Spring 1-1-2015

Riparian Evapotranspiration Estimation Using a Subsurface-Surface Water Balance Approach

Jose Alejandro Solis
University of Colorado at Boulder, jose.solis@colorado.edu

RIPARIAN EVAPOTRANSPIRATION ESTIMATION USING A SUBSURFACE-SURFACE WATER BALANCE APPROACH

by

Jose Alejandro Solis

B.S., New Mexico State University, 2005

M.S. New Mexico State University, 2008

A dissertation submitted to the

Faculty of the Graduate School of the

University of Colorado in partial fulfillment

of the requirements for the degree of

Doctor of Philosophy

Civil Engineering

2015

This thesis entitled:
Riparian Evapotranspiration Estimation Using A Subsurface-Surface Water Balance Approach
written by Jose Alejandro Solis
has been approved for the Department of Civil and Environmental Engineering

_____

Harihar Rajaram, Advisor

_____

Donald O. Whittemore

_____

James J. Butler, Jr.

_____

Roseanna Marie Neupauer

_____

John Scott McCartney

_____

Holly R. Barnard

Date_____

The final copy of this thesis has been examined by the signatories, and we find that both the content and the form meet acceptable presentation standards of scholarly work in the above mentioned discipline.

Solis, Jose, Alejandro (Ph.D., Civil Engineering)

Riparian Evapotranspiration Estimation Using a Subsurface-surface Water Balance Approach

Dissertation directed by Professor and President's Teaching Scholar Harihar Rajaram

ABSTRACT

Riparian evapotranspiration (RET) is an important component of basin-wide evapotranspiration (ET), especially in subhumid to semi-arid regions, with significant impacts on water management and conservation. A common method of measuring ET is using the eddy correlation technique. However, since most riparian zones are narrow, eddy correlation techniques are not applicable because of limited fetch distance. Techniques based on surface-subsurface water balance are applicable in these situations, but their accuracy is not well constrained. In this study, we estimated RET within a 100 meter long by 45 meter wide riparian zone along Rock Creek in the Whitewater Basin (1,100km) in central Kansas using a subsurface water balance (SSWB) approach. The soils were comprised largely of silty loam and clay, with gravel fragments at higher depths. Deeper alluvial sediment in the riparian zone is primarily clay that acts as an aquitard overlying the bedrock and overlying this layer is more permeable alluvial sediment and soil. The soil moisture contribution to RET is expected to be large in this setting. The SSWB approach was based on a monitoring network that included six soil moisture profilers with capacitance sensors at 4-6 depths (during different periods of the study), 4 water table wells, a deep bedrock well, and a weather station.

Continuous data collection and analysis extended from July 2010 to December 2013. The RET estimates obtained from the different profile locations vary significantly, even though they typically exhibit coherent trends. Results are presented on an annual and inter-annual (three periods within the year) basis. This variability results from the highly

heterogeneous soils in the vadose zone (2-3 m thick), where soil moisture (rather than groundwater) is the major source of water for riparian vegetation. Variable vegetation density and species also likely contribute to the variability.

The water-balance based approach is very cost-effective, even with the large number of soil moisture sensors deployed. However, the high degree of variability in RET estimates from individual profiles even within a relatively short reach, suggests caution in the application and interpretation of water balance based techniques in vadose zones with natural vegetation, unless large sensor networks are used.

DEDICATION

I would like to dedicate this work to my parents Humberto and Martha Solis who have taught me that hard work pays off and that the only inheritance that no one can take away from you is your education. To all of the people who have come to this country and strived for a better future for their family. To my precious wife Rosario Vanessa and son Emanuel Alejandro.

ACKNOWLEDGEMENTS

I would like to thank God for having put all the people in my life and given me health and patience through one my hardest endeavors. I would like to thank my advisor, mentor, and friend Dr. Harihar Rajaram for accepting me as a student and for all of his patience through these seven years. If it wasn't for his patience, understanding and constant encouragement I would have not finished this PhD. To my family in always being there, supporting and encouraging me to continue on and to always look forward.

This research was funded by the Nation Science Foundation, grant EAR-0741397; Project Title: Collaborative Research: Refinement of Techniques for Estimating Evapotranspiration from Narrow Riparian Zones--Water Balance and Atmosphere Measurements. I would like to thank the Colorado Diversity Initiative (CDI) along with Alliance for Graduate Education and the Professoriate (AGEP) program, the Cooperative Institute for Research in Environmental Sciences (CIRES) graduate student award program, and the Civil Environmental and Architectural Engineering (CEAE) Department Fellowship who further supported and funded me during my time at CU Boulder.

I would like to thank Bill Watson (land owner, during this research) for his cooperation in allowing us to use his property for this study. Also, would like thank all the collaborators of this project such as Bill Eichinger, Dan Ceynar and Anton Kruger from the University of Iowa and in particular to Don Whittemore, Jim Butler, Ed Reboulet Steve Knobbe, Mike Dealy from the Kansas Geologic Survey (KGS), for their help and contribution through this research project.. Who if it wasn't for all their help in the field and mitigation with the land owner, this project would have not been possible.

I am very grateful for all the faculty and professors from the CEAE department for all their help during my time at CU Boulder. Thanks to John McCartney for allowing me to use his lab for soil analysis. Thanks to all the undergraduate students who helped me in the lab and in the field in particular Danny Birdsell, Austin Nossokoff, Matt Schwartz. Thanks to all of my committee members: Don Whittemore, Jim Bulter, Roseanna Neupauer, John McCartney and Holly Barnard, for agreeing to be part of my committee.

CONTENTS

CHAPTER I 1

INTRODUCTION AND OBJECTIVES 1

1.1 Introduction 1
1.2 Riparian zone Hydrology and RET 2
1.3 Other Impacts of RET 4
1.4 Past Efforts at RET Measurement 5
1.5 Thesis Objectives and Outline 8

CHAPTER II 10

SITE DESCRIPTION 10

2.1 Hydrogeology of study site 11
2.1.1 Soil Characterization: 19
2.1.2 Soil Analyses for profile A: 20
2.1.3 Soil Analyses for profile C: 24
2.1.4 Soil Analyses for profile D: 28
2.1.5 Soil Analyses for profile E: 32
2.1.6 Soil Analyses for profile F: 36
2.1.7 Summary of Soil Property Variations: 40
2.2. Topography of study site 40
2.3 Vegetation of the study site 41

CHAPTER III 42

MONITORING NETWORK DESIGN 42

3.1 Soil moisture profiler network 43
3.2 Ground water network 46
3.3 Stream gaging system 48
3.4 Weather station 49

CHAPTER IV 52

REPRESENTATIVE OBSERVATIONS AND CONCEPTUAL MODEL 52

4.1 Observations from Well Data 52
4.2 Observations from Soil Moisture Data 56
4.3 Hydrogeological connectivity 60
4.4 Conceptual Model 62

CHAPTER V 66

FRAMEWORK FOR WATER BALANCE ANALYSIS 66

CHAPTER VI 74

ANNUAL CYCLE AND ESTIMATES OF RIPARIAN EVAPOTRANSPIRATION 74

6.1 Precipitation 74
6.2 Total Soil Moisture, TSM 75
6.3 Groundwater inflow(+) / outflow (−), $G'_{in/out}$ 81
6.4 Riparian Evapotranspiration Estimation, RET 86
6.5 Discussion 91
6.5.1 Heterogeneity across profile locations 91
6.5.2 Inter-annual variability 91
6.5.3 Comparison to other sites 92
6.5.4 Limitations 94

CHAPTER VII 96

INTER-ANNUAL VARIABILITY DURING THREE PERIODS WITHIN THE GROWING SEASON AND COMPARISON TO LIDAR ESTIMATES OF RIPARIAN EVAPOTRANSPIRATION 96

7.1 Inter-annual variability during three periods within the growing season 96
7.1.1 Year 2011 98
7.1.2 Year 2012 100
7.1.3 Year 2013 102
7.2 Lidar Comparison 110

CHAPTER VIII 118

1D VERTICAL NUMERICAL MODEL USING INSIGHTS FROM THE CONCEPTUAL MODEL AND FIELD AND LABORATORY MEASUREMENTS 118

CHAPTER IX 139

SUMMARY AND CONCLUSIONS 139

REFERENCES 147

APPENDIX A: Visual Soil Analysis 154

APPENDIX B: Laboratory Soil Analysis 156

APPENDIX C: Normalized Total Soil Moisture Time Series 177

APPENDIX D: Annual Soil Moisture Time Series Plots 179

APPENDIX E: Annual Reference Evapotranspiration on a monthly time scale. 190

APPENDIX F: Annual water table hydrograph measurements for shallow wells 191

TABLES

Table
2. 1 Soil properties and van Genuchten parameters with depth for Profile A.....21

2. 2. Soil properties and van Genuchten parameters with depth for Profile C.....25

2. 3. Soil properties and van Genuchten parameters with depth for Profile D.....29

2. 4. Soil properties and van Genuchten parameters with depth for Profile E.....33

2. 5. Soil properties and van Genuchten parameters with depth for Profile F.....37

3. 1. Sensor location with respect to the ground surface for profile A. 45

3. 2. Sensor location with respect to the ground surface for profile B. 45

3. 3. Sensor location with respect to the ground surface for profile C. 45

3. 4. Sensor location with respect to the ground surface for profile D. 45

3. 5. Sensor location with respect to the ground surface for profile AA, E. 45

3. 6. Sensor location with respect to the ground surface for profile AB, F.....45

3. 7. Sensor type, model, and location placed on the weather station.....51

6. 1. Annual change in total soil moisture at each profile location along with the average of all the profiles and yearly measured precipitation. 78

6. 2. Annual summaries for minimum, maximum, average, and total annual change in total soil moisture spatially across all profile locations.....79

6. 3Table 6.3. Minimum, maximum and average $G'_{in/out}$ values for of the profiles corresponding to the figures 6.6 through 6.11.....85

6. 4. Yearly summary of estimated RET from all profile locations and comparison to the ETsz and percentage of filtered GDD for 2010. 89

6. 5. Yearly summary of estimated RET from all profile locations and comparison to the ETsz and percentage of GDD of filtered estimates for 2011.....89

6. 6. Yearly summary of estimated RET from all profile locations and comparison to the ETsz and percentage of GDD of filtered estimates for 2012.....90

6. 7. Yearly summary of estimated RET from all profile locations and comparison to the ETsz and percentage of GDD of filtered estimates for 2013.....90

6. 8. Comparative riparian evapotranspiration results from various locations and authors. Describes the vegetation type, the location of where the measurements were made, the depth to water table, evapotranspiration derived from groundwater measurements and the corresponding citation†. 93

7. 1. Durations of the three periods analyzed in each year 105

7. 2. Daily averaged RET for profile locations A, B, and F during the three selected periods during 2011, 2012 and 2013. Numbers in parentheses is the ratio of estimated RET to the ASCE standardized ET....109

7. 3. Comparative riparian evapotranspiration estimates from previous studies. The table describes the vegetation type, the location of where the measurements were made, the depth to water table, evapotranspiration derived from water table fluctuations (ETgw) and the corresponding citation† (Note that the Nachabe et al. 2005 study employed TSM balance rather than water table measurements). 110

7. 4. Equivalent depth of water and/or ET from the EC flux tower and ET estimates from the Lidar and change in soil water moisture (dS/dt) from the all the soil moisture profiles (A-F) over same duration. 113

8. 1. Soil properties that were used in the numerical model for Profile D. 120

A 1. Visual inspection of soil core sample no. 4 (Well D, furthest from creek) 154

A 2. Visual inspection of soil core sample no. 5 (Well C, 2nd furthest from creek) 154

A 3. Visual inspection of soil core sample no. 6 (Well B, 2nd closest to creek) 155

A 4. Visual inspection of soil core sample no. 10 (Well A, closest to creek) 155

B 1. Mass of soil samples retained in each sieve, cumulative percent retained, and percent finer for soil at Profile A at 0.13 m from the surface. 157

B 2. Mass of soil samples retained in each sieve, cumulative percent retained, and percent finer for soil at Profile A at 0.53 m from the surface. 157

B 3. Mass of soil samples retained in each sieve, cumulative percent retained, and percent finer for soil at Profile A at 0.84 m from the surface. 157

B 4. Mass of soil samples retained in each sieve, cumulative percent retained, and percent finer for soil at Profile A at 1.44 m from the surface. 158

B 5. Values of D_{10}, D_{30}, and D_{60} along with the C_u and C_c from soil at Profile A at four distinct depths and their most probable classifications. 158

B 6. Mass of soil samples retained in each sieve, cumulative percent retained, and percent finer for soil at Profile C at 0.15 m from the surface. 160

B 7. Mass of soil samples retained in each sieve, cumulative percent retained, and percent finer for soil at Profile C at 0.56 m from the surface. 160

B 8. Mass of soil samples retained in each sieve, cumulative percent retained, and percent finer for soil at Profile C at 1.05 m from the surface. 160

B 9. Mass of soil samples retained in each sieve, cumulative percent retained, and percent finer for soil at Profile C at 1.77 m from the surface. 161

B 10. Values of D_{10}, D_{30}, and D_{60} along with the C_u and C_c from soil at Profile C at four distinct depths and their most probable classifications. 161

B 11. Mass of soil samples retained in each sieve, cumulative percent retained, and percent finer for soil at Profile D at 0.08 m from the surface. 163

B 12. Mass of soil samples retained in each sieve, cumulative percent retained, and percent finer for soil at Profile D at 0.48 m from the surface. 163

B 13. Mass of soil samples retained in each sieve, cumulative percent retained, and percent finer for soil at Profile D at 0.89 m from the surface. 163

B 14. Mass of soil samples retained in each sieve, cumulative percent retained, and percent finer for soil at Profile D at 1.60 m from the surface. 164

B 15. Values of D_{10}, D_{30}, and D_{60} along with the C_u and C_c from soil at Profile D at four distinct depths and their most probable classifications. 164

B 16. Mass of soil samples retained in each sieve, cumulative percent retained, and percent finer for soil at Profile E at 0.18 m from the surface. 166

B 17. Mass of soil samples retained in each sieve, cumulative percent retained, and percent finer for soil at Profile E at 0.58 m from the surface. 166

B 18. Mass of soil samples retained in each sieve, cumulative percent retained, and percent finer for soil at Profile E at 1.08 m from the surface. 166

B 19. Mass of soil samples retained in each sieve, cumulative percent retained, and percent finer for soil at Profile E at 1.59 m from the surface. 167

B 20. Values of D_{10}, D_{30}, and D_{60} along with the C_u and C_c from soil at Profile E at four distinct depths and their most probable classifications. 167

B 21. Mass of soil samples retained in each sieve, cumulative percent retained, and percent finer for soil at Profile F at 0.11 m from the surface. 169

B 22. Mass of soil samples retained in each sieve, cumulative percent retained, and percent finer for soil at Profile F at 0.52 m from the surface. 169

B 23. Mass of soil samples retained in each sieve, cumulative percent retained, and percent finer for soil at Profile F at 1.03 m from the surface.....169

B 24. Mass of soil samples retained in each sieve, cumulative percent retained, and percent finer for soil at Profile F at 1.63 m from the surface.....170

B 25. Values of D_{10}, D_{30}, and D_{60} along with the C_u and C_c from soil at Profile F at four distinct depths and their most probable classifications.....170

FIGURES

Figure

1. 1. (a) and (b) Aerial photographs of two 3.5 X 3.5 *km* sections of Whitewater basin. Strahler stream orders label the riparian zones (dark bands) in each image. Riparian zone widths do not increase systematically with an increase in order but appear to fluctuate around a constant mean value. (c) vegetation cover that typifies the riparian zones in Whitewater is shown for the Rock Creek stream. Hackberry, Elm, and Green Ash are the dominant species of trees that cover the basin..... 4

2.1. Location of study site.....10

2. 2. Map of Rock Creek watershed above a temporary gaging station installed several years ago as a part of HydroKansas research activities. The general location of the riparian evapotranspiration (RET) study is shown by the red rectangle, which is in the northern half of Sec. 20, T. 25 S., R 04 E., Butler County, Kansas. The fine red lines and the west boundary of the watershed form the north and parts of the west and east lines of Sec. 20. 12

2. 3. The same area as in Figure 2.2 but taken from an aerial photograph (Google earth: 37°51'54.42" N 97°00'58.18" W, image taken on 2/25/2012) during the winter when there was little leaf material left on the deciduous trees. The dark sinuous line through the riparian area is the channel of Rock Creek. The blue rectangle represents the area shown at higher resolution in Figure 2.4.....13

2. 4. Enlargement of the area within the blue rectangle in Figure 2.3 showing the location of the Rock Creek research site and the nine Geoprobe DPEC logs. The orange and green circles represent locations of stakes used for site reference and measurements. The blue lines (about 100 m apart) bound the main study section. The dark curved band is the channel of Rock Creek (water and shadow caused by southeast sun location). The darker gray shades indicate the area of riparian vegetation. Note that the south bank of the creek is a shale bedrock outcrop with very little vegetation. 14

2. 5 North-south cross section of electrical conductivity logs of the unconsolidated sediment at the study site. The areal location of each log is indicated in Figure 2.4 within the white filled circle with the same number as at the end of the label above the log. The filled blue triangles represent the water-level surface. The open triangle represents the last measured value of a water level that was slowly rising in the direct-push hole before the hole was sealed with bentonite. 16

2. 6. West-northwest to east-southeast cross section of electrical conductivity logs of the unconsolidated sediment at the study site. See Figure 2.5 for explanation of blue triangles and area location of logs. A water-level measurement was not made for DPEC log 1. 17

2. 7. Northeast to southwest cross section of electrical conductivity logs of the unconsolidated sediment at the study site. See Figure 2.5 for explanation of blue triangles and area location of logs. A water-level measurement was not made for DPEC log 3. 18

2. 8. Soil water retention curves for profile A at various depth. 21

2. 9. Hydraulic Conductivity versus depth for profile A. 22

2. 10. Porosity versus depth for profile A. 22

2. 11. van Genuchten n parameter versus depth for profile A. 23

2. 12. van Genuchten α, parameter versus depth for profile A. 23

2. 13. Soil water retention curves for profile C at various depths. 25

2. 14. Hydraulic Conductivity versus depth for profile C. 26

2. 15. Porosity versus depth for profile C. 26

2. 16. van Genuchten n parameter versus depth for profile C. 27

2. 17. van Genuchten α, parameter versus depth for profile C. 27

2. 18. Soil water retention curves for profile D at various depth. 29

2. 19. Hydraulic Conductivity versus depth for profile D. 30

2. 20. Porosity versus depth for profile D. 30

2. 21. van Genuchten n parameter versus depth for profile D. 31

2. 22. van Genuchten α, parameter versus depth for profile D. 31

2. 23. Soil water retention curves for profile E at various depth. 33

2. 24. Hydraulic Conductivity versus depth for profile E. 34

2. 25. Porosity versus depth for profile E. 34

2. 26. van Genuchten n parameter versus depth for profile E. 35

2. 27. van Genuchten α, parameter versus depth for profile E. 35

2. 28. Soil water retention curves for profile F at various depth. 37

2. 29. Hydraulic Conductivity versus depth for profile F. 38

2. 30. Porosity versus depth for profile F. 38

2. 31. van Genuchten n parameter versus depth for profile F. 39

2. 32. van Genuchten α, parameter versus depth for profile F. 39

3. 1. Location of sensors within the riparian zone which include ground water observation wells, stream gages and soil moisture profiles. The soil moisture sensors are positioned within 2 m (6.6 ft) of the alluvium wells. The stream flow goes from East to West....43

3. 2. Sentek EnviroSCAN soil moisture profiler system customized for our application. The 6 pairs of gold-colored rings (No. 1) constitute the capacitance sensors set at 6 different depths that slide along a plastic type cartridge (No.2) and all connected to an electronic interface (No. 3) that communicates with a centralized external data logger (No.5). The cartridge is then placed inside the access tube (No. 4, white PVC pipe). 44

3. 3. (**a**) Dual-rod Geoprobe direct push system that was used in drilling the deep alluvium wells (KGS, Ed Robelet and Steve from right to left). (**b**) RotoSonic drill rig that was used to make the bedrock well. 47

3. 4. Vertical cross-section through the main transect showing locations of soil moisture sensors, shallow well screens and deep alluvial well screens (figure is not to scale). 48

3. 5. **(a)** Two pressure sensors mounted on a plastic ring and covered by two plates, which allows unimpeded flow and protection from debris. **(b)** The downstream gage placed in the stream (No. 1) and a stake embedded in the ground to prevent gage movement during a flood event. **(c)** The bifurcated access tube that allows easy access to each sensor's data logger for manual download (No.3). 49

3. 6. Weather station located on the prairie as depicted by the red arrow on the satellite image at the top right corner. The weather station measures: precipitation (No. 1), wind speed and direction (No. 2), solar radiation (No. 3), air temperature and humidity (No. 4), and the barometric sensor is located inside the enclosure (No. 5) along with the data logger, and telemetry system. 50

4. 1. Hydrographs of wells screened in the bedrock and alluvial base/weathered bedrock top, in two of the shallow alluvial (water table) wells, and in the shallow stream bed well during a two-week period in June 2011. The hydrographs in red (wells C-WT and C) and green (wells B-WT and B) represent pairs of nearby alluvial base and shallow alluvium wells; the bedrock well hydrograph is the black line....53

4. 2. Aerial view of the study site and showing the location of the pumping wells. 54

4. 3. Hydrograph of the alluvial base wells and the temperature of the discharge pipes of the supply wells during the summer. A decrease in temperature occurred when the pumps started as indicated at the locations of the vertical lines. 55

4. 4. A closer view of the continuous soil moisture measurements by 4 sensors for profile AA (upstream profile, also referred to as profile E). 56

4. 5. Soil moisture profile taken every 0.15 meters starting from a depth of 0.15m to 1.40m, at profile A (closest to the stream), taken on 7/7/2011.....58

4. 6. Soil moisture profile taken every 0.15 meters starting from a depth of 0.13m to 1.65m, at profile B (2nd closest to the stream), taken on 7/7/2011. 58

4. 7. Soil moisture profile taken every 0.15 meters starting from a depth of 0.08m to 1.75m, at profile C (3rd closest to the stream), taken on 7/7/2011. 59

4. 8. Soil moisture profile taken every 0.15 meters starting from a depth of 0.08m to 1.6m, at profile D (furthest from the stream), taken on 7/7/2011.....59

4. 9. Hydrographs of wells screened in the bedrock and alluvial base/weathered bedrock top, in two of the shallow alluvial (water table) wells, and in the shallow stream bed well during a period in May through June 2012. The hydrographs in red and green represent pairs of nearby alluvial base and shallow alluvium wells; the bedrock well hydrograph is the black line. 61

4. 10. Soil water content at six different depths during a period in May through June 2012. The top most sensor (brown line) shows the effect of the precipitation and the others do not show the infiltration sharp front. 62

4. 11. Visual interpretation of the conceptual model for the study site. Direct precipitation, streambank infiltration, and upward leakage are the main sources to the shallow water table. Plant transpiration and, when the water table is substantially higher than the stream, discharge to the stream, are the main avenues by which water leaves the uppermost saturated zone. The faint dashed blue line indicates the stream stage and water table conditions under very short lived high flow events, when recharge from overbank flow can occur. The bottom dashed blue line represents the typical water table position during most of the year. The deep alluvium and bedrock wells have a higher potentiometric head than the shallow water table that can be up to a difference of two feet (Note: diagram is not to scale). 64

5. 1. Reach-scale schematic of for the water balance equation (schematic modified from Mac Nish et al., 2000) 67

5. 2. Diagram for equation 5.3a TSM_{top} representation 69

5. 3. Diagram for equation 5.3b TSM_{full} representation 70

5. 4. Examples of estimated RET by looking at the TSM_{top} from two locations a) profile location E (upstream); b) profile location F (downstream); and examples of estimated RET by looking at the TSM_{full} from two locations c) profile location B (2^{nd} furthest from stream); d) profile location C (3^{rd} furthest from stream). The nighttime behavior is reasonably well approximated with a constant slope. Location F behaves like a discharge zone (exhibiting nighttime recovery in TSM_{top}, i.e. $G' = G'_{in} - G'_{out} > 0$), while locations E and C exhibits nigh-time decrease in TSM_{top} and TSM respectively, thus behaving like a recharge zone (i.e. G' or $G = G_{in} - G_{out} < 0$). At location B, the behavior is different across the different days. For the duration shown, it is behaving like a discharge zone with $G > 0$. 71

5. 5. Illustration of the three different time duration approaches for the estimation of G' or G-values. G'_1 represents a time duration from midnight to 4AM, G'_2 represents from 8pm of the previous day to 8AM of the current day and finally G'_3 represents from 10pm of the previous day to 6am of the current day. 72

6. 1. Monthly precipitation for the entire research period, 2010 through 2013.....75

6. 2. Total soil moisture for all profiles (A, B, C, D, E, F) and precipitation during 2010. 76

6. 3. Total soil moisture for all profiles (A, B, C, D, E, F) and precipitation during 2011. 77

6. 4. Total soil moisture for all profiles (A, B, C, D, E, F) and precipitation during 2012. 77

6. 5. Total soil moisture for all profiles where data was available (A, B, E, F) and precipitation during 2013. 78

6. 6. Average monthly inflows comparison and TSM for Profile A during the entire research period.....82

6. 7. Average monthly inflows comparison and TSM for Profile B during the entire research period.....82

6. 8. Average monthly inflows comparison and TSM for Profile C during the entire research period.....83

6. 9. Average monthly inflows comparison and TSM for Profile D during the entire research period.....83

6. 10. Average monthly inflows comparison and TSM for Profile E during the entire research period.....84

6. 11. Average monthly inflows comparison and TSM for Profile F during the entire research period.....84

6. 12. Daily RET estimates averaged over each month for all the profiles during the growing season and the ASCE standardized reference evapotranspiration (ET_{sz}) in 2010. The colored lines represent the profiles, the dotted line the average of all profile locations, and the light blue shaded area is the ET_{sz}. 86

6. 13. Daily RET estimates averaged over each month for all the profiles during the growing season and the ASCE standardized reference evapotranspiration (ET_{sz}) in 2011. The colored lines represent the profiles, the dotted line the average of all profile locations, and the light blue shaded area is the ET_{sz}. 87

6. 14. Daily RET estimates averaged over each month for all the profiles during the growing season and the ASCE standardized reference evapotranspiration (ET_{sz}) in 2012. The colored lines represent the profiles, the dotted line the average of all profile locations, and the light blue shaded area is the ET_{sz}. 87

6. 15. Daily RET estimates averaged over each month for all the profiles during the growing season and the ASCE standardized reference evapotranspiration (ET_{sz}) in 2013. The colored lines represent the profiles, the dotted line the average of all profile locations, and the light blue shaded area is the ET_{sz}. 88

7. 1. Three period comparison of soil moisture profiles over three years (2011, 2012, and 2013). First row shows profiles in 2011: (a) average soil moisture profile location A; (b) average soil moisture profile location B; (c) average soil moisture profile location F. Second row shows profiles in 2012: (d) average soil moisture profile location A; (e) average soil moisture profile location B; (f) average soil moisture profile location F. Third row shows profiles in 2013: (g) average soil moisture profile location A; (h) average soil moisture profile location B; (i) average soil moisture profile location F. 105

7. 2. Comparison of soil moisture changes during three periods in 2011 from three different profile locations (A, B and F). The total soil moisture (TSM) trends during the three periods are also shown at each profile location. Note that the y-axis ranges are different for each plot. Each row shows soil moisture changes during a specific period (2011, 2012, 2013), and each column shows behavior at a specific profile (A, B, F). 106

7. 3. Comparison of soil moisture changes during three periods in 2012 from three different profile locations (A, B and F). The total soil moisture (TSM) trends during the three periods are also shown at each profile location. Note that the y-axis ranges are different for each plot. Each row shows soil moisture changes during a specific period (2011, 2012, 2013), and each column shows behavior at a specific profile (A, B, F). 107

7. 4. Comparison of soil moisture changes during three periods in 2013 from three different profile locations (A, B and F). The total soil moisture (TSM) trends during the three periods are also shown at each profile location. Note that the y-axis ranges are different for each plot. Each row shows soil moisture changes during a specific period (2011, 2012, 2013), and each column shows behavior at a specific profile (A, B, F). 108

7. 5. Location of study site. The red rectangle corresponds to the riparian vegetation where the soil moisture profiles are located. The triangle with the letter L corresponds to the location of where the Raman LIDAR was placed for measurements and the circle with the letter W corresponds to the location of the weather station. 111

7. 6 Equivalent depth of water and/or ET per 30 minutes from the EC flux tower, ET estimates from the Lidar, ASCE Standardized ET (ETsz) and soil moisture based RET estimates from the all the soil moisture profiles (A-F). [Daily ASCE ETsz values = 5.19, 5.94, 7.52 mm/day for days 7,8, and 9 of July respectively] 113

7. 7. Equivalent depth of water and/or ET per 30 minutes from the EC flux tower, ET estimates from the Lidar, ASCE Standardized ET and, change in soil water moisture (dS/dt) from the all the soil moisture profiles (A-F) using only the TSM_Top. [ASCE ETsz = 5.19, 5.94, 7.52 mm/day for days 7,8, and 9 of July respectively] 114

7. 8. Wind velocity and direction for the duration of the Lidar measurements (see table 7.4). Meteorological measurements which include air temperature, relative humidity, solar radiation and barometric pressure during the study period.....116

8. 1. One-dimensional representation of the soil layers used in the numerical model.....121

8. 2. Photograph of an incised bank at the study site showing the depth to which roots can extend. The height of the bank was measured at approximately 4.5 meters.....126

8. 3. Modeled soil moisture profile with depth and observed soil moisture values in the field. Model was run for 60 days. The blue solid line is the modeled soil moisture profile results and the red dashed line is the initial condition prescribed from which the model was initiated. The red +'s are the field observations at the beginning of the simulation and the blue x's are the field observations at the end of the simulation period.....127

8. 4. Model run with RW = 82 $mm3$(root density), Cs = 400, Cr = 1.0 × 105 $daysm$, $Zrmax$ = 3.25 m (the rooting depth, from the surface to a length of 3.25 meters). 128

8. 5. Model run with RW = 50 $mm3$(root density), Cs = 995, Cr = 1.5 × 104 $daysm$, $Zrmax$ = 3.29 m (the rooting depth, from the surface to a length of 3.29 meters). 128

8. 6. Model run with RW = 85 $mm3$(root density), Cs = 920, Cr = 1.0 × 105 $daysm$, $Zrmax$ = 3.29 m (the rooting depth, from the surface to a length of 3.29 meters). 129

8. 7. Modeled RET by integrating the TSM across the entire depth(red line), RET estimated by using six discrete points and the water table location (blue line) and RET estimated by only using six discrete points for period 1. 131

8. 8. Calculated daily Q_{in} or Q_{out} values that were determined from the nighttime TSM slope from the three different methods for period 1. 132

8. 9. Change in soil moisture at six depth locations for period 1 (5/21-28/2012); a) modeled results; b) field observations. 133

8. 10. Change in total soil moisture using three different approaches. Red dotted line uses the results from the entire profile, green dashed line uses values from six depths, and the blue dashed line also uses the same six depth location in addition to location of the water table. 134

8. 11. Modeled RET by integrating the TSM across the entire depth(red line), RET estimated by using six discrete points and the water table location (blue line) and RET estimated by only using six discrete points for period 2. 134

8. 12. Calculated daily Q_{in} or Q_{out} values that were determined from the nighttime TSM slope from the three different methods for period 2. 135

8. 13. Change in soil moisture at six sensor locations. (a) modeled results (b) field observations. 135

8. 14. Change in total soil moisture using three different approaches for period 2. Red dotted line uses the results from the entire profile, green dotted line uses values from six depths, and the blue dotted line also uses the same six depth location in addition to location of the water table. 136

8. 15. Modeled RET by integrating the TSM across the entire depth(red line), RET estimated by using six discrete points and the water table location (blue line) and RET estimated by only using six discrete points for period 3. 136

8. 16. Calculated daily Q_{in} or Q_{out} values that were determined from the nighttime TSM slope from the three different methods for period 3. 137

8. 17. Change in soil moisture at six sensor locations. (a) modeled results (b) field observations. 137

8. 18. Change in total soil moisture using three different approaches for period 3. Red dotted line uses the results from the entire profile, green dotted line uses values from six depths, and the blue dotted line also uses the same six depth location in addition to location of the water table. 138

B 1. Percent finer vs. Grain size relationship for soil located at Profile A at various depths from the surface. 156

B 2. Percent finer vs. Grain size relationship for soil located at Profile C at various depths from the surface. 159

B 3. Percent finer vs. Grain size relationship soil located at Profile D at various depths from the surface. 162

B 4. Percent finer vs. Grain size relationship for soil located at Profile E at various depths from the surface. 165

B 5. Percent finer vs. Grain size relationship for soil located at Profile F at various depths from the surface. 168

C 1. Normalized total soil moisture for all profiles in 2010....177

C 2. Normalized total soil moisture for all profiles in 2011....177

C 3. Normalized total soil moisture for all profiles in 2012....178

C 4. Normalized total soil moisture for all profiles in 2013....178

D 1. Soil moisture and total soil moisture for profile A in 2010....179

D 2. Soil moisture and total soil moisture for profile A in 2011....179

D 3. Soil moisture and total soil moisture for profile A in 2012....180

D 4. Soil moisture and total soil moisture for profile A in 2013....180

D 5. Soil moisture and total soil moisture for profile B in 2010....181

D 6. Soil moisture and total soil moisture for profile B in 2011....181

D 7. Soil moisture and total soil moisture for profile B in 2012....182

D 8. Soil moisture and total soil moisture for profile B in 2013....182

D 9. Soil moisture and total soil moisture for profile C in 2010....183

D 10. Soil moisture and total soil moisture for profile C in 2011....183

D 11. Soil moisture and total soil moisture for profile C in 2012....184

D 12. Soil moisture and total soil moisture for profile D in 2010....184

D 13. Soil moisture and total soil moisture for profile D in 2011....185

D 14. Soil moisture and total soil moisture for profile D in 2012....185

D 15. Soil moisture and total soil moisture for profile E in 2010....186

D 16. Soil moisture and total soil moisture for profile E in 2011....186

D 17. Soil moisture and total soil moisture for profile E in 2012....187

D 18. Soil moisture and total soil moisture for profile E in 2013....187

D 19. Soil moisture and total soil moisture for profile F in 2010....188

D 20. Soil moisture and total soil moisture for profile F in 2011. 188

D 21. Soil moisture and total soil moisture for profile F in 2012. 189

D 22. Soil moisture and total soil moisture for profile F in 2013. 189

F 1. 2011 Annual water table hydrograph measurements for shallow wells B (green line) and C (red line), and deep bedrock well (well H, black line) and for the well located in the stream (well G, light blue line).....191

F 2. 2012 Annual water table hydrograph measurements for shallow wells B (green line) and C (red line), and deep bedrock well (well H, black line) and for the well located in the stream (well G, light blue line).....192

F 3. 2013 Annual water table hydrograph measurements for shallow wells B (green line) and C (red line), and deep bedrock well (well H, black line) and for the well located in the stream (well G, light blue line).....193

F 4. 2013 Annual water table hydrograph measurements for shallow wells B (green line) and C (red line), and deep bedrock well (well H, black line) and for the well located in the stream (well G, light blue line).....194

CHAPTER I

INTRODUCTION AND OBJECTIVES

1.1 Introduction

Riparian evapotranspiration (RET) is an important component of the water balance of watersheds. It is poorly quantified in many areas such as the mid-western and south-western U.S. because riparian zones are narrow along streams with a width on the order of less than 20-50m (Lee et al., 2004; Smiley et al., 2011). Traditional methods of measuring evapotranspiration (ET), such as eddy covariance methods that require a large homogeneous vegetated area are thus not applicable in riparian zones. The recommended ratio of fetch distance for applicability of eddy covariance measurements is about 1:100 (Westenburg et al., 2006). One method where fetch is not a limiting factor is the Sub-Surface Water Balance (SSWB) method, which is the main method to be used in this study. In this method, RET is estimated as a residual in a water balance equation where all other terms (change in storage, other inflows, outflows) are independently constrained. This research was part of the Hydro-Kansas (HK) project, involving collaboration between the Kansas Geological Survey (KGS), the University of Iowa (UI) and, University of Colorado at Boulder (CU). The study site is within the Whitewater basin in south-central Kansas. The study was carried out between July 2010 and December 2013.

Previous large-scale field experiments aimed at measuring RET include the Semi-Arid Land-Surface-Atmosphere (SALSA) program in the Upper San Pedro Basin (USPB) in southeastern Arizona (Goodrich et al., 2000; Mac Nish et al., 2000). The SALSA study consisted of a combination of ET measurement techniques. These techniques included water balance, sap flow and, remote sensing. One main difference between the SALSA study and our study is that there was no significant vadose zone contribution to RET at the

SALSA site because of very coarse-grained sandy alluvium in the riparian zone. In contrast, at our study site the alluvium consists of fine-grained soils and sediment such as silt, clay and, loam.

1.2 Riparian zone Hydrology and RET

Riparian zones in a grassland setting are ribbon-like rows of trees and underbrush that follow along perennial and intermittent streambeds (Figure. 1.1). The National Research Council (NRC, 2002) defines riparian areas as follows:

> *"Riparian areas are transitional between terrestrial and aquatic ecosystems and are distinguished by gradients in biophysical conditions, ecological processes, and biota. They are areas through which surface and subsurface hydrology connect water bodies with their adjacent uplands. They include those portions of terrestrial ecosystems that significantly influence exchanges of energy and matter with aquatic ecosystems (i.e. a zone of influence). Riparian areas are adjacent to perennial, intermittent, and ephemeral streams, lakes, and estuarine-marine shorelines."*

Of primary interest in this dissertation are riparian zones along streams. Potential sources of water to such riparian zones include groundwater inflows, surface and shallow subsurface flow on hillslopes following precipitation events, and seepage from the stream. In the same riparian zone, different sources may be dominant at different times. Groundwater inflows are often driven by hydraulic gradients that are closely related to topographic gradients. The stream network serves as a drain in such situations, and receives baseflow from the groundwater system. Previous studies summarized in NRC (2002) suggest that there is significant spatial variability in groundwater inflows to riparian zones due to heterogeneity in riparian sediments and focused regions of local inflows. In the Whitewater basin, alternating limestone units (the primary bedrock strata transmitting groundwater) and shales adds to the spatial variability of groundwater inflows to streams. Temporal variability in groundwater inflows is typically less significant than

inflows from hillslope sources and seepage from the stream. Inflows from hillslope sources vary significantly in response to precipitation, and seepage from the stream varies on daily to seasonal time scales in response to individual storm events and seasonal variations in precipitation.

RET intercepts a portion of the groundwater inflow that would otherwise be discharged to the stream as baseflow (NRC, 2002). RET commonly produces a diurnal pattern of water-level fluctuations in shallow water-table wells in riparian zones (e.g., White, 1932; Loheide et al., 2005; Butler et al., 2007; Scott et al., 2008; Schilling and Jacobson, 2009; Williams and Scott, 2009; Jobbágy et al., 2011; Rahgozar et al., 2012). In smaller streams, RET is substantial enough to produce similar diurnal variations in stream flows (e.g., Troxell, 1936; Wicht, 1941; Bren, 1997; Lundquist and Cayan, 2002; Bond et al., 2002). In streams with permeable hyporheic zones, the size of the hyporheic zone has been observed to expand during the day as RET causes more water to seep out of the stream (Harvey et al., 1991). In addition to playing an important role in riparian hydrology (and ecology), RET is also an important, but poorly quantified, component of basin-wide ET. In the example shown in Figure 1.1, fields of various crops and pastureland are only a short distance (Figure 1.1a,b) from the dense canopy streambed shown in Figure 1.1c. Although riparian zones make up only a small percent of the total landscape (Fig. 1a,b), RET may have a much larger impact on basin-wide ET because:

i) Riparian zones are located in areas of persistent high soil moisture and groundwater storage; the root systems of the trees and underbrush are extensive and tap into groundwater.

ii) The height and structure of the tree canopy promotes a more efficient exchange with the atmosphere compared to nearby grass canopies.

iii) Riparian vegetation typically has a longer growing season than surrounding crops and grasses.

These assertions are consistent with one of the important conclusions of the Department of Energy Water Cycle Pilot Study (DOE WCPS conducted in the Whitewater basin) (Miller et al., 2005), i.e. that ET is highly variable over small spatial scales (< 1 km), because of spatial variability in vegetation and soil moisture, and because deep-rooted plants access groundwater.

Figure 1. 1. (a) and (b) Aerial photographs of two 3.5 X 3.5 *km* sections of Whitewater basin. Strahler stream orders label the riparian zones (dark bands) in each image. Riparian zone widths do not increase systematically with an increase in order but appear to fluctuate around a constant mean value. (c) vegetation cover that typifies the riparian zones in Whitewater is shown for the Rock Creek stream. Hackberry, Elm, and Green Ash are the dominant species of trees that cover the basin.

1.3 Other Impacts of RET

RET is an important but poorly understood watershed flux. Because it is so difficult to measure, it is often ignored. Its importance ranges from negligible in low, heavily forested areas (northern Wisconsin, Minnesota) to being the **only** major river-loss

mechanism (for example, the Rio Grande). Phreatophyte water consumption is a widespread concern in water management in the semi-arid regions of the U.S. and has been the subject of many studies (e.g. Stromberg, 1993; Busch et al., 1992, Grimm et al., 1997; Hipps et al., 1998). The loss of water in riparian areas is critical to water management efforts in arid and semi-arid regions (e.g. Newman et al., 2006). In most parts of the country, RET is a significant fraction of the basin-wide ET, but large-scale measurements typically cannot resolve the RET contribution and so it is generally ignored.

1.4 Past Efforts at RET Measurement

The eddy correlation method is considered to be the most direct estimate of ET and a *de facto* standard. The standard formulation of the eddy correlation (Stull, 1988) calculates the moisture flux from $\overline{w'q'}$ where w' and q' are the fluctuations in vertical wind speed and specific humidity. However, the method has limited applicability for measuring RET because of the small size of most riparian areas. In past land-atmosphere interaction field experiments, surface flux towers were normally placed away from tree lines because of fetch and 'representativeness' requirements (Westenburg et al., 2006). Estimating RET in grassland biomes is extremely difficult because of the narrow width of the riparian zones, precluding the use of techniques that can be utilized in areas of more extensive vegetation (Moncrieff *et al.*, 2000; Goodrich *et al.*, 2000). Datasets obtained in previous atmospheric field campaigns directed at assessing land-atmosphere interactions in grassland biomes have proven of little utility because:

1. Flux towers placed within the riparian zone are likely to give biased results due to being placed between trees (so-called 'chimney' areas). A substantial

array of towers would be needed to account for the heterogeneity typical of riparian areas. Canopy towers have not been operated in grassland biome riparian zones; being more common in large forested areas.

2. Previous aircraft investigations used 30-60 km transects to obtain sufficient 'fetch', a practice that poorly represents ET in riparian zones; crossing only a few in a single transect.

3. Past atmospheric water vapor budget studies (for example, Grossman, 1992; LeMone et al., 2002) did not focus on riparian zones and were subject to large uncertainties. It is possible that the large uncertainty is related to the contribution of riparian zones.

Though attempts at estimating RET in a desert landscape have been reported (Gatewood et al., 1950; Goodrich *et al*., 2000), similar attempts in a grassland biome have not been reported beyond that of Weeks and Sorey (1973) and Butler et al. (2007). Most previous efforts have been performed over vegetation in a riparian floodplain, which covers a much larger area than mid-western riparian zones and is generally a shorter canopy so that conventional ET techniques could be used (Unland *et al.,* 1998; Goodrich et al., 2000; Scott et al., 2000; 2002, 2003, 2004; Schilling, 2007). When riparian forest canopies are studied, they cover an area large enough for conventional ET techniques, (for example Schilling, 2007; Cooper et al., 2003; Nagler et al., 2005). An exception is Goodrich et al., (2000); Cooper et al., (2000) and Schaeffer et al. (2000), who used sap flow gages on a limited number of trees and scaled the measurements to a larger area. These estimates were verified using estimates from the LANL/UI Raman lidar.

Alternative approaches based on water balance analyses are cost-effective and have a long history (White, 1932; Gatewood et al., 1950; Goodrich et al., 2000; Mac Nish et al., 2000; Loehide et al., 2005; Nachabe et al., 2005; Butler et al., 2007; Rahgozar et al., 2012). The SSWB approach is capable of providing nearly continuous time estimates of RET, over durations as long as desired, provided the basic measurement network is in place and functioning. Most of these previous studies were set in a desert landscape, where there is little ET outside the riparian zone and these zones are considerably wider than in a grassland biomes. As noted by NRC (2002), "*there is no universally acceptable approach to characterizing water balance of riparian areas and many studies employ significant simplifications, assumptions or other qualifications*". For instance, in the SALSA study (Goodrich et al., 2000; Mac Nish et al., 2000), the coarse-grained streambed sediments justified the neglect of vadose zone contributions, and only water table and stage measurements were used to quantify the SSWB. Of particular significance is the fact that unlike at these previously studied sites, the alluvial deposits and overlying soils in the Whitewater Basin are comprised of low-permeability silty clay and silty clay loam. Thus, the vadose-zone contribution to RET, which was largely ignored in the aforementioned studies, cannot be neglected. The work presented in this dissertation builds on the previous SSWB work by following up on suggested improvements to the methodology (e.g., Mac Nish *et al.*, 2000) as well as extending it to a setting in which the vadose-zone contribution to RET is expected to be significant. Although Nachabe et al. (2005) and Rahgozar et al. (2012) demonstrated the use of total soil moisture in a vertical column as an effective approach to estimating local RET in a relatively small area in Florida, these studies were based on a single vertical profile where the water table was very shallow (approximately 1.5 meters)

and therefore had a small vadose zone contribution, and the accuracy of such an isolated RET estimate for a large riparian zone is poorly understood.

1.5 Thesis Objectives and Outline

The objectives of the thesis are to:

1. Implement and evaluate the SSWB approach for RET estimation in a challenging setting with a thick vadose zone and complex subsurface stratigraphy, alluvium containing mostly fine-grained soils and sediments, and a deeper water table than many alluvial systems.

2. Evaluate the reliability of SSWB-based reach-scale RET estimates and compare them with other estimates.

3. Quantify uncertainty in the SSWB based on observations from multiple soil profilers and the variability among RET estimates obtained with different profile locations, supplemented with numerical modeling incorporating heterogeneity in soils properties and root distributions.

The subsequent chapters of the thesis are organized as follows: A detailed site description along with soil characterization and laboratory soil analysis is presented in chapter II. Chapter III describes the monitoring network that was used in this research, and the rationale for its design. Representative observations from groundwater well and soil moisture profiles data describe the hydrogeological connection that led to the formulation of the conceptual model of site hydrology in Chapter IV. The following chapter (Chapter V) describes the framework for the water balance analysis that was implemented

in this thesis, which draws upon the conceptual model in Chapter IV. Chapters VI and VII contain the core of the results from the field measurements. Precipitation, total soil moisture, groundwater table elevations and RET estimates are shown on an annual basis (with monthly averaging) in Chapter VI, at all profile locations. Inter-annual variability during three shorter periods at different stages of the growing season is presented in Chapter VII. The RET estimates were also compared with LIDAR estimates of RET during one of these periods. Chapter VIII described insights that were obtained by using a 1D vertical numerical model. Lastly, chapter IX summarizes and discusses all of findings from this research work. Further details are shown in appendices A through F. These include results of visual and laboratory analysis of soil properties, normalized total soil moisture time series plots, annual soil moisture time series plots, annual reference evapotranspiration on a monthly time scale, and annual water table hydrograph measurements for shallow wells.

CHAPTER II

SITE DESCRIPTION

The study site is located in south-central Kansas just Northwest of El Dorado. The site lies within the lower portion of the Rock Creek Watershed and is along a 5th order stream in the middle part of the Whitewater River Basin (1,100 km²). The study area has a length of 100 m (330 ft) and a width of 45 m (150 ft) as indicated by the red box in Figure 2.1. To the north of the study site, brome hay is grown and to the south, pasture grass grows naturally.

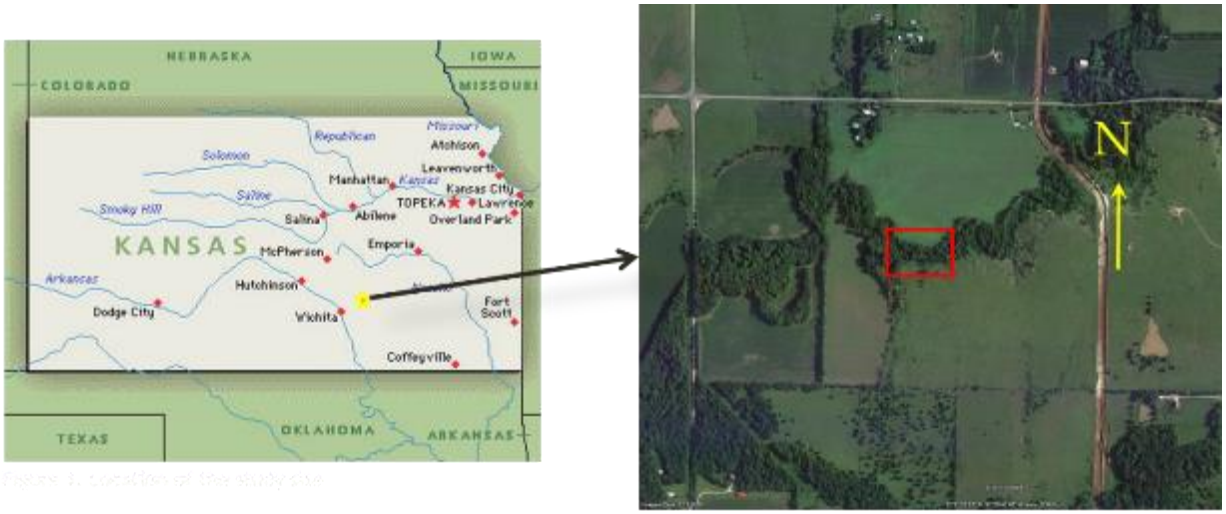

Figure 2.1. Location of study site.

The study site was selected based on several features, including the following:

- Tributary to the Whitewater River with sufficient baseflow for stream gaging.
- Presence of a substantial riparian zone to generate significant evapotranspiration.

- East to west stretch of riparian zone of a few hundred meters (~0.2 mi) to allow north-south deployment of LIDAR on north side of zone for measurement of vapor plume in summer during predominantly southerly winds.
- Sufficient alluvial sediment allowing for installation of wells and soil moisture sensors.
- Absence of factors potentially interfering with SSWB and LIDAR activities, such as high-tension power lines and substantial animal activity (cattle).

2.1 Hydrogeology of study site

The underlying bedrock of the watershed is mainly composed of alternating layers of Permian shale and limestone (Zeller, 1968). Along the study reach there are unconsolidated alluvial and terrace deposits, as shown in Figure 2.2. The alluvial deposits consist mainly of Verdigris, Vanoss, Ladysmith, Irwin, Clime-Sogn, and Norge soils (NRCS web soil survey, http://websoilsurvey.sc.egov.usda.gov/App/WebSoilSurvey.aspx). Verdigris Series soils consist of silt loam and silty clay loam type soils (Penner et al., 1975). This type of soil is the main type that underlies the riparian zone. The stream runs east to west and is bounded on the south bank by an outcrop of predominantly shale with some limestone. There is very little riparian type vegetation to the south of the stream which makes the entire riparian zone north of the stream, therefore only one side of the stream was instrumented. Figure 2.3 is a satellite photograph using GoogleEarth©, which was taken on 2/25/2012 when the vegetation was in its dormant stage, and clearly shows the location of the stream.

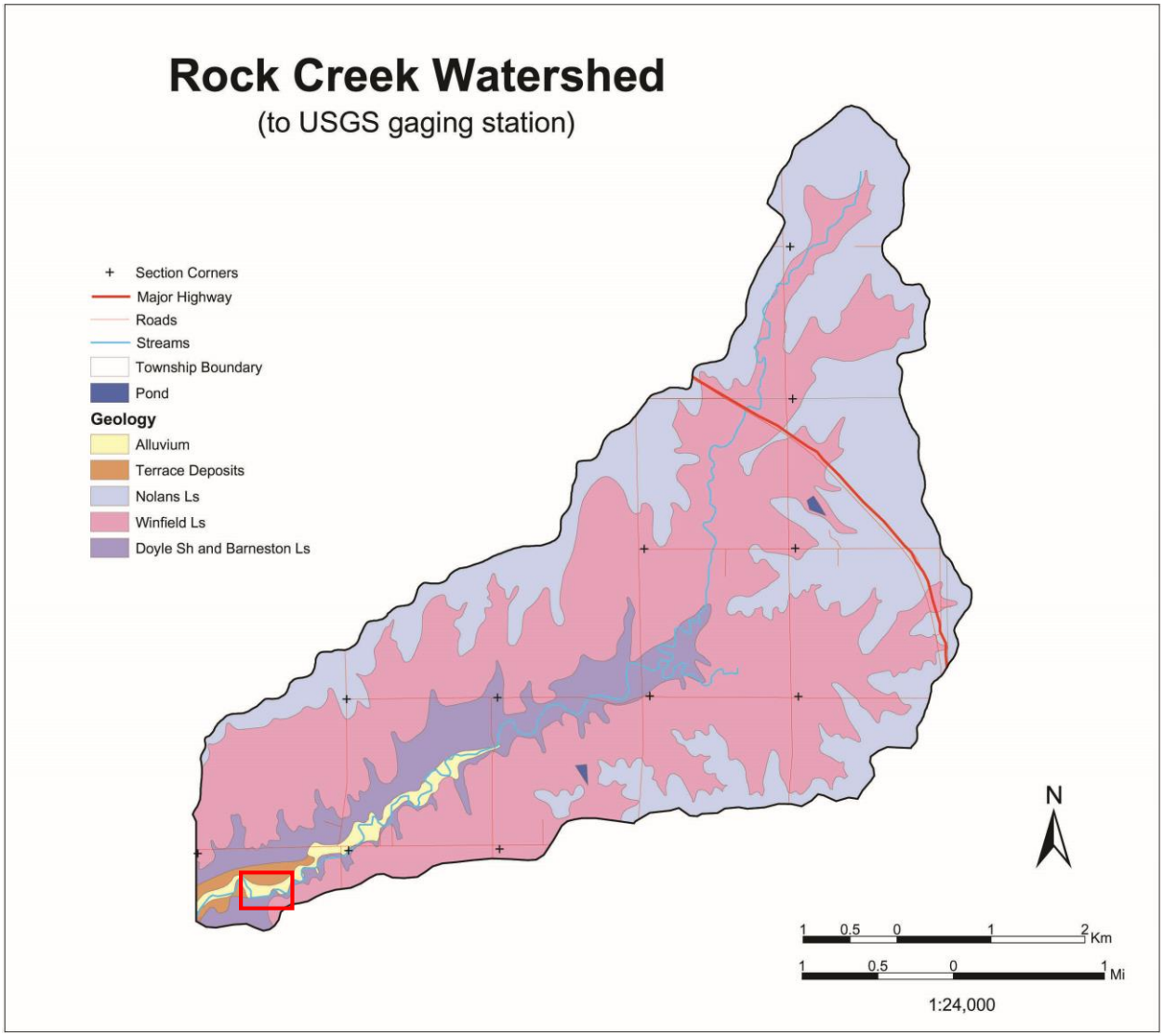

Figure 2. 2. Map of Rock Creek watershed above a temporary gaging station installed several years ago as a part of HydroKansas research activities. The general location of the riparian evapotranspiration (RET) study is shown by the red rectangle, which is in the northern half of Sec. 20, T. 25 S., R 04 E., Butler County, Kansas. The fine red lines and the west boundary of the watershed form the north and parts of the west and east lines of Sec. 20.

Figure 2. 3. The same area as in Figure 2.2 but taken from an aerial photograph (Google earth: 37°51'54.42" N 97°00'58.18" W, image taken on 2/25/2012) during the winter when there was little leaf material left on the deciduous trees. The dark sinuous line through the riparian area is the channel of Rock Creek. The blue rectangle represents the area shown at higher resolution in Figure 2.4.

The shale outcropping along the south bank of Rock Creek within the research site matches the description of the Holmesville Shale Member of the Doyle Shale, which Zeller (1968) describes as green, gray, yellow, and red, unfossiliferous shale containing argillaceous limestone. Slabs of limestone in the grass field to the south of the creek fit the description of the Towanda Limestone Member above the Holmesville Shale Member. The lowermost portion of the Holmesville Shale or the top of the Fort Riley Limestone Member of the Barneston Limestone is expected to form the bedrock underlying the alluvium at the research site. The KGS conducted direct-push electrical conductivity (DPEC) logging of the

alluvial sediment at 9 locations within and adjacent to the riparian zone selected for the research site (Figure 2.4).

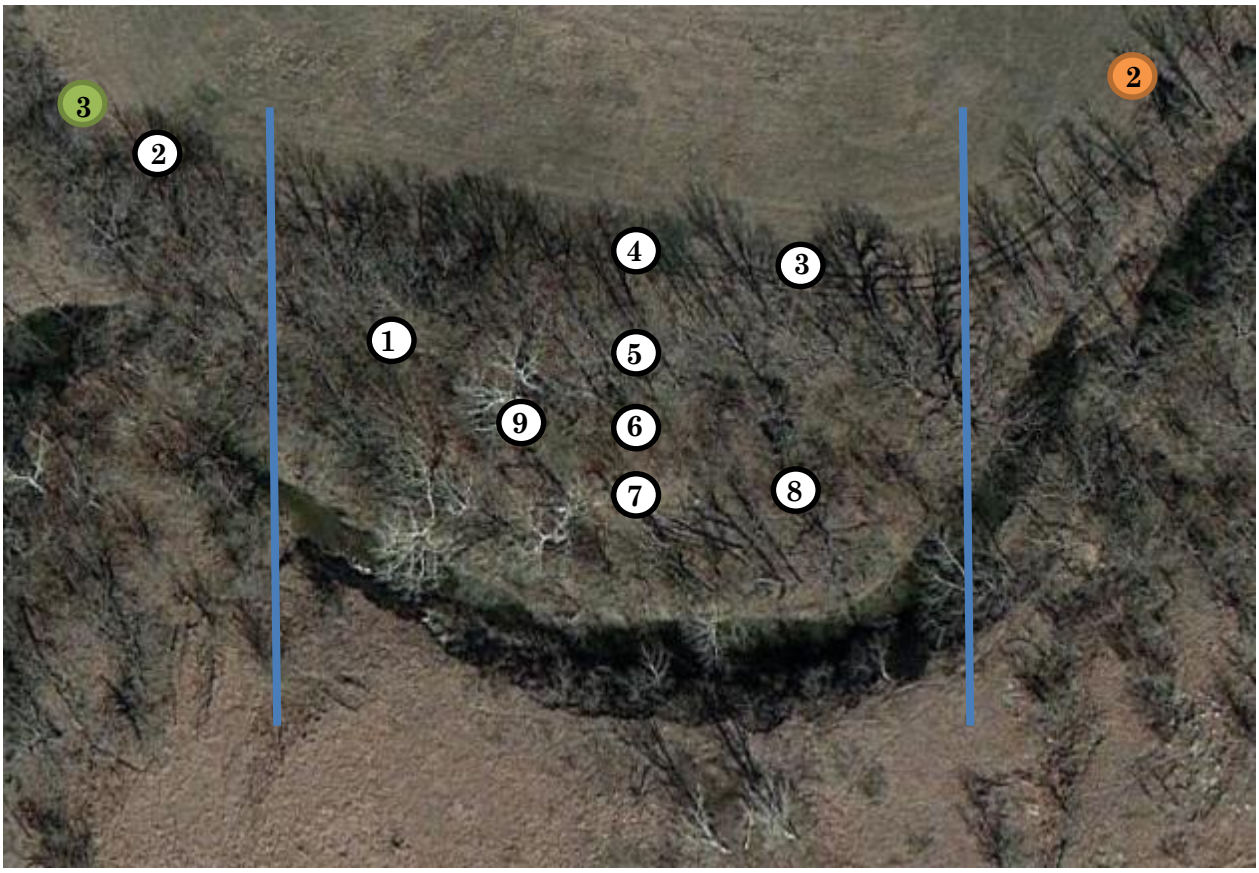

Figure 2. 4. Enlargement of the area within the blue rectangle in Figure 2.3 showing the location of the Rock Creek research site and the nine Geoprobe DPEC logs. The orange and green circles represent locations of stakes used for site reference and measurements. The blue lines (about 100 m apart) bound the main study section. The dark curved band is the channel of Rock Creek (water and shadow caused by southeast sun location). The darker gray shades indicate the area of riparian vegetation. Note that the south bank of the creek is a shale bedrock outcrop with very little vegetation.

The depths to bedrock from the land surface through the soil and alluvial deposits range from about 5.5 to 7.6 m (~18-25 ft) within the study site (DPEC log locations 1 and 3-9 in Figure 2.4). The DPEC logs shown in Figures 2.5-2.7 suggest that most of the alluvial deposits are fine-grained materials (silts and clays) as indicated by relatively high electrical conductivities. The conductivity was approximately constant or generally increased in the

upper third of the logs. This zone represents soil altered by mechanical, biological (including roots), and chemical processes within the riparian area. Thin zones of both lower and higher conductivity material occurring within the middle of the logged depth range represent coarser alluvial sediment, such as fine to medium sands, to finer sediment (clay), respectively. The conductivity generally decreases in the bottom half of the logs to relatively low values just above the bedrock.

The lowest part of the logs has a zone of relatively low electrical conductivity indicating somewhat higher permeability material. As indicated above, this zone is more difficult to push through than the overlying sediment. The material appears to supply water to the DPEC holes relatively quickly after completion. This zone could possibly represent chert or limestone gravel or weathered limestone bedrock. Gravel in and along the stream channel is nearly all limestone. Some of the limestone strata in the Rock Creek watershed upstream of the research site contain some siliceous geodes and concretions and also chert (Zeller, 1968). Physical weathering of the chert and other siliceous material in the rocks upstream of the study site could have produced sand and gravel sediment that could be incorporated in the alluvial deposits. Sleezer (1990) described alluvial deposits in Butler County containing chert gravel. Aber (1991) described an alluvial deposit in west-central Butler County as including limestone gravel, quartz pebbles, and coarse sand in the lower part of predominantly silty-clay and clayey-silt deposits.

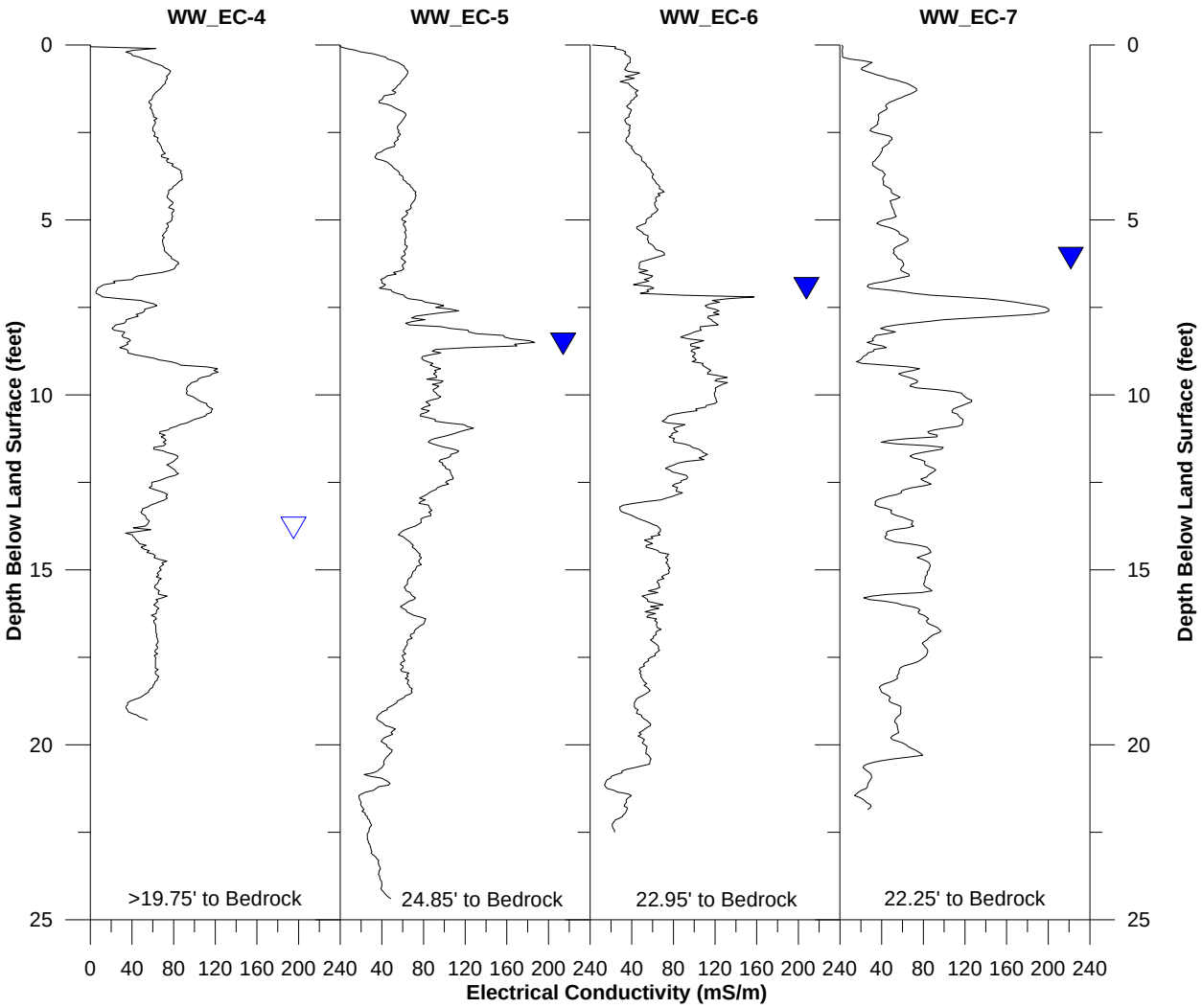

Figure 2. 5 North-south cross section of electrical conductivity logs of the unconsolidated sediment at the study site. The areal location of each log is indicated in Figure 2.4 within the white filled circle with the same number as at the end of the label above the log. The filled blue triangles represent the water-level surface. The open triangle represents the last measured value of a water level that was slowly rising in the direct-push hole before the hole was sealed with bentonite.

The water levels in the wells indicate significant saturated thickness (10-16 ft). The top of the DPEC logs in Figures 2.5-2.7 represent the land surface, which generally slopes towards the creek from north to south. Thus, the relative depths of the water levels cannot be interpreted in the figures in terms of ground-water flow directions. However, groundwater wells later discussed in the following chapters indicate a higher water level closer to the stream and lower water levels away from the stream when stream levels are

higher than very low-flow conditions. This indicates that the stream is a losing type stream for these conditions.

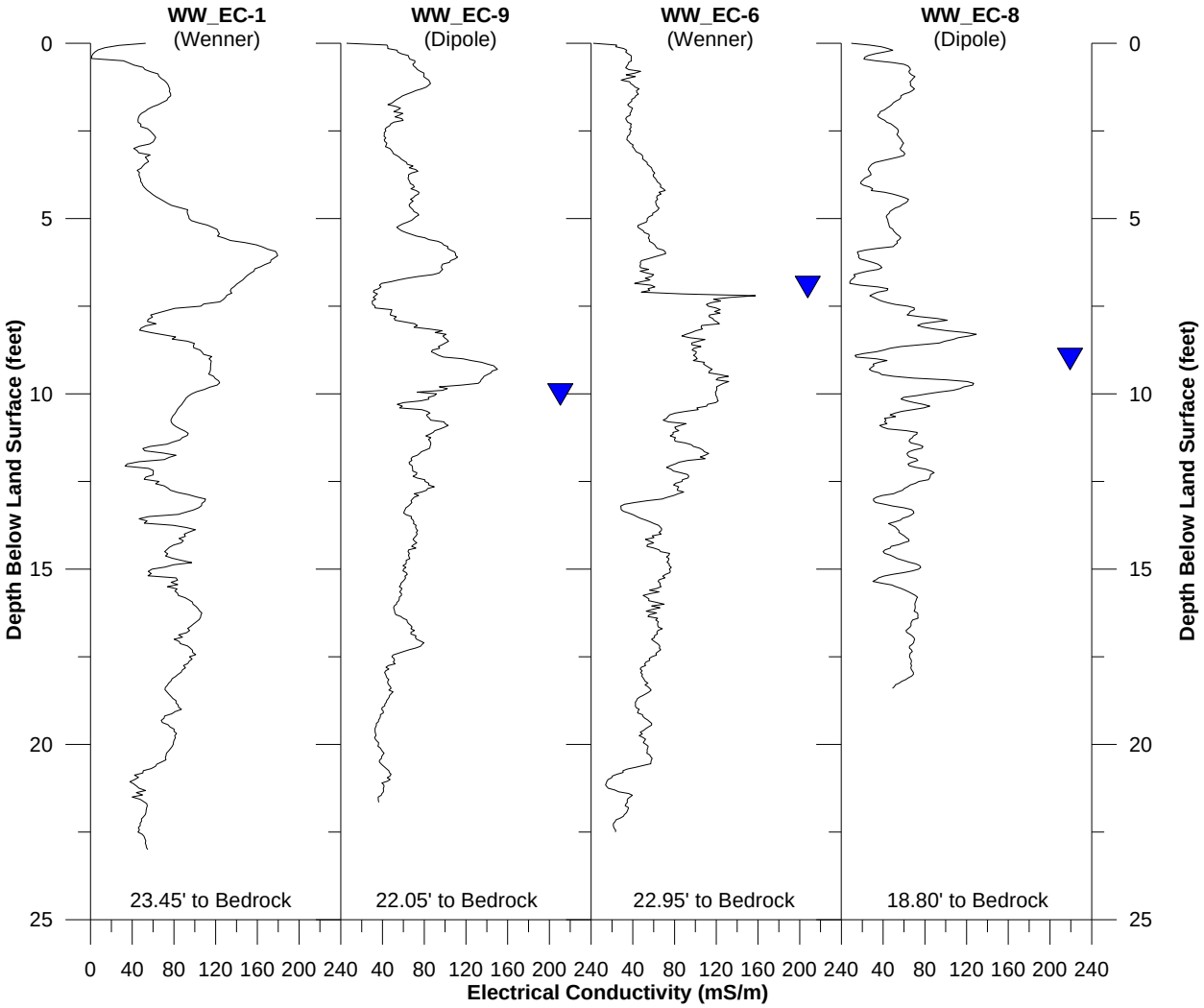

Figure 2. 6. West-northwest to east-southeast cross section of electrical conductivity logs of the unconsolidated sediment at the study site. See Figure 2.5 for explanation of blue triangles and area location of logs. A water-level measurement was not made for DPEC log 1.

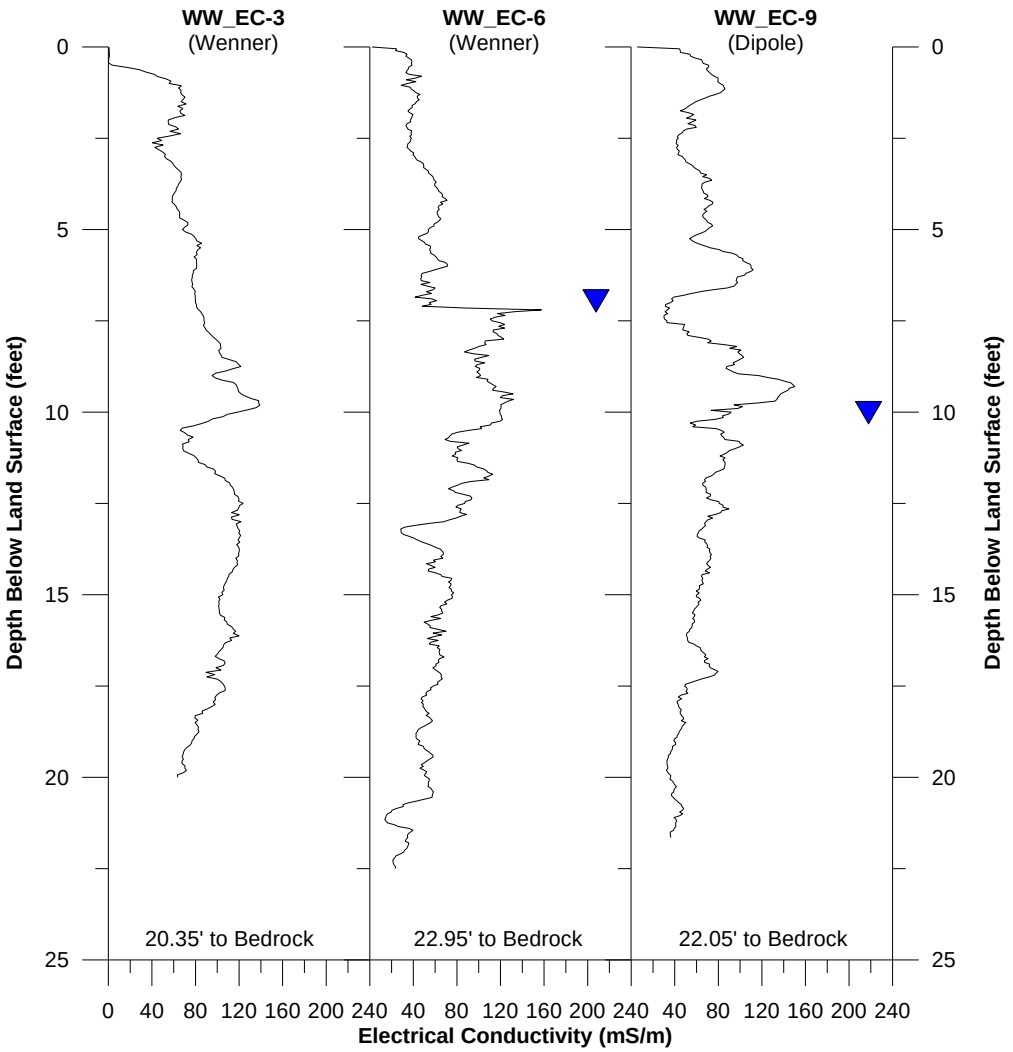

Figure 2. 7. Northeast to southwest cross section of electrical conductivity logs of the unconsolidated sediment at the study site. See Figure 2.5 for explanation of blue triangles and area location of logs. A water-level measurement was not made for DPEC log 3.

During installation of monitoring wells, soil cores were collected from near locations 4, 5, 6 and, 7 which will be referred to as locations “D”, “C”, “B” and “A” respectively. The cores were collected by KGS staff using a Geo-Probe and analyzed at CU Boulder. Visual analysis of these cores and showed a pattern consisting of about 6 visually different soil layers. The top layer was a dark brown unconsolidated soil type that ranged from 2.1 to 2.4 m (7-8 ft) in thickness. The visual analysis was consistent as it was described by Penner (1975) as a Verdigris Series type soil. The second layer had a reddish-

brown color and appeared to be of clayish-silt texture with a thickness of about 1.7 m (5.5 ft). In the third layer the soil changed to a light-brown color and had very clay like texture. The fourth layer was again of a reddish-brown color but had more of a red hue compared to the second layer and the texture was reflective of a more crumbly and shale type material. The fifth layer was predominantly grey with a little tan color as well and appeared very silty. The final layer (sixth layer) was a tan light-brown with a little grey and was of silty-clay texture. A more detailed visual analysis presented in Tables A1-A4 in appendix A.

2.1.1 Soil Characterization:

Several laboratory soil analyses were conducted to measure soil hydraulic properties including soil water retention curves (SWRC) and saturated hydraulic conductivity (K_s) as well as texture and soil classification. These analyses were performed on soil that was collected from the Geoprobe cores as well as cores obtained during installation of access tubes for the soil moisture profilers.

Sieve analyses were performed on soils from four different depths within the first layer for profiles A, C, D, E, and F. Seven different sieves were used to classify the soil. The sieves were used were a No. 4 (4.750mm), 10 (1.981mm), 20 (0.833 mm), 40 (0.419 mm), 60 (0.246 mm), 140 (0.104 mm), and a No. 200 (0.074 mm). In addition to the sieve analysis a SWRC was measured for the soils at various depths throughout the profile using a laboratory apparatus known as the HYPROP© (UMS GmbH München) which uses a simplified evaporation method as described by Peters and Durner (2008). This system uses a combination of sensitive tensiometers to measure soil suction and a scale that measures sample weight which can be converted to soil water content. The unsaturated hydraulic

conductivity is also inferred from the difference in suction between the tensiometers at different depths within the sample, which is used to define a gradient and hence an evaporative flux (Peters and Durner, 2008). A software analysis program fit curves to the HYPROP data using different constitutive models. The van Genuchten model (van Genuchten, 1980) was used for the analysis and also in the numerical model (explained in further detail in the later chapters). In addition to the HYPROP apparatus a permeameter was used to measure the saturated hydraulic conductivity of the soil as an independent verification of values obtained from the HYPROP data analysis software.

2.1.2 Soil Analyses for profile A:

Soil samples for the sieve analysis were taken from 0.13 m (0.43 ft), 0.53 m (1.7 ft), 0.94 m (3.1 ft), and 1.44 m (4.7 ft). Detailed analyses are shown in Appendix B. By using the Unified Soil Classification Systems (USCS) it was determined that the most probable classifications of these soils are:

0.13 m = Well graded, coarse-grained, silty, clayey sand

0.53 m = Poorly graded, coarse-grained, silty, clayey sand.

0.94 m = Poorly graded, coarse-grained, silty, clayey sand.

1.44 m = Poorly graded, coarse-grained, silty, clayey sand.

Figure 2.8 shows the soil-water retention curves (SWRC) for profile A at various depths. Table 2.1 and Figures 2.9-2.12 show the variation of soil properties and van Genuchten SWRC model parameters with depth.

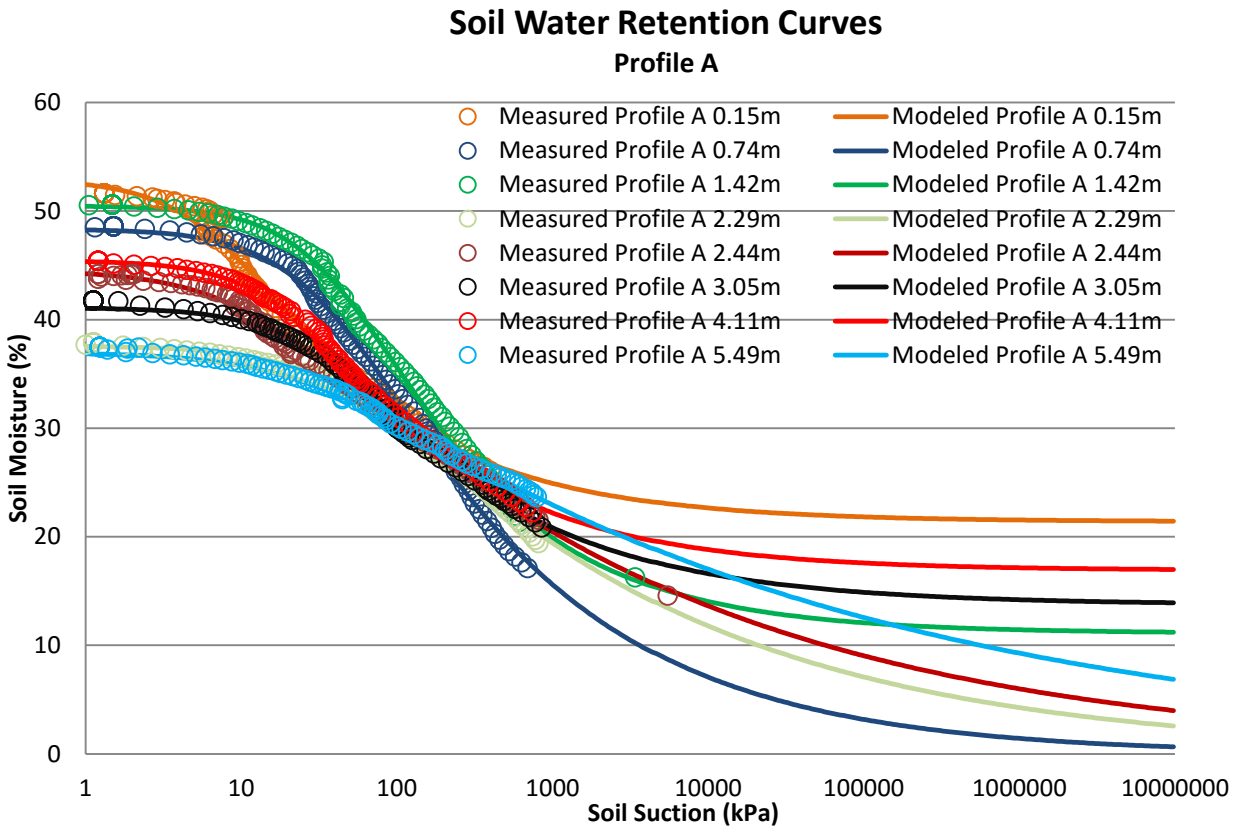

Figure 2. 8. Soil water retention curves for profile A at various depth.

Table 2. 1 Soil properties and van Genuchten parameters with depth for Profile A.

Depth Range (m)	Hydraulic Conductivity, K_s (m/d)	Porosity, ϕ	van Genuchten, n	van Genuchten, α (1/m)
0.50	0.150*	0.53	1.281	16.1
1.25	0.030*	0.48	1.546	2.14
2.00	0.039*	0.51	1.481	2.18
2.65	0.093‡	0.38	1.221	1.90
3.40	0.945‡	0.44	1.176	7.38
4.40	0.006‡	0.41	1.399	2.85
4.90	0.026‡	0.45	1.415	4.41
6.00	0.002*	0.37	1.132	3.60

*Measured with a permeameter
‡Estimated from HYPROP© system

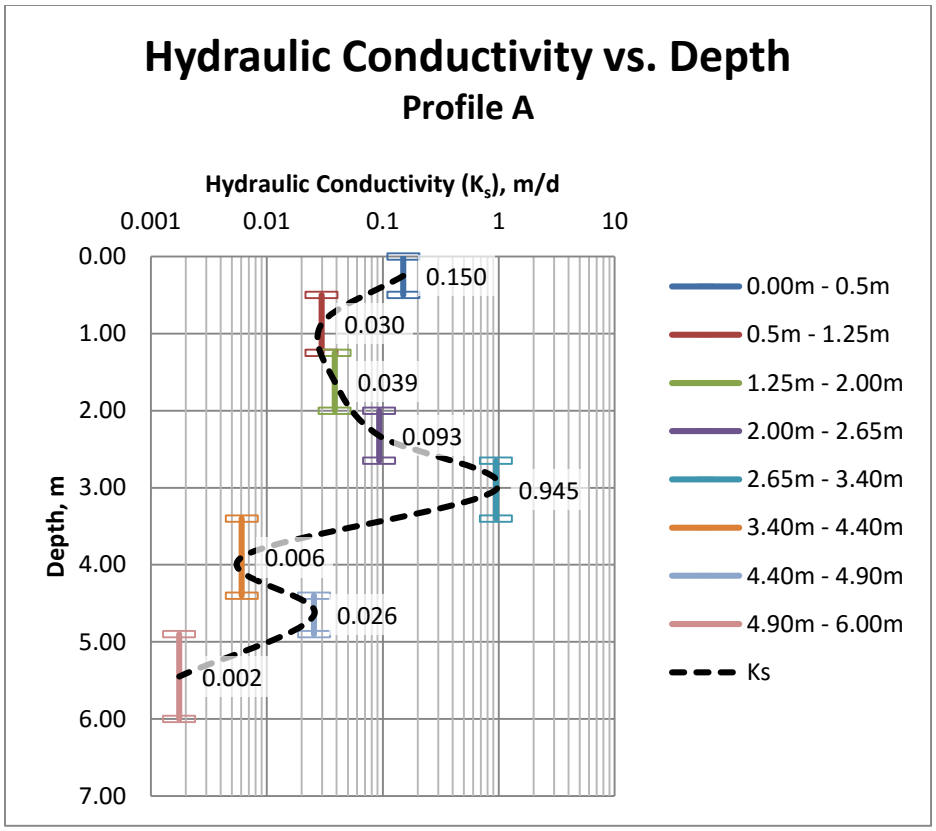

Figure 2. 9. Hydraulic Conductivity versus depth for profile A.

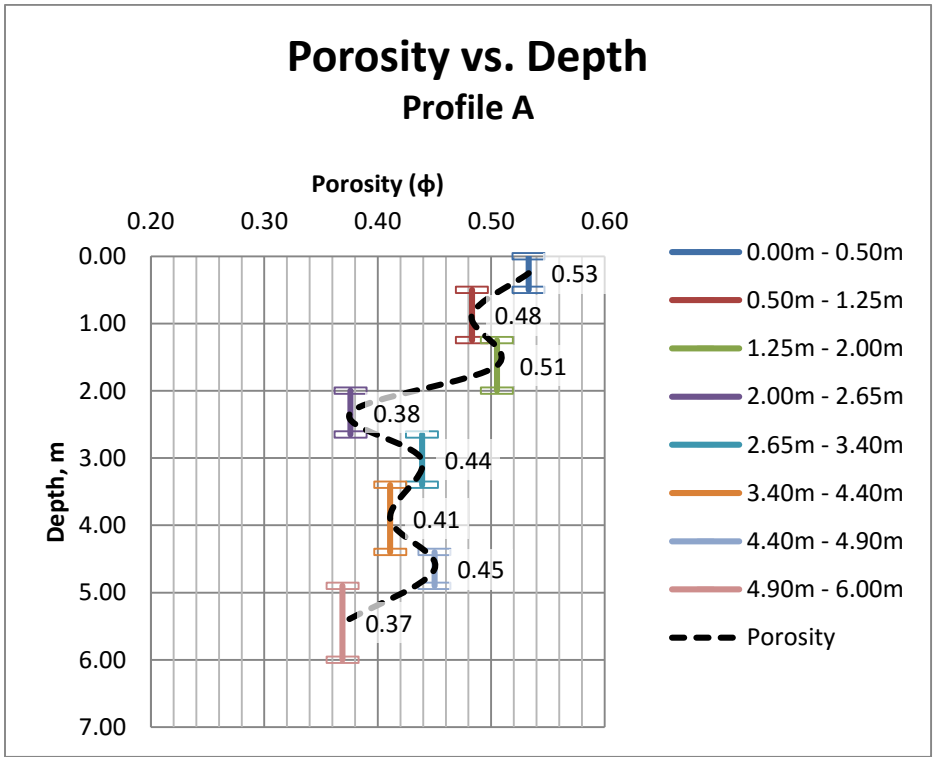

Figure 2. 10. Porosity versus depth for profile A.

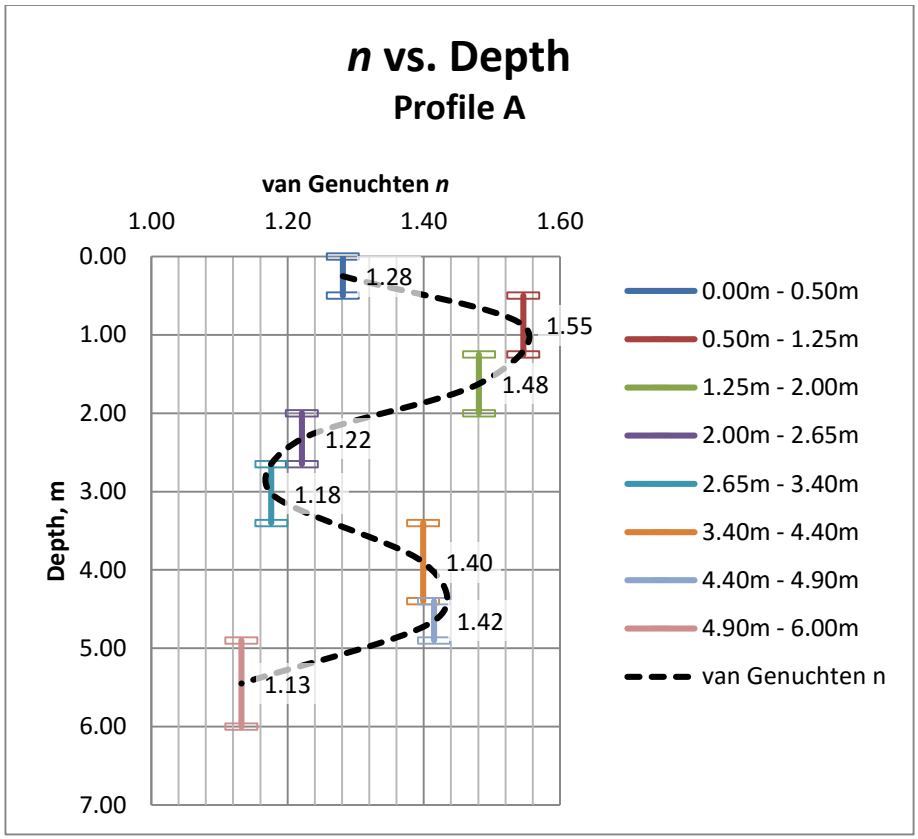

Figure 2. 11. van Genuchten n parameter versus depth for profile A.

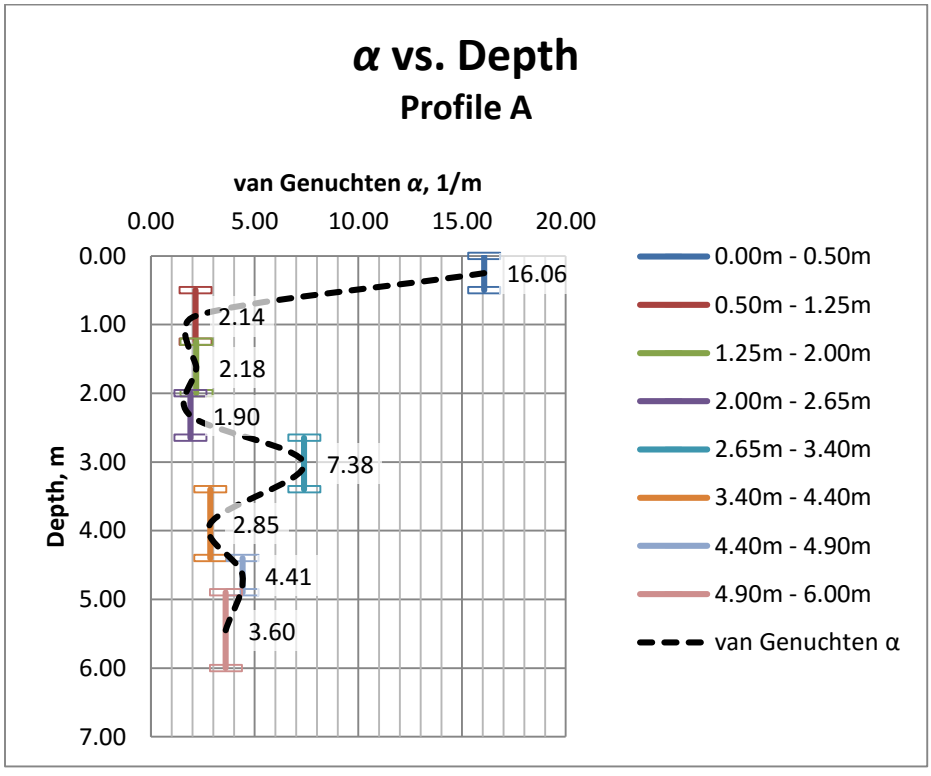

Figure 2. 12. van Genuchten α, parameter versus depth for profile A.

2.1.3 Soil Analyses for profile C:

Soil samples for the sieve analysis were taken from 0.15 m (0.49 ft), 0.56 m (1.8 ft), 1.05 m (3.4 ft), and 1.77 m (5.8 ft). Detailed analyses are shown in Appendix B. By using the USCS systems it was determined that the most probable classifications of these soils are:

0.15 m = Poorly graded, coarse-grained, silty, clayey sand.

0.56 m = Poorly graded, coarse-grained, silty, clayey sand.

1.05 m = Well graded, coarse-grained, silty, clayey sand.

1.77 m = Well graded, coarse-grained, silty, clayey sand.

Figure 2.13 shows the SWRCs for profile C at various depths. Table 2.2 and Figures 2.14-2.17 show the variation of soil properties and van Genuchten SWRC model parameters with depth.

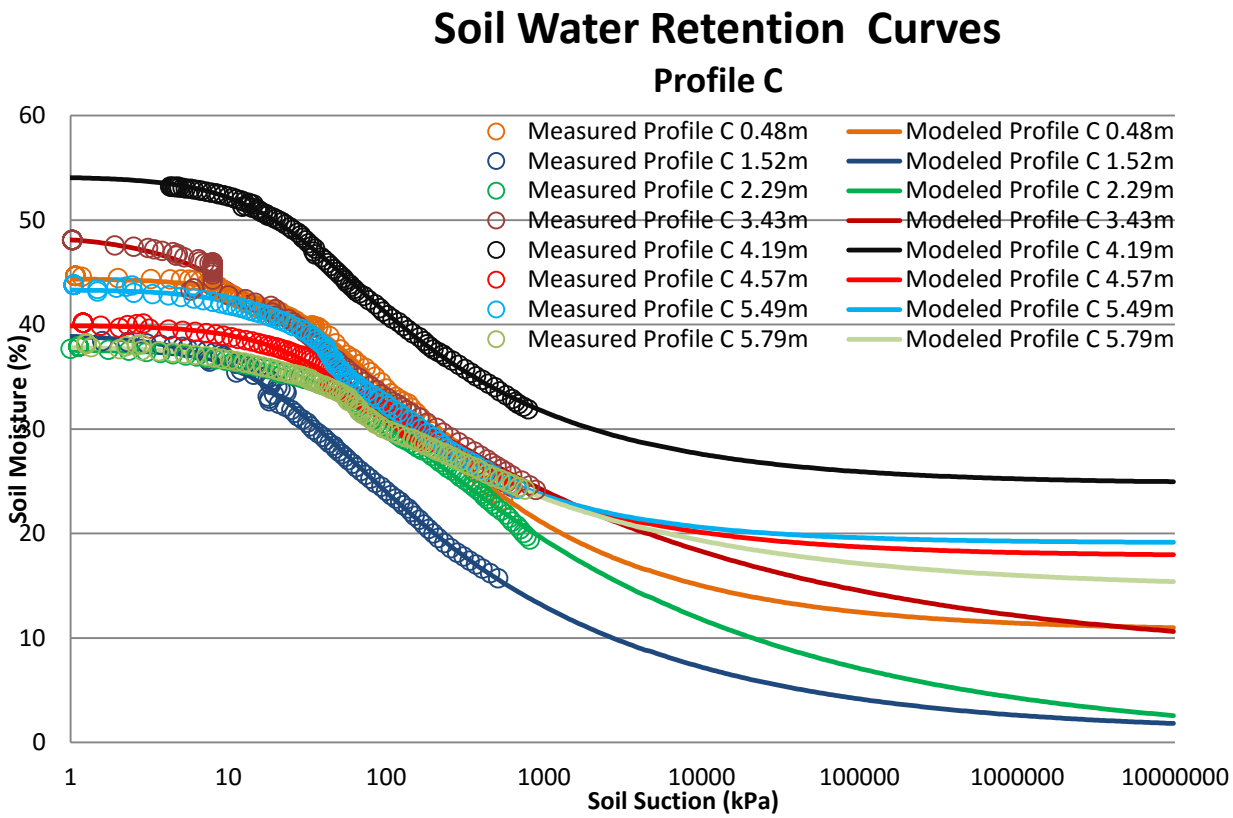

Figure 2. 13. Soil water retention curves for profile C at various depths.

Table 2. 2. Soil properties and van Genuchten parameters with depth for Profile C.

Depth Range (m)	Hydraulic Conductivity, K_s (m/d)	Porosity, ϕ	van Genuchten, n	van Genuchten, α (1/m)
1.00	0.103*	0.44	1.38	2.18
2.00	0.047*	0.49	1.29	5.08
3.00	0.093‡	0.38	1.22	1.90
4.00	0.109‡	0.49	1.96	10.7
5.20	0.213‡	0.54	1.39	3.99
5.70	0.003‡	0.40	1.41	2.69
5.90	0.002‡	0.43	1.49	2.96
6.00	0.005‡	0.40	1.28	3.25

*Measured with a permeameter
‡Estimated from HYPROP© system

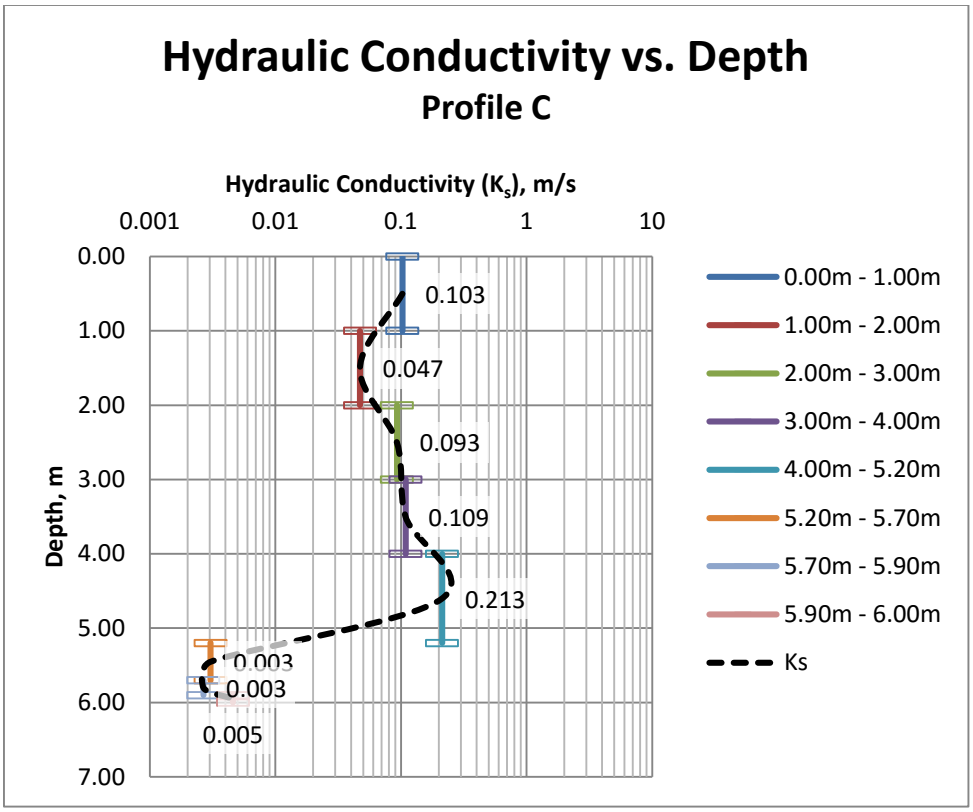

Figure 2. 14. Hydraulic Conductivity versus depth for profile C.

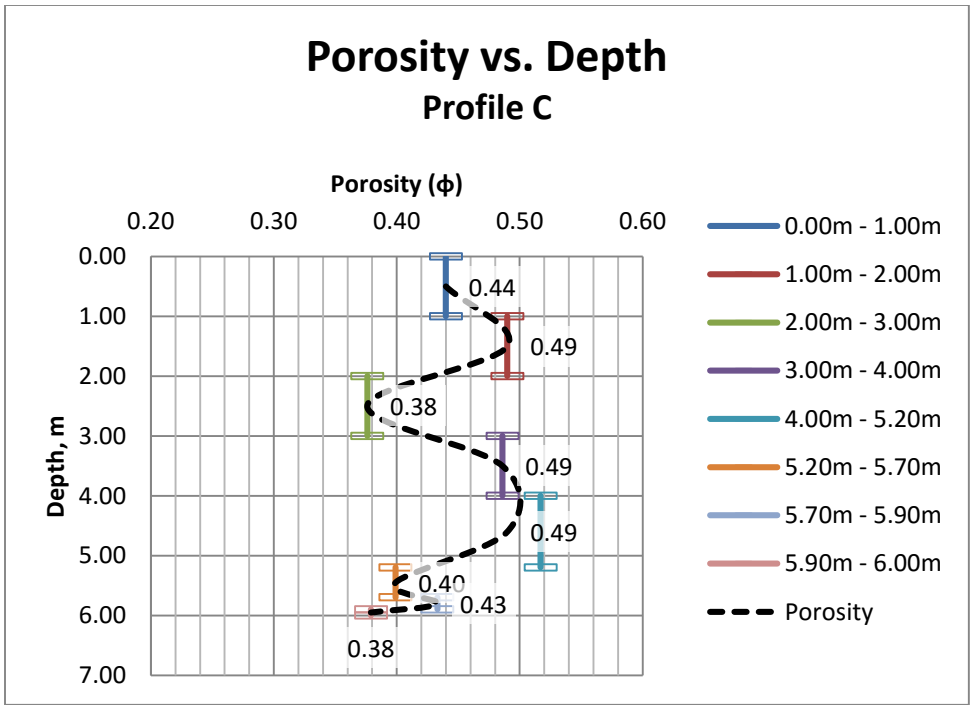

Figure 2. 15. Porosity versus depth for profile C.

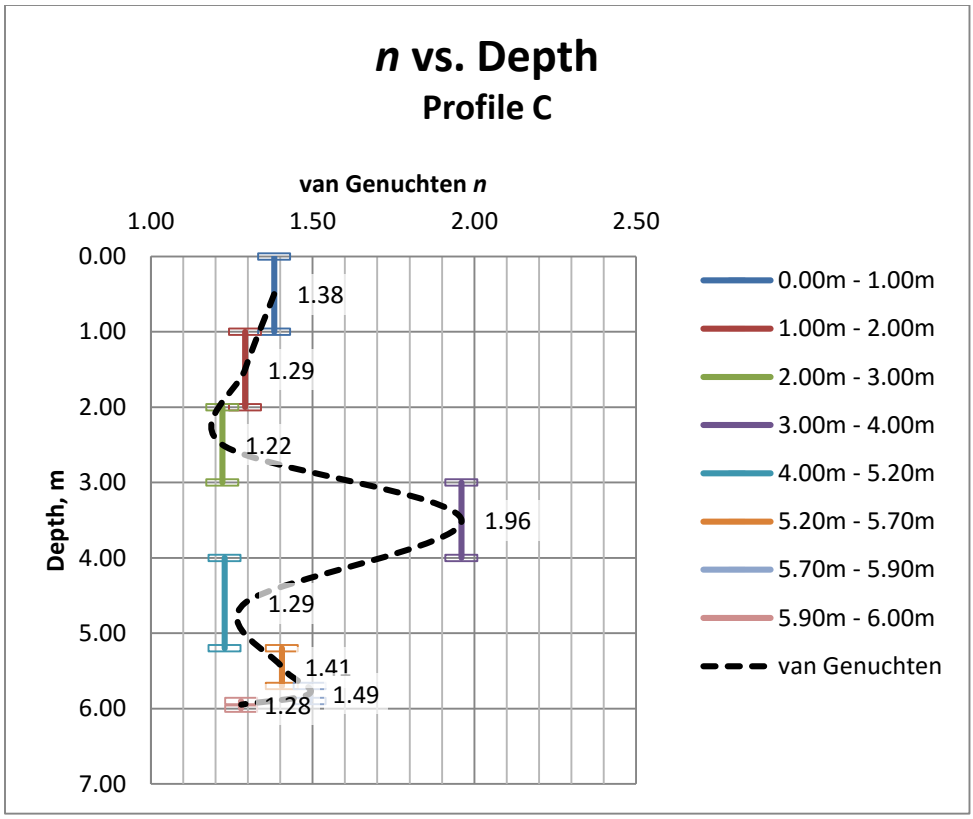

Figure 2. 16. van Genuchten n parameter versus depth for profile C.

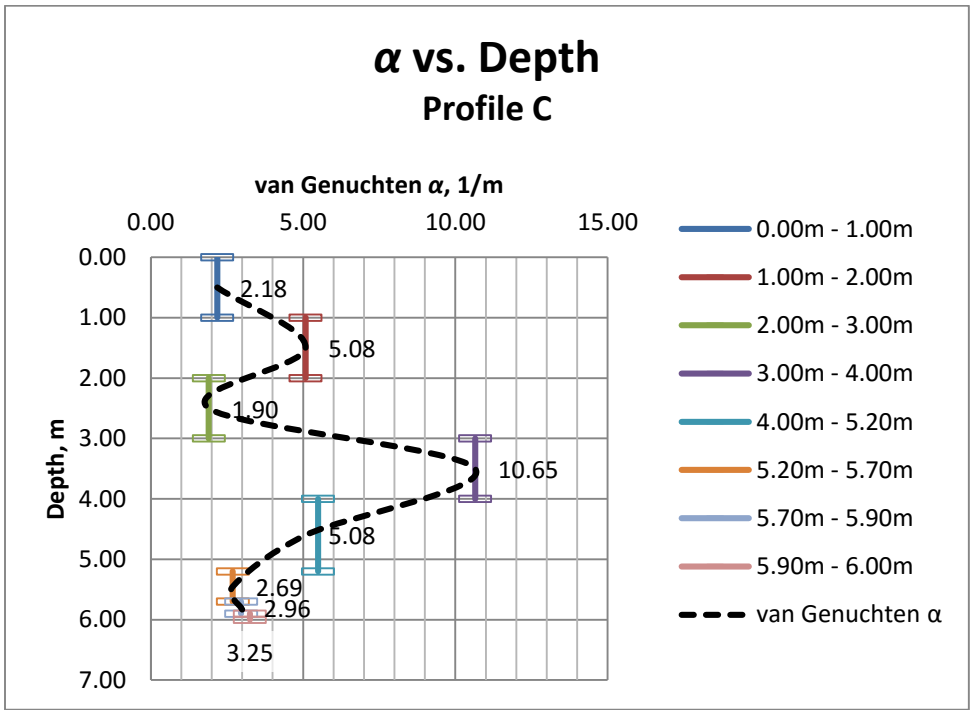

Figure 2. 17. van Genuchten α, parameter versus depth for profile C.

2.1.4 Soil Analyses for profile D:

Soil samples for the sieve analysis were taken from 0.08 m (0.26 ft), 0.48 m (1.6 ft), 0.89 m (2.9 ft), and 1.60 m (5.2 ft). Detailed analyses are shown in Appendix B. By using the USCS systems it was determined that the most probable classifications of these soils are:

0.08 m = Poorly graded, coarse-grained, silty, clayey sand.

0.48 m = Poorly graded, coarse-grained, silty, clayey sand.

0.89 m = Poorly graded, coarse-grained, silty, clayey sand.

1.60 m = Well graded, coarse-grained, silty, clayey sand.

Figure 2.18 shows the SWRCs for profile D at various depths. Table 2.3 and Figures 2.19-2.22 show variation of soil properties and van Genuchten SWRC model parameters with depth.

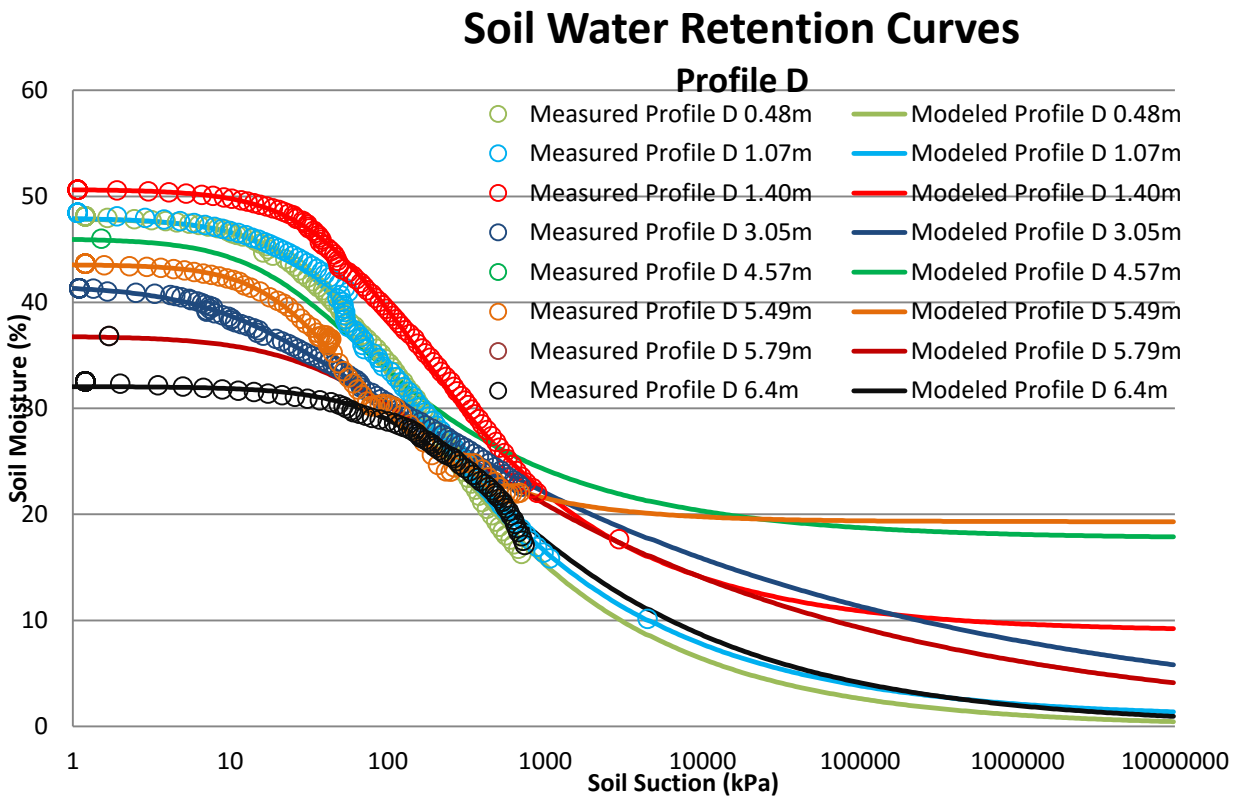

Figure 2. 18. Soil water retention curves for profile D at various depth.

Table 2. 3. Soil properties and van Genuchten parameters with depth for Profile D.

Depth Range (m)	Hydraulic Conductivity, K_s (m/d)	Porosity, ϕ	van Genuchten, n	van Genuchten, α (1/m)
0.67	0.079*	0.48	1.38	1.89
1.33	0.009*	0.48	1.36	2.07
2.00	0.006*	0.51	1.41	1.57
3.89	0.011‡	0.42	1.14	7.64
4.98	0.007‡	0.46	1.40	3.71
5.51	0.000095*	0.44	1.69	3.11
5.92	0.003‡	0.37	1.18	2.26
6.00	0.00057*	0.32	1.32	0.60

*Measured with a permeameter
‡Estimated from HYPROP© system

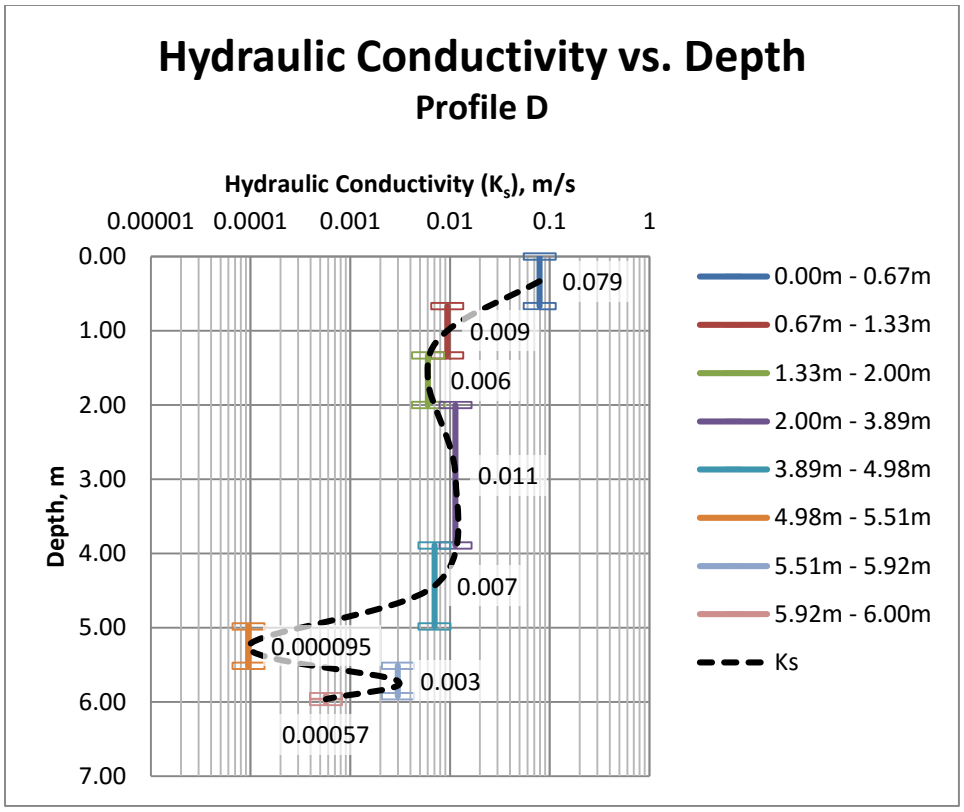

Figure 2. 19. Hydraulic Conductivity versus depth for profile D.

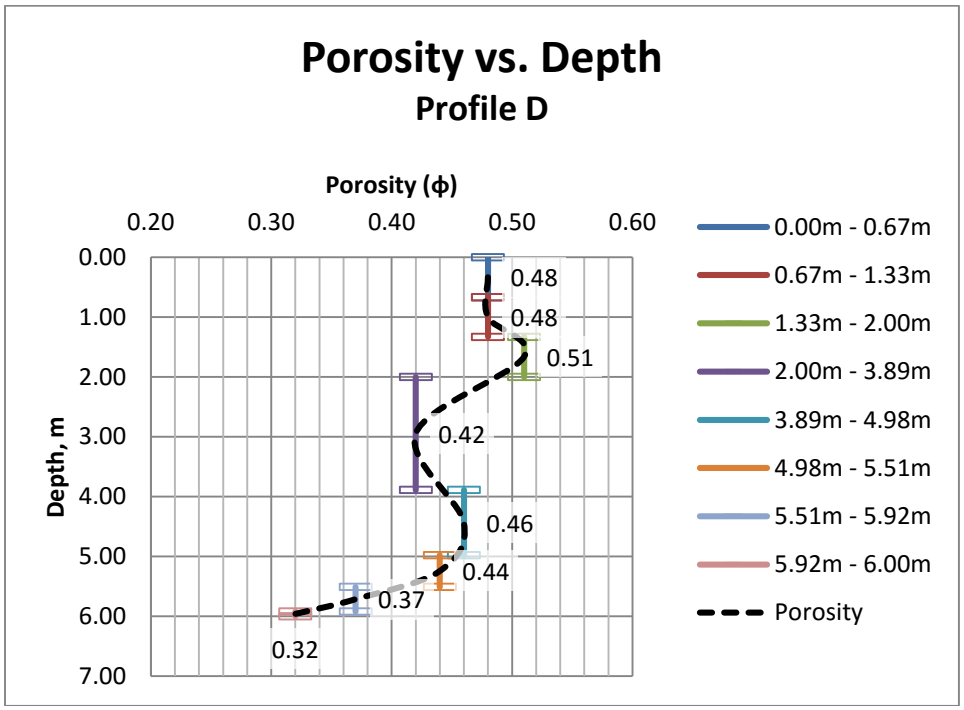

Figure 2. 20. Porosity versus depth for profile D.

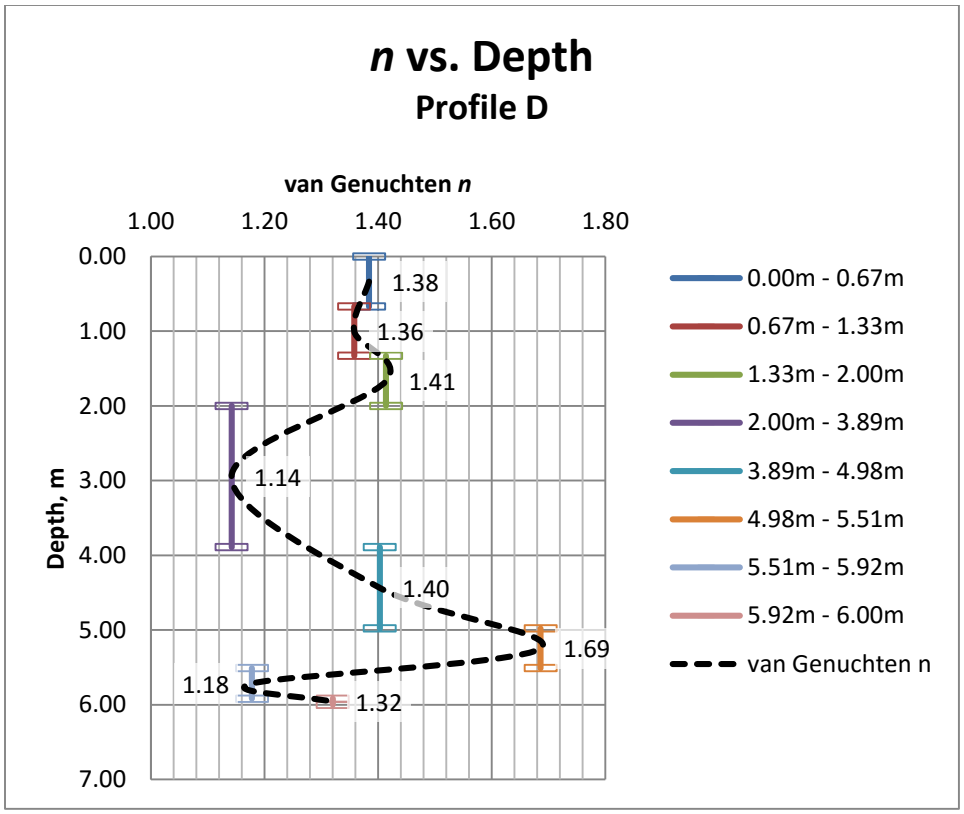

Figure 2. 21. van Genuchten n parameter versus depth for profile D.

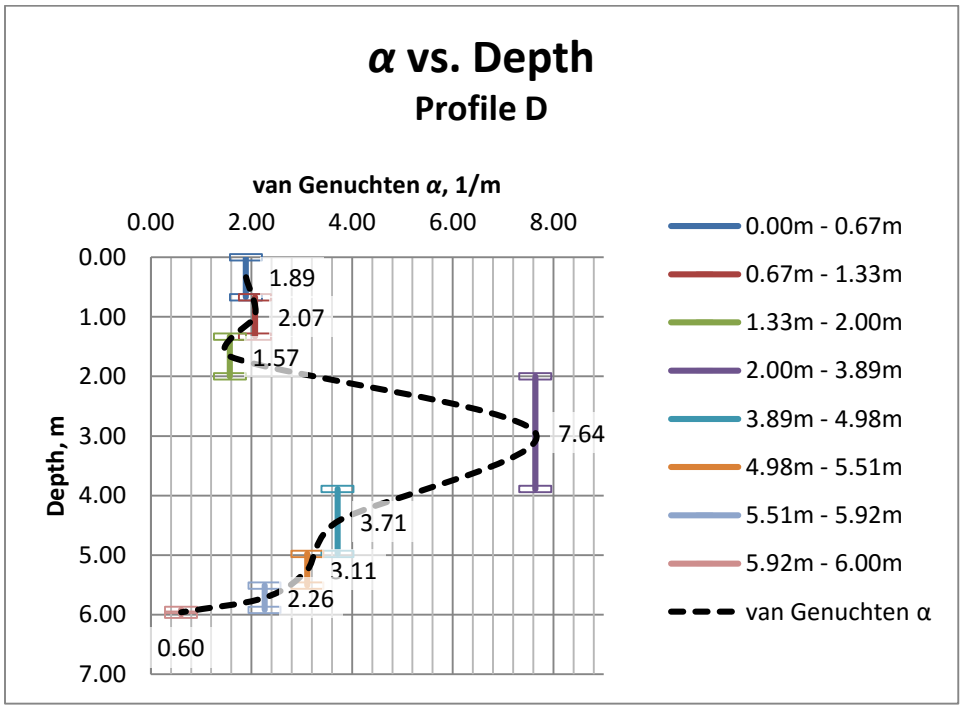

Figure 2. 22. van Genuchten α, parameter versus depth for profile D.

2.1.5 Soil Analyses for profile E:

Soil samples for the sieve analysis were taken from 0.18 m (0.59 ft), 0.58 m (1.9 ft), 1.07 m (3.5 ft), and 1.58 m (5.2 ft). Detailed analyses are shown in Appendix B. By using the USCS systems it was determined that the most probable classifications of these soils are:

0.18 m = Well graded, coarse-grained, silty, clayey sand.

0.58 m = Well graded, coarse-grained, silty, clayey sand.

1.06 m = Well graded, coarse-grained, silty, clayey sand.

1.59 m = Well graded, coarse-grained, silty, clayey sand.

Figure 2.23 shows the SWRCs for profile E at various depths. Table 2.4 and Figures 2.24-2.27 show the variation of soil properties and van Genuchten SWRC model parameters with depth.

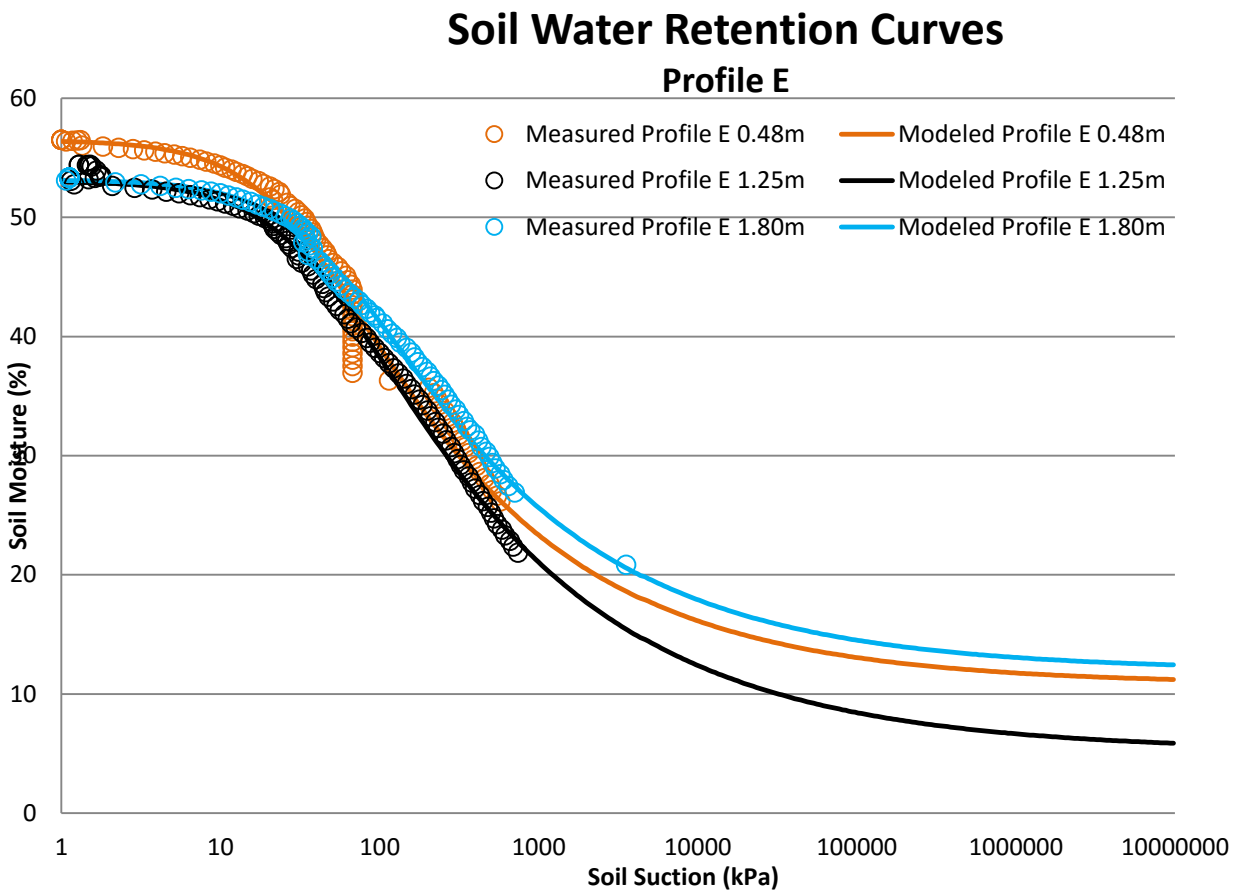

Figure 2. 23. Soil water retention curves for profile E at various depth.

Table 2. 4. Soil properties and van Genuchten parameters with depth for Profile E.

Depth Range (m)	Hydraulic Conductivity, K_s (m/d)	Porosity, ϕ	van Genuchten, n	van Genuchten, α (1/m)
0.67	1.054*	0.56	1.38	3.03
1.33	2.295*	0.46	1.35	2.31
2.00	1.430*	0.53	1.37	1.95

*Measured with a permeameter

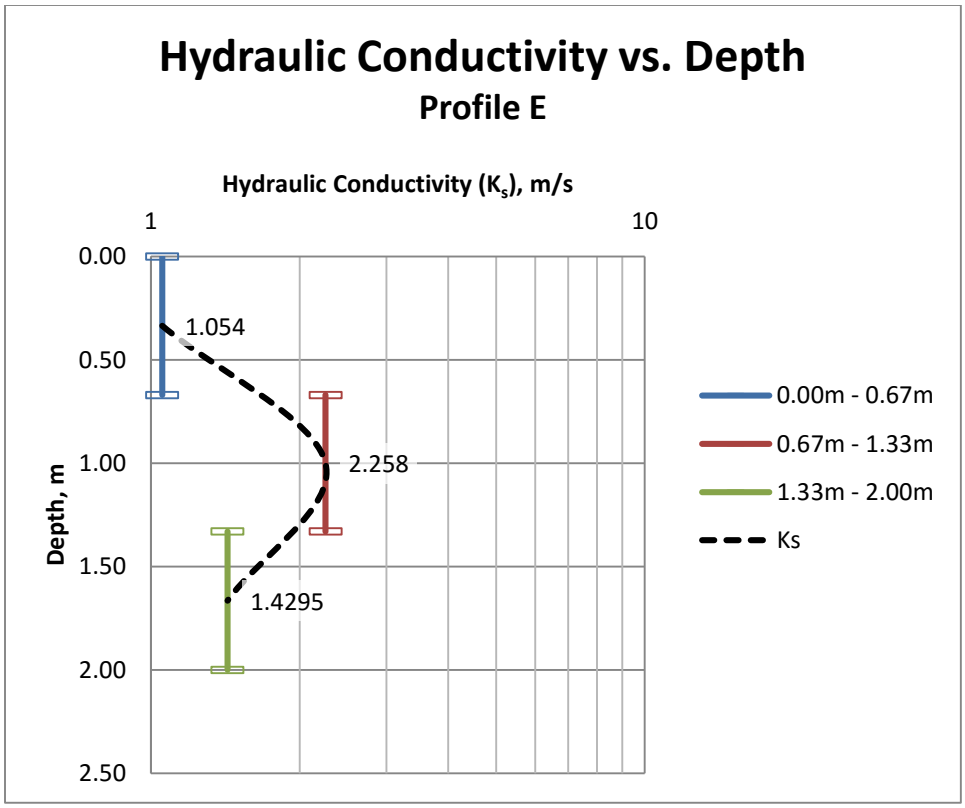

Figure 2. 24. Hydraulic Conductivity versus depth for profile E.

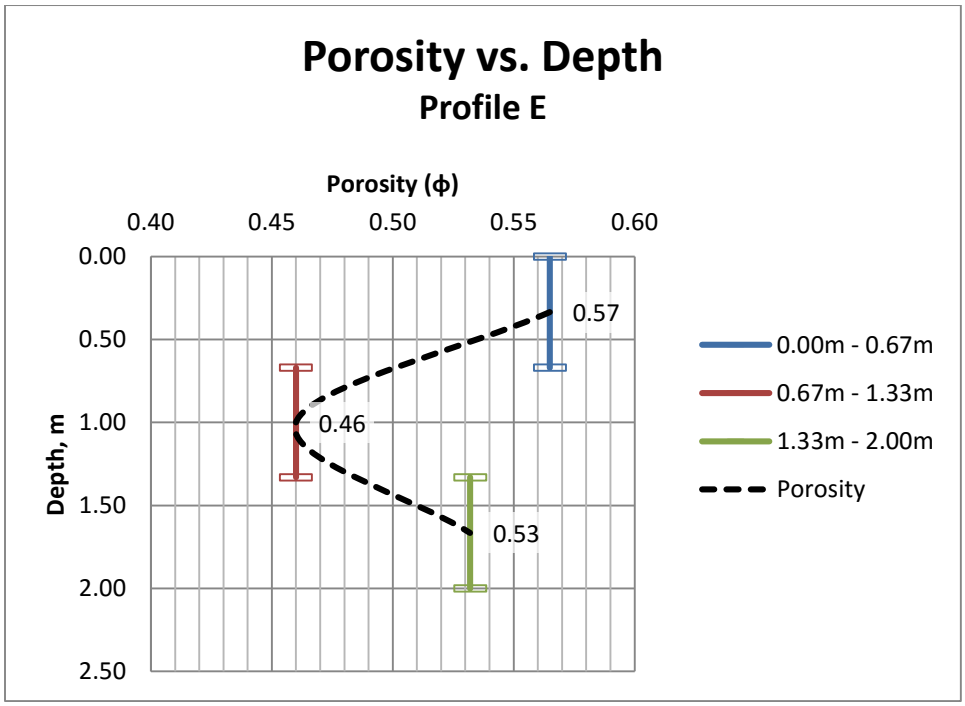

Figure 2. 25. Porosity versus depth for profile E.

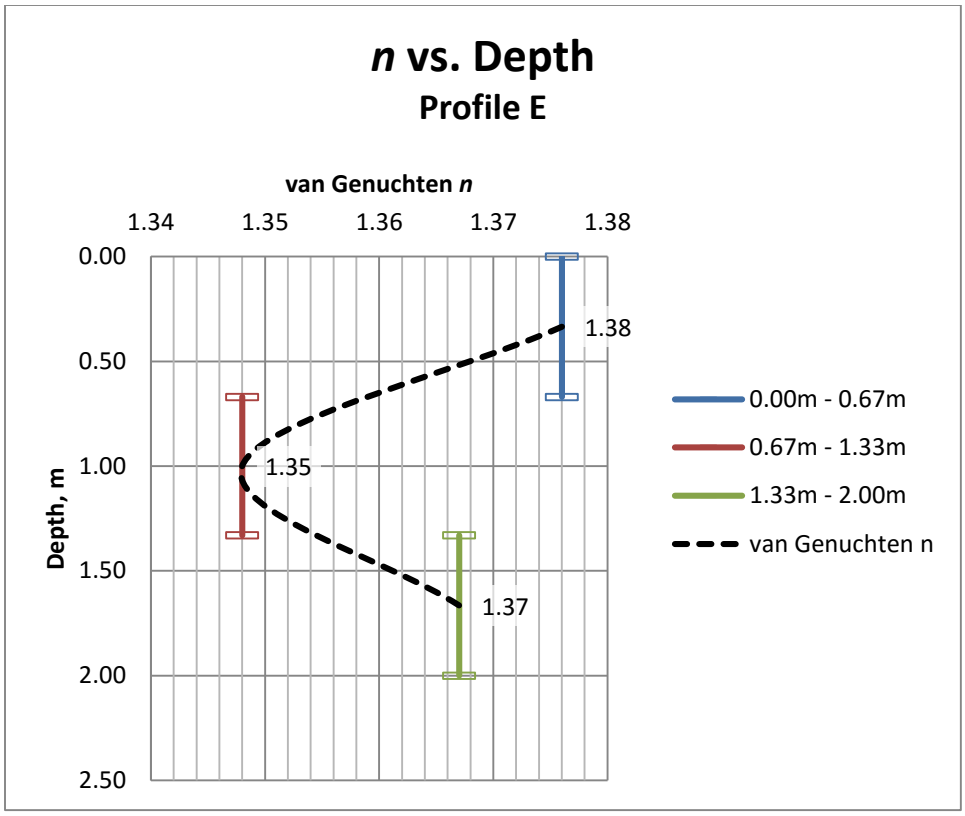

Figure 2. 26. van Genuchten n parameter versus depth for profile E.

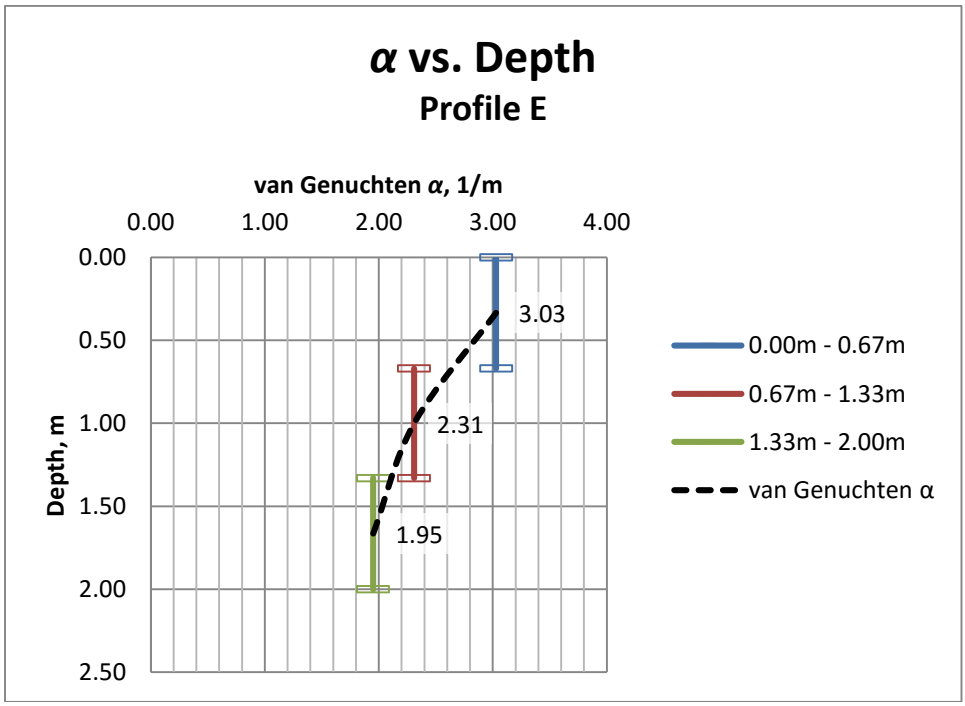

Figure 2. 27. van Genuchten α, parameter versus depth for profile E.

2.1.6 Soil Analyses for profile F:

Soil samples for the sieve analysis were taken from 0.11 m (0.36 ft), 0.52 m (1.7 ft), 1.03 m (3.4 ft), and 1.63 m (5.3 ft). Detailed analyses are shown in Appendix B. By using the USCS systems it was determined that the most probable classifications of these soils are:

0.11 m = Well graded, coarse-grained, silty, clayey sand.

0.52 m = Well graded, coarse-grained, silty, clayey sand.

1.03 m = Well graded, coarse-grained, silty, clayey sand.

1.63 m = Well graded, coarse-grained, silty, clayey sand.

Figure 2.28 shows the SWRCs for profile F at various depths. Table 2.5 and Figures 2.29-2.32 show the variation of soil properties and van Genuchten SWRC model parameters with depth.

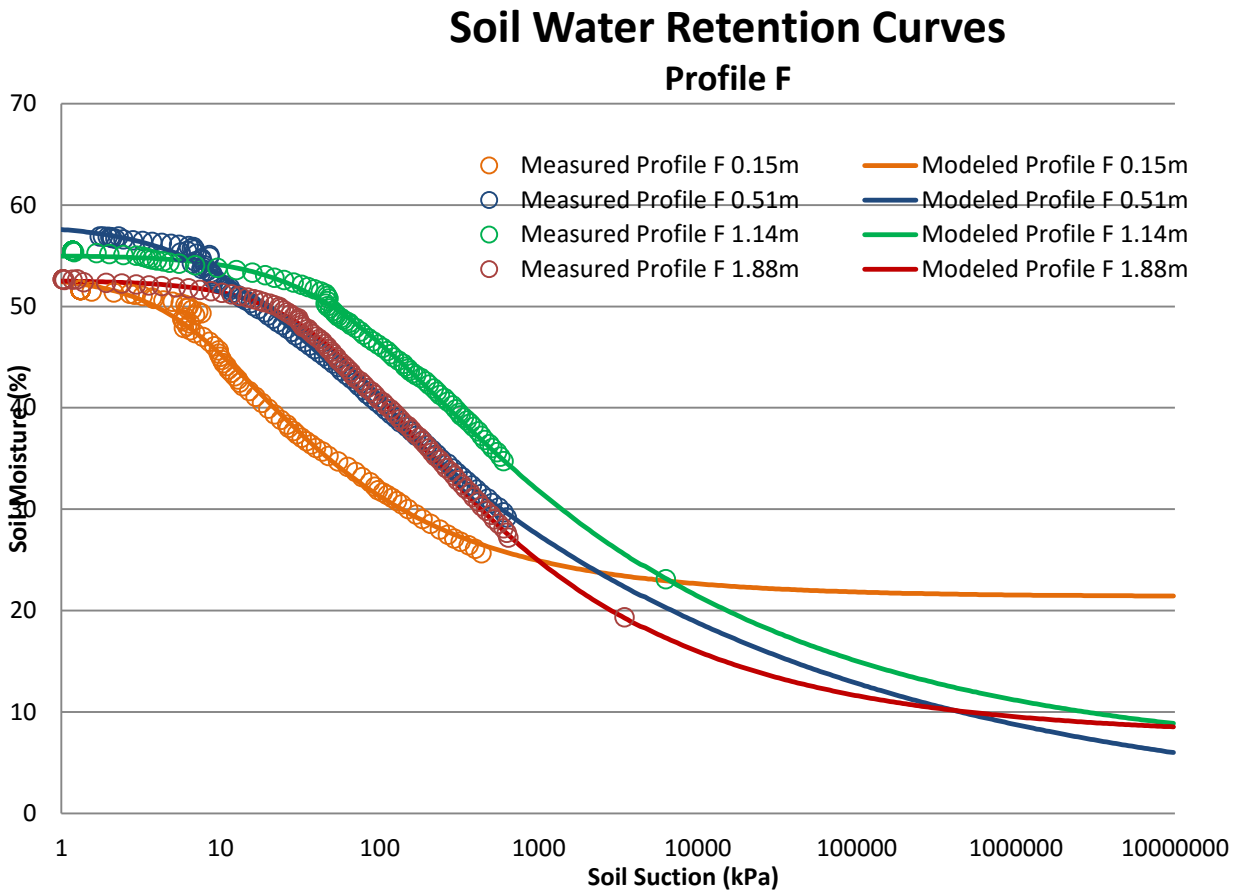

Figure 2. 28. Soil water retention curves for profile F at various depth.

Table 2. 5. Soil properties and van Genuchten parameters with depth for Profile F.

Depth Range (m)	Hydraulic Conductivity, K_s (m/d)	Porosity, ϕ	van Genuchten, n	van Genuchten, α (1/m)
0.27	0.075*	0.53	1.28	16.1
0.67	0.18*	0.58	1.17	8.97
1.34	0.012‡	0.55	1.46	0.83
2.00	1.012*	0.53	1.32	1.89

*Measured with a permeameter
‡Estimated from HYPROP© system

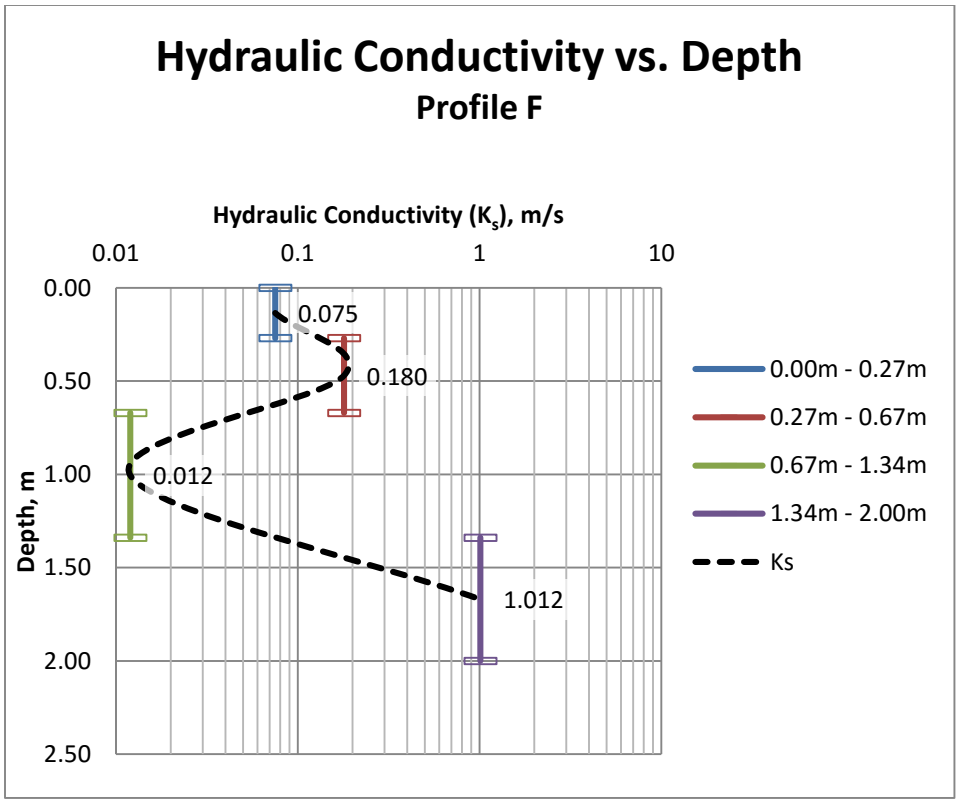

Figure 2. 29. Hydraulic Conductivity versus depth for profile F.

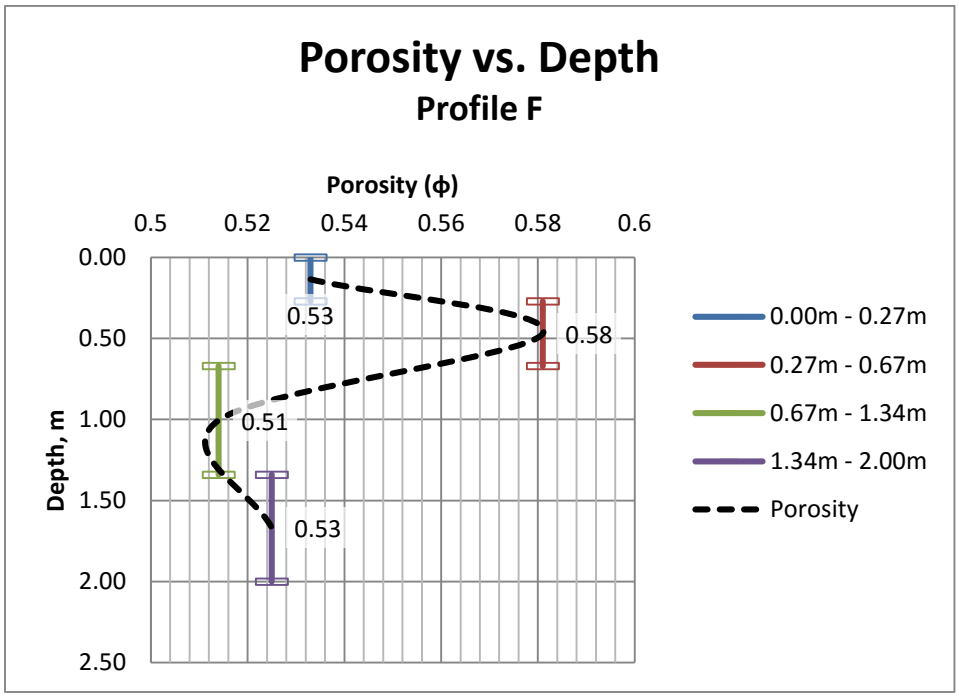

Figure 2. 30. Porosity versus depth for profile F.

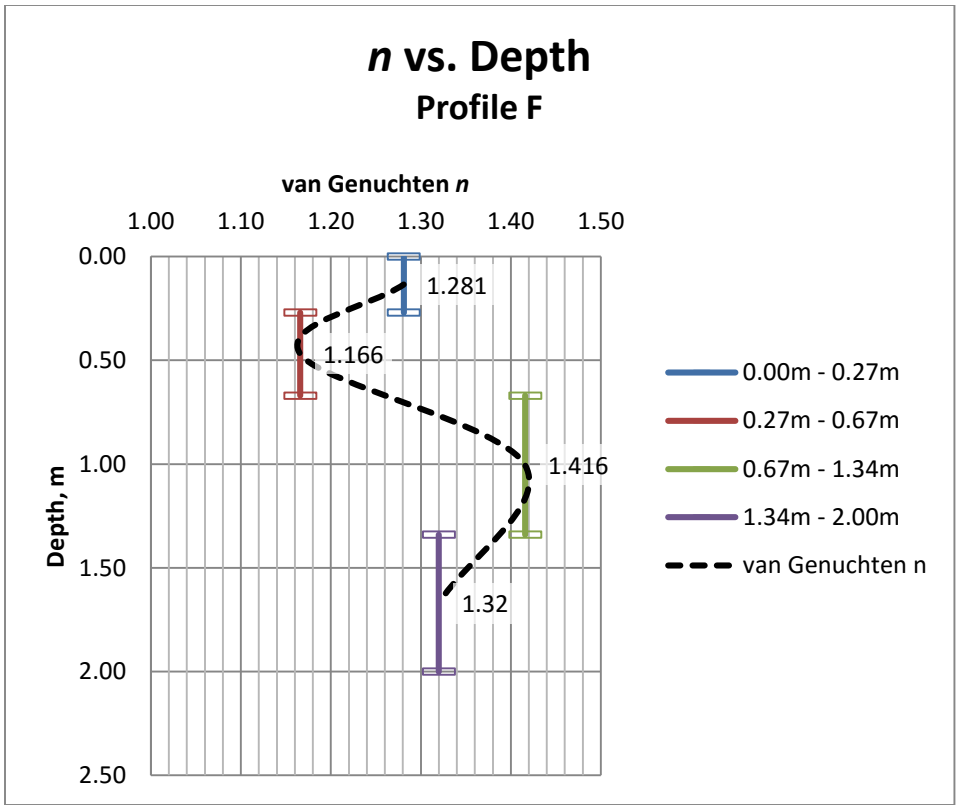

Figure 2. 31. van Genuchten n parameter versus depth for profile F.

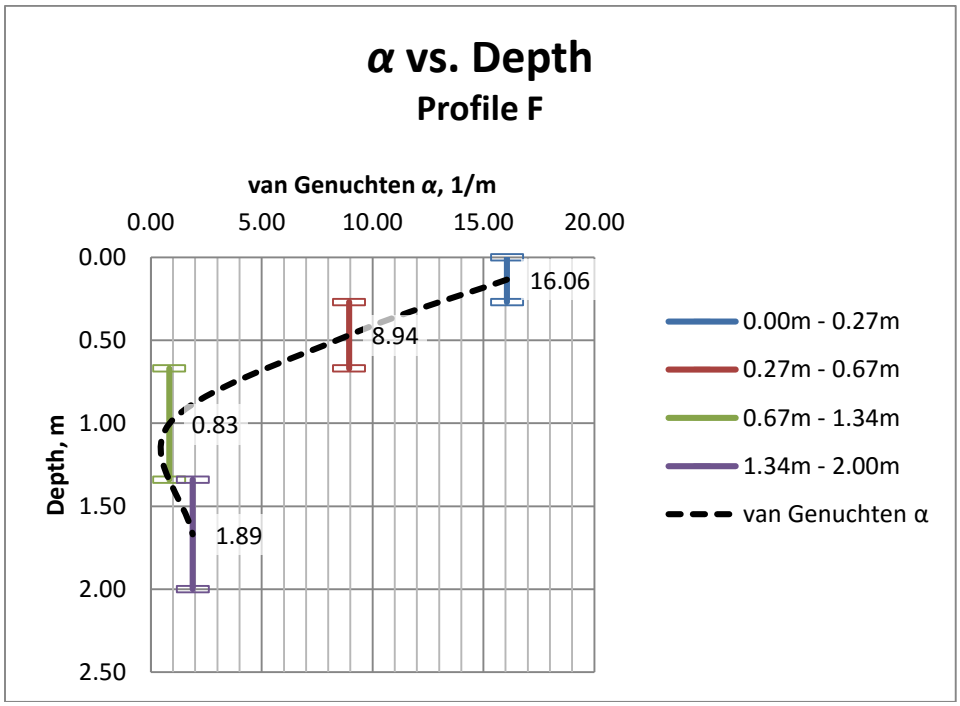

Figure 2. 32. van Genuchten α, parameter versus depth for profile F.

2.1.7 Summary of Soil Property Variations:

From the detailed soil analyses of different profiles, it can be concluded that the top layer generally has a high saturated hydraulic conductivity that ranges between 0.006 and 0.47 m/day (0.02-1.54 ft/day), with the higher values being in the upper portion and the lower values in the deeper portion of this layer. There is also evidence of the second through the sixth layer tend to act as a semi-confining unit (ranges around 3-4 m (9.8-13.1 ft) in thickness) with very low hydraulic conductivity between 0.000095 and 0.003 m/day (0.000031-0.0098 ft/day). As later will be discussed in Chapter IV, the potentiometric heads measured in the deeper portion of the alluvium or alluvium-bedrock interface are higher than the measured water table elevations (2.4 m (8 ft) depth to water). Thus, we infer that the low conductivity layers 2-6 act as a semi-confining unit.

2.2. Topography of study site

The topography of the surrounding area consists mainly of rolling hills. At the study site there is a generally gentle slope along Rock Creek, a tributary to the Whitewater River. The stream meanders throughout its length and its morphology is controlled by rock outcrops and deep incisions which are caused by erosion during high flows. The banks along the stream are steep in some areas, with varying bank heights (about 4.5 m (15 ft) high in many areas) and in other places the banks have a gentle slope going away from the stream. Along the stream there are sections where woody debris has accumulated during storm events; these sections create dammed pools of waters.

2.3 Vegetation of the study site

The riparian vegetation consists of a variation of phreatic vegetation. The larger vegetation includes oaks, locust, hawthorn, sycamore, coffee, hackberry, cottonwood, elm, willow, and other trees. Smaller vegetation includes grass and forbs among small shrubs. To the north of the riparian vegetation, Brome grass is cultivated and cut twice a year. On the south side of the stream, the vegetation consists of prairie type grass and has been left to grow naturally. The Prairie grass field is subject to controlled burning every one to two years.

CHAPTER III

MONITORING NETWORK DESIGN

The overall monitoring network at the field site is composed of three distinct sensor networks: a soil moisture sensor network, a groundwater measurement network, stream gaging system, and a weather station. The soil moisture sensor network is comprised of six different profilers. Four profilers are distributed along a central transect in the riparian zone and the other two are located at the upstream and downstream end. Six deep alluvium wells, five shallow groundwater-table wells, one deep bedrock well, and one stream well make up the groundwater monitoring network. The deep alluvium wells are located in the same configuration as the soil moisture network and penetrate just into the top of the weathered bedrock. Three of the shallow water-table wells are located along the central transect and the other two are at the downstream and upstream ends of the study reach. The bedrock well is located on the edge of the riparian zone and one well is located within the streambed. The stream gaging system has two gaging locations, one upstream and one downstream. The locations of all the sensors are shown in Figure 3.1.

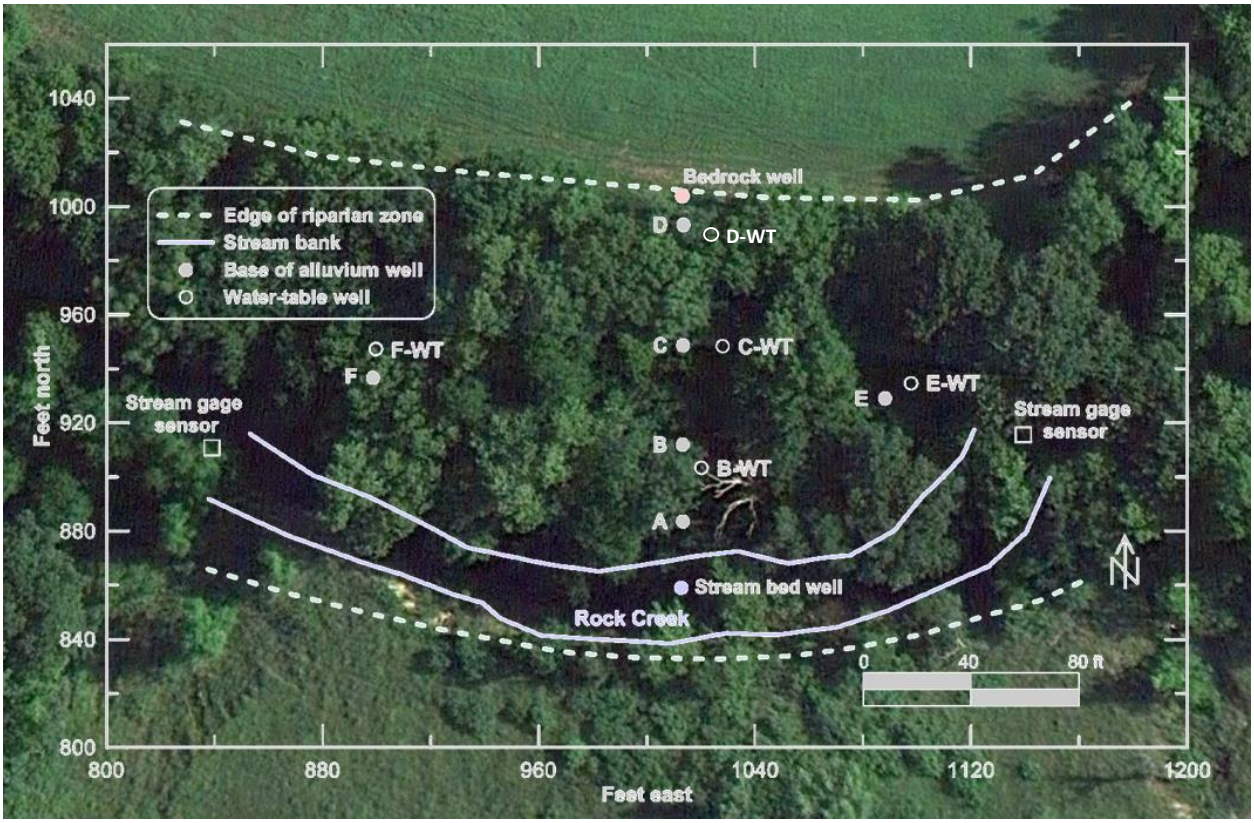

Figure 3. 1. Location of sensors within the riparian zone which include ground water observation wells, stream gages and soil moisture profiles. The soil moisture sensors are positioned within 2 m (6.6 ft) of the alluvium wells. The stream flow goes from East to West.

3.1 Soil moisture profiler network

After careful evaluation of alternative soil moisture measurement technologies and the difficulties involved in installation at the site due to highly silty and clayey soils, we decided to use the EnviroSCAN probe system from Sentek technologies. The advantages of this system are the ease of installation (requiring no digging of deep pits, just auguring a single borehole at each location) and accuracy/reliability as documented in recent publications from the U.S. Department of Agriculture (Alva, 2008; Jabro et al., 2005; Paltineanu and Starr, 1998; Paltineanu and Starr, 2000; Rowland et al., 2011; Starr and Paltineanu, 1998). One of the limitations is the depth range, where the access tubes were only able to penetrate into the ground to a depth that ranged from 1.4 to 1.8 m (4.6-5.9 ft).

The EnviroSCAN system uses the capacitance method to determine the relative dielectric permittivity of the soil and therefore the water content of the soil (Paltineanu and Starr, 1997). Each soil moisture measurement is obtained by a capacitance sensor which is comprised of two cylindrical capacitance plates (brass rings) separated by a plastic ring, which can be positioned at different depths along a cartridge unit that rides within an access tube (see Figure 3.2). Each of the profilers was initially installed with four capacitance sensors and later updated to six sensors to better resolve the vertical variation of soil moisture resolution in the profile.

Figure 3. 2. Sentek EnviroSCAN soil moisture profiler system customized for our application. The 6 pairs of gold-colored rings (No. 1) constitute the capacitance sensors set at 6 different depths that slide along a plastic type cartridge (No.2) and all connected to an electronic interface (No. 3) that communicates with a centralized external data logger (No.5). The cartridge is then placed inside the access tube (No. 4, white PVC pipe).

Tables 3.1-3.6 indicate the location of the sensors relative to the ground.

Table 3. 1. Sensor location with respect to the ground surface for profile A.

PROFILE A	
Sensor No.	**Meters**
Sensor No. 1	0.140
Sensor No. 2	0.432
Sensor No. 3	0.718
Sensor No. 4	1.019
Sensor No. 5	1.222
Sensor No. 6	1.441

Table 3. 2. Sensor location with respect to the ground surface for profile B.

PROFILE B	
Sensor No.	**Meters**
Sensor No. 1	0.187
Sensor No. 2	0.476
Sensor No. 3	0.781
Sensor No. 4	1.092
Sensor No. 5	1.394
Sensor No. 6	1.692

Table 3. 3. Sensor location with respect to the ground surface for profile C.

PROFILE C	
Sensor No.	**Meters**
Sensor No. 1	0.168
Sensor No. 2	0.565
Sensor No. 3	0.768
Sensor No. 4	1.064
Sensor No. 5	1.368
Sensor No. 6	1.781

Table 3. 4. Sensor location with respect to the ground surface for profile D.

PROFILE D	
Sensor No.	**Meters**
Sensor No. 1	0.095
Sensor No. 2	0.307
Sensor No. 3	0.605
Sensor No. 4	0.905
Sensor No. 5	1.208
Sensor No. 6	1.611

Table 3. 5. Sensor location with respect to the ground surface for profile AA, E.

PROFILE AA, E	
Sensor No.	**Meters**
Sensor No. 1	0.146
Sensor No. 2	0.451
Sensor No. 3	0.849
Sensor No. 4	1.153
Sensor No. 5	1.438
Sensor No. 6	1.661

Table 3. 6. Sensor location with respect to the ground surface for profile AB, F.

PROFILE AB, F	
Sensor No.	**Meters**
Sensor No. 1	0.210
Sensor No. 2	0.511
Sensor No. 3	0.810
Sensor No. 4	1.095
Sensor No. 5	1.400
Sensor No. 6	1.619

All profiles sensor units were connected to a centralized CR1000 data logger (Campbell Scientific) enclosed in a weather resistant enclosure as shown in Figure 3.2, label *No. 5*. Measurements were recorded on a 15 minutes interval. The data logger was powered by a 12-Volt 24-AMP sealed battery that was recharged by a solar panel. The data logger also transmitted data through a radio telemetry system (RF401 900-MHz Spread-Spectrum Radio, Campbell Scientific) where it is communicated to another radio that was connected to the weather station datalogger. Data were then retrieved remotely using the weather station telemetry system.

3.2 Ground water network

All 13 wells were installed within the riparian zone by the KGS. The 6 alluvium wells were constructed by using a dual-rod Geoprobe direct-push system as shown in Figure 3.3 (a). As the Geoprobe penetrated the ground a plastic liner was used to retrieve soil cores. Before the coring drive casing was removed, a PVC well screen and casing were inserted in the borehole. A sand filter pack was placed in the annular space above the screened interval and the rest of the annular space was sealed with Bentonite pellets. The wells were then developed with a surge block and pumped. The shallow well in the stream bed and the two shallowest alluvial wells (B-WT and C-WT in Figure 3.1) were installed by hand auguring into the upper gravel zone that is embedded in silty clay in the alluvium. This approach was necessary for the streambed well, and was useful for the shallowest two water-table wells because it allowed detailed sensing of the character of the alluvial sediment with depth, especially the moisture content. Water flowed relatively rapidly into the boreholes of water-table wells B-WT and C-WT during auguring. Although moisture increased with depth in the other three boreholes, water did not enter rapidly and the

boreholes could not be advanced by hand to the depth needed due to the resistance of an unsaturated gravel layer. The Geoprobe direct-push unit was then used to deepen these boreholes to the desired depth. PVC well screen and casing were inserted in the boreholes and a sand filter pack was placed in the annular space to above the screened interval and the rest of the annular space was sealed with Bentonite (except for the streambed well in which stream gravel was placed above the sand pack). The bedrock well, which was installed with a RotoSonic drill rig (see Figure 3.3 (b)), penetrated a few zones of void space totaling about 1.5 m in the limestone, and was developed by bailing. An Instrumentation Northwest (Kirkland, WA) pressure transducer/data logger unit was placed in the water column of each well. A barometer was hung above the water level and below ground surface in one of the wells (Well B). Measurements of pressure (head of water) was recorded on a 15 minute interval and was collected manually on a regular basis (~2-4 months) by the KGS.

Figure 3. 3. (**a**) Dual-rod Geoprobe direct push system that was used in drilling the deep alluvium wells (KGS, Ed Robelet and Steve from right to left). (**b**) RotoSonic drill rig that was used to make the bedrock well.

A schematic of a vertical cross-section of the main transect with the location of the different wells and soil moisture profile is shown in Figure 3.4. This figure can be compared to Figure 3.1 that shows the plan view.

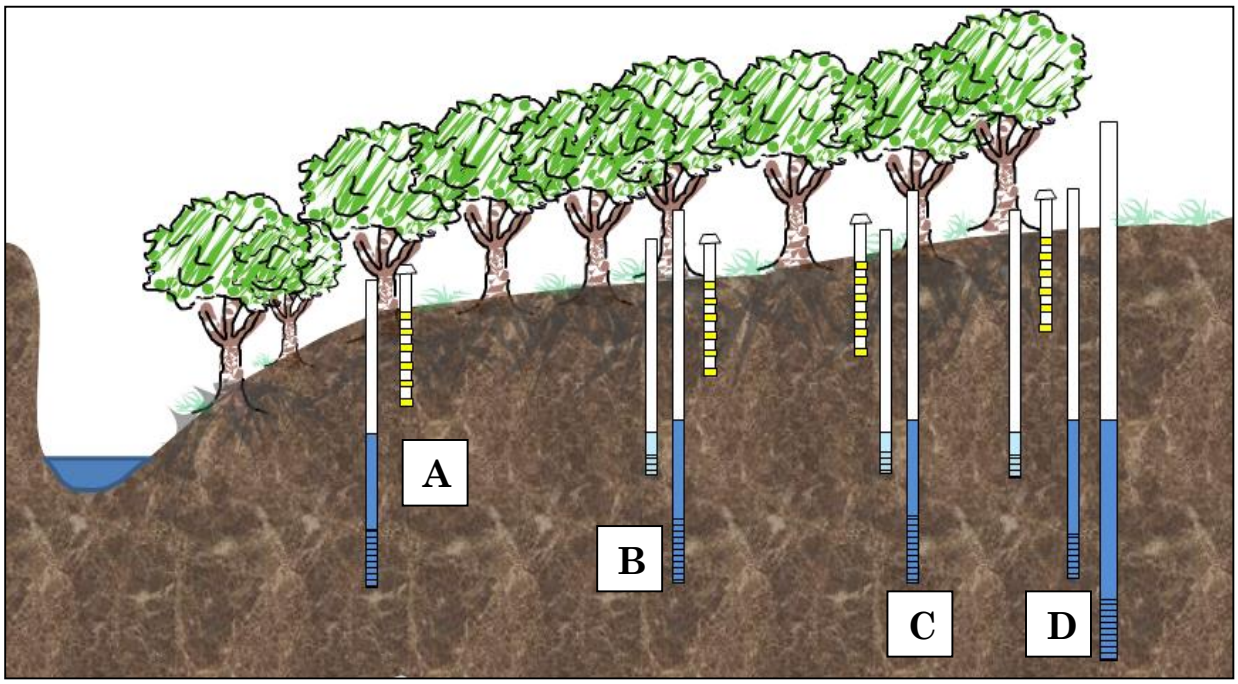

Figure 3. 4. Vertical cross-section through the main transect showing locations of soil moisture sensors, shallow well screens and deep alluvial well screens (figure is not to scale).

3.3 Stream gaging system

The University of Iowa (UI) installed a stream gaging system. The gaging system consisted of two pressure transducers with different optimum pressure ranges in deeper portions of the stream channel at both the upstream and downstream ends of the stream study reach of Figure 3.1. The cables between the sensors and data loggers are covered with stainless steel strap to prevent damage from rodents and any debris that may be present in the stream during high water flows. The data loggers for the transducers are enclosed in PVC casing on trees at a level that would be above a very substantial flood level

as shown in Figure 3.5(c). Each stream gage contains two sensors (see Figure 3.5(a)). The first sensor has a maximum effective depth range of 1.5 m (4.9 ft), which allows for a change in depth sensitivity of about 1 mm. Since small changes in depth were expected during the periods of interest, this allowed for maximum sensitivity. The second sensor has an effective depth range of 15 m (49.2 ft), which is approximately the maximum depth that might occur. Although this sensor has a change in depth sensitivity of about 1 cm, the combination allows for effective measurement of flow depths for all likely conditions in the stream. Figure 3.5(b) shows the gage as it is installed in the stream.

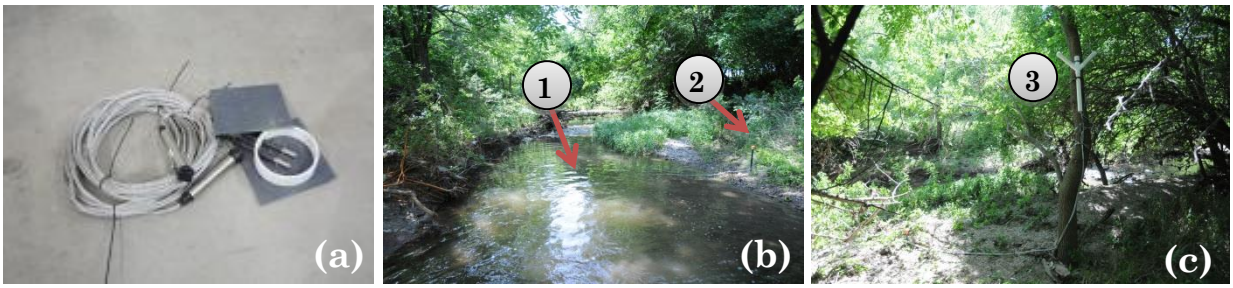

Figure 3. 5. **(a)** Two pressure sensors mounted on a plastic ring and covered by two plates, which allows unimpeded flow and protection from debris. **(b)** The downstream gage placed in the stream (No. 1) and a stake embedded in the ground to prevent gage movement during a flood event. **(c)** The bifurcated access tube that allows easy access to each sensor's data logger for manual download (No.3).

3.4 Weather station

The weather station was installed in the prairie land which is to the south of the study reach and about 100 meters (328 ft) to the south-southeast of the main line of wells as shown in Figure 3.6. A chain-link fence was placed around the weather station to prevent wildlife disturbance. The station includes instruments for measurement of precipitation, wind speed and direction, barometric pressure, solar radiation, and air temperature and humidity. Table 3.7 shows the sensors used and their placement. Data is stored on a CR1000 data logger (Campbell Scientific) and collected on a daily, hourly, and

15-minute interval. The weather station is powered by a 12Volt-24AMP sealed battery and recharged with a solar panel. The station also has a telemetry system which is composed of digital cellular modem (RAVENXTG Cellular Digital Modem for AT&T, Campbell Scientific) and radio (RF401 900-MHz Spread-Spectrum Radio, Campbell Scientific) that allows communication to the soil moisture profile network. Data can be collected remotely with the use of a computer software (LoggerNet 4.1) and an internet connection.

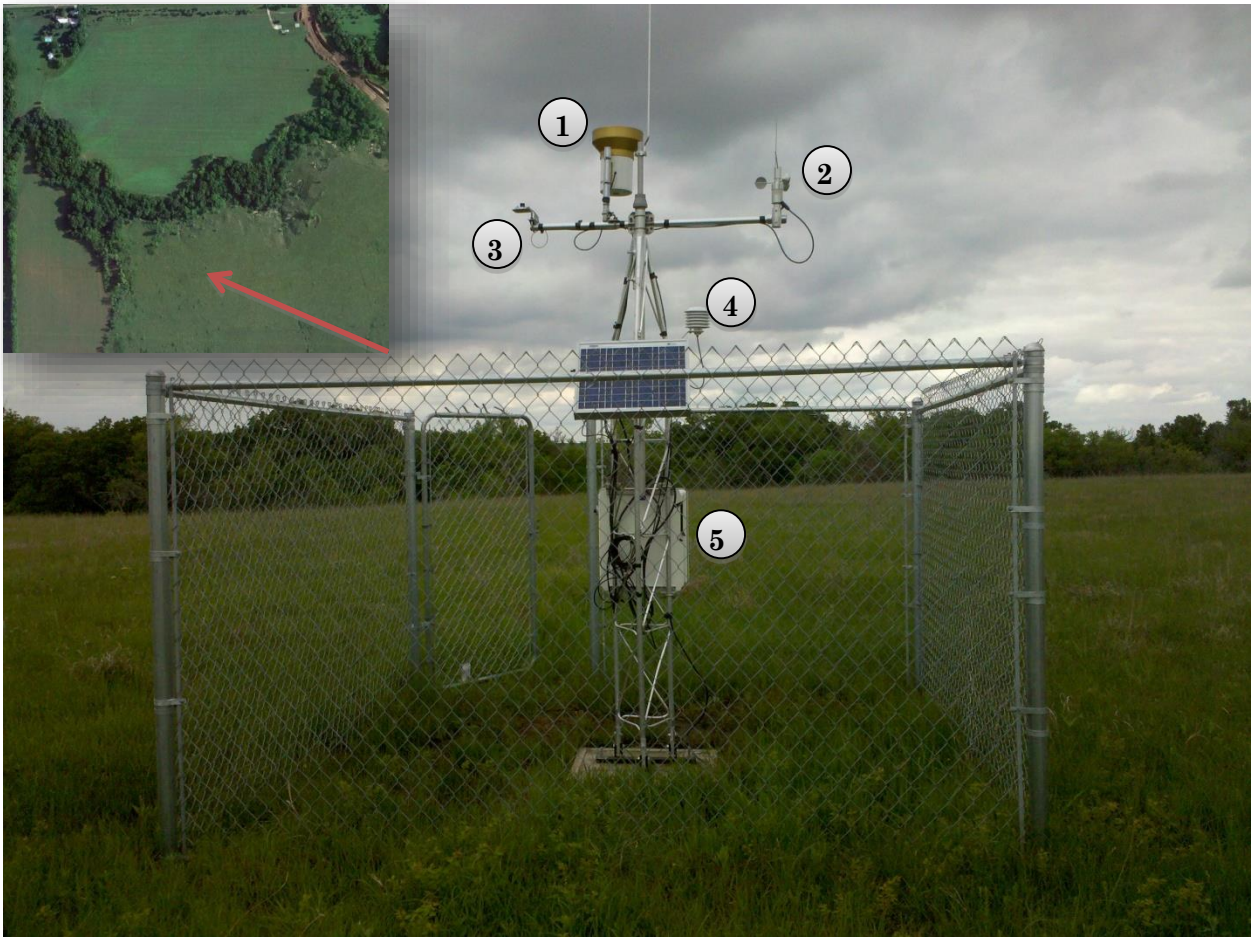

Figure 3. 6. Weather station located on the prairie as depicted by the red arrow on the satellite image at the top right corner. The weather station measures: precipitation (No. 1), wind speed and direction (No. 2), solar radiation (No. 3), air temperature and humidity (No. 4), and the barometric sensor is located inside the enclosure (No. 5) along with the data logger, and telemetry system.

Table 3. 7. Sensor type, model, and location placed on the weather station.

Measurement	Sensor Type	Placement
Solar radiation	LI200X Pyronometer	2.74 m *
Air temperature and relative humidity	HMP50, Temperature and relative humidity sensor	2.13 m *
Atmospheric Pressure	CS 106 Vaisala PTB110 Barometer	1.27 m *
Wind speed and direction	Met One 034B-L Windset	2.74 m *
Precipitation	TE525WS Tipping bucket	3.05 m ‡

* Measured from ground surface

‡ Measured from the top of the tipping bucket to the ground surface

CHAPTER IV

REPRESENTATIVE OBSERVATIONS AND CONCEPTUAL MODEL

In this chapter, a conceptual model of the subsurface system underlying the riparian zone is developed based on interpretation of representative observations. The key inferences are from water level data for both shallow and alluvium wells, soil moisture profiles, and soil property characterization (Chapter II). Water-level and soil moisture measurements were taken continuously from as early as July of 2010 to the present. Other measurements began later in the study, where additional wells and more soil moisture sensors were added to further understand the dynamic complexities of the hydrogeology of the studied riparian zone.

4.1 Observations from Well Data

Some key features contributing to the conceptual model are the head changes and head differences among the bedrock well, alluvium base wells and the shallower water table wells. The first important observation is that the potentiometric head elevation in the bedrock well, the alluvium base wells, and the streambed well were higher than the water table elevation observed in the shallow water table wells during the dry summer season (approximately 0.5 m (1.6 ft) for the bedrock and alluvium base wells and 0.2 m (0.7 ft) for the streambed well). This is clearly evident from Figure 4.1 where the head elevations are shown for a period during June 2011.

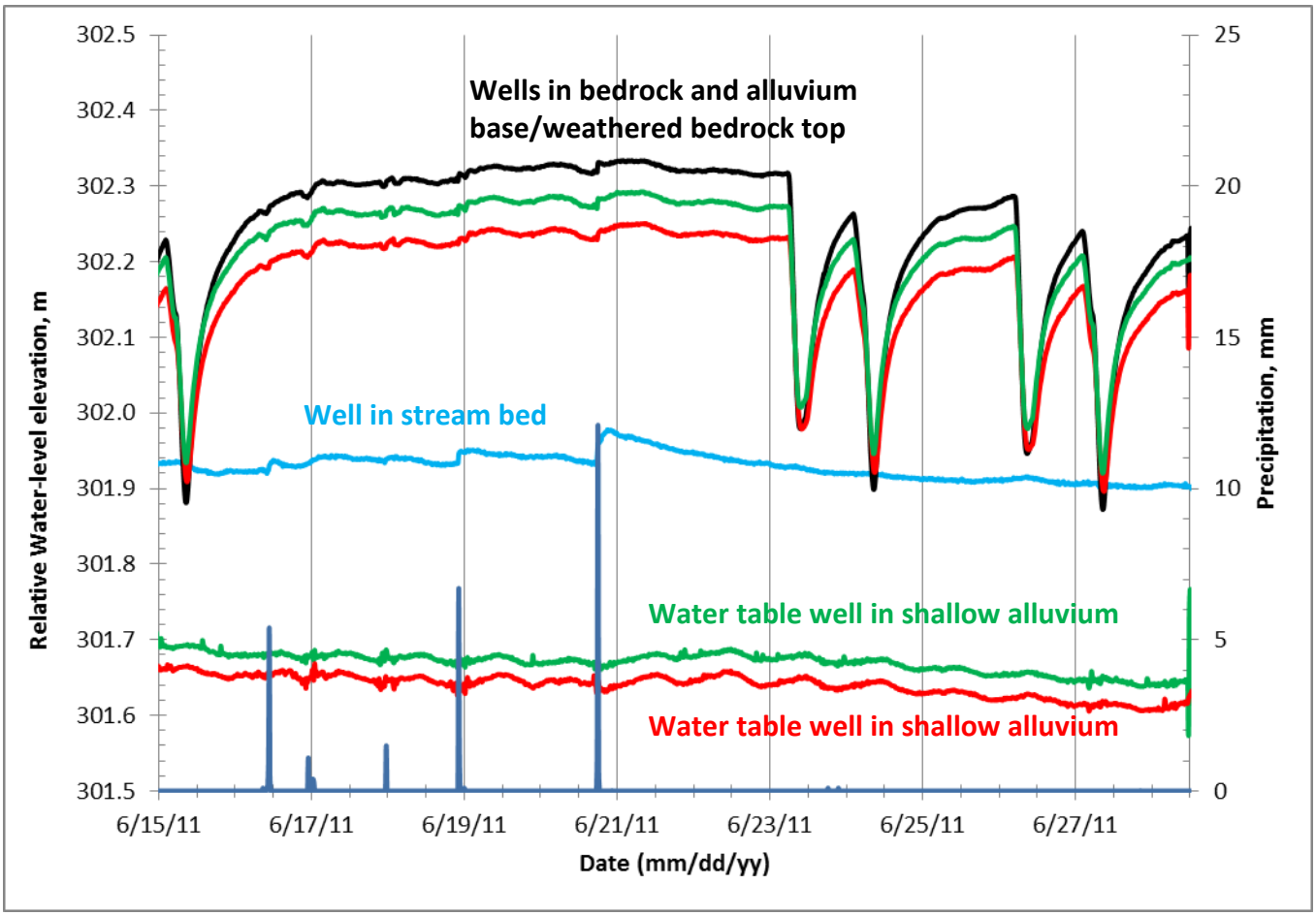

Figure 4. 1. Hydrographs of wells screened in the bedrock and alluvial base/weathered bedrock top, in two of the shallow alluvial (water table) wells, and in the shallow stream bed well during a two-week period in June 2011. The hydrographs in red (wells C-WT and C) and green (wells B-WT and B) represent pairs of nearby alluvial base and shallow alluvium wells; the bedrock well hydrograph is the black line.

Another important feature evident from the deep wells is the pronounced drawdown in the water level that occurs due to pumping of nearby wells. The landowner has two wells that are approximately 400 m (quarter mile) from the riparian study site and mainly used for lawn and garden watering, as shown on Figure 4.2. As can be seen from Figure 4.1, the drawdown spikes only occur in the bedrock and deep alluvium wells and not in the stream

well or the shallow wells. This suggests that the hydraulic connection between the deep and shallow subsurface systems is not strong, which is consistent with the hydrogeological description of the soils and sediments (Chapter II); the deeper alluvium consists of fine-grained sediments with very low hydraulic conductivity. Thus suggests that the lower alluvium acts as a confining aquitard layer between the deep alluvium (including either gravel on or a weathered zone in the top of the weathered bedrock) and the shallow alluvium (water table) wells. The thickness of the aquitard varies within the riparian zone. Locations at the edges of the riparian zone have a thicker confining layer than at the center, as inferred from the hydraulic conductivity and soil core samples, which show that the middle of the transect has a greater depth of unconsolidated alluvium (see Chapter II). Another important key feature to note is the diurnal fluctuation that occurs in the shallow water table wells. These fluctuations are indicative of a RET signal. It is also noteworthy that the diurnal fluctuations are not evident in the streambed well.

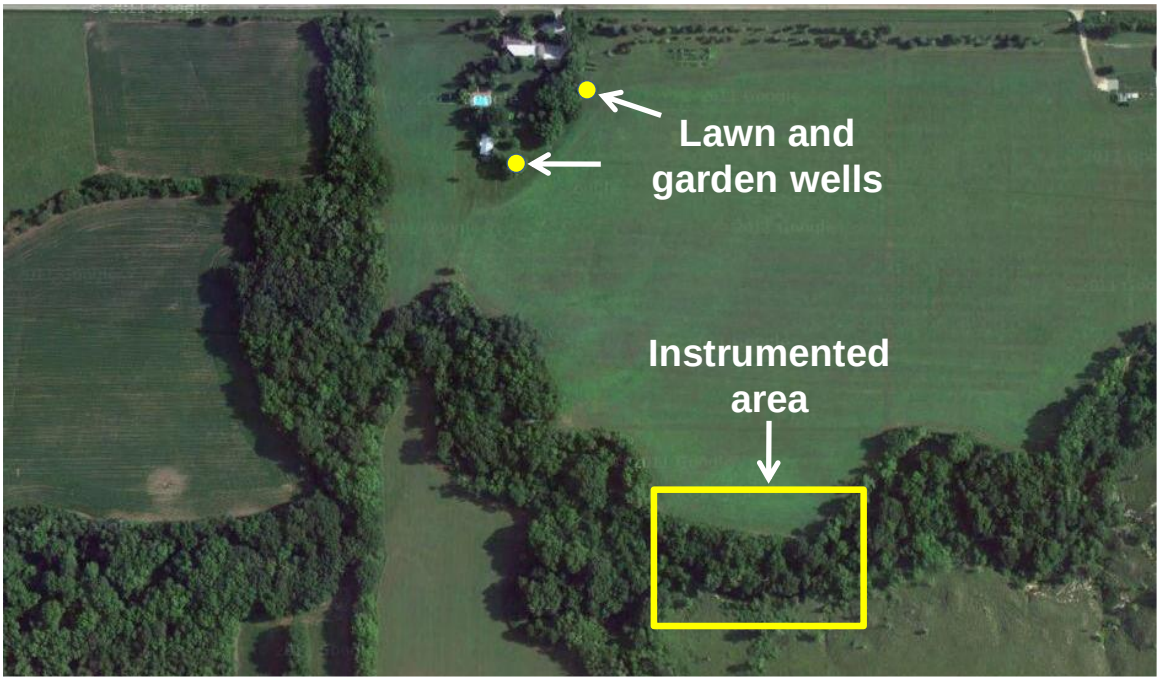

Figure 4. 2. Aerial view of the study site and showing the location of the pumping wells.

The estimated time from when the pumping starts and the influence of pumping reaches the deep wells is approximately 15-30 minutes. This was found by applying a temperature micro data logger (Hobo, Tidbit) on each of the discharge pipes of each pumping well. During the summer, the groundwater temperatures are cooler than the land surface and thus show a drop in temperature due to pumping. An example of this relationship between deep alluvium and bedrock well heads and well pipe temperature is shown in Figure 4.3. These observations suggest relatively high permeability of the bedrock aquifer in which the lawn and garden wells are screened.

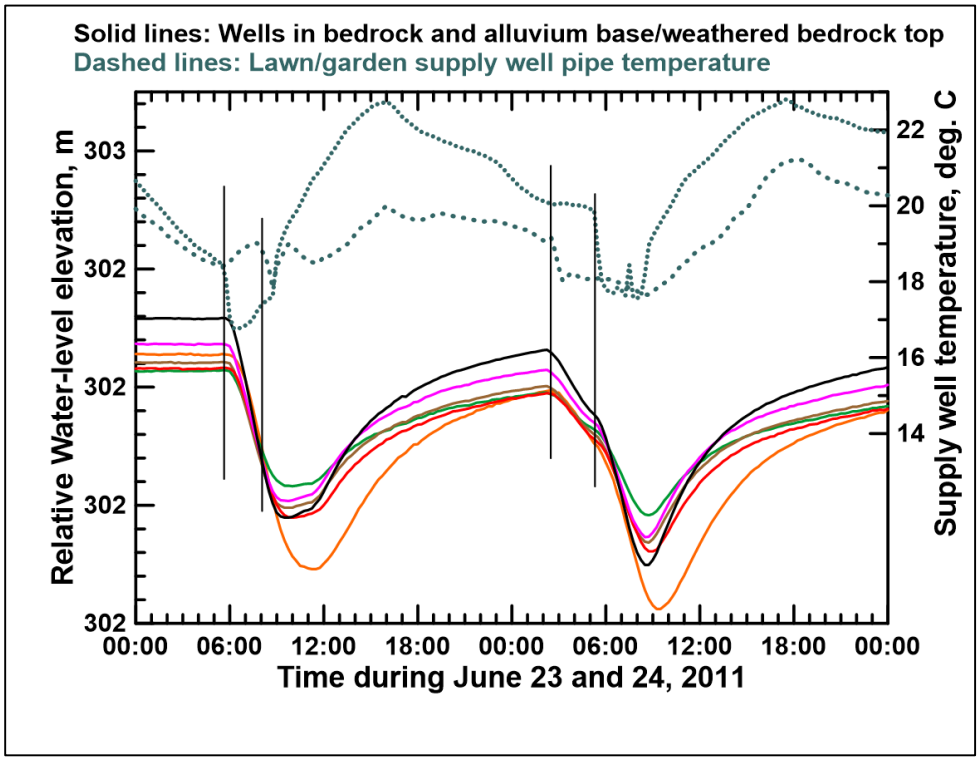

Figure 4. 3. Hydrograph of the alluvial base wells and the temperature of the discharge pipes of the supply wells during the summer. A decrease in temperature occurred when the pumps started as indicated at the locations of the vertical lines.

4.2 Observations from Soil Moisture Data

Figure 4.4 shows soil moisture measurements taken at four different depths at one of the soil moisture profiles (upstream profile E). The soil moisture sensors exhibit diurnal fluctuations that are similar to the fluctuations seen in the water table in the shallow alluvium as previously shown in figure 4.1. These fluctuations are most likely due to the water uptake by the riparian vegetation, i.e. RET, which exhibits diurnal oscillations (Butler et al., 2007).

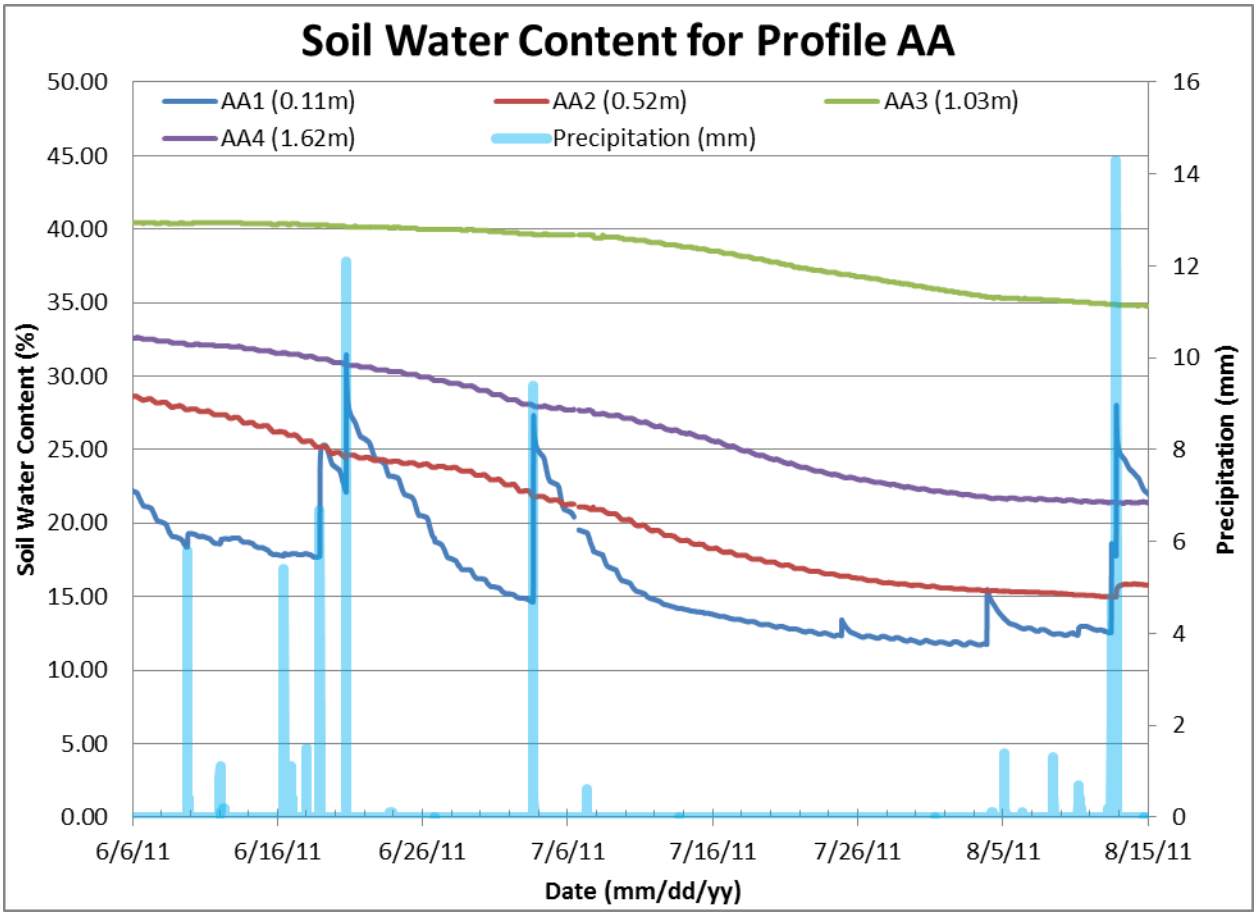

Figure 4. 4. A closer view of the continuous soil moisture measurements by 4 sensors for profile AA (upstream profile, also referred to as profile E).

An additional observation from Figure 4.4 is the pronounced response of the shallowest soil moisture sensors to precipitation events. The deeper sensors do not show this substantial response to smaller precipitation events. However, the two intermediate depth sensors display a slightly slower rate of decrease in soil water content immediately after the largest two precipitation events in June and July, followed by a resumption of the soil moisture decrease during the dry spells. The dependence of the soil moisture response on the magnitude of precipitation is seen from the sensor located at 0.52 meters (1.71 ft) below the surface, which did not show an abrupt increase in soil water content after the earlier events (between 6/7/2011 and 7/7/2011) but displays a small spike after the largest precipitation event shown in Figure 4.4 that occurred on 8/13/2011.

Another important feature that is demonstrated by analysis of the soil moisture measurements from the different profiles is the highly heterogeneous nature of the alluvium. An example of the variability of the soil moisture is shown in figures 4.5 through 4.8. These figures show measurements taken in 0.15 m (0.49 ft) increments throughout the profile (by raising the capacitance sensors manually in steps to achieve closely spaced measurements). The sharp changes in soil moisture content at intermediate depths suggest abrupt changes in soil texture which is verified by soil characterization done in the laboratory. In some portions of the soil profile, fine grained soils retain more water when compared to adjacent soils that are coarser grained. The water table depth varies from profile to profile. For example the depth to water table at "Profile C" was 3.11 m (10.2 ft) below ground surface on 7/7/2011 while it was 2.84 m (9.3 ft) at "Profile B", just a small distance (0.27 m (0.89 ft)) apart.

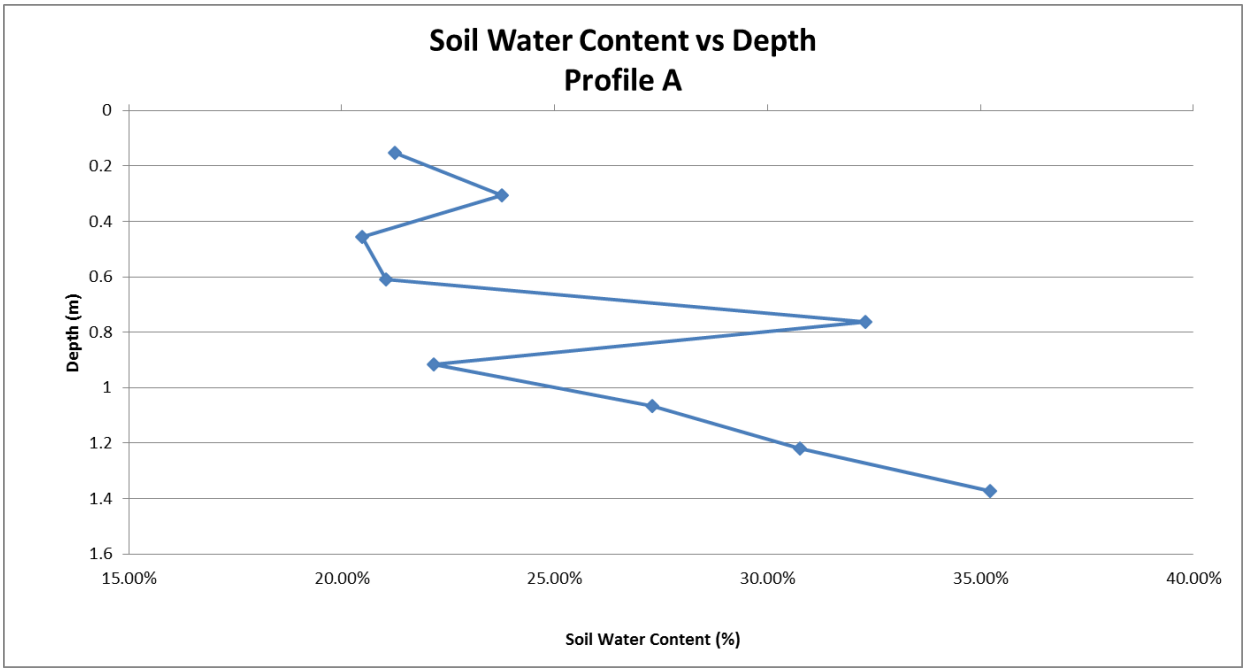

Figure 4. 5. Soil moisture profile taken every 0.15 meters starting from a depth of 0.15m to 1.40m, at profile A (closest to the stream), taken on 7/7/2011.

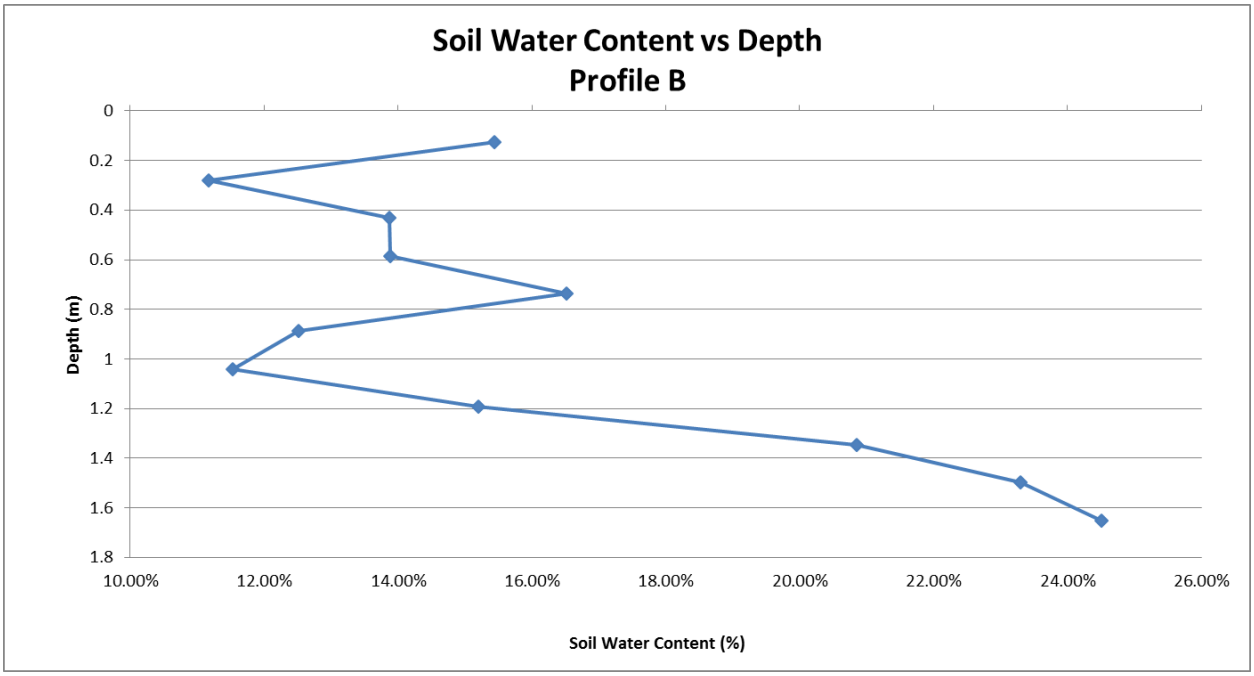

Figure 4. 6. Soil moisture profile taken every 0.15 meters starting from a depth of 0.13m to 1.65m, at profile B (2nd closest to the stream), taken on 7/7/2011.

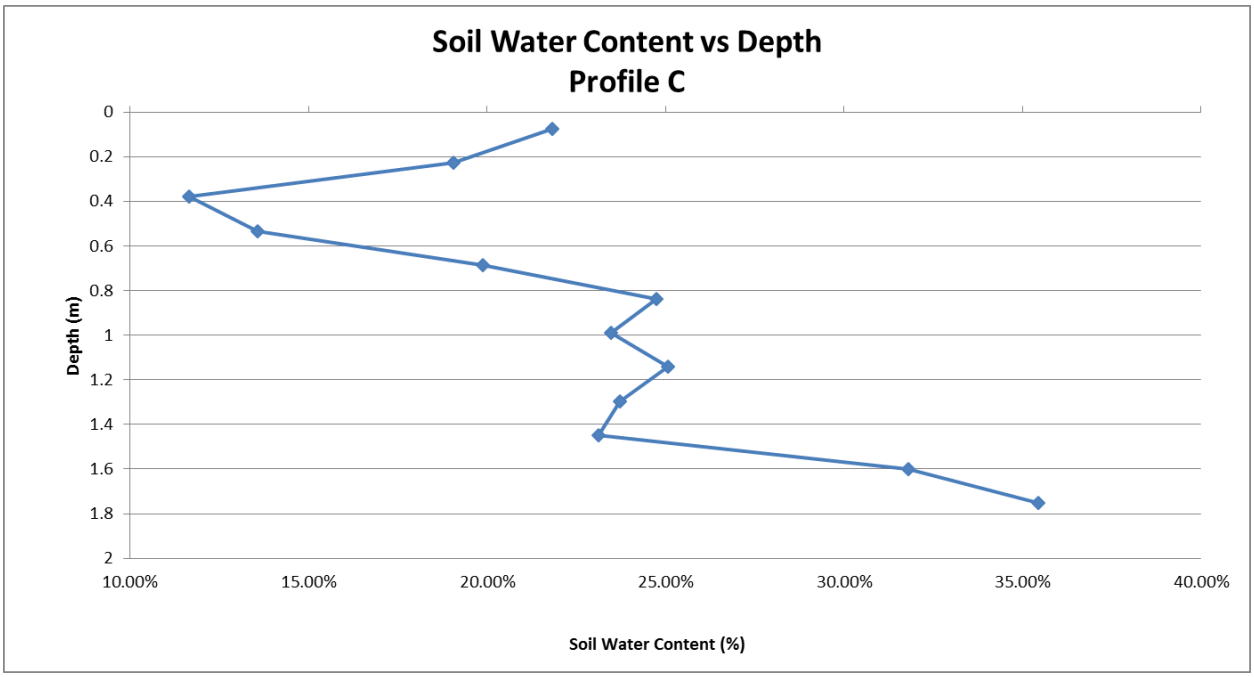

Figure 4. 7. Soil moisture profile taken every 0.15 meters starting from a depth of 0.08m to 1.75m, at profile C (3rd closest to the stream), taken on 7/7/2011.

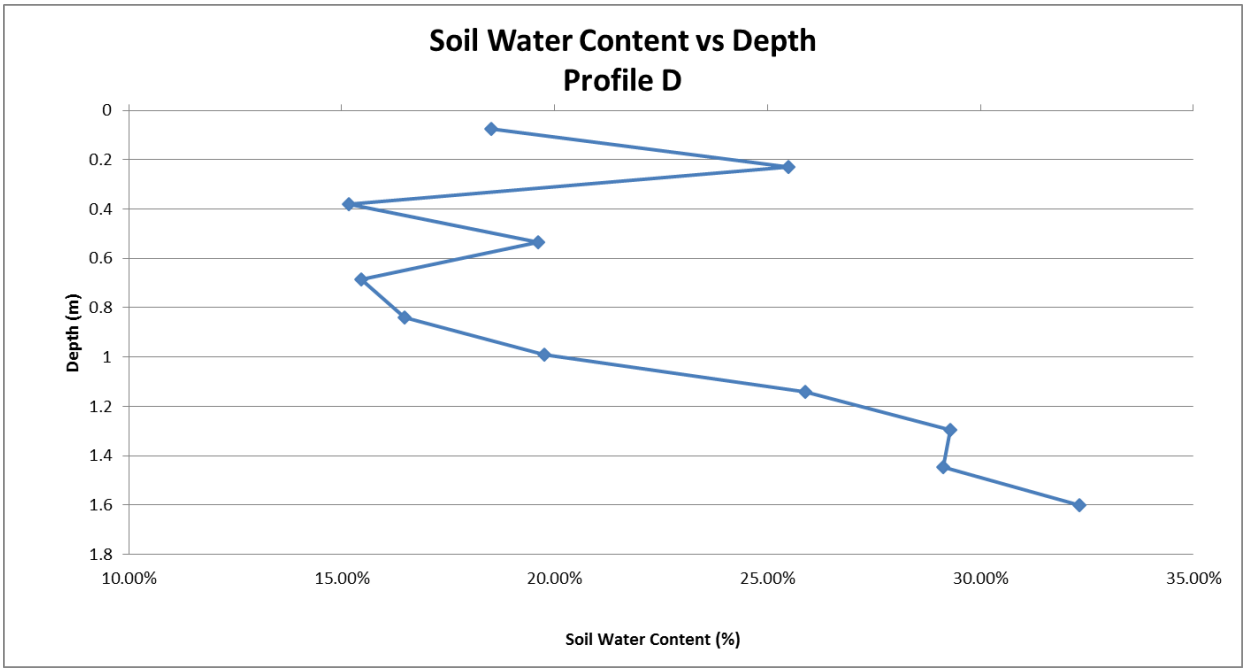

Figure 4. 8. Soil moisture profile taken every 0.15 meters starting from a depth of 0.08m to 1.6m, at profile D (furthest from the stream), taken on 7/7/2011.

4.3 Hydrogeological connectivity

It is useful to evaluate the hydrogeological connectivity in the riparian zone. As previously stated there appears to be very little hydraulic connection between the bedrock and shallow alluvium (water table) wells since the latter do not respond to pumping, while the former do. As noted previously, the streambed well does not respond to pumping, nor does it exhibit diurnal oscillations that would suggest connectivity to the shallow alluvium. Figure 4.1 indicates that during very low flows no significant increase occurs in the water table recorded by the shallow alluvium wells due to precipitation events. The limited response of deeper soil moisture sensors to precipitation events in Figure 4.4 is also consistent with the behavior of the water table trends, and in general confirms the low permeability of the alluvium. However, the stream appears to have a hydrogeological connection with the shallow alluvium wells at higher stages, as discussed below.

During moderate to high flows there is an increase in water level in both the streambed well and the shallow alluvium wells in response to a precipitation event (for example, the event on 6/3/12, Figure 4.9). Figure 4.10 demonstrates the influence of precipitation on the uppermost soil moisture measurement as a sharp change for the same event. Although the sensor at 0.48 m (1.6 ft) depth shows a gradual soil moisture increase after the 6/3/12 event, the deeper sensors show no significant change. Thus, there is no indication of rapid infiltration following the 6/3/12 precipitation event. Yet, the water levels in the streambed and shallow water table wells respond to the 6/3/12 precipitation event. There is a lag between the response of water table wells B and C and the streambed well, with a slightly longer lag at well C (farther from the stream) compared to well B. The above observations suggest that the response to the 6/3/12 event is caused by a connection

between the stream and the shallow water table that drives flow from the stream into the alluvium, rather than direct infiltration of precipitation through the soil. The Whitewater basin is known to be prone to flash flooding with limited infiltration due to the low soil permeabilities. The 6/3/12 event highlights a mechanism by which isolated high flow events deliver water to the shallow alluvial groundwater system by leakage from the stream. However, during the low flow periods that characterize most of the growing season, the absence of diurnal fluctuations in the streambed well suggests lack of connection between the stream and the shallow alluvium in which the water table wells are screened.

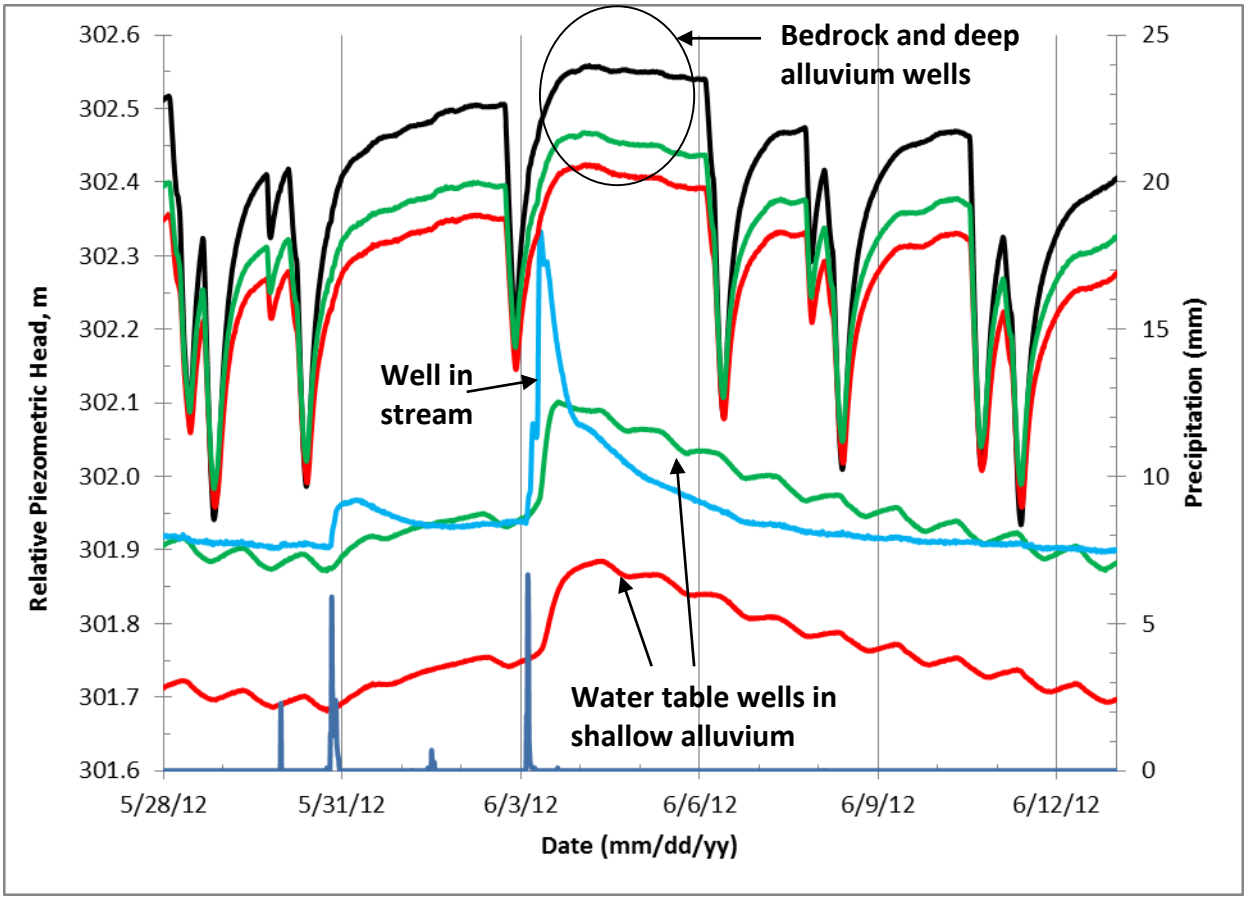

Figure 4. 9. Hydrographs of wells screened in the bedrock and alluvial base/weathered bedrock top, in two of the shallow alluvial (water table) wells, and in the shallow stream bed well during a period in May through June 2012. The hydrographs in red and green represent pairs of nearby alluvial base and shallow alluvium wells; the bedrock well hydrograph is the black line.

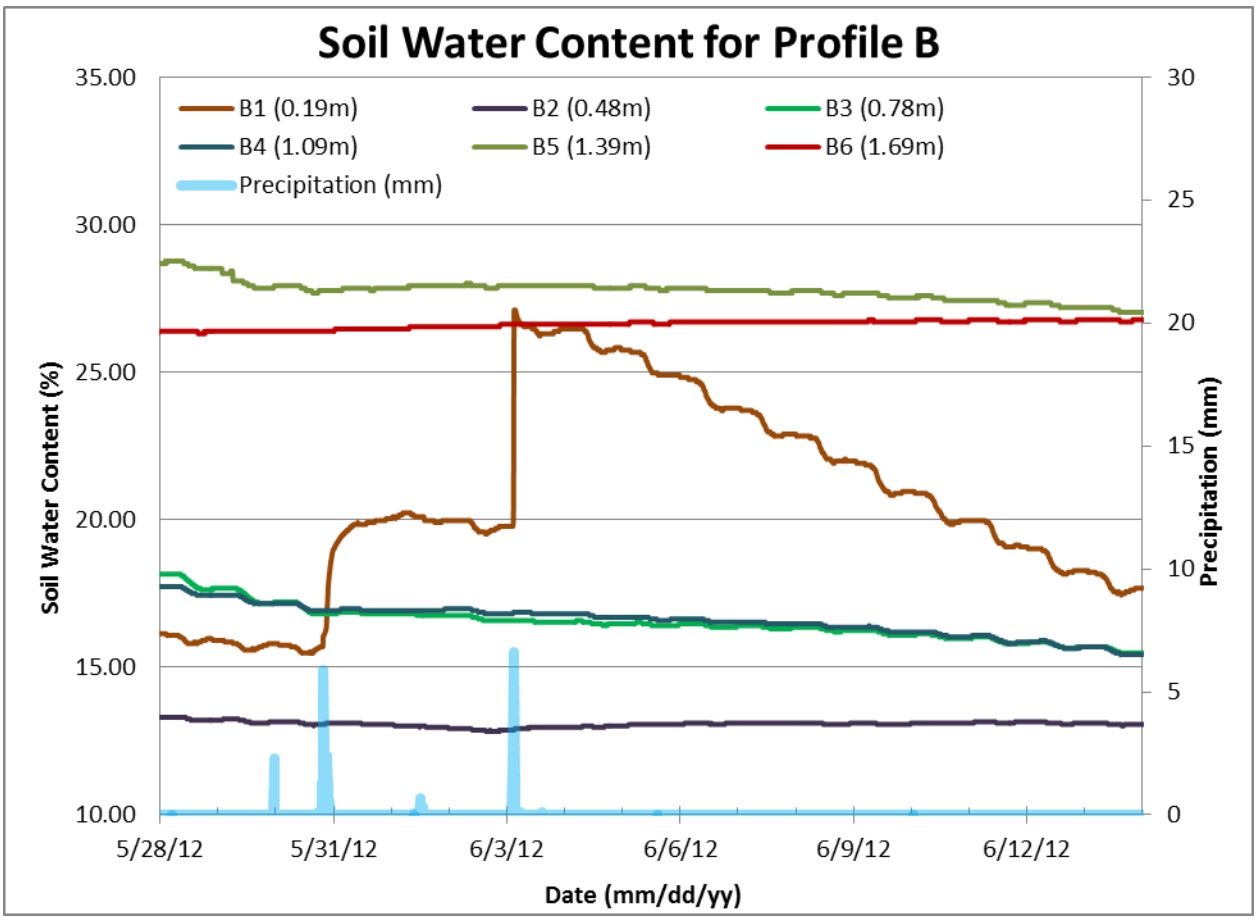

Figure 4. 10. Soil water content at six different depths during a period in May through June 2012. The top most sensor (brown line) shows the effect of the precipitation and the others do not show the infiltration sharp front.

4.4 Conceptual Model

The soil moisture and water level records, coupled with observations from Geoprobe electrical conductivity profiles, sediment cores collected during well installation, and general site characteristics (including riparian distribution, surface topography, stream morphology, and sediment and bedrock geology) allow formulation of conceptual hypotheses on the hydrologic cycle in the study reach. These conceptual hypotheses provide a framework for developing and testing a hydrologic model for water balance in the system, from which RET can be estimated.

The deeper alluvial sediment in the riparian zone is primarily clay that acts as an aquitard overlying the bedrock and overlying this layer is more permeable alluvial sediment and soil. The alluvial sediment is very heterogeneous and includes layers of predominantly fine-grained material and some layers of limestone gravel imbedded in the fine-grained material. The substantially different rate at which water entered the shallow alluvium wells after boring and laboratory analysis indicates significant heterogeneity in the hydraulic conductivity on a small scale.

The upper two meters of the alluvial sediment is a developed soil that has a greater permeability than that of the underlying alluvial clay. The roots of vegetation in the riparian zone extend through this soil zone to the water table as indicated by the diurnal fluctuations in the shallow alluvium wells. The fine-grained alluvial sediment is expected to generate a capillary fringe of substantial thickness that ranges around 0.5 m (1.6 ft) (bubbling pressure of the soil can be related to $1/\alpha$, based on the values of the van Genuchten parameter α reported in Table 2.1 of Chapter II). During much of the growing season when evapotranspiration is active in the riparian zone, the shallow alluvium is likely the main reservoir supplying water to the riparian vegetation. The root zone is expected to extend over depths of 2-4 m (6.6-13.1 ft) in the shallow alluvium. Soil moisture in the root zone is recharged by slow infiltration from rainfall and capillary rise from the shallow water table. The shallowest groundwater in the upper alluvium acts as in an unconfined aquifer. The unconfined aquifer is also slowly recharged by upward flow from the deeper alluvium/bedrock aquifer where the head is higher. However, we expect these recharge rates to be very small due to the low permeability of the aquitard layer. The water table in the unconfined aquifer also rises in response to short-lived moderate to high-

flow events in the stream when the stream level rises high enough to allow bank infiltration into more permeable sediment and soil (Figure 4.9). Based on all the above observations, Figure 4.11 summarizes and gives a visual interpretation of our conceptual model of the hydrogeology at the study reach.

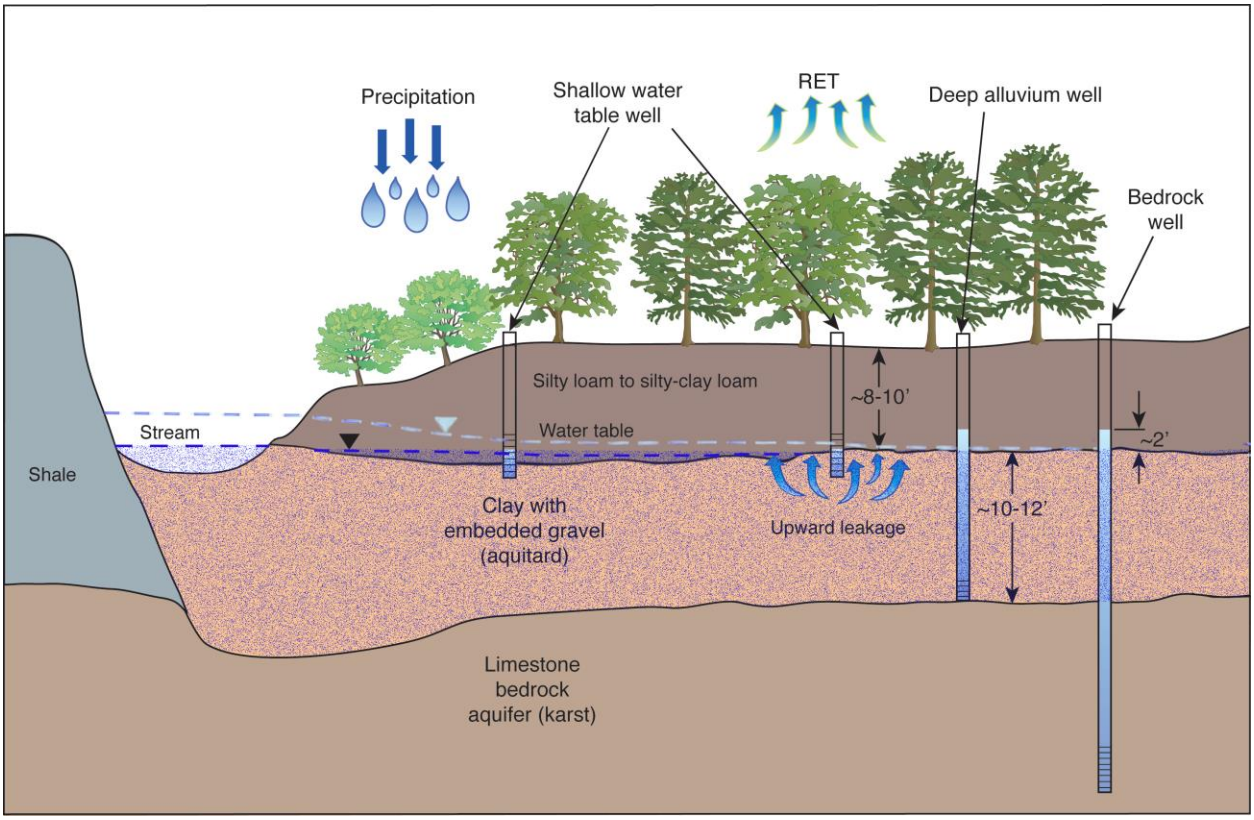

Figure 4. 11. Visual interpretation of the conceptual model for the study site. Direct precipitation, streambank infiltration, and upward leakage are the main sources to the shallow water table. Plant transpiration and, when the water table is substantially higher than the stream, discharge to the stream, are the main avenues by which water leaves the uppermost saturated zone. The faint dashed blue line indicates the stream stage and water table conditions under very short lived high flow events, when recharge from overbank flow can occur. The bottom dashed blue line represents the typical water table position during most of the year. The deep alluvium and bedrock wells have a higher potentiometric head than the shallow water table that can be up to a difference of two feet (Note: diagram is not to scale).

This conceptual model is in contrast with locations elsewhere in Kansas and the U.S. where alluvial sediment is primarily sand or sand and gravel that allows stream-

aquifer interactions to be primary controls on subsurface water supply to riparian plants (Nachabe et al., 2005; Butler et al., 2007; Goodrich et al., 2000; Mac Nish et al., 2000). During leaf-out stage in the riparian area, the vegetation extracts moisture from both the unsaturated zone and capillary fringe. The rate of water flow from capillary rise is too slow to replenish soil moisture during root uptake of water in the daylight hours but can replenish soil moisture during the night when transpiration is not occurring. Therefore, the coupled processes of plant transpiration and slow capillary action are substantial enough to produce observable diurnal fluctuations in soil moisture and in the shallow water table. The relative amount of the unsaturated soil moisture compared to capillary fringe water derived from ground water being taken up by roots depends on the antecedent precipitation. The combination of all observations and data collected thus far was used to create the proposed conceptual model. This model will be used to quantitatively evaluate processes occurring in the riparian zone and for estimation of RET. The water balance framework is discussed in the following chapter.

CHAPTER V

FRAMEWORK FOR WATER BALANCE ANALYSIS

In general, a reach-scale surface-subsurface water balance equation for a riparian zone can be written as:

Equation (5.1)

$$\frac{d}{dt}\left[\int_{x} A(x,t)dx + \iint_{x,y}\left(fH(x,y,t) + \int_{H}^{z_{surface}} q(x,y,z,t)dz\right)dx\,dy\right] = Q_{in} - Q_{out} - ET_s + G_{in} - G_{out} + P - RET$$

where x (streamwise) and y (normal to stream) are horizontal coordinates; A(x,t) denotes the stream cross-section; ϕ = porosity; H=water table elevation; θ = water content; z is a vertical coordinate; $z_{surface}$ denotes the elevation of the ground surface; Q_{in} and Q_{out} represent streamflow at the top and bottom of the reach, ET_s represents the volumetric evaporation rate from the stream, G_{in} and G_{out} represent groundwater inflows and outflows (volume per time); RET and P denote the reach-integrated riparian evapotranspiration and precipitation (volume per time, i.e. corresponding rates multiplied by the reach area). The water balance equation (5.1) generalizes the approach of Mac Nish et al. [2000] to include soil moisture storage (also see Figure 5.1). Previous water balance studies in riparian zones with shallow water tables have largely employed a groundwater balance, using the specific yield to quantify change in groundwater storage (White, 1932; Goodrich et al., 2000; Mac Nish et al., 2000; Butler et al., 2007; Lautz, 2008; Schilling and Jacobson, 2009). Nachabe et al. [2005] estimated RET based on diurnal changes in vertically integrated soil moisture storage in groundwater discharge and recharge zones in Florida. In their application, a

single soil moisture profile was used; it is unclear how the number of profiles impacts accuracy of the RET estimate.

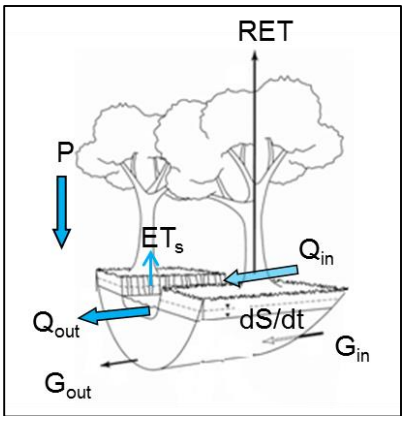

Figure 5. 1. Reach-scale schematic of for the water balance equation (schematic modified from Mac Nish et al., 2000)

Based on the conceptual model described in chapter IV, we note that the stream and the alluvium within the riparian zone are largely disconnected most of the time (except during very rare high flow events). For this reason, the surface and subsurface systems within the riparian zone can be decoupled, and the water balance equation for the alluvium can be treated separately for almost the entire growing season. Correspondingly, (5.1) is simplified to:

Equation (5.2)

$$\frac{d}{dt}\left[\iint_{x,y}\left(fH(x,y,t)+\int_{H}^{z_{surface}} q(x,y,z,t)dz\right)dx\,dy\right]=G_{in}-G_{out}+P-RET$$

In (5.2), G_{in} and G_{out} represent the groundwater inflows and outflows to the entire reach. In principle, (5.2) can form the basis for a reach-integrated subsurface water balance. However, considering the significant heterogeneity in soil properties and soil moisture profiles across the six profile locations, obtaining a reach-scale picture from only

these six profile locations may not be very accurate. For this reason, we also consider each profiler location independently, and consider a one-dimensional vertical water balance similar to that of Nachabe et al. [2005]. Additionally, because the soil moisture sensors do not extend down to the water table, we cannot directly use (5.2) to estimate RET from a water balance. At profilers B and C, and for some periods at profiler E and F, water table elevations were reliably recorded and offer an additional datapoint ($\theta = \phi$ at the water table elevation, which was determined from the soil characterization described in Chapter II). Correspondingly, we use two modified forms of (5.2) in our water balance analysis. For profilers without water table measurements (A and D, and some periods for E and F), we employ a water balance over the depth interval from the ground surface to the deepest sensor (z_d), as shown in equation (5.3a) below:

Equation (5.3a)

$$\frac{d}{dt}\left(\int_{z_d}^{z_{surface}} q(x,y,z,t)dz \right) = \frac{dTSM_{top}}{dt} = G'_{in} - G'_{out} + P - RET_{top}$$

In (5.3a), TSM_{top} refers to the total soil moisture between the ground surface and the deepest sensor (units of mm); P represents the precipitation rate (mm/day), RET_{top} represents the riparian evapotranspiration rate (mm/day) from the depth horizon between $z_{surface}$ and z_d (specific to each profiler location). Assuming that there are no lateral fluxes within the vadose zone, the fluxes G'_{in} and G'_{out} (mm/day) could be interpreted as fluxes across a horizontal plane at elevation z_d. Typically, at a location where deep percolation dominates, G'_{out} would represent the deep percolation rate and G'_{in} would be zero. Alternatively, if there is significant capillary rise and uptake of water by vegetation, G'_{in} would be positive (see Figure 5.2).

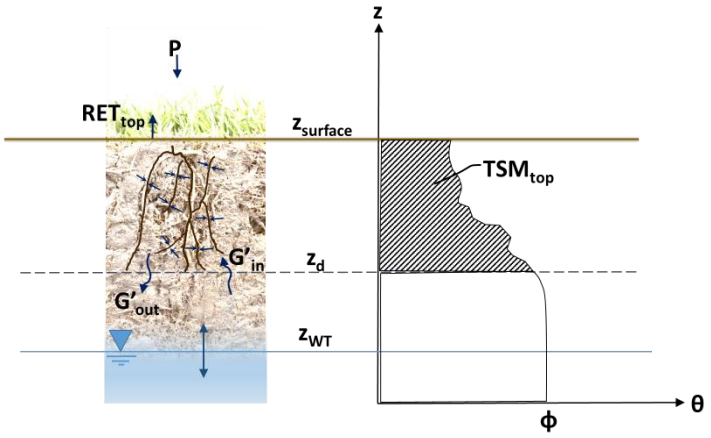

Figure 5. 2. Diagram for equation 5.3a TSM_{top} representation

For cases where water table data are also available, the modified form of (5.2) is:

Equation (5.3b)

$$\frac{d}{dt}\left(f\left(z_{WT} - z_{bot}\right) + \int_{z_d}^{z_{surface}} q(x,y,z,t)dz \right) = \frac{dTSM_{full}}{dt} = G_{in} - G_{out} + P - RET$$

In (5.3b), TSM_{full} (units of mm) refers to the total soil moisture in the entire vertical column from the ground surface to elevation z_{bot} (which could be an arbitrary elevation below the range of fluctuation of the water table), RET represents the riparian evapotranspiration rate from the profiler location, and G_{in} and G_{out} represent lateral groundwater inflows and outflows at the profiler location. In a recharge zone, G_{out} will be positive and G_{in} will be zero, whereas in a discharge zone G_{in} will be positive and G_{out} will be zero (see Figure 5.3). For the water balance analyses in the remainder of the thesis, it is pertinent to note that TSM_{full} and TSM_{top} were calculated using trapeziodal integration of the discrete soil moisture measurements at different depths to evaluate the integrals on the left hand side of equations 5.3a and b. Although some interpolation errors will be incurred as a result, we believe that this is a reasonable approach for integration. Higher-order integration schemes introduce more curvature into the soil moisture profiles, and may not be entirely realistic. However, we acknowledge that due to the heterogeneity evident in the

soil properties, it is entirely possible that there are extremely nonlinear soil moisture variations between the individual sensor locations.

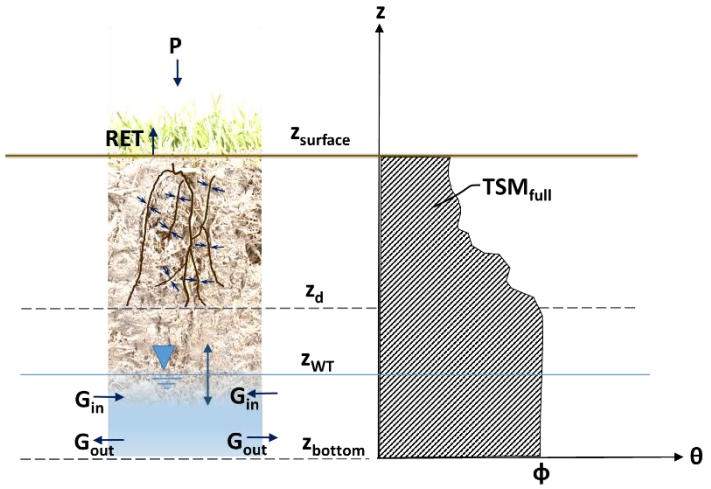

Figure 5. 3. Diagram for equation 5.3b TSM_{full} representation

Integration of (5.3a) and (5.3b) over the duration of a day leads to the following discrete equations that were used in the water balance analysis:

Equation (5.4a)

$$TSM_{top,(i+1)} - TSM_{top,(i)} = \left(P - RET_{top,}\right) + (G'_{in} - G'_{out})$$

Equation (5.4b)

$$TSM_{(i+1)} - TSM_{(i)} = (P - RET) + (G_{in} - G_{out})$$

where P, RET, $RET_{top,}$ G_{in}, $G_{out,}$ G'_{in} and G'_{out} in (5.4a and 5.4b) represent daily total values (in mm). Application of (5.4a) for calculation of RET or RET_{top} requires estimates of the fluxes G_{in}, $G_{out,}$ G'_{in} and G'_{out}. Following the approaches of White [1932] for the groundwater component of RET, and Nachabe et al. [2005] for total RET, we assume that these fluxes are invariant over a 24-hour period, and may be determined from the slope of the TSM (or TSM_{top}) variations during the night, when RET or RET_{top} is inactive. This assumption is justified in part by the slow response time scales associated with groundwater flow in the low-permeability alluvium and the deeper vadose zone (see Figures 5.4 and 5.5). Figures

5.4 and 5.5 below illustrate the determination of G_{in}, G_{out}, G'_{in} and G'_{out} from the nighttime trends in TSM and TSM_{top}. They demonstrate two types of behavior locally - either as a recharge zone (profiles E and C, with net outflow) or as a discharge zone (profiles F and B, with net inflow). The values of TSM_{top} and TSM were determined by trapezoidal integration using the discrete soil moisture and water table measurements, respectively.

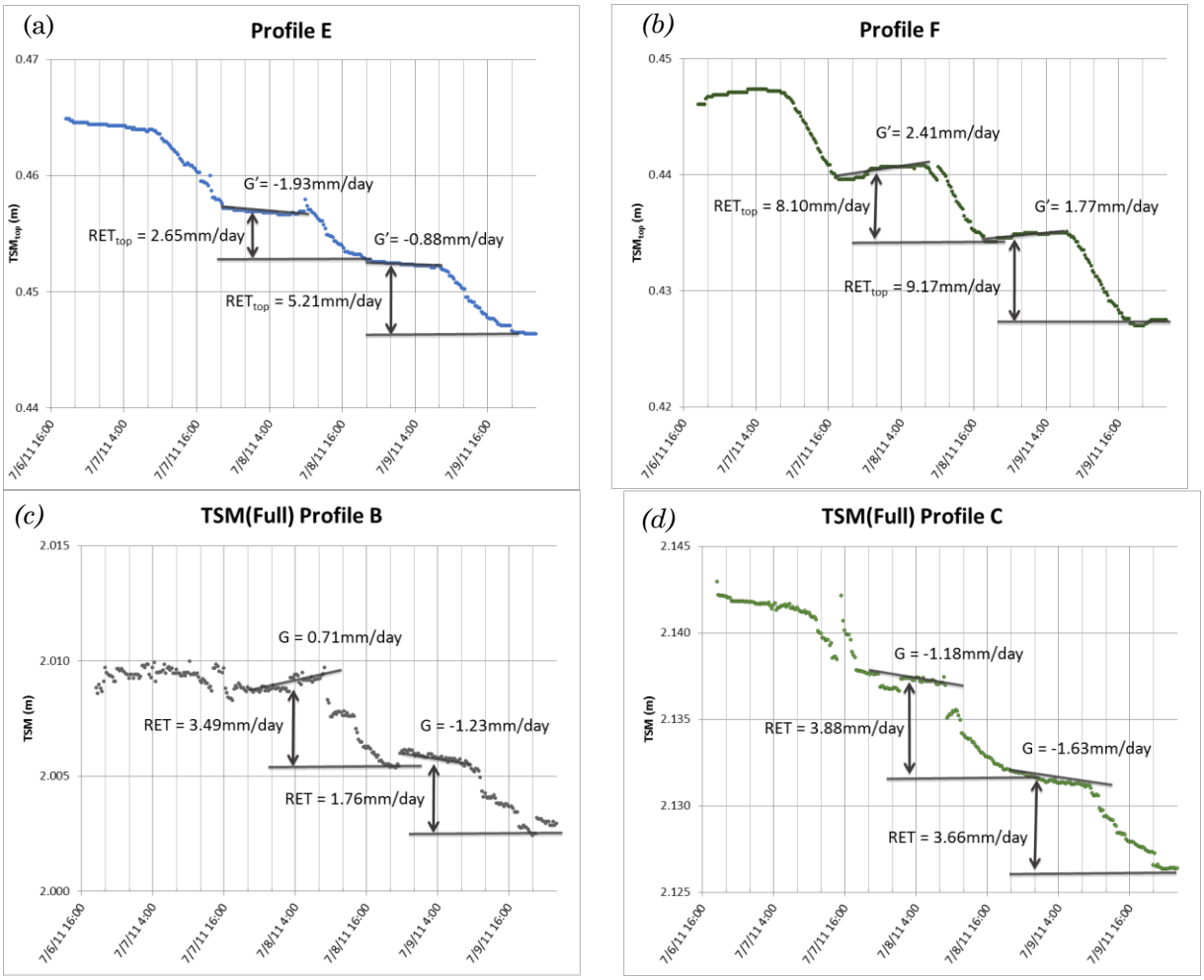

Figure 5. 4. Examples of estimated RET by looking at the TSM_{top} from two locations a) profile location E (upstream); b) profile location F (downstream); and examples of estimated RET by looking at the TSM_{full} from two locations c) profile location B (2nd furthest from stream); d) profile location C (3rd furthest from stream). The nighttime behavior is reasonably well approximated with a constant slope. Location F behaves like a discharge zone (exhibiting nighttime recovery in TSM_{top}, i.e. $G' = G'_{in} - G'_{out} > 0$), while locations E and C exhibits nigh-time decrease in TSM_{top} and TSM respectively, thus behaving like a recharge zone (i.e. G' or $G = G_{in} - G_{out} < 0$). At location B, the behavior is different across the different days. For the duration shown, it is behaving like a discharge zone with $G > 0$.

Figure 5.4 a and b demonstrate how the estimated RET was determined by using equation 5.4a where only soil moisture measurements were made, while Figure 5.4 c and d are based on equation 5.4b where both water table and soil moisture measurements are used. These figures include the slope of the soil moisture recovery during the night time from which the G' and G-values are determined. In the approach of Nachabe [2005] the recovery of the TSM is observed between midnight and 4AM to estimate G (this approach is labeled G'_1 in figures 5.6 and 5.7 below). One of the observable concerns that can be seen from using this soil moisture balance method is whether the estimated G_{in}, G_{out}, G'_{in} and G'_{out} values are sensitive to the duration of the night over which the slopes are determined. To address this concern two additional time durations were used. Figure 5.6 illustrates the estimation of G' for profile location F using three time duration approaches - the first approach was based on the TSM_{top} slope from midnight to 4AM, the second approach was based on the TSM_{top} slope from 8PM of the previous day to 8AM of current day (this approach is labeled G'_2) and the third approach that was based on the change in TSM_{top} from 10PM of the previous day to 6AM of the current day (this approach is labeled G'_3).

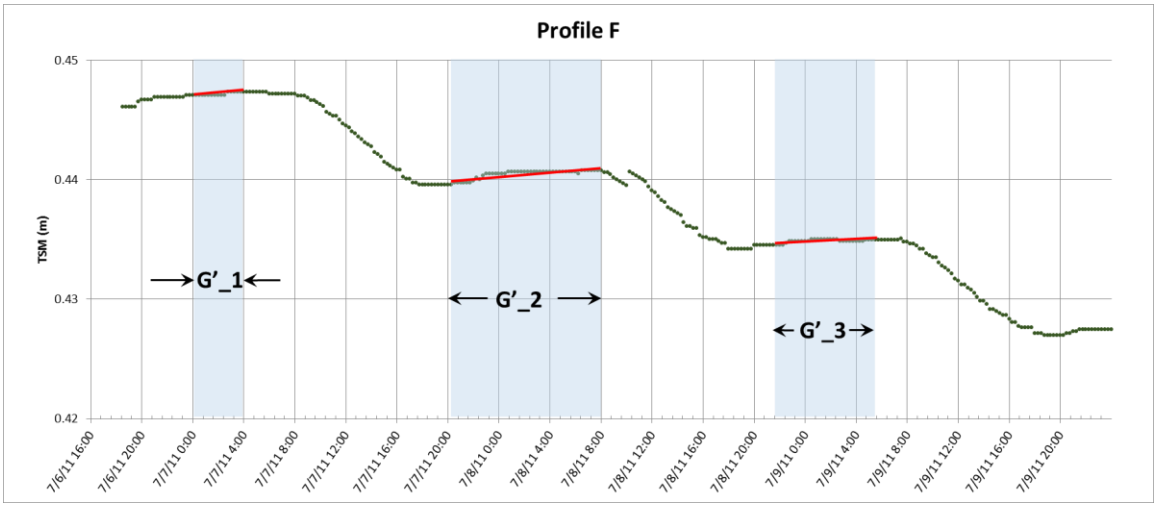

Figure 5. 5. Illustration of the three different time duration approaches for the estimation of G' or G-values. G'_1 represents a time duration from midnight to 4AM, G'_2 represents from 8pm of the previous day to 8AM of the current day and finally G'_3 represents from 10pm of the previous day to 6am of the current day.

A comparison of G' or G estimated obtained using the three different time durations is presented in the next chapter. The assumption of constant inflow/outflow over a 24-hour period is an acknowledged limitation of our approach. Although we acknowledge this assumption, we do recognize and estimate the inflow or outflow on daily basis where on some days there could be an inflow and on other days there could be an outflow. This approach accounts for the temporal variations. In general, the assumption of constant inflow/outflow over a 24-hour period is more likely to be valid in the case of G_{in}/G_{out} as opposed to G'_{in}/G'_{out} because groundwater response time are usually longer than vadose zone response times. However, for thick vadose zones as at our study site, representative soil moisture trends suggest that assuming constant G'_{in}/G'_{out} over a 24-hour period is a reasonable approximation. Any diurnal variation of G'_{in}/G'_{out} will lead to errors in the estimates of RET_{top}. Another limitation of the approach to estimating RET_{top} based on (5.3a) and (5.4a) is that any other diurnally varying flux will be mistakenly included as RET_{top}. One such diurnally varying flux is related to snowmelt: when there is a snowpack on the ground and no precipitation is recorded, but snowmelt occurs during the warmer daytime temperatures. In such situations, there will be an increase in TSM_{top}, and blind application of Equation (5.4a) would lead to the estimation of a negative RET. However, it is unlikely that RET and snowmelt are occurring simultaneously, since much of the snow and snowmelt occur outside the growing season. We were able to filter out these instances effectively.

CHAPTER VI

ANNUAL CYCLE AND ESTIMATES OF RIPARIAN EVAPOTRANSPIRATION

The following is a summary of the annual results at this study site for the different water balance variables. This includes precipitation (P), total soil moisture (TSM_{top} or TSM), groundwater inflow or outflow depending on its sign ($G'_{in/out}$ or $G_{in/out}$) and lastly the estimated RET as a residual. As previously discussed in Chapter V, the total soil moisture was derived by using equations 5.4a and 5.4b depending on the availability of groundwater data at the specific profile location. In order to be consistent in comparing all the profiles with each other, the calculated total soil moisture was calculated between the ground surface and the lowest sensor (TSM_{top}). In the remainder of this chapter, total soil moisture will be referred to as total soil moisture or TSM (used interchangeably with TSM_{top}, which is the most extensively analyzed variable here). Additionally, the variables TSM_{total} will be used to refer to the total soil moisture down to the water table.

6.1 Precipitation

Precipitation varied from year to year, and significant differences between the different years covered by the study are that 2012 was an extremely dry year, especially during the growing season; and 2013 was a very wet year. Figure 6.1 below shows the monthly precipitation over the entire research period. Total annual precipitation was 237 mm in 2010 (measurements began in July of 2010 and the entire year was not measured), 366 mm in 2011, 198 mm in 2012, and 524 mm in 2013. These measurements were done by using the rain gage from the weather station at the study site and seem to have some discrepancies when compared to the National Weather Service (NWS,

http://water.weather.gov/precip/) precipitation data. Where, measured values are lower than those reported by the NWS.

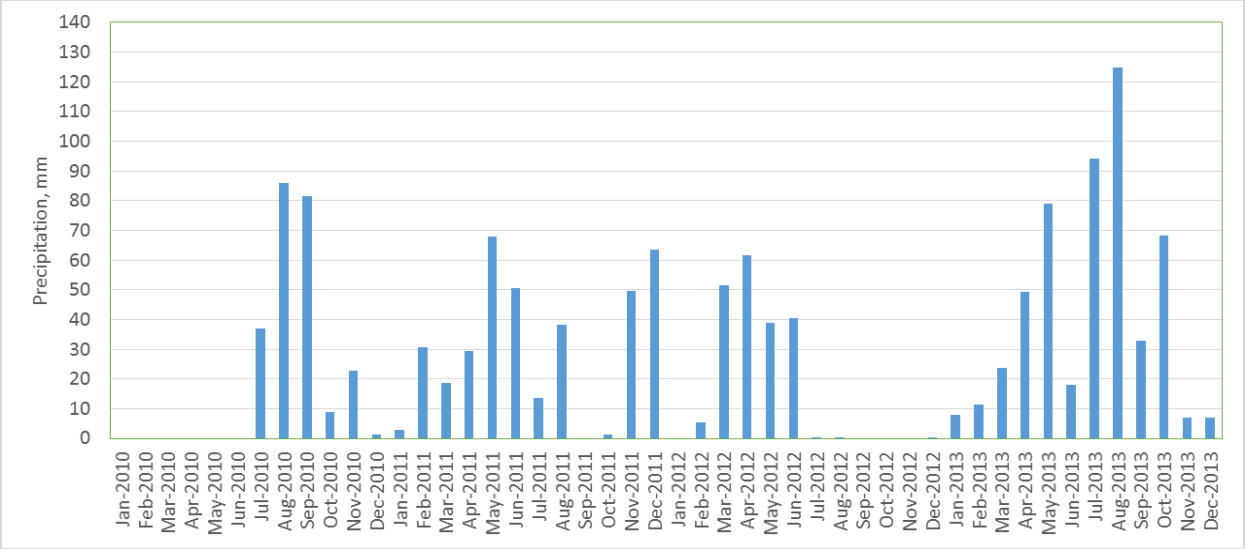

Figure 6. 1. Monthly precipitation for the entire research period, 2010 through 2013.

6.2 Total Soil Moisture, TSM

Figures 6.2 through 6.5 show the combined TSM_{top} trends from each profile location throughout the entire research period (2010-2013; 3.5 years). Figures 6.2 to 6.4 show the TSM_{top} trends for 2012-2014 respectively. Unlike the previous years, in 2013 the only available data was for profiles A, B, E, and F; these are shown in figure 6.5. The precipitation is included along with the derived TSM_{top} values in the figures. The precipitation values generally explain the sharp increases in TSM_{top} at several times throughout the year. Many smaller TSM spikes corresponding to lower precip events are not accompanied by precipitation events as recorded by the rain gage at the study site. There are discrepancies between the rain gage data from the study site and the NWS precipitation data. However, these discrepancies do not alter the qualitative

interpretations of TSM trends in the remaining chapters. However, quantitative estimation of RET by water balance will no doubt be influenced by the magnitude of the precipitation events and any biases between the site-specific and NWS data. The monthly RET estimates presented in Chapter VI reflect the influence of this discrepancy. However, the choice of the three periods in each year (analysis reported in Chapter VII) intentionally avoided durations with any precipitation events. Thus, we believe that errors in the precipitation data do not influence the quantitative estimates of RET during these periods

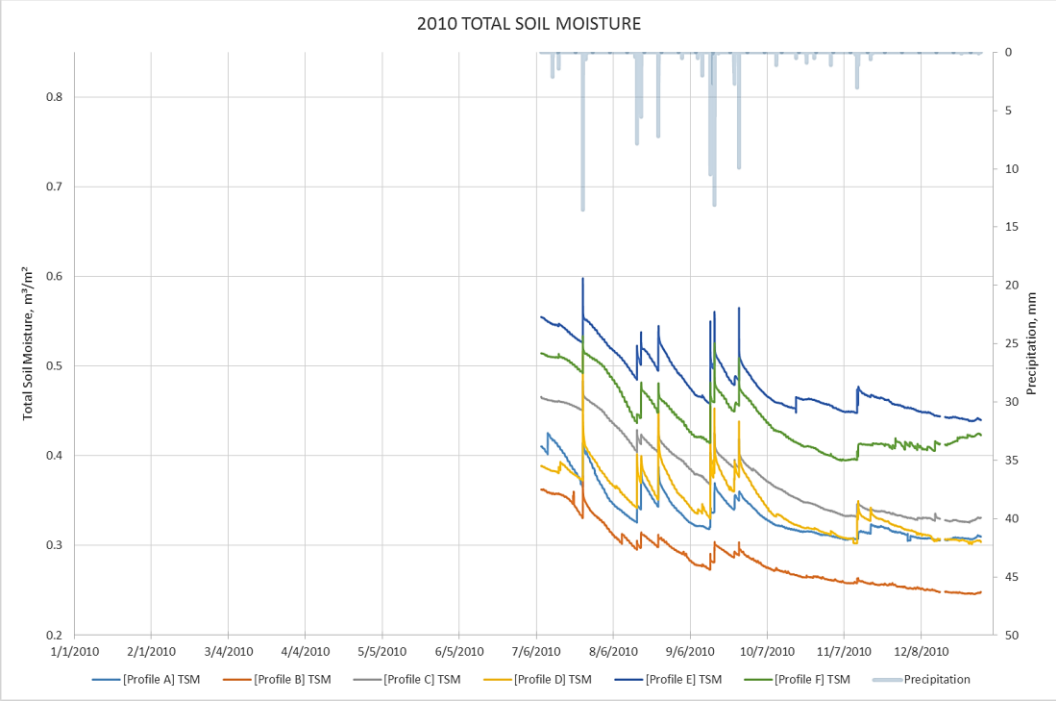

Figure 6. 2. Total soil moisture for all profiles (A, B, C, D, E, F) and precipitation during 2010.

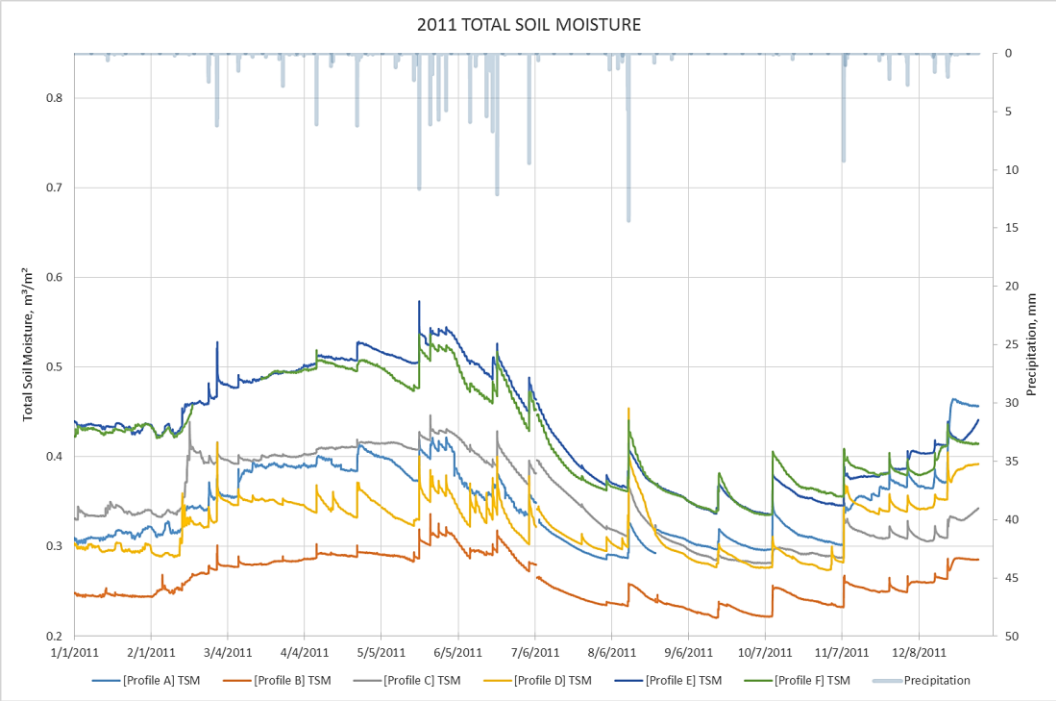

Figure 6. 3. Total soil moisture for all profiles (A, B, C, D, E, F) and precipitation during 2011.

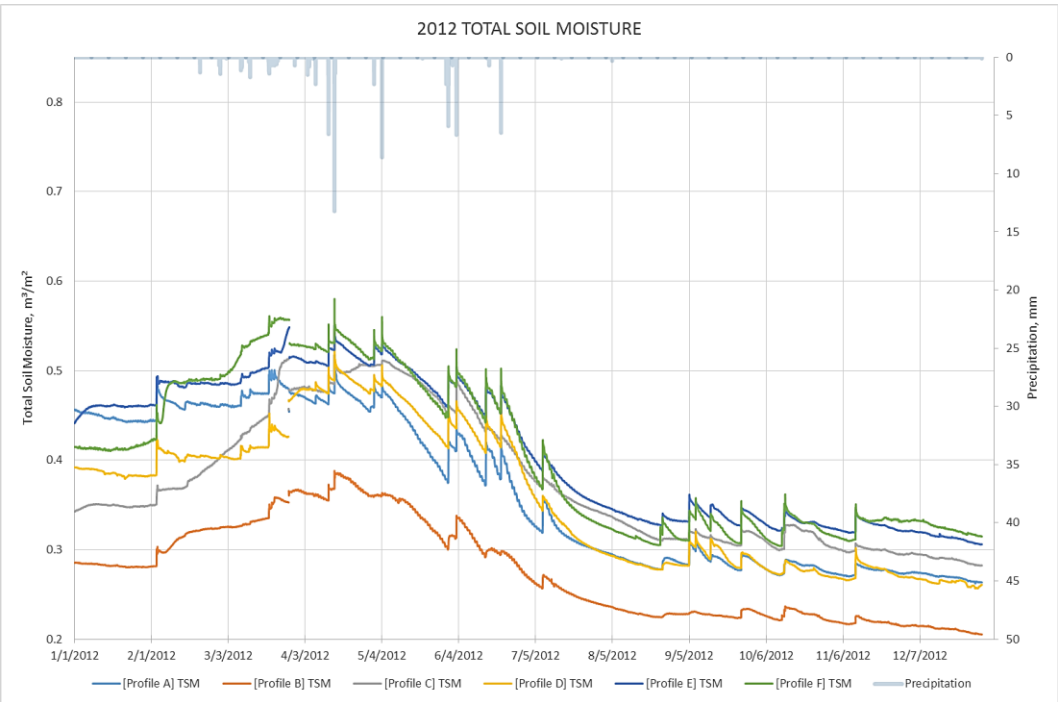

Figure 6. 4. Total soil moisture for all profiles (A, B, C, D, E, F) and precipitation during 2012.

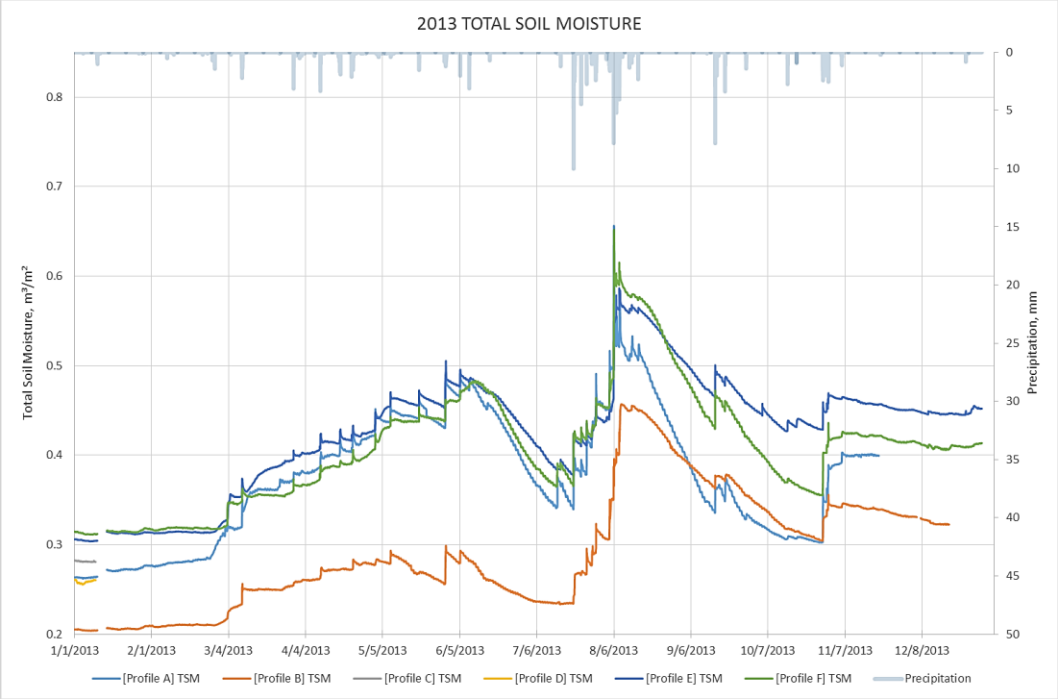

Figure 6. 5. Total soil moisture for all profiles where data was available (A, B, E, F) and precipitation during 2013.

In addition to the above figures, tables 6.1 and 6.2 also show a summary of the annual change in total soil moisture (ΔTSM_{top}).

Table 6. 1. Annual change in total soil moisture at each profile location along with the average of all the profiles and yearly measured precipitation (2010 measurements are not for the entire year).

Profile Location	2010 (Jul-Dec) ΔTSM (mm)	2011 (Jan-Dec) ΔTSM (mm)	2012 (Jan-Dec) ΔTSM (mm)	2013 (Jan-Dec) ΔTSM (mm)
Profile A	-101	147	-193	136*
Profile B	-114	37	-80	118
Profile C	-135	12	-88	No Data Available
Profile D	-85	88	-189	No Data Available
Profile E	-115	1	-135	146
Profile F	-91	-8	-100	99
Average:	-107	31	-117	125
Precipitation	237	366	198	524

**only up to the end of November*

Table 6. 2. Annual summaries for minimum, maximum, average, and total annual change in total soil moisture spatially across all profile locations (2010 measurements are not for the entire year).

TSM	Year 2010		Year 2011		Year 2012		Year 2013	
min | max | avg (VALUE)	TSM (mm)	Profile location	TSM (mm)	Profile location	TSM (mm)	Profile location	TSM (mm)	Profile location
Highest TSM	555	E	540	E	542	F	600	F
Lowest TSM	362	B	315	B	205	B	203	B
Highest ΔTSM	-85	C	147	C	-80	B	146	E
Lowest ΔTSM	-135	D	-8	F	-193	A	99	F
Average TSM at beginning of Year (mm)	449		343		389		272	
Average TSM at end of Year (mm)	343		389		272		404	
Total Change in Moisture (mm)	-106		46		-117		132	

The figures and tables presented above suggest that there is substantial inter-annual and spatial variability across all the profile locations. Comparing 2011 through 2013 shows that 2012 was the driest of the all the years and 2013 was the wettest. Correspondingly there is a net loss in soil moisture storage in 2012 at all profile locations, whereas there is a general gain in soil moisture storage in the other two years. At this study site, it was also interesting to note when the soil water replenishment and or recovery occurred. The recovery tended to be highest during the spring, between around March and May on a consistent basis. In 2013, a relatively dry winter and spring led to low total soil moisture values, which began to recover as a result of several small precipitation events in late spring/early summer. Subsequently a rapid drying occurred during a dry spell in June and there was significant late summer increase in soil moisture due to higher than normal precipitation events in July and August. Continued precipitation events in the fall resulted in persistence of high soil moisture through the end of the year. It is interesting to note that the general trends of the TSM_{top} are similar across all profile locations, although the individual soil moisture values are different.

Table 6.2 summarizes the overall dynamics across the profile locations on an annual time scale showing which profiles had the highest and lowest TSM_{top}-values. The highest TSM_{top}-value was seen in profile E for 2010 and 2011, and for 2012 and 2013 the highest value was from profile F. The lowest TSM_{top}-value was consistently seen in profile B over the entire research period. The profile locations at which the maximum and minimum annual change in total soil moisture (ΔTSM) occurred varied from year to year. The highest ΔTSM-value was seen in profile C for 2010 and 2011. For 2012 and 2013 profiles B and E had the highest ΔTSM-value, respectively. The lowest ΔTSM-value occurred in profiles D

for 2010, F for 2011, A for 2012 and again in F for 2013. There was a net loss of 106 mm of TSM on average across all profile locations in 2012. There was a net soil moisture gain of 132 mm for 2013 meaning that there was a higher soil moisture at the end of the year than at the beginning. In 2011 there was also a gain but only by a slight increase of 12%.

Other figures showing annual normalized total soil moisture are included in appendix C titled "Normalized Total Soil Moisture Time Series". These figures compare the TSM with each other in relation to one another by fixing the initial TSM value at the beginning of the year and looking at the change in TSM throughout the year. What this helps visualize is the net total change in TSM from all the profiles in relation to each other. Additional annual time-series plots of individual soil moisture measurements from each profile are also shown in the appendix where they show how the soil moisture over depth varied through the year.

6.3 Groundwater inflow(+) / outflow (−), $G'_{in/out}$

As mentioned in the previous chapter, three different nighttime intervals were evaluated for estimating groundwater inflow/outflow. Figures 6.6 through 6.11 shown below illustrate the variability of the estimated groundwater inflow/outflow. Since there is substantial variability in groundwater inflow/outflow rates from day to day, we decided to examine the monthly-averaged G'-values to determine general trends in the behavior of groundwater inflow/outflows. It should also be noted that since the G'-values here are based on TSM_{top}, they could also represent net vertical flows at the depth corresponding to the lowest sensor in each profile (i.e. infiltration - loss of TSM_{top} or exfiltration - gain of TSM_{top}).

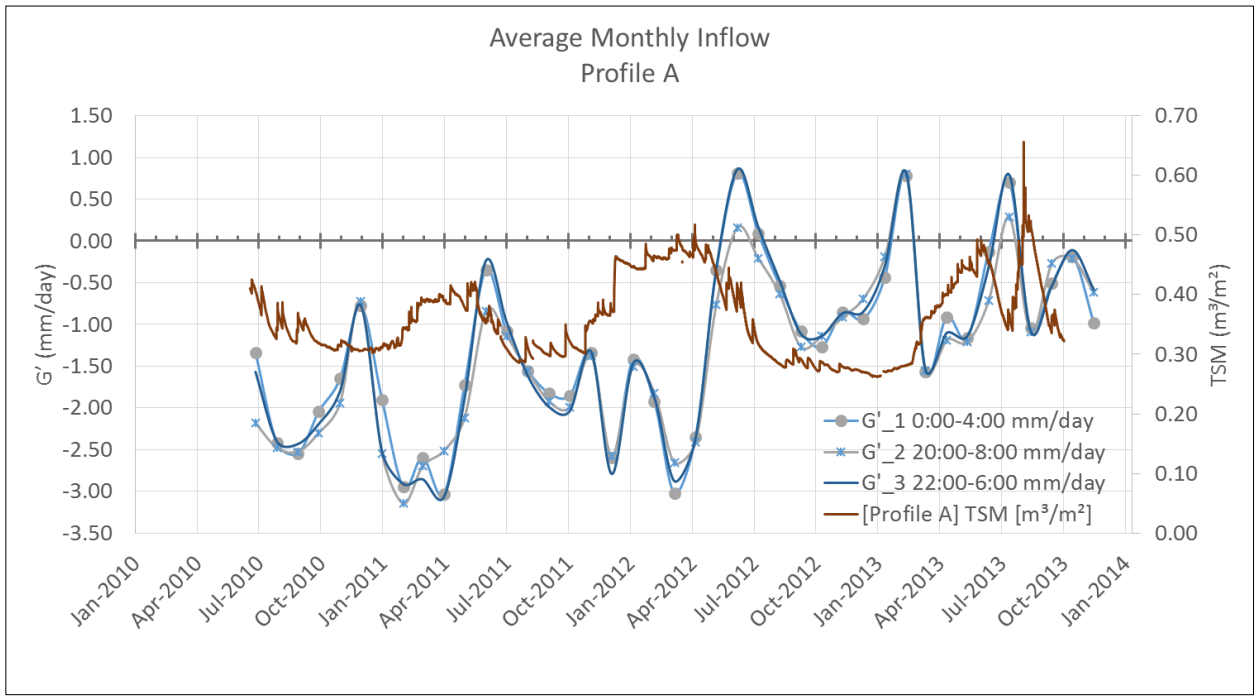

Figure 6. 6. Average monthly inflows comparison and TSM for Profile A during the entire research period.

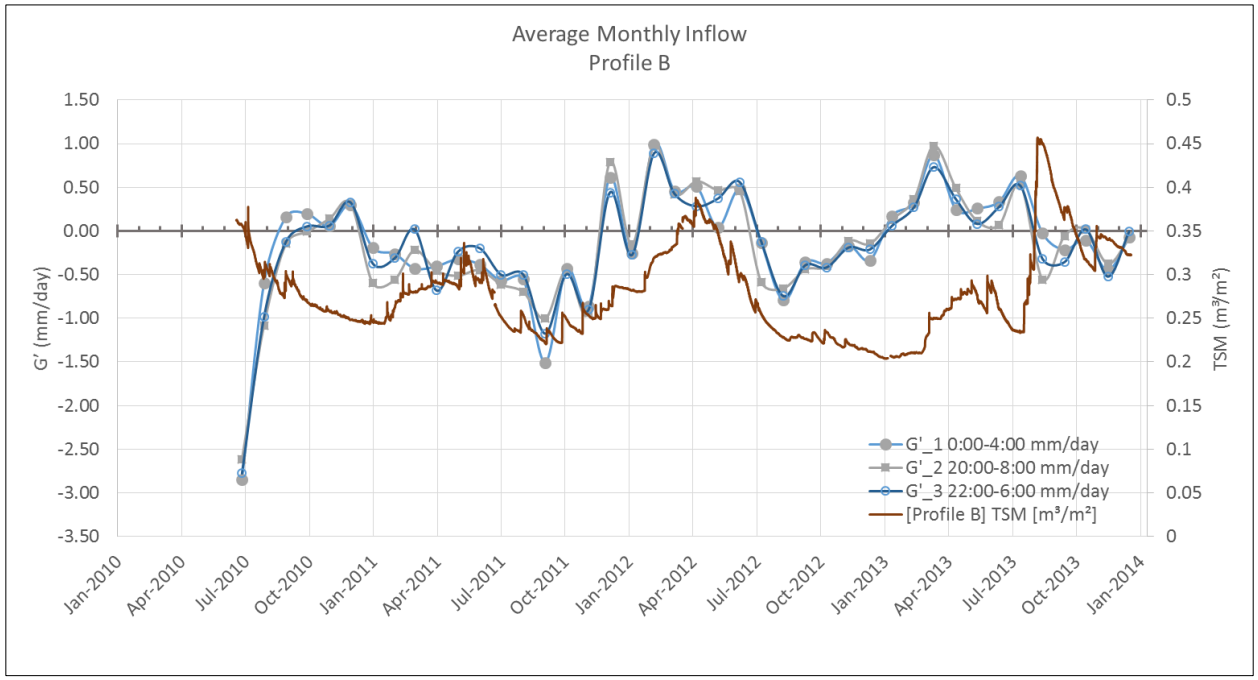

Figure 6. 7. Average monthly inflows comparison and TSM for Profile B during the entire research period.

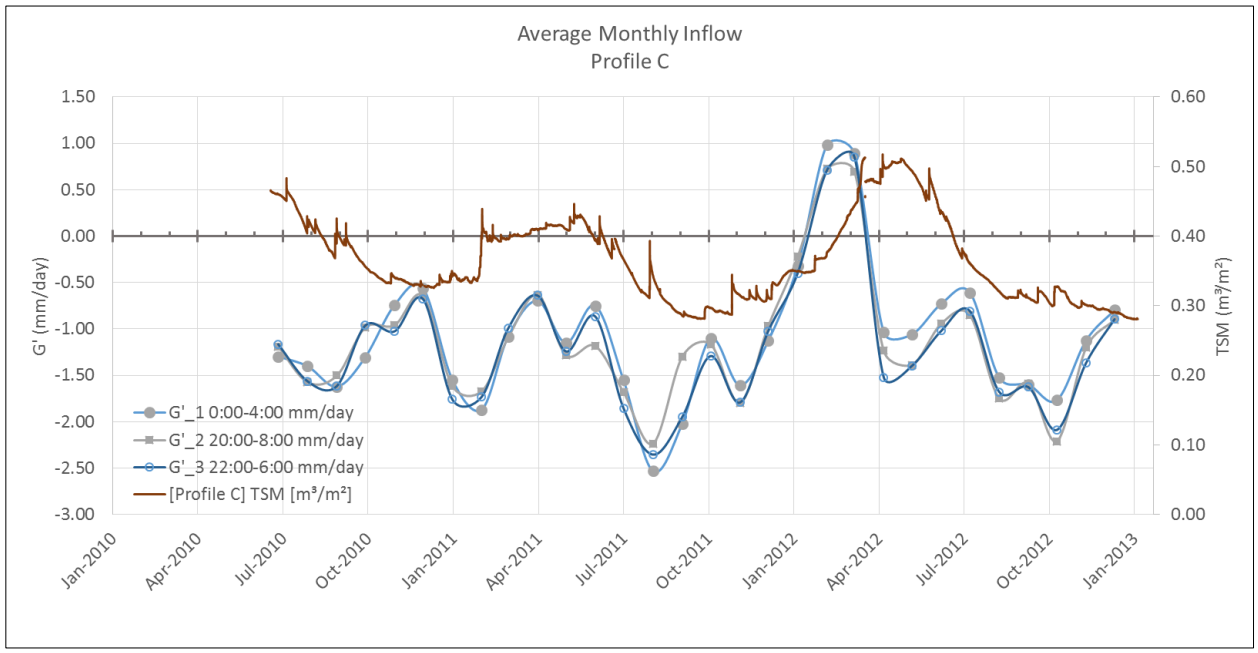

Figure 6. 8. Average monthly inflows comparison and TSM for Profile C during the entire research period.

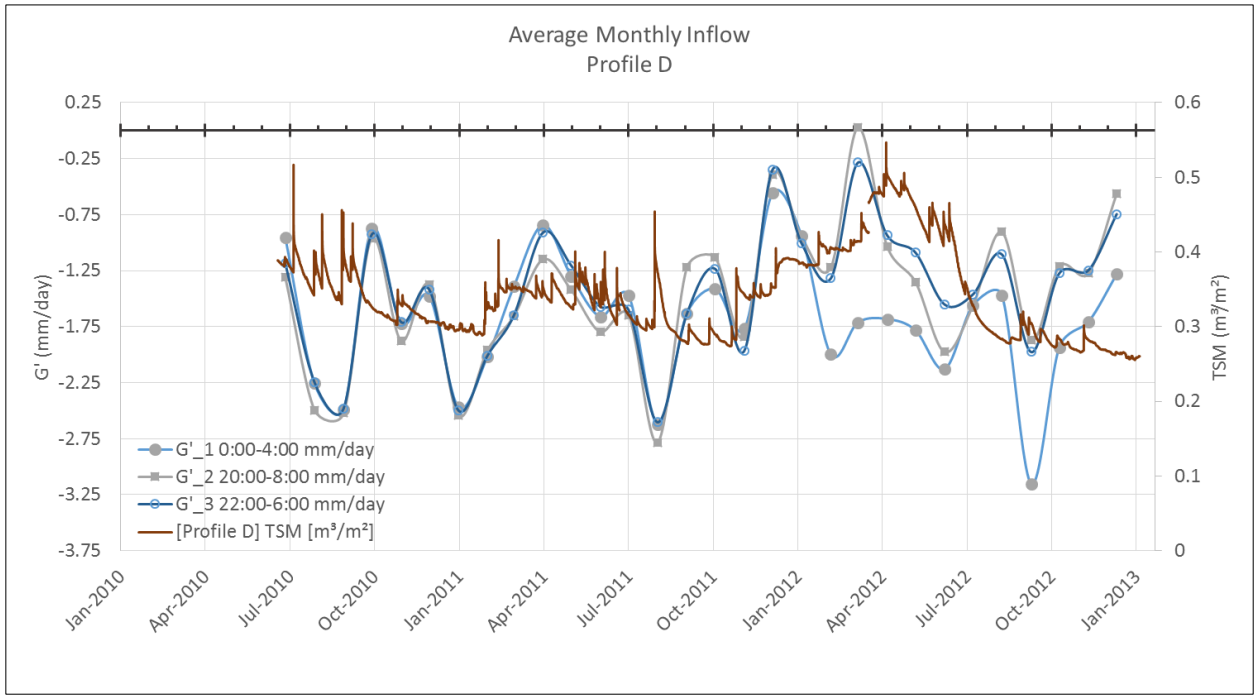

Figure 6. 9. Average monthly inflows comparison and TSM for Profile D during the entire research period.

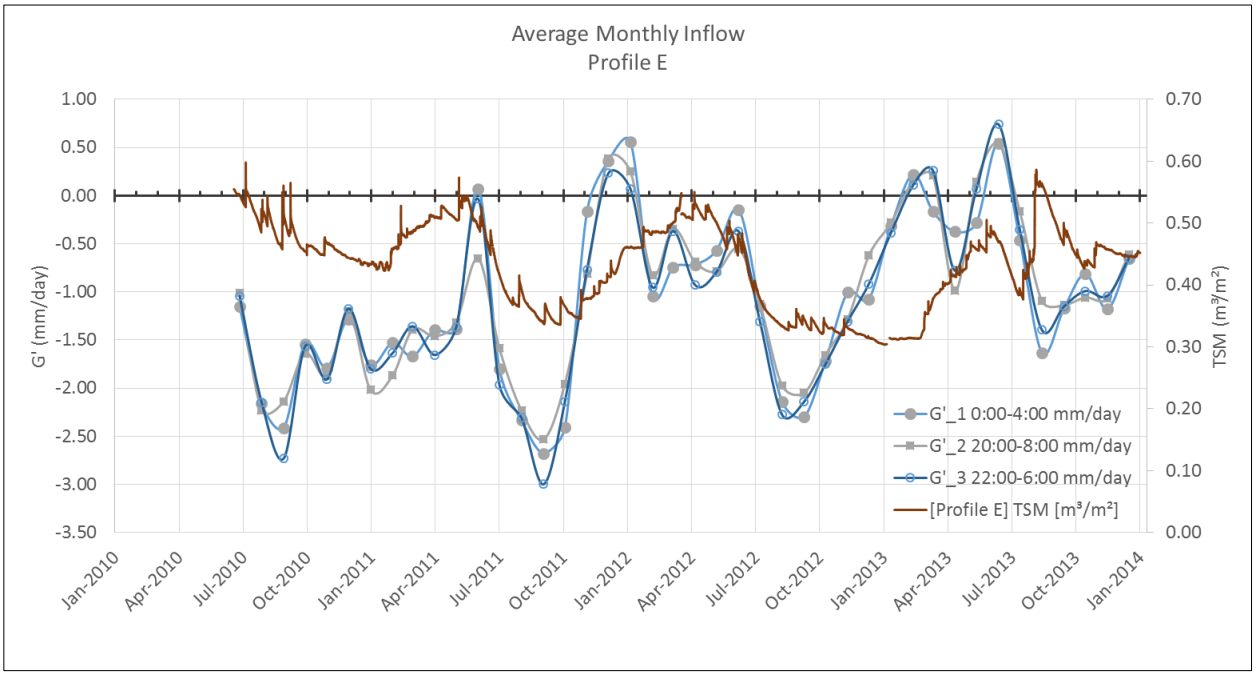

Figure 6. 10. Average monthly inflows comparison and TSM for Profile E during the entire research period.

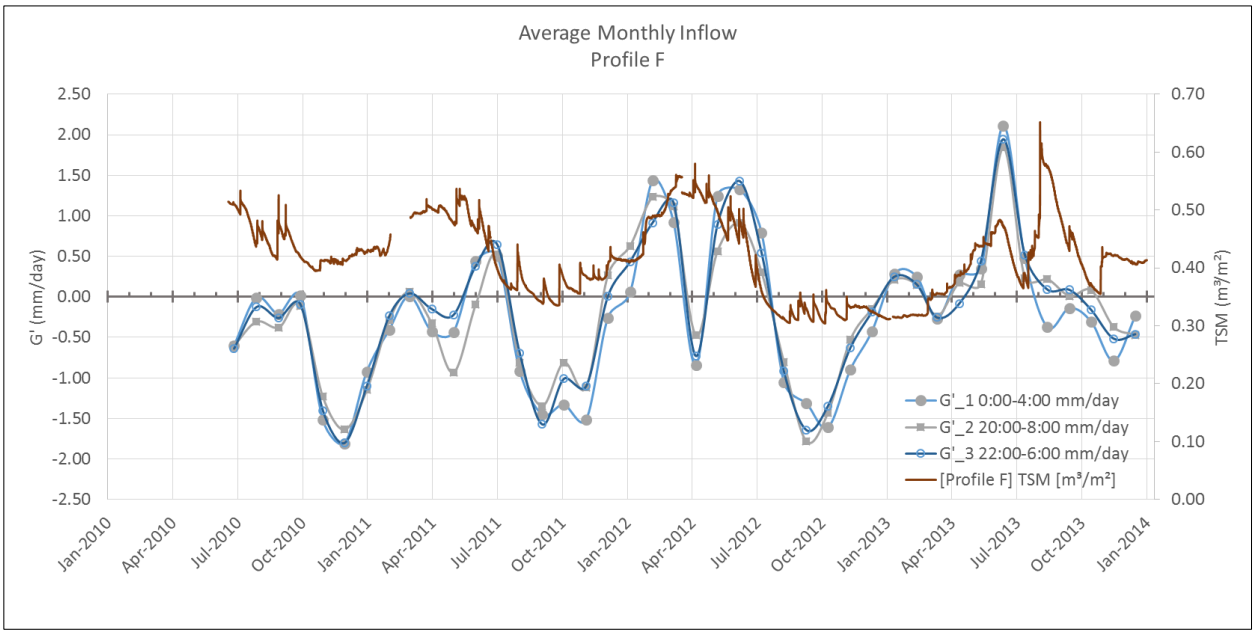

Figure 6. 11. Average monthly inflows comparison and TSM for Profile F during the entire research period.

The above figures indicate there is not much variation between the G' estimates obtained using the three different nighttime intervals. The nature of G' provides insights into the hydrogeologic behavior at the different profile locations. During the summer growing season, profiles A, C, D and E tend to behave more like recharge zones (the G'-values are mostly negative), whereas profiles B and F (and to a small extent profile E) behave like discharge zones (positive G' values). There are unique characteristics at each profile as can be seen in the summary table 6.3 shown below.

Table 6. 3. Minimum, maximum and average $G'_{in/out}$ values for of the profiles corresponding to the figures 6.6 through 6.11.

Profile Location	Minimum $G'_{in/out}$ (mm/day)	Maximum $G'_{in/out}$ (mm/day)	Average $G'_{in/out}$ (mm/day)
Profile A	-3.08	0.82	-1.31
Profile B	-2.75	0.95	-0.16
Profile C	-2.37	0.85	-1.13
Profile D	-2.85	-0.27	-1.52
Profile E	-2.74	0.62	-1.09
Profile F	-1.80	1.97	-0.20

The average values of G' in Table 6.3 reveal that on average, all profile locations behave like recharge zones, which is consistent with the general behavior of thick vadose zones. During the growing season, some of the profile locations (B and F) act like discharge zones with a net nighttime increase in TSM_{top}, likely representing exfiltration, which supplies evapotranspiration at these locations.

6.4 Riparian Evapotranspiration Estimation, RET

RET was estimated on an annual time scale using the soil water balance as shown previously in equation 5.3a and 5.3b. Days with precipitation events, and outliers (values that were outside of the normal range) were filtered out. Monthly RET estimates were calculated as a monthly average of daily RET calculated for all days of the particular month, which are shown in figures 6.12 through 6.15. RET estimates were only obtained for the growing season, when RET values are positive. The American Society of Civil Engineers (ASCE) standardized reference evapotranspiration equation (ET_{sz}) [Allen et al. 2005], which corresponds to uniformly dense, well-watered (not short of soil water) short crop that is similar to a clipped grass (approximate height of 0.12 m) and is actively growing over a distance of at least 100 m, was used as a baseline to show the maximum amount of ET that could occur for meteorological conditions based on the weather station data from the site.

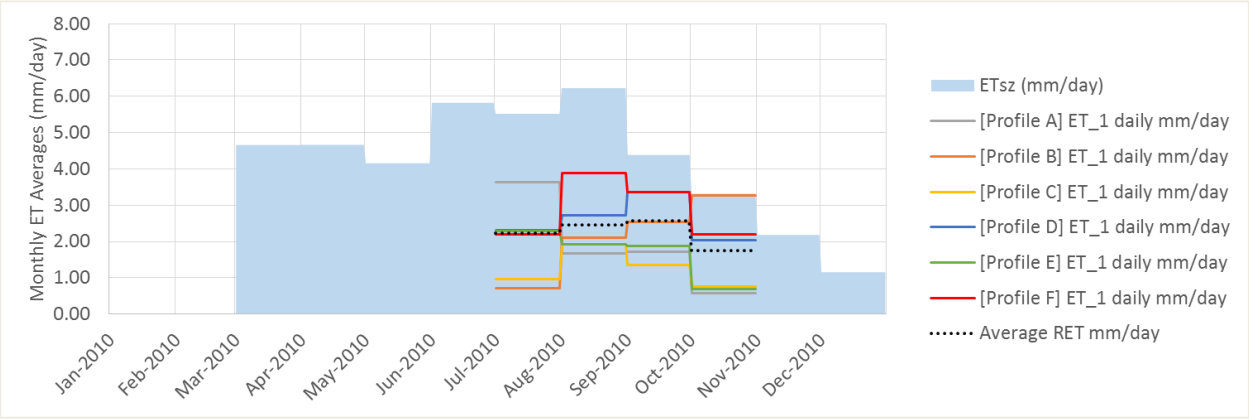

Figure 6. 12. Daily RET estimates averaged over each month for all the profiles during the growing season and the ASCE standardized reference evapotranspiration (ET_{sz}) in 2010. The colored lines represent the profiles, the dotted line the average of all profile locations, and the light blue shaded area is the ET_{sz}.

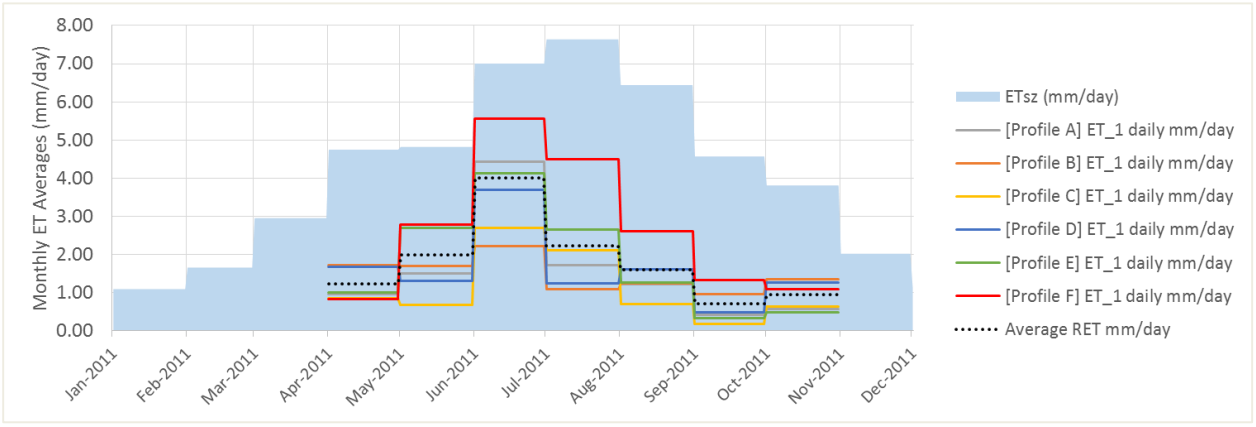

Figure 6. 13. Daily RET estimates averaged over each month for all the profiles during the growing season and the ASCE standardized reference evapotranspiration (ET_{sz}) in 2011. The colored lines represent the profiles, the dotted line the average of all profile locations, and the light blue shaded area is the ET_{sz}.

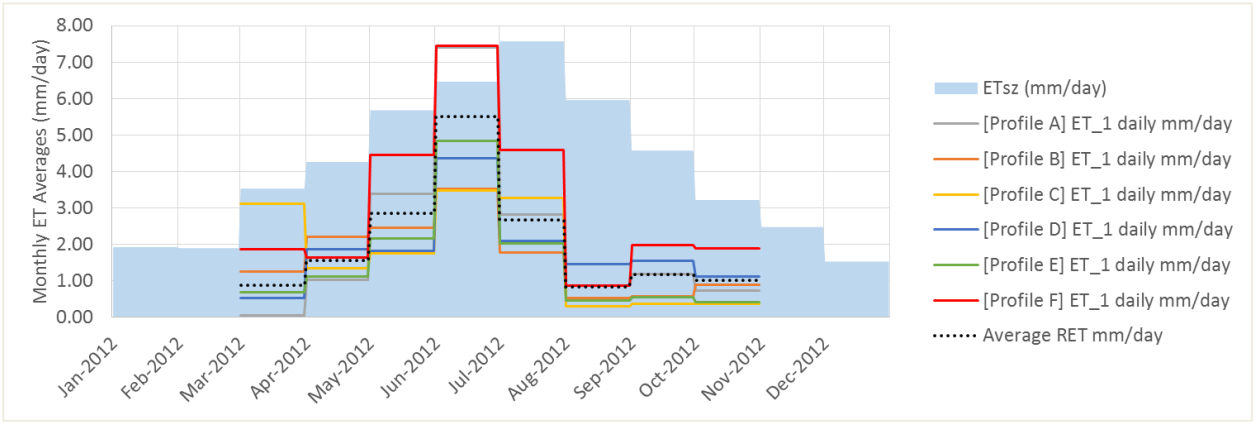

Figure 6. 14. Daily RET estimates averaged over each month for all the profiles during the growing season and the ASCE standardized reference evapotranspiration (ET_{sz}) in 2012. The colored lines represent the profiles, the dotted line the average of all profile locations, and the light blue shaded area is the ET_{sz}.

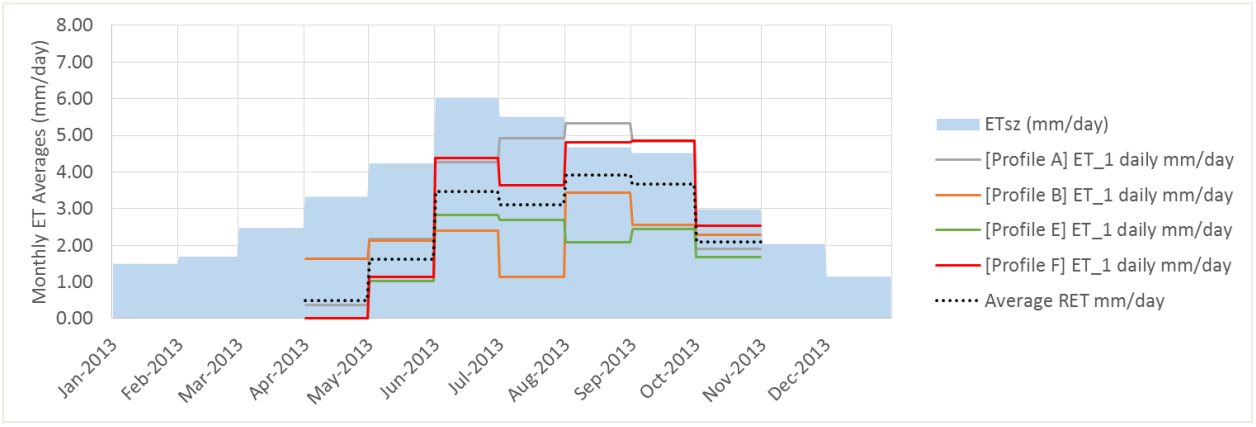

Figure 6. 15. Daily RET estimates averaged over each month for all the profiles during the growing season and the ASCE standardized reference evapotranspiration (ET_{sz}) in 2013. The colored lines represent the profiles, the dotted line the average of all profile locations, and the light blue shaded area is the ET_{sz}.

A more in depth analysis and comparison of the results from the previous figures is shown in Tables 6.4 through 6.7. Table 6.4 shows the percentage of days during the growing period that were available for comparison after filtering out days with precipitation and other outliers at each profile location. The growing period was determined was by computing the growing degree days (GDD) which is determined by using the following equation [McMaster and Wilhelm 1997]:

Equation (6.1)

$$GDD = \frac{T_{max} + T_{min}}{2} - T_{base}$$

Where, T_{max} is the maximum temperature of the day and T_{min} is the minimum temperature of the day, and the T_{base} is the base temperature for the particular vegetation that is being grown. At this particular site the vegetation consisted of riparian vegetation such as cottonwood trees (populus, spp.), willow trees (salix spp.) among other hardwood trees. A base temperature value of 10℃ was used [Zalesny et al. 2004]. In general, GDD extends between the last freeze at the end of winter and the first freeze at the beginning of winter. Since data collection started on 7/8/2010 the RET values were only estimated up until

10/31/2010 for 2010. In 2011 the growing season extended from 4/5 to 10/17, and in 2012 it extended from 3/12 to 10/4. For 2013 the growing season started somewhat late in comparison to the previous years, beginning on 4/25 and ending around 10/14. The total number of GDD is shown at the top-left of each table. The filtered GDD for every profile consists of days where no precipitation occurred, and also involved filtering out outliers. The annual RET estimates from each profile consisted of the summation of filtered RET values for that particular year. The reported ETsz values consisted of the summation of filtered ETsz values for the same days that remained after filtering.

Table 6. 4. Yearly summary of estimated RET from all profile locations and comparison to the ETsz and percentage of filtered GDD for 2010.

YEAR 2010 Total No. of GDD 116	Filtered GDD (days)	% of filtered GDD $\frac{Filtered\ GDD_{profile}}{GDD_{total}}$	RET (mm)	ETsz (mm)	% of ETsz $\frac{RET_{profile}}{ET_{sz}}$
Profile A	60	52%	129	354	36%
Profile B	65	56%	151	344	44%
Profile C	77	66%	104	411	25%
Profile D	82	71%	210	441	48%
Profile E	68	59%	125	394	32%
Profile F	93	80%	279	485	58%
Average	74	64%	166	405	41%

Table 6. 5. Yearly summary of estimated RET from all profile locations and comparison to the ETsz and percentage of GDD of filtered estimates for 2011.

YEAR 2011 Total No. of GDD 196	Filtered GDD (days)	% of filtered GDD $\frac{Filtered\ GDD_{profile}}{GDD_{total}}$	RET (mm)	ETsz (mm)	% of ETsz $\frac{RET_{profile}}{ET_{sz}}$
Profile A	80	41%	172	534	32%
Profile B	84	43%	138	579	24%
Profile C	61	31%	104	428	24%
Profile D	99	51%	177	652	27%
Profile E	67	34%	173	472	37%
Profile F	119	61%	379	764	50%
Average	85	73%	191	572	33%

Table 6. 6. Yearly summary of estimated RET from all profile locations and comparison to the ETsz and percentage of GDD of filtered estimates for 2012.

YEAR 2012 Total No. of GDD 207	Filtered GDD (days)	% of filtered GDD $\frac{Filtered\ GDD_{profile}}{GDD_{total}}$	RET (mm)	ETsz (mm)	% of ETsz $\frac{RET_{profile}}{ET_{sz}}$
Profile A	124	60%	386	804	48%
Profile B	114	55%	264	748	35%
Profile C	82	40%	211	556	38%
Profile D	112	54%	273	702	39%
Profile E	105	51%	245	673	36%
Profile F	140	68%	524	876	60%
Average	113	97%	317	727	44%

Table 6. 7. Yearly summary of estimated RET from all profile locations and comparison to the ETsz and percentage of GDD of filtered estimates for 2013.

YEAR 2013 Total No. of GDD 173	Filtered GDD (days)	% of filtered GDD $\frac{Filtered\ GDD_{profile}}{GDD_{total}}$	RET (mm)	ETsz (mm)	% of ETsz $\frac{RET_{profile}}{ET_{sz}}$
Profile A	110	64%	464	615	75%
Profile B	116	67%	292	682	43%
Profile C	No Data	No Data	No Data	No Data	No Data
Profile D	No Data	No Data	No Data	No Data	No Data
Profile E	108	62%	255	621	41%
Profile F	112	65%	452	624	72%
Average	112	96%	366	636	58%

Profile location F showed the highest estimated RET more or less consistently, except in 2013, when RET estimated at profile F is slightly lower than that at Profile A. This result made sense since the vegetation was very lush and green with smaller grasses covering the ground and a full canopy from the larger trees at Profile F. Profile locations B and C showed lower RET estimates, which coincided with the surrounding profile area where a full canopy was not present, and smaller vegetation.

6.5 Discussion

6.5.1 Heterogeneity across profile locations

It is evident from the results that there is significant heterogeneity across all profiles both spatially and with depth in each profile. This is particularly surprising because the profile locations are relatively close to each other. Profile location F and B behave as discharge zones while the RET estimates at location F are much higher than RET estimates than profile B. Profile location D always behaves as a recharge zone, which makes sense since it is the location furthest away from the stream and at the edge of the riparian zone. The remaining profiles behaved mostly as recharge zones. In addition, the RET estimates along with the TSM_{top} and G' results varied significantly among the different profile locations. The G'-values exhibited the highest variability when compared to the other water balance variables. During the growing season G' ranged from minimum of -3 mm/day seen at profile A to a maximum of 2 mm/day seen at profile F.

6.5.2 Inter-annual variability

As noted above there is significant inter-annual variability in the total soil moisture trends. The year 2013 started off as a very dry year due to the drought that had occurred in 2012, but later around August of 2013 a higher than average series of precipitation events replenished the riparian's zone soil water. Replenishment usually occurs at the beginning of the year (January to around May), rather than towards the latter part of the growing season.

6.5.3 Comparison to other sites

This study site consisted of a relatively deep vadose zone with low permeability soils, and a perched aquifer that is recharged in a variety of ways, either from snow melt, high precipitation events or potentiometric head difference from the deeper bedrock groundwater system. A summary of RET estimates and measurements is compiled in table 6.8, showing the general rate of RET for similar riparian vegetation at distinct locations. These results from previous studies help confirm that the RET estimates from this study site and our methodology are reasonable.

Table 6. 8. Comparative riparian evapotranspiration results from various locations and authors. Describes the vegetation type, the location of where the measurements were made, the depth to water table, evapotranspiration derived from groundwater measurements and the corresponding citation†.

Vegetation	Location	Depth to Water Table, m	ET_{gw}, mm/yr	Reference
Oak savanna	Iowa, USA	0.5–2.5	404	Schilling and Jacobson [2009]
Prosopis flexuosa	western Argentina	6–15	200–300	Jobbágy et al. [2011]
Prosopis velutina (woodland)	Arizona, USA	Avg. of 10	475–517	Scott et al. [2008][(a)]
Sporobolus wrightii (grassland)	Arizona, USA	Avg. of 5.3	330–403	Scott et al. [2008][(b)]
Shrubland	Arizona, USA	Avg. of 2.5	340–421	Scott et al. [2008][(c)]
Mixed Wetland vegetation	Florida, USA	0.6-.8	106–746	Rahgozar et al. [2012]
Forest vegetation (slash pine/hardwood trees)	Florida, USA	0.5-1.3	178–816	Rahgozar et al. [2012]
Pasture grass to a mixture of Forest vegetation (Mixture of Quercus spp. and Acer spp.)	Florida, USA	0-1.2	700 - 1320	Nachabe et al. [2005]
Populus spp. and *Salix spp.*	Arizona, USA	0.5-2	755	Williams and Scott [2009][(a)]
Populus spp.	Arizona, USA	1.6	966	Williams and Scott [2009][(b)]
Populus spp.	Arizona, USA	3.3	410 r	Williams and Scott [2009][(c)]
Mixed Riparian Vegetation *(Populus spp., salix spp., Acer spp,* among others)	Kansas, USA	2-4	191-366	Current Study Solis J. A. Dissertation [2015]

†This table was modified from Orellana et al. [2012]

The majority of the RET estimates included water table measurements. Although water table measurements were made in our study, the measurements were limited to only a few profile locations as mentioned in the previous chapter (see appendix F for annual hydrographs). Even though the estimated RET was only derived from TSM top measurements that cover the upper 2 m beneath the ground surface, they compare well with previous studies as shown above.

Scott et al. [2008][a] reported ET_{gw} values of 517, 477, and 475 mm/yr based on precipitation, soil water storage and ET derived from remote sensing measurements, for 2003, 2004, and 2005 respectively. Their study was for woodland vegetation similar to this research site, in a semi-arid climate in Arizona. The estimated RET for our site ranged from a minimum of 104 mm/yr (profile C, 2011) to a maximum of 524 mm/yr (profile F, 2013) at a given profile location and an average of 291 mm/yr for the three years (2011, 2012, and 2013). The amount of precipitation at the Scott et al. [2008] site averaged to 232 mm/yr compared to 363 mm/yr at our site. At their study site, the annual ET_{gw} variability was much smaller (annual ET_{gw} ranged from 475-517 mm for the three years, range 42 mm) than the variability at our site (profile annual reach average RET ranged from 191-366 mm across the three years, range 175 mm).

6.5.4 Limitations

There are potential errors in the above estimates of RET. The soil moisture profile sensors only reach to a maximum depth that ranges between 1.42-1.75 m, depending on the location of the profile. Depending on the water-table level, a substantial part of the vadose zone often exists from the deepest soil-moisture sensor to the top of the water table (~1 m of depth not being measured). The TSM is estimated by using the trapezoidal integration and an associated linear interpolation between sensors may not capture the more complicated variations reflected in the soil moisture profile as previously shown in Chapter IV, which is also a source of error. Another potential source of error is the limited number of water-table wells and the substantial heterogeneity in the permeability of the shallow alluvium at each location. Although five water-table wells exist in the study area, only two show relatively

rapid responses to changes in hydrologic conditions. These two are located where a saturated gravel zone exists near the water table. In addition, the hydraulic conductivity and piezometric head vary among the six alluvium base wells, although, in general, the aquitard acts similarly at each site to confine the bedrock aquifer. Another limitation that affected the interpretation and comparison of results was the amount of data that was processed, analyzed, and filtered varied among the profile locations

CHAPTER VII

INTER-ANNUAL VARIABILITY DURING THREE PERIODS WITHIN THE GROWING SEASON AND COMPARISON TO LIDAR ESTIMATES OF RIPARIAN EVAPOTRANSPIRATION

In this chapter, we present soil moisture profiles, changes in soil moisture and estimates of riparian evapotranspiration (RET) during three periods within the growing season for each year from 2011-2013. During one of the three periods in 2011, simultaneous measurements of RET using a three-dimensional LIDAR system were available through a collaborative effort with the University of Iowa. This provided a unique opportunity to compare RET estimated based on TSM water balance with the LIDAR-based measurements. As noted in previous chapters, a unique feature of this site is the significant heterogeneity across the different soil profile locations. Thus, soil moisture profiles, soil moisture variations and RET estimates all vary significantly by profile. The observations presented in this chapter further document this heterogeneity.

7.1 Inter-annual Variability During Three Periods Within the Growing Season

The three periods of interest were chosen to represent three distinct stages within the growing seasons in 2011-2013, and are described below:

- Period 1 – May - early in the growing season, when the soil moisture is in a highly replenished state, following recharge from precipitation and no depletion by RET during the winter.

- Period 2 – June - during the peak growing season when RET is generally at its highest. Although we selected periods between rainfall events, period 2 in each year typically reflects the influence of antecedent rainfall events

- Period 3 – July/August - representing the late growing season, when the soil moisture is typically depleted and RET drops significantly

The durations corresponding to the three periods in each year are listed in Table 7.1. The durations of the selected periods range from 5 to 18 days. Figure 7.1 shown below, has a total of nine plots, describing behavior at three different profile locations (profiles A, B and F; the three columns in the figure), in each year between 2011 and 2013 (the three rows in the figure). In each plot, the time-averaged soil moisture profiles across the duration of each of the three periods for are shown for the corresponding year. Figures 7.2 through 7.4 (containing 9 plots each) show the changes in soil moisture content at individual sensor locations and the changes in total soil moisture (TSM) for profiles A, B, and F during each of the three periods analyzed in 2011, 2012 and 2013 respectively. Table 7.2 shows the average daily RET for profile locations A, B and F during the three periods analyzed in each year. Together, these figures and tables provide a framework for analyzing the behavior during the three periods across three years. Additionally, the precipitation record and TSM trends during the growing seasons, which include these periods, is evident from Figures 6.3-6.5 in chapter VI.

7.1.1 Year 2011

In 2011, the precipitation record reveals fairly wet conditions with several rainfall events between periods 1 and 2. The duration between periods 2 and 3 was largely dry, with the exception of a large rainfall event just prior to period 3. There was also a significant decrease in TSM in all profiles between periods 2 and 3. Figure 7.1 (a, b, c for 2011) shows highest soil moisture contents in period 1. Figure 7.2 (a, b, c) shows higher rates of soil moisture depletion at shallower depths during period 1, and small increases in soil moisture at the two deepest sensor locations (likely reflecting drainage following the large rainfall event in late April). Diurnal oscillations including strong nighttime recovery are clearly discernible at the shallowest sensor location in profile B, and the two shallowest sensor locations in profile F. The TSM also shows significant diurnal oscillations at these two profile locations, indicating behavior similar to that in a groundwater discharge zone. Diurnal variations are not clearly discernible at the shallowest sensor location in profile A, although the sensor at the next depth exhibits diurnal variations in the later portion of period 1. The highest RET rates during this period are in profile F, followed by profiles A and B. This trend is consistent with the behavior seen in Figures 7.2 (a, b, c).

At shallower depths, the soil moisture profiles in Figure 7.1 (a, b, c) show significant drying between periods 1 and 2 in profile A, while there is little change in soil moisture in profiles B and F (F shows a slight wetting). At profile F, there is a noticeable decrease in soil moisture at depths > 0.6m. The changes in the soil moisture profiles between periods 1 and 2 are influenced by both RET and the recharge from rainfall events.

To a large extent, the soil moisture profiles for periods 1 and 2 are not very different (except for the slight drying at shallow depths in profile A and greater depths in profile F), because the rainfall events between periods 1 and 2 offset the loss of water due to RET.

During period 2, the soil moisture depletion rates suggested by Figure 7.2 (d, e, f) are substantially larger than in period 1. The shallowest soil moisture sensors at each profile location continue to show the greatest soil moisture depletions. Significant diurnal oscillations in TSM continue at profiles B and F, although the nighttime recovery is less pronounced at profile B. Diurnal variations are also seen in the TSM of profile A. Diurnal oscillations with much smaller amplitudes and low soil moisture decline rates are discernible in the deeper sensors. The RET rates at profile locations A, B and F in period 2 are respectively 1.4, 1.9 and 3.2 times higher than in period 1. Between periods 2 and 3 the soil moisture profiles in Figures 7.1 (a, b, c) show significant drying at shallow depths in profile B, with relatively less drying at profiles A and F. Profile A shows relatively uniform drying across the entire depth covered by the sensors. At deeper locations, profile F exhibits significant drying. The differences between the profiles for periods 2 and 3 are influenced to some extent by a large rainfall event just before period 3.

During period 3, the soil moisture depletion rates seen in Figure 7.2 (g, h, i) are much smaller than in period 2 at profiles A and B, but much larger than in period 1 at all profiles. Very little nighttime recovery in TSM is observed even in profile F, where pronounced nighttime recoveries in TSM are seen in periods 1 and 2. Almost no change in soil moisture contents is discernible in the two deepest sensors at all profile locations. The average daily RET rates at profile locations A and B are smaller than in period 1, while the

RET rate at profile F continues to be high (about 1.8 times that in period 1). The fact that the rates of decline of TSM at profiles A and B during period 3 are higher than in period 1, despite lower RET rates in period 3, likely reflects the influence gravity drainage.

7.1.2 Year 2012

In spring 2012, before the start of the growing season, the TSM values at most profiles are larger than the corresponding values in 2011, due to significant recharge events in the late 2011. However, subsequently, 2012 turned out to be a very dry year, with very little summer rainfall and virtually no precipitation during the fall and winter. In period 1, the soil moisture at intermediate depths is higher than during period 1 in 2011. Period 2 was just after the few summer rainfall events, and period 3 was late in the growing season, during an extended dry spell. The TSM trends in Figure 6.4 show a sustained decrease down to very low levels after period 2. Figure 7.1 (d, e, f, for 2012) shows significant drying at deeper locations (due to RET) and wetting at shallower locations between periods 1 and 2 (due to rainfall events). Between periods 2 and 3, there is substantial drying at all depths at all profile locations, and the soil moisture profiles in late July 2012 are the driest profiles seen in Figure 7.1.

In period 1, Figures 7.3 (a, b, c) show the highest soil moisture depletion rates at the three shallowest sensor locations at profiles A and F, while the sensor at the third depth shows the highest depletion rates at profile B. Significant diurnal variations in moisture depletion rate are observed in TSM and at the shallowest three sensors at all profile locations. Smaller diurnal variations and depletion rates are observed in the deeper

sensors, while the deepest sensor at profile B shows a very small increase in soil moisture. To some extent, the higher depth range over which soil moisture depletion occurs is due to the higher soil moisture contents at intermediate depths during period 1. The highest average daily RET rates during these periods are seen at profile A, followed by profiles F and B. These rates are more than 2.5 times larger than during period 1 in 2011. This difference in RET between periods 1 in 2012 and 2011 is also corroborated by the soil moisture variations in Figures 7.1 and 7.3 (a, b, c), especially the greater depth over which soil moisture depletion occurs in 2012.

In period 2, which followed one of the rare summer rainfall events of 2012, the highest soil moisture depletion rates were seen at the shallowest sensor at all three profiles (Figure 7.3, d, e, f). Moderate depletions and diurnal variations continued at the deeper sensors. The shallowest sensor and TSM at all profile locations showed significant diurnal variations, including nighttime recovery. The RET rates are highest at profile A, followed by profiles F and B. The average daily RET rates at profiles A and B are respectively 2.6 and 1.9 times higher than in period 1 of 2011, while the RET rate at profile F is slightly smaller, by a factor 0.94. Following the extremely dry spell between periods 2 and 3, Figure 7.1 (d, e, f) shows significant soil moisture depletion at all depths at all three profiles, leading to very low soil moisture contents in period 3.

In period 3, the soil moisture depletions (Figure 7.3 g, h, i) are much smaller than in period 1 at profiles A and B. While the shallowest sensor still shows the highest depletions at these profiles, the deepest sensor and the sensor at the fifth depth show the next highest depletion rates. Diurnal variations continue to be observed at the sensors exhibiting the

highest soil moisture depletion rates. At profile F, the soil moisture depletion is higher than in period 1, despite the extremely dry conditions. The highest depletion rates are seen in the deepest sensor and the sensor just above it. The fact that all three profiles show relatively high depletion rates in the deeper sensors suggest that trees were attempting to extract water from deeper locations due to the extremely dry surface conditions. The daily average RET rates during period 3 are much lower than in period 3 of 2011 at profiles B and F (76% and 65% of the 2011 values respectively), and slightly higher than in 2011 at profile A.

7.1.3 Year 2013

The TSM values at all profiles start out at extremely low values in 2013 (see Figure 6.5 in Chapter 6), due to the dry conditions in 2012. The TSM increases gradually in response to spring precipitation events prior to the start of the growing season, although the spring precipitation was lower than in 2011 and 2012. Correspondingly, the soil moisture profiles in period 1 of 2013 reflect wetting near the surface (Figure 7.1 g, h, i). Period 2 was in the middle of the growing season following a relatively dry spell, and significant drying is evident between periods 1 and 2. The later portion of the growing season is marked by several high rainfall events (Figure 6.5), leading to steep increases in TSM and wetter soil moisture profiles in period 3.

In period 1, Figures 7.4 (a, b, c) show the highest soil moisture depletion rates at the shallowest sensors at all profiles. The highest TSM declines are seen in profile A, while profile F shows a relatively low decline in TSM compared to other periods in all years. Soil

moisture at most deeper sensors increases significantly at all profile locations, reflecting the influence of wetting fronts from antecedent rainfall events. Diurnal variations in soil moisture depletion rates are observed at all shallow sensors, including nighttime recovery. The highest RET rate was observed at profile A and the lowest was at profile F. The RET rate observed at profile F (1.36 mm/day) was the lowest of all periods analyzed, and is consistent with the low rates of decline in soil moisture in Figure 7.4 c. Between periods 1 and 2 in 2013, there is an extended dry spell and correspondingly there is a significant decline in soil moisture except at the deepest two sensors at all profile locations (Figure 7.1 g, h, i). At the deepest two sensor locations in profile F, there is a significant increase in soil moisture, reflecting continued drainage of moisture that was not consumed due to low RET rates in period 1.

In period 2, significantly higher soil moisture decline rates were observed at all profile locations compared to period 1. At profile A, the highest declines occurred at intermediate depths, and declines were seen at all depths. Diurnal variations with nighttime recovery were seen at all but the shallowest sensor. By this time the surface moisture content had reduced significantly (Figure 7.1g). Profile B showed much lower soil moisture decline rates than profile A. The greatest decline rates were at the two shallowest sensors, while the changes at deeper locations were very small. Diurnal variations with nighttime recovery were observed at the shallowest sensor and in the TSM. At profile F, significant soil moisture decline rates were observed (including diurnal variations with nighttime recovery) at all but the deepest two sensors. The RET rates in Table 7.2 are consistent with the TSM decline rates, with profiles A and F showing very similar rates,

and much lower rates at profile B. The RET rates at profiles B and F were significantly lower than in period 2 of 2011 and 2012, while that at profile A was in between those rates. Between periods 2 and 3, there was a significant amount of rainfall leading to a steep increase in TSM at all profile locations (Figure 6.5) and period 3 reflects the dry spell that follows. The soil moisture profiles in Figure 7.1 (g, h, i) show significant increases in soil moisture at profiles B and F at all depths. However, there is only a slight increase at profile A. In period 3, Figure 7.4 (g, h, i) shows that the highest soil moisture decline rates were observed in profile A, with slightly lower rates in profile F and much lower rates in profile B. At profile A, the sensors at intermediate depths (2, 3, 4 and 5) showed the greatest declines (including diurnal oscillations in the decline rates and nighttime recovery). At profile B, the shallowest two sensors showed the highest decline rates and diurnal oscillations, while sensor 5 showed an increasing soil moisture for the earlier part of period 3. At profile F, all but the deepest two sensors continued to show significant soil moisture decline rates, including diurnal oscillations and nighttime recovery. The RET estimates reported in Table 7.2 are consistent with these observations with significantly higher rates at profiles A and F, compared to profile B. RET rates at all profiles were substantially higher than in period 3 of 2011 and 2012, due to the significantly higher soil moisture and TSM resulting from the continued rainfall between mid-July and August 2013 (see Figures 6.3, 6.4 and 6.5 in chapter VI).

Table 7. 1. Durations of the three periods analyzed in each year

Year	Period 1 (early growing season)	Period 2 (peak growing season)	Period 3 (late growing season)
2011	5/11 - 5/17	6/21 - 7/2	8/13 - 8/23
2012	5/21 - 5/28	6/8 - 6/13	7/18 - 7/27
2013	5/23 - 5/29	6/25 - 7/13	8/29 - 9/11

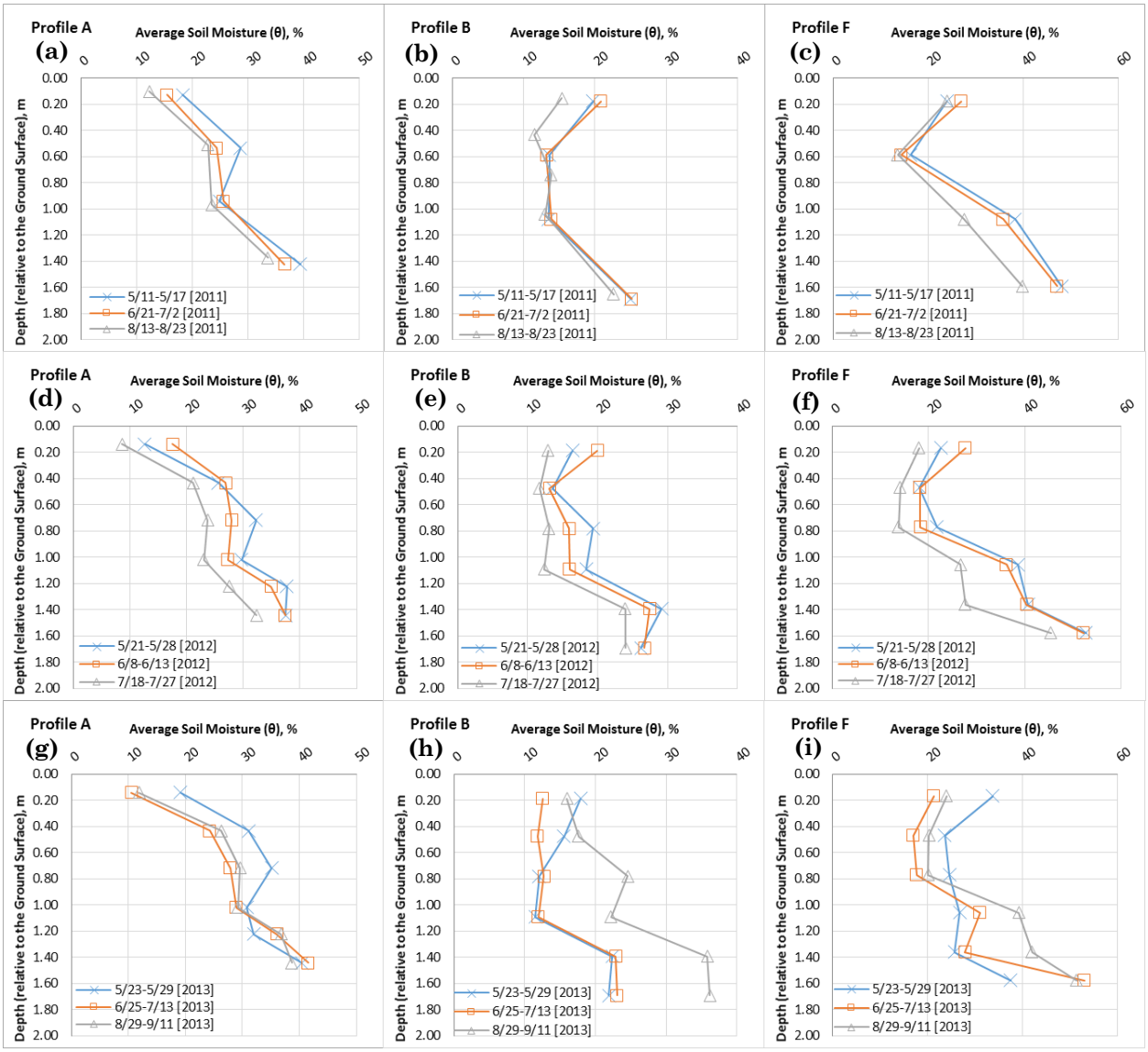

Figure 7. 1. Three period comparison of soil moisture profiles over three years (2011, 2012, and 2013). First row shows profiles in 2011: (a) average soil moisture profile location A; (b) average soil moisture profile location B; (c) average soil moisture profile location F. Second row shows profiles in 2012: (d) average soil moisture profile location A; (e) average soil moisture profile location B; (f) average soil moisture profile location F. Third row shows profiles in 2013: (g) average soil moisture profile location A; (h) average soil moisture profile location B; (i) average soil moisture profile location F.

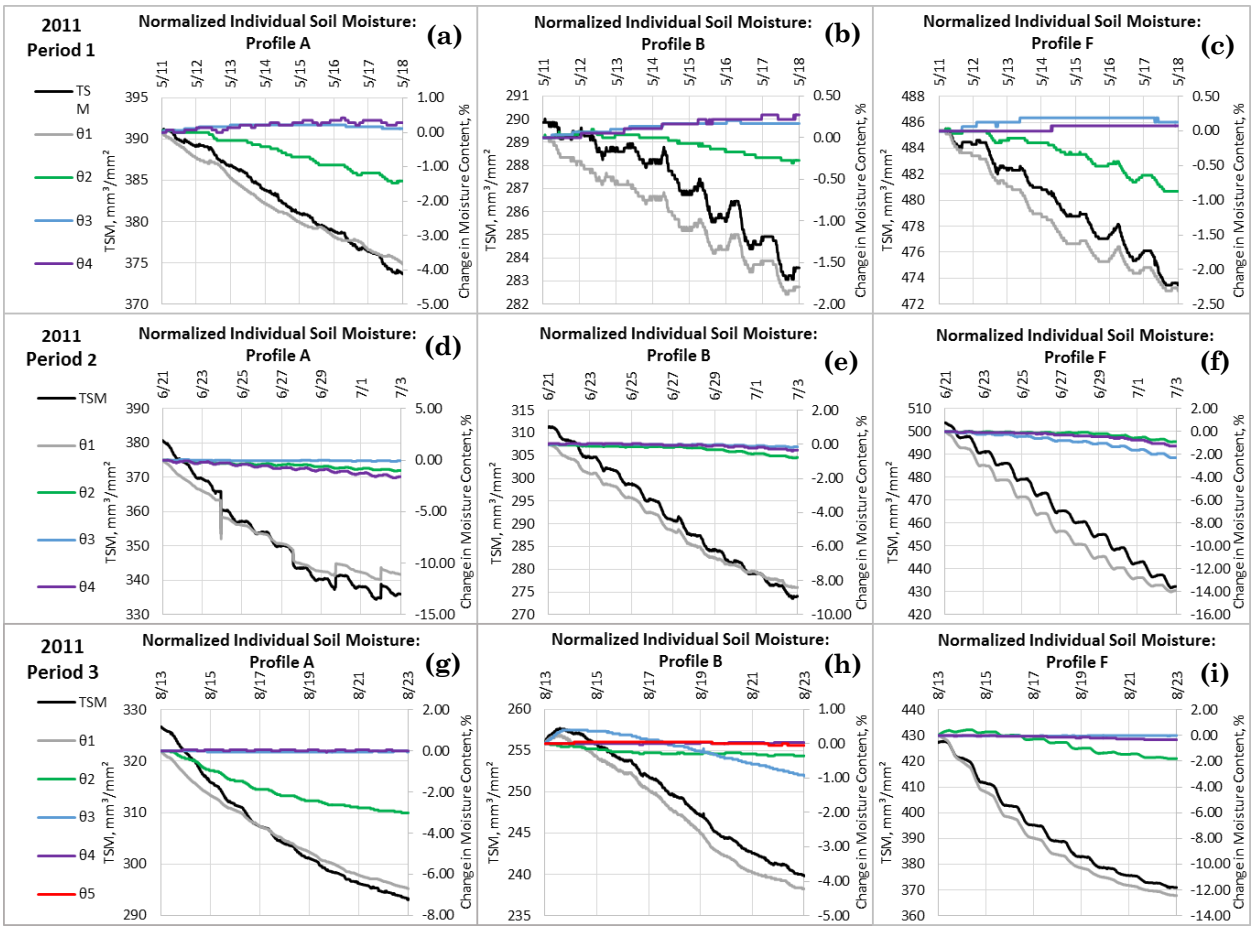

Figure 7. 2. Comparison of soil moisture changes during three periods in 2011 from three different profile locations (A, B and F). The total soil moisture (TSM) trends during the three periods are also shown at each profile location. Note that the y-axis ranges are different for each plot. Each row shows soil moisture changes during a specific period (2011, 2012, 2013), and each column shows behavior at a specific profile (A, B, F).

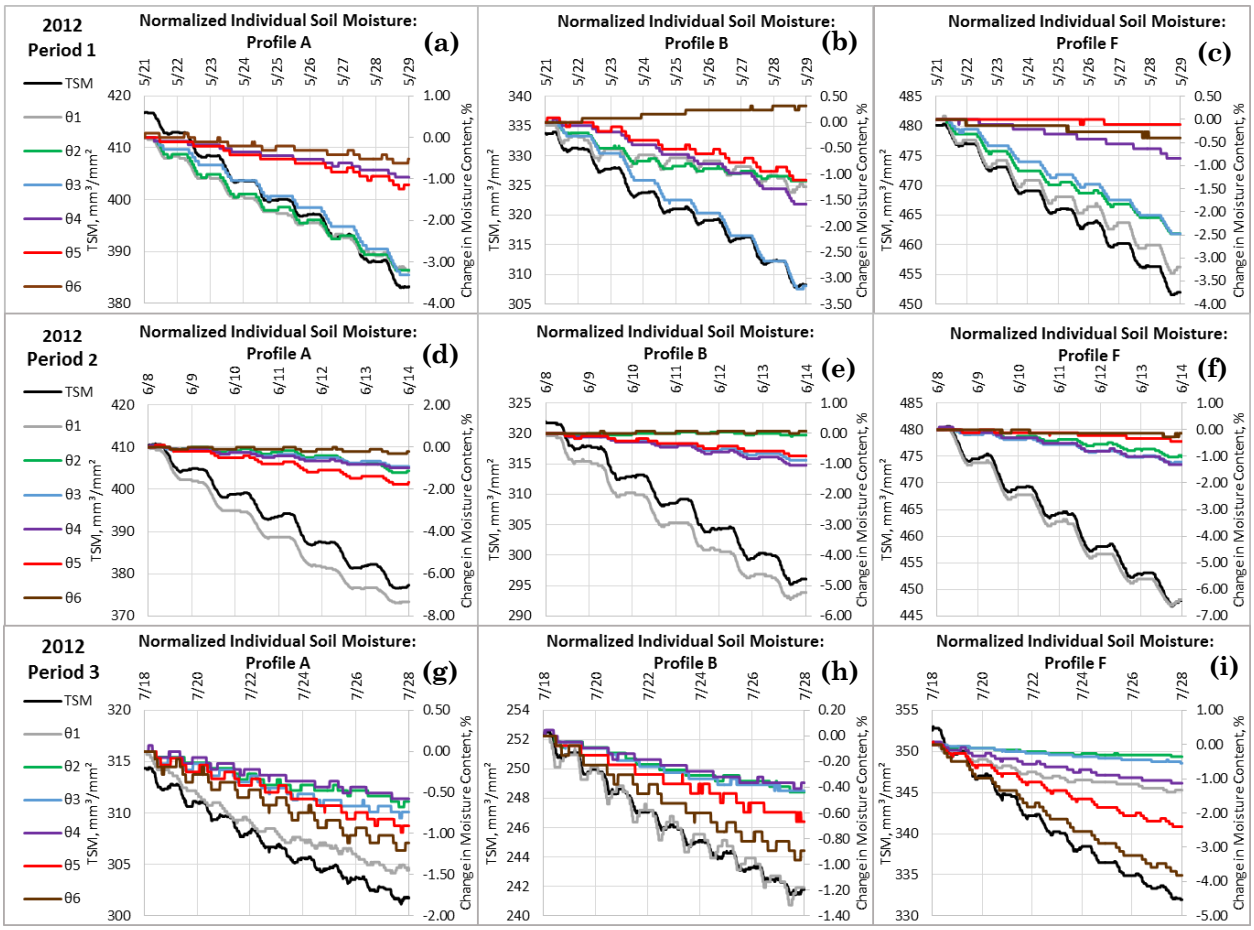

Figure 7. 3. Comparison of soil moisture changes during three periods in 2012 from three different profile locations (A, B and F). The total soil moisture (TSM) trends during the three periods are also shown at each profile location. Note that the y-axis ranges are different for each plot. Each row shows soil moisture changes during a specific period (2011, 2012, 2013), and each column shows behavior at a specific profile (A, B, F).

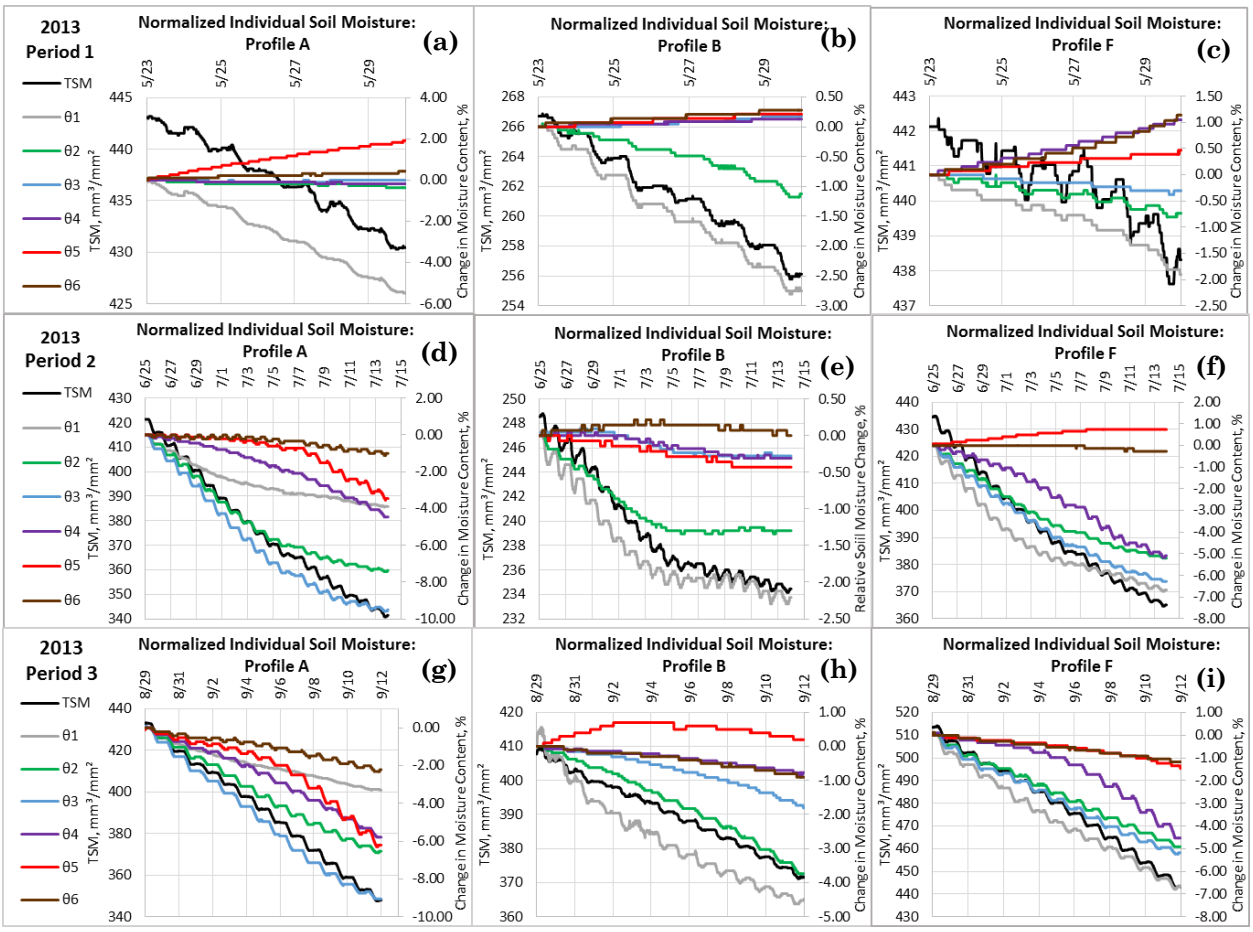

Figure 7. 4. Comparison of soil moisture changes during three periods in 2013 from three different profile locations (A, B and F). The total soil moisture (TSM) trends during the three periods are also shown at each profile location. Note that the y-axis ranges are different for each plot. Each row shows soil moisture changes during a specific period (2011, 2012, 2013), and each column shows behavior at a specific profile (A, B, F).

Table 7.2 summarizes the daily average RET estimates from the three profile locations during the selected periods from the three years. These estimates range from a minimum average of 0.83 mm/day to maximum of 7.13 mm/day. The highest RET estimates varied between profile locations A and F, while at location B the RET estimates were consistently lower in comparison. Even though these estimates are highly variable they are still within a reasonable range when compared to studies at other sites, as shown in table 7.3. It is also interesting to note that the ratio of the estimated RET to the ASCE

standardized ET varies widely across profile locations even in the same period, and across different periods at a given location. In general (except for Period 1 in 2013), the ratio is highest at profile F. In 2011, the ratios are quite similar at profiles A and B, while it is much higher at profile F. During the extremely dry conditions in Period 3 of 2012, the ratios at each profile location take on the smallest values across all periods (except at profile F, where the ratio is slightly smaller in Period 1 of 2013, which may be a result of compromised vegetation health due to the extreme dry conditions in late 2012).

Table 7. 2. Daily averaged RET for profile locations A, B, and F during the three selected periods during 2011, 2012 and 2013. Numbers in parentheses is the ratio of estimated RET to the ASCE standardized ET.

Year	Period	Date Range	Profile A Avg. RET, mm/day	Profile B Avg. RET, mm/day	Profile F Avg. RET, mm/day	ASCE Avg. ETsz, mm/day
2011	Period 1	5/11 - 5/17	1.87 (0.45)	1.18 (0.29)	2.23 (0.54)	4.12
	Period 2	6/21 - 7/2	2.63 (0.38)	2.25 (0.32)	7.13 (1.02)	7.01
	Period 3	8/13 - 8/23	1.10 (0.18)	1.08 (0.18)	4.07 (0.67)	6.03
2012	Period 1	5/21 - 5/28	4.37 (0.64)	3.59 (0.53)	3.78 (0.56)	6.78
	Period 2	6/8 - 6/13	6.75 (1.06)	4.36 (0.68)	6.70 (1.05)	6.38
	Period 3	7/18 - 7/27	1.25 (0.16)	0.83 (0.10)	2.64 (0.33)	8.00
2013	Period 1	5/23 - 5/29	2.55 (0.57)	1.60 (0.36)	1.36 (0.31)	4.44
	Period 2	6/25 - 7/13	4.66 (0.70)	1.34 (0.20)	4.43 (0.67)	6.62
	Period 3	8/29 - 9/11	5.78 (1.08)	3.15 (0.59)	5.13 (0.96)	5.33

Table 7. 3. Comparative riparian evapotranspiration estimates from previous studies. The table describes the vegetation type, the location of where the measurements were made, the depth to water table, evapotranspiration derived from water table fluctuations (ETgw) and the corresponding citation† (Note that the Nachabe et al. 2005 study employed TSM balance rather than water table measurements).

Vegetation	Location	Depth to Water Table, m	ET_{gw}, mm/day	Reference
Wetland vegetation	North Dakota, USA	up to 1.7	3–5	Rosenberry and Winter [1997]
Riparian vegetation	Arizona, USA	3.0	2.58–5.99	Mac Nish et al. [2000]
Forest vegetation (Mixture of Quercus spp. and Acer spp.)	Florida, USA	1.4-1.5	5.76-6.30	Nachabe et al. [2005]
Primarily Populus spp.	Kansas, USA	1.9	3.5-4.8	Butler et al. [2007]
Alnus glutinosa (L.) Gaertn.	western Hungary	0.6–0.9	3.2-10.5 (growing season)	Gribovszki et al. [2008]
Phreatophytic vegetation	Wyoming, USA	1–3	0.0–3.1	Lautz [2008]
dominantly Populus deltoids spp. wislizeni	Albuquerque, New Mexico, USA	1.03	7.01–16.84	Martinet et al. [2009]
dominantly Populus deltoids spp. wislizeni	Belen, New Mexico, USA	0.0–0.78	6.24–15.70	Martinet et al. [2009]
Wetland vegetation	southeast England	3.0	5.50 (max)	Mould et al. [2010]
Wetland vegetation	northern Germany	0.1–0.6	5.91 (max)	Mould et al. [2010]
Mixed Riparian Vegetation *(Populus spp., salix spp., Acer spp,* among others)	Kansas, USA	2-4	0.83–7.13	Current Study Solis J. A. Dissertation [2015]

†This table was modified from Orellana et al. [2012]

7.2 Lidar Comparison

During the growing season in 2011, there was a collaborative opportunity to compare the TSM based RET estimates with a LIDAR based measurement. A team from the University of Iowa led by William Eichinger employed the Los Alamos National Laboratory (LANL)-University of Iowa (UI) Raman LIDAR to measure the water vapor concentrations in three dimensions in the plume emanating off the riparian canopy.

Monin-Obukhov similarity theory was then used to obtain the spatially resolved water vapor fluxes [Cooper et al., 2000; Eichinger et al., 2000; Eichinger et al., 2006; Eichinger and Cooper, 2007]. The LIDAR system included a 1.064 micron Nd:YAG laser with a Cassagrain telescope with a laser pulse of 50Hz with 25mJ of energy per pulse. Flux measurements from the LIDAR were taken north of the riparian vegetation shown below in figure 7.5 as a triangle with a letter "L" inside. An eddy covariance tower was also installed in the field between the study reach and the LIDAR system. During the comparison period, the brome field north of the riparian zone had already been harvested to avoid interference with the water vapor plume from the riparian zone. The LIDAR system estimates a reach-averaged RET rate.

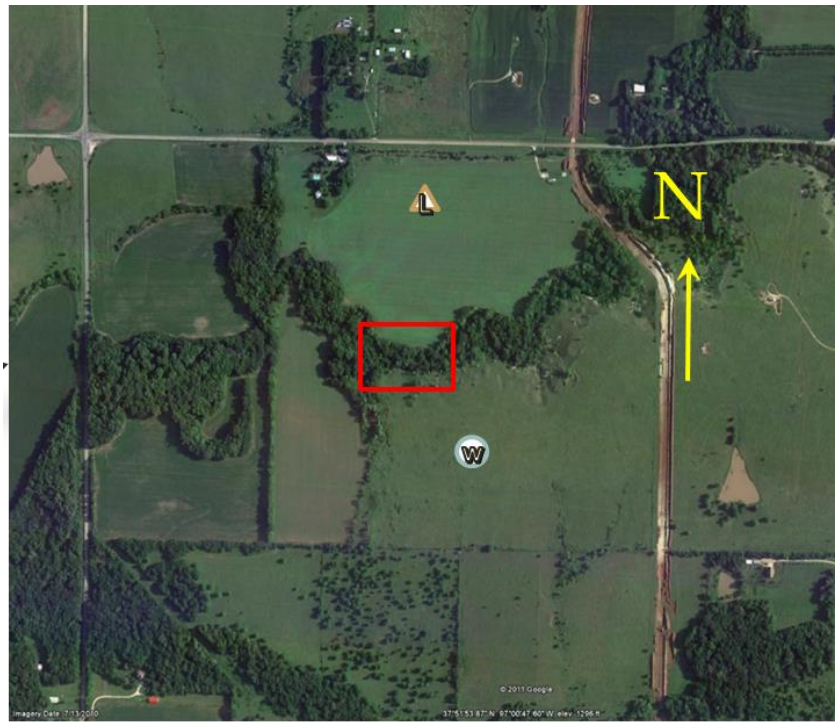

Figure 7. 5. Location of study site. The red rectangle corresponds to the riparian vegetation where the soil moisture profiles are located. The triangle with the letter L corresponds to the location of where the Raman LIDAR was placed for measurements and the circle with the letter W corresponds to the location of the weather station.

Estimates of RET from the Raman LIDAR and estimates from the sub-surface water balance (TSM) method were compared over the three day period when LIDAR measurements were available (July 7, 8, 9; 2011) and are shown in Figures 7.6, 7.7 and Table 7.4. Figure 7.6 shows the ET trends for the three days from each soil moisture profile, the LIDAR and the eddy covariance estimates. The ASCE reference evapotranspiration (ASCE ETsz) (ASCE-EWRI 2005) is also shown for comparison. The ASCE ETsz reference is defined as the ET rate from a uniform surface of dense actively growing vegetation having specified height and surface resistance, not short of soil water and representing an expanse of at least 100m of the same or similar vegetation. The ASCE ETsz for a short grass was used as the reference ET in Figure 7.6 - it is used mainly to illustrate the calculated diurnal variations in ET based on meteorological variables. The ASCE ETsz calculation is based on a Penman-Montieth equation. We did not attempt to convert the ASCE ETsz estimates to riparian vegetation because of the mixed vegetation at the site, which includes many species of trees and shrubs.

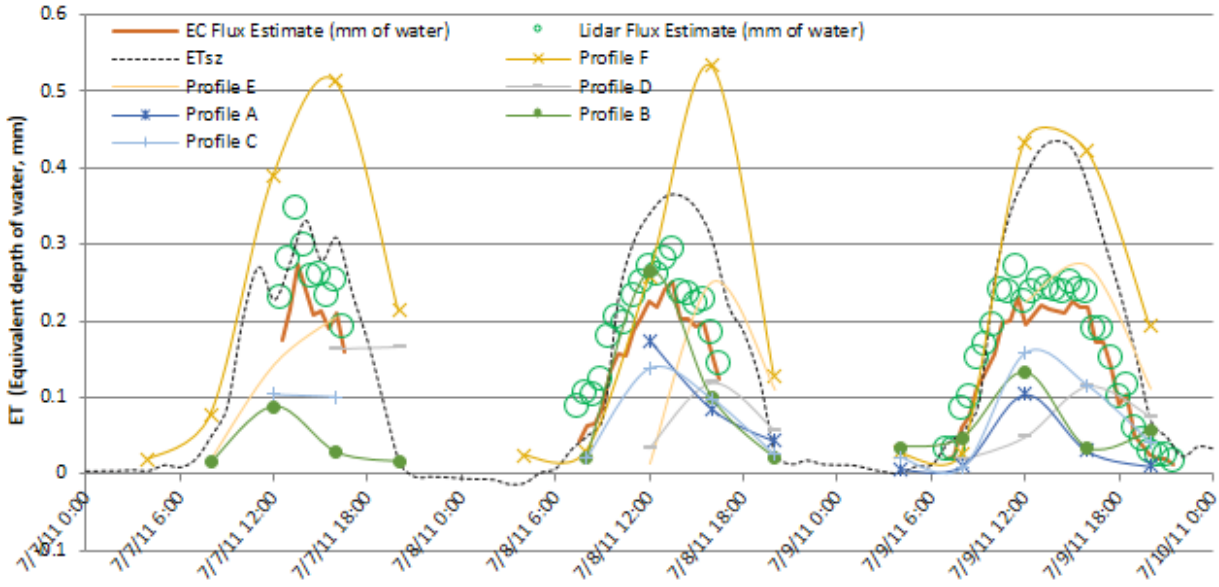

Figure 7. 6 Equivalent depth of water and/or ET per 30 minutes from the EC flux tower, ET estimates from the Lidar, ASCE Standardized ET (ETsz) and soil moisture based RET estimates from the all the soil moisture profiles (A-F). [Daily ASCE ETsz values = 5.19, 5.94, 7.52 mm/day for days 7,8, and 9 of July respectively]

Table 7. 4. Equivalent depth of water and/or ET from the EC flux tower and ET estimates from the Lidar and change in soil water moisture (dS/dt) from the all the soil moisture profiles (A-F) over same duration.

				Profile A	Profile B	Profile C	Profile D	Profile E	Profile F
		EC Flux Estimate	Lidar Flux Estimate	**RET**	**RET**	**RET**	**RET**	**RET**	**RET**
	HOURS	(mm of water)	(mm of water)	(mm of water)	(mm of water)	(mm of water)	(mm of water)	(mm of water)	(mm of water)
7/7/2011 12:30 7/7/2011 16:30	4	1.88	2.34		0.86	0.80		1.51	4.22
7/8/2011 7:30 7/8/2011 16:30	9	3.11	3.83	2.05	3.18	1.84	1.25	2.36	6.57
7/9/2011 7:00 7/9/2011 21:30	14.5	3.98	4.60	1.15	1.66	2.64	2.06	4.69	8.21

There are lags in the timing of peak RET estimated by the different profiles, and as noted earlier, there is significant variability in the RET estimated from each profile in Figure 7.6. In particular, the RET estimated at profile F is significantly larger than at other profile locations, which is consistent with the behavior during period 2 in 2011 (see Table 7.2). To facilitate a reach scale comparison, the integrated dTSM/dt was computed on a four-hour time interval and a spatial trapezoidal integration was performed to obtain the integrated RET for the central transect (A, B, C, D). The integrated RET along the

entire reach length which includes all the soil moisture profiles (E, [integrated (A, B, C, D)], F) was also calculated. These spatially integrated estimated are compared against the LIDAR measurements in Figure 7.7 below. The reach-integrated RET estimates obtained using TSM changes from all of the six profiles compare very well with the LIDAR estimates. RET estimates obtained from the LIDAR were 3.83 mm for the period 7:30-16:30 on 7/8/2011 and 4.60 mm for the period 7:00-21:30 on 7/9/2011. The corresponding RET estimates obtained from TSM based measurements were 3.44 mm and 4.36 mm. The integrated TSM based only on the central transect did not match the LIDAR measurements very well. Inclusion of profile F is critical to obtaining a good match between the LIDAR and TSM measurements.

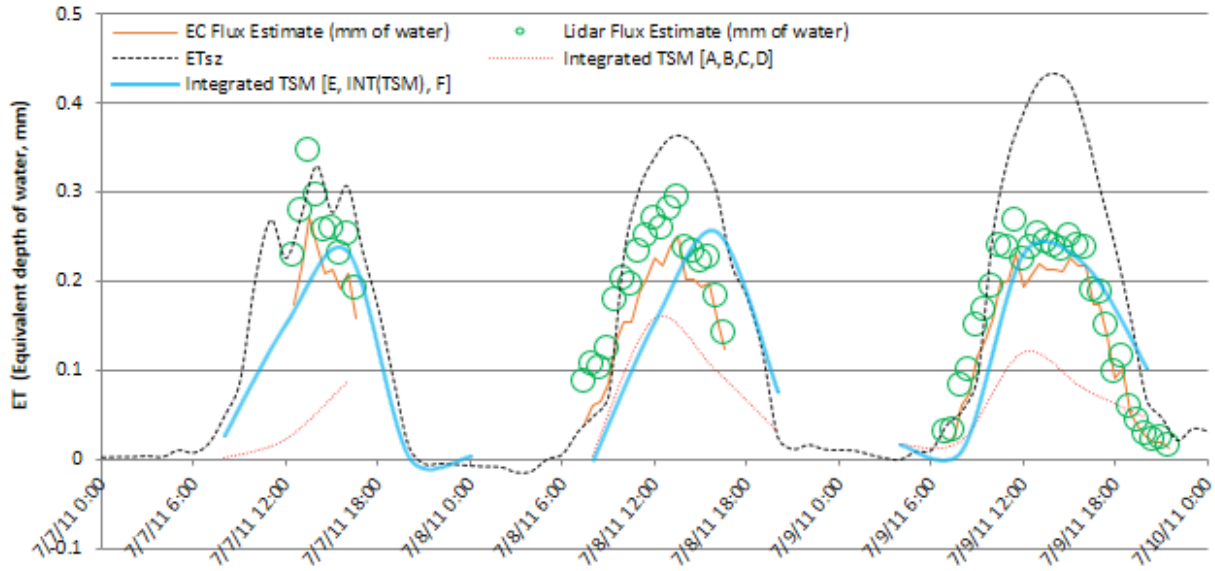

Figure 7. 7. Equivalent depth of water and/or ET per 30 minutes from the EC flux tower, ET estimates from the Lidar, ASCE Standardized ET and, change in soil water moisture (dS/dt) from the all the soil moisture profiles (A-F) using only the TSM_Top. [ASCE ETsz = 5.19, 5.94, 7.52 mm/day for days 7,8, and 9 of July respectively]

Figures 7.6 and 7.7 include periods when the RET estimates are higher than ETsz. Part of this discrepancy owes to the differences between crop coefficients for short grass versus riparian vegetation. Additional factors contributing to the discrepancy are related to weather, as shown in figure 7.8. During the time of Lidar measurements on the first day, the wind was blowing from a Northwest direction rather than the south, which would have influenced the behavior of the water vapor plume captured by the Lidar. However, the wind velocity was not very high. The windrose plots in figure 7.8 show that during that time the wind speed was between 2.1 and 3.6 m/s (4.7-8.05 mph). Other explanations could be because solar data show that there were clouds (dips in Rs) and higher relative humidity on the first day. Other factors that influence the ASCE ETsz estimates include the vegetation height, canopy resistance, and the albedo also known as the reflectance of the riparian vegetation and soil surface (Allen et al. 1998).

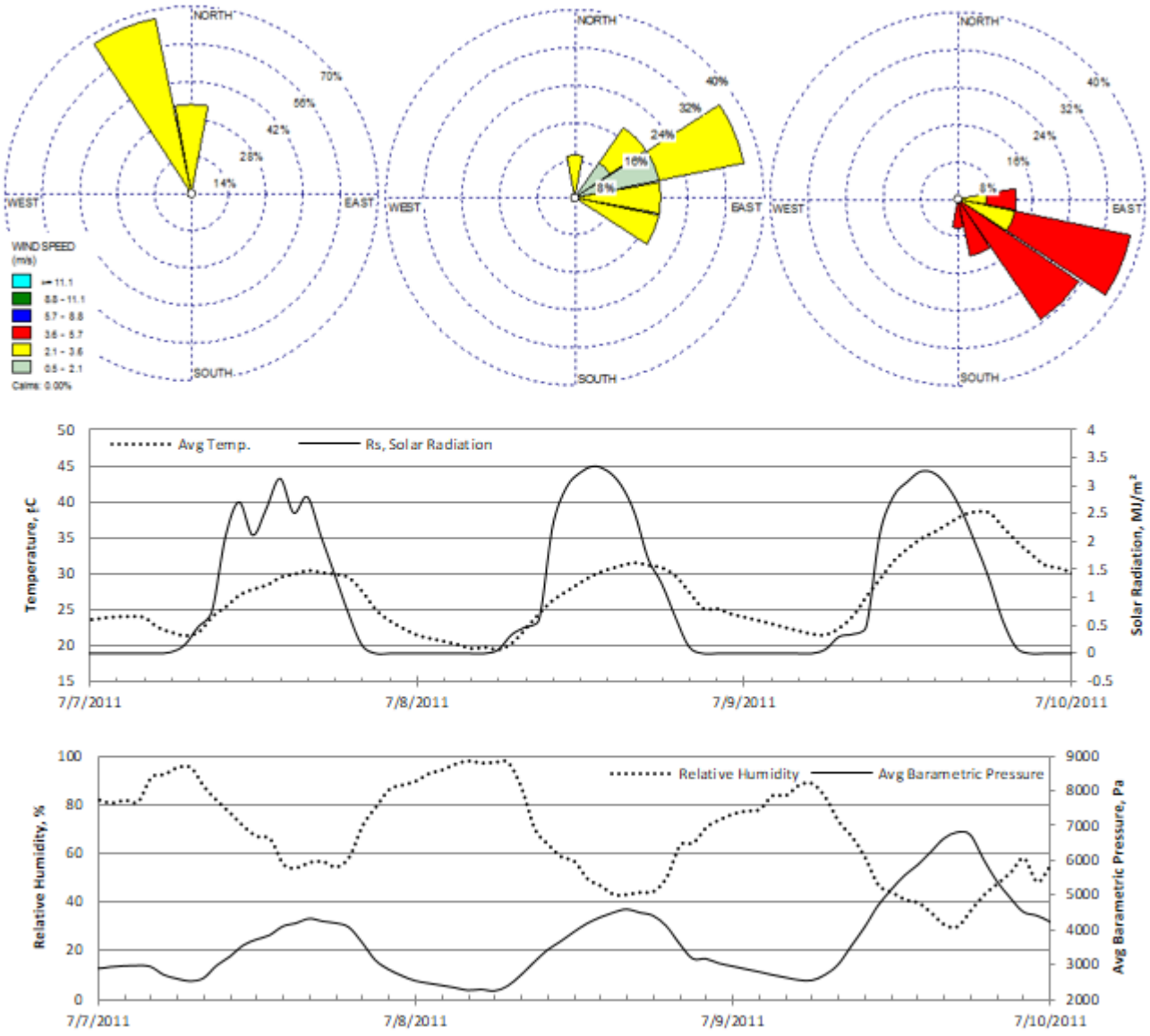

Figure 7. 8. Wind velocity and direction for the duration of the Lidar measurements (see table 7.4). Meteorological measurements which include air temperature, relative humidity, solar radiation and barometric pressure during the study period.

RET estimates obtained from TSM changes in individual soil moisture profiles exhibited a large variability (up to a factor 8). This variability results from the variable vegetation density and species, and the highly heterogeneous soils in the vadose zone (2-3 m thick), where soil moisture (rather than groundwater) is the major source of water for

riparian vegetation. The Heterogeneity across the study site is also evident from the inter-annual three period comparisons (Figures 7.1-7.4). It appears that the Lidar and EC flux estimates of ET (RET estimates obtained from LIDAR: 3.83 mm on 7/8/2011 and 4.60 mm on 7/9/2011) fall within the range of soil moisture profile ET estimates (RET estimates obtained from TSM based measurements: 3.44 mm and 4.36 mm for the same time), which is encouraging. There is significant variability between ET estimates obtained with single vertical profile analysis, which is likely caused by heterogeneity in soil properties, nearby vegetation, root density and other factors. While water Balance based estimation of RET is cost-effective, variability in vegetation density and type, and subsurface heterogeneity can potentially lead to inaccuracies in water-balance based RET estimates, under natural vegetation in thick vadose zones, as vividly illustrated in Figures 7.6 and 7.7.

CHAPTER VIII

1D VERTICAL NUMERICAL MODEL USING INSIGHTS FROM THE CONCEPTUAL MODEL AND FIELD AND LABORATORY MEASUREMENTS

Based on the conceptual model numerical simulation models were developed using Richards Equation in the mixed form. Previous studies established that the soil moisture (θ) based form is problematic because the unsaturated diffusivity function $\left(D(\theta) = K(\theta)/C(\theta)\right)$ blows up and the pressure head (ψ or h) based form produces mass conservation errors (Celia M. A. et al., 1990). The mixed form of the Richards equation works best for numerical simulation. Since the conceptual model includes a water table above the aquitard, the equation was modified to a saturated-unsaturated flow equation as shown in equation 8.1. This unsaturated-saturated flow equation has been used previously by Clement, et al. (1994) and Akindunni and Gillham, R. W. (1992), among others. In addition to the change in soil water content, there is a change in the volume of water stored per unit volume of porous medium, due to the compressibility of the medium. With the Richards equation, positive values of water pressure cannot be handled, and the storage term should be augmented to account for compressibility under saturated conditions. The Richards equation is also modified by including a plant-water uptake term in the form of a distributed sink. The plant-water uptake rate is represented as a function of pressure head (also known as suction), following recent approaches in ecohydrologic studies (Guswa et al., 2002; Guswa, 2005; Ojha et al., 2009).

Equation (8.1)

$$\frac{\partial\theta(\psi)}{\partial t} - \frac{\theta(\psi)}{\phi}S_s\frac{\partial\psi}{\partial t} - \frac{\partial K(\psi)}{\partial z} + \frac{\partial}{\partial z}\left(K(\psi)\frac{\partial\psi}{\partial z}\right) = -ET(\psi)$$

Where:

$\theta(\psi)$ = soil water content as function of pressure head *[l^3 l^{-3}],*

ψ = pressure head [l],

S_s = specific storage *[l^{-1}],*

z = vertical coordinate pointing upwards [l],

$ET(\psi)$ = plant-water uptake rate as a volumetric water loss [l^3 l^{-3} t^{-1}],

ϕ = porosity *[unit less],*

$K(\psi)$ = hydraulic conductivity as a function of pressure head *[t l^{-1}],*

The simulation model was formulated using a finite difference implicit Euler Backward approach with a Picard iteration (Celia et al., 1990; Clement et al. 1994). Two different versions of this model were developed. The two main differences between these two versions were in the grid spacing and the implementation of the ET signal. In the first version of the model the grid spacing was specified at 0.01 meters and 0.001m in the second version. The implementation of the ET signal within the first version used a plant water uptake function that is also dependent on meteorological factors and is uniformly distributed over the specified rooting depth (will be discussed further in detail later in the text) while in the second version the ET was fully prescribed uniformly distributed over the specified rooting depth and does not have the plant-water uptake function incorporated in it.

Both versions consisted of eight soil layers, each containing different soil properties (obtained from laboratory analysis, see chapter 2). The following boundary conditions were used for the first version of the numerical model: at the top of the domain precipitation (P)

is added during rainy periods, with a no flux boundary condition during dry periods (this is consistent with the representation of ET as a distributed sink term rather than as a surface flux). At the bottom of the domain the actual piezometric head is input from the deep alluvium base well. Table 8.1 shows the different property values that were used in the eight layers and figure 8.1 illustrates the one-dimensional representation of the model.

Table 8. 1. Soil properties that were used in the numerical model for Profile D.

Layer	Length (m)	Depth Range (m)	Hydraulic Conductivity, K_s (m/d)	Porosity, ϕ	Van Genuchten, n	Van Genuchten, α (1/m)
8	0.67	0.67	0.0793*	0.48	1.384	1.89
7	0.67	1.33	0.00942*	0.48	1.358	2.07
6	0.67	2.00	0.00601*	0.51	1.414	1.57
5	1.89	3.89	0.01134‡	0.42	1.142	7.64
4	1.09	4.98	0.007‡	0.46	1.403	3.71
3	0.53	5.51	0.000095*	0.44	1.686	3.11
2	0.41	5.92	0.003‡	0.37	1.178	2.26
1	0.08	6.00	0.000569*	0.32	1.32	0.60

*Measured with a permeameter
‡Estimated from HYPROP© system

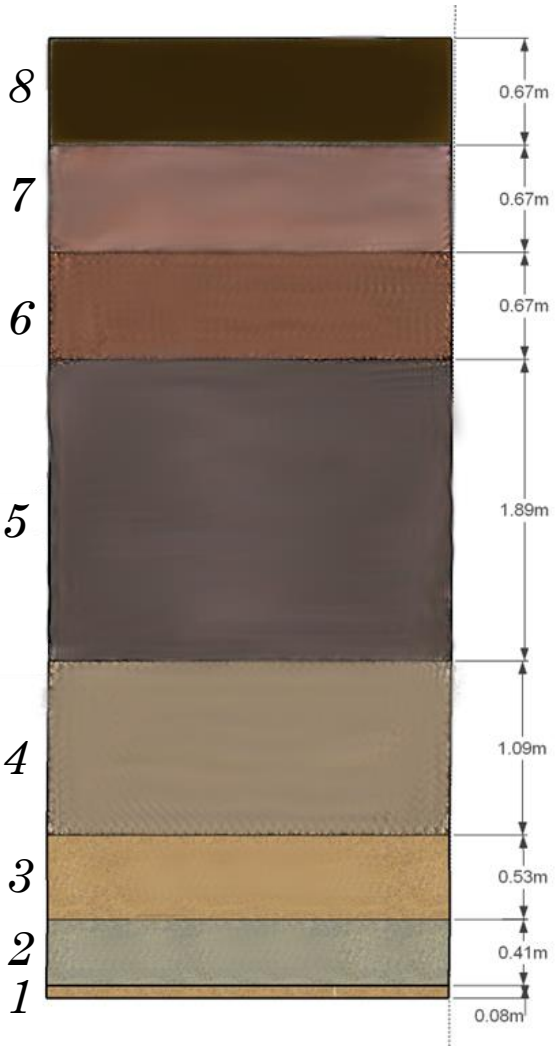

Figure 8. 1. One-dimensional representation of the soil layers used in the numerical model.

The soil properties were characterized by using van Genuchten's model (van Genuchten, 1980) as shown by the following equations. The parameters for the Van Genuchten model were obtained from soil laboratory analysis using the HYPROP© apparatus:

Equation (8.2)

$$Se = \Theta = \left[\frac{1}{(1 + (\alpha\psi)^n)}\right]^m$$

Where:

Equation (8.2b)

$$m = 1 - \frac{1}{n}$$

Then, based on Mualem's model (Mualem, 1976) the unsaturated hydraulic conductivity for the soil was represented using the following equations:

Equation (8.3)

$$\Theta = \frac{\theta - \theta_r}{\theta_s - \theta_r}$$

Equation (8.4a)

$$K_r = \sqrt{\Theta}\left(1 - \left(1 - \Theta^{\frac{1}{m}}\right)\right)^2$$

Equation (8.4b)

$$K = K_s\, K_r$$

The variable $ET(\psi)$in equation 8.1 includes a plant water uptake function that is a function of ψ (soil suction). The function that was used in the model is shown below and was obtained from Guswa, et al. (2002):

Equation (8.5)

$$\sigma_i = \Delta z_i \cdot rw_i \cdot \frac{(\psi_p - \psi_i)}{\frac{C_s}{K(\psi_i)RW_o} + \frac{C_r}{RW_o}}$$

Where:

σ_i = local plant uptake function *[l t^{-1}]*,

Δz_i = thickness of soil layer [*l*],

rw_i = relative root density as a function of depth *[unit less]*,

ψ_i = suction head of the soil at a specific computational node [*l*],

ψ_p = suction head of the plants [*l*],

C_s = constant that accounts for root diameter, geometry, and arrangement *[unit less],*

C_r = constant parameter of the plant *[t l-1],*

$K(\psi_i)$ = hydraulic conductivity as a function of suction head *[l t-1]* , and

RW_o = average root density over the root zone *[l l-3, length of roots per volume of soil].*

Equation 8.5 was then modified to a volumetric water loss function that accounts for the maximum evapotranspiration rate that occurs for that given time of day.

Equation (8.6)

$$ET(\psi_i) = \frac{\sigma_i}{\Delta z_i} = RW_i \left[\frac{\psi_p - \psi_i}{\frac{C_s}{K(\psi_i)} + C_r} \right] \left(ET_{signal} \right)$$

Where:

Equation (8.7)

$$RW_i = rw_i \cdot RW_o$$

Equation (8.8)

$$rw_i = \begin{cases} 1, & z_i \leq Zr_{max} \\ 0, & z_i > Zr_{max} \end{cases}$$

Where:

Zr_{max} = maximum rooting depth *[m]*

Equation (8.9)

$$ET_{signal} = \frac{ET_{sz}}{ET_{sz\,max}}$$

Where:

ET_{signal} = normalized multiplier that captures the diurnal variation of ET [*unitless],* obtained as the ratio of PET to PET_{max}.

ET_{sz} = ASCE Standardized Reference Evapotranspiration *[mm hr^{-1}]*

$ET_{sz\,max}$ = the maximum ET_{sz} on the day of interest *[mm hr^{-1}]*

The ASCE standardized reference ET (ET_{sz}) is in reference to the ET of a well-watered short grass (Allen et al., 2005). This ET_{sz} value captures the diurnal variation resulting from solar radiation, temperature and atmospheric deficit (humidity from the weather station) but does not capture the soil moisture influence. For our study site we have riparian vegetation, not grass, so we combine this normalized diurnal signal from ET_{sz} with our plant water uptake function to represent diurnal variations in plant water uptake. The plant water uptake function also takes into account plant parameters and the soil water potential influence. For example, at night the ET_{signal} variable defined above will be small and therefore there is less plant water uptake. Equation 8.10 shows how ET_{sz} is calculated (Allen et al. 2005):

Equation (8.10)

$$ET_{sz} = \frac{0.408\Delta(R_n - G) + \gamma \frac{C_n}{T + 273} u_2 (e_s - e_a)}{\Delta + \gamma(1 + C_d u_2)}$$

Where:

ET_{sz} = standard reference crop evapotranspiration for short (ET_{os}) or tall (ET_{rs}) surfaces *[mm d^{-1} for daily time steps or mm h^{-1} for hourly time steps]*

ET_{sz} = calculated net radiation at the crop surface *[MJ m^{-2} d^{-1} for daily time steps or MJ m^{-2} h^{-1} for hourly time steps]*

G = soil heat flux density at the soil surface *[MJ m^{-2} d^{-1} for daily time steps or MJ m^{-2} h^{-1} for hourly time steps, most of the time this number is taken as zero since this number is very small compared to R_n and is nearly zero in a period of 24 hours]*

T = mean daily or hourly air temperature at 1.5 to 2.5-m height *[°C]*

u_2 = mean daily or hourly wind speed at 2-m height *[m s^{-1}]*

e_s = saturation vapor pressure at 1.5 to 2.5-m height *[kPa]* (*calculated for daily time steps as the average of saturation vapor pressure at maximum and minimum air temperature*)

e_a = mean actual vapor pressure at 1.5 to 2.5-m height *[kPa]*

Δ = slope of the saturation vapor pressure from the temperature curve, *[kPa °C^{-1}]*

γ = pyschrometric constant *[kPa °C^{-1}]*

C_n = numerator constant that changes with reference type and calculation time step *[K mm s^3 Mg^{-1} d^{-1} or K mm s^3 Mg^{-1} h^{-1}]*

C_d = denominator constant that changes with reference type and calculation time step *[s m^{-1}]*

The plant water uptake parameters were adjusted by trial and error to obtain reasonable behavior in the results shown here. The soil property functions were prescribed based on the measured values and not adjusted. One of the motivations for this version of model was to evaluate the influence of the plant-water uptake function and the response to the varying field conditions, such as the shallow water table location, to verify whether an appropriately parameterized numerical model can produce diurnal variations in water-table elevation and TSM, which are the key modeling targets. Such a modeling exercise provides confidence in interpreting RET based on these diurnal variations, by partially validating the conceptual model developed in Chapter 4. Four plant water uptake parameters of importance are the rooting depth (Zr_{max}), the root density (RW_o), the root diameter, geometry and arrangement (C_s), and the root-plant conductivity (C_r). Although the root density may be expected to vary with depth, we used a constant value to simplify

an already complex and poorly constrained system. The rooting depth is the depth to which the plant water uptake function is distributed. Figure 8.2 shows an example of what typical rooting depths look like at the study site and are comparable to similar studies (Orellana et al., 2012).

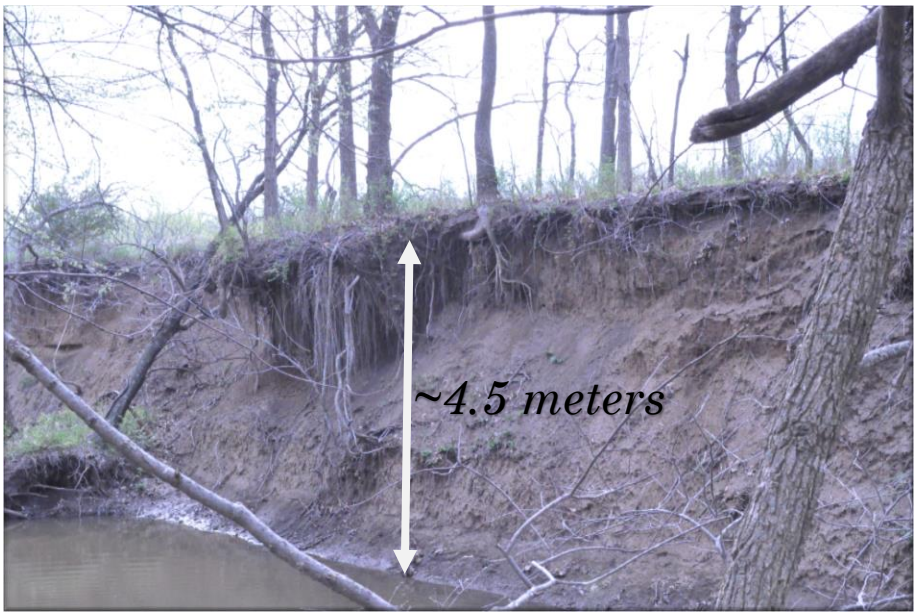

Figure 8. 2. Photograph of an incised bank at the study site showing the depth to which roots can extend. The height of the bank was measured at approximately 4.5 meters.

Initial conditions were developed by choosing soil moisture values from the field at a specific time from a specific profile location (profile D for this version of the model that is presented in this chapter). We then used the soil properties that were derived from laboratory analysis (see table 8.1), and then used the van Genuchten model (equation 8.1) to solve for pressure head (ψ). We used hydrostatic conditions below the water table ($z = \psi$) and interpolated between known ψ values every 0.01m. Once the pressure head was calculated every 0.01m the van Genuchten model was used again and solved for the soil moisture (θ). The initial conditions are shown in Figure 8.3 with the red dashed line; the

figure includes the model results (blue solid line) of the soil moisture profile along with initial (red +) and final (blue x) field observations. The model overestimates the soil moisture showing slightly wetter conditions at the end of the simulation.

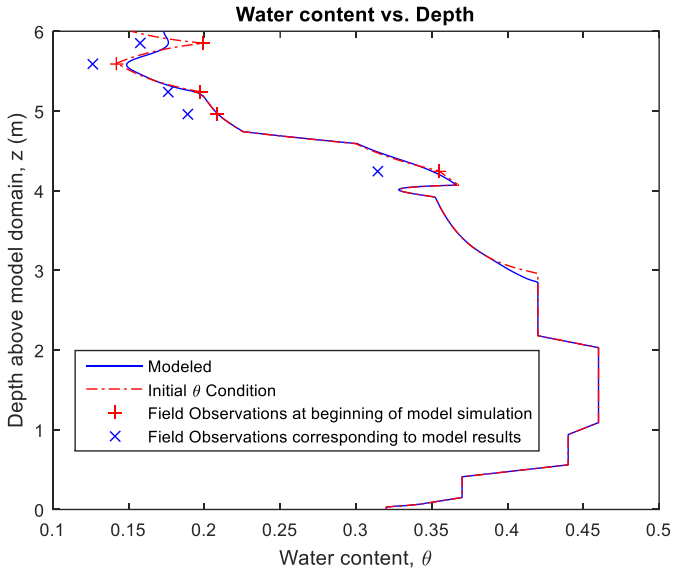

Figure 8. 3. Modeled soil moisture profile with depth and observed soil moisture values in the field. Model was run for 60 days. The blue solid line is the modeled soil moisture profile results and the red dashed line is the initial condition prescribed from which the model was initiated. The red +'s are the field observations at the beginning of the simulation and the blue x's are the field observations at the end of the simulation period.

Figures 8.4 through 8.6 compare the measured and modeled water table diurnal fluctuations for three plant water uptake parameter combinations that produce a good match. The water-table measurements are from the shallow alluvium well at location C (C-WT) from 6/13/2011 to 8/15/2011. These values for the plant water uptake parameters are shown in the caption of each figure). These parameters ranged from 50 to 85 m/m^3 for the root density parameter (RW_o), 400 to 995 for the root diameter, geometry, and arrangement parameter (C_s), 1.0×10^4 to 1.5×10^5 days/m for the root and plant conductivity parameter (C_r), and 3.25 to 3.29 m for the rooting depth (Zr_{max}) which corresponds to the relative root density function (rw_i) as seen in equation 8.8.

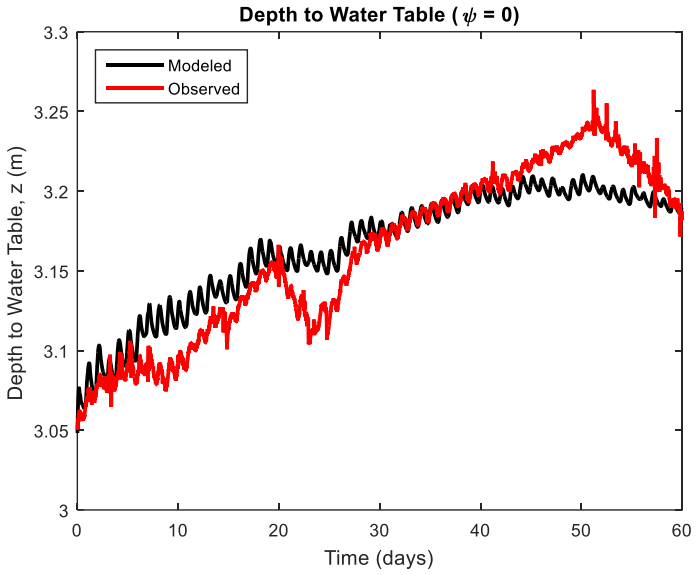

Figure 8. 4. Model run with $RW = 82\ m/m^3$(root density), $C_s = 400$, $C_r = 1.0 \times 10^5\ days/m$, Zr_{max} = 3.25 m (the rooting depth, from the surface to a length of 3.25 meters).

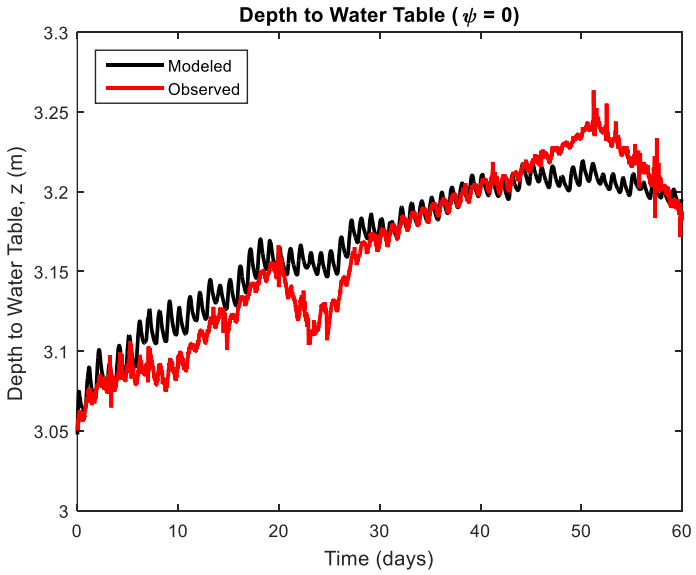

Figure 8. 5. Model run with $RW = 50\ m/m^3$(root density), $C_s = 995$, $C_r = 1.5 \times 10^4\ days/m$, Zr_{max} = 3.29 m (the rooting depth, from the surface to a length of 3.29 meters).

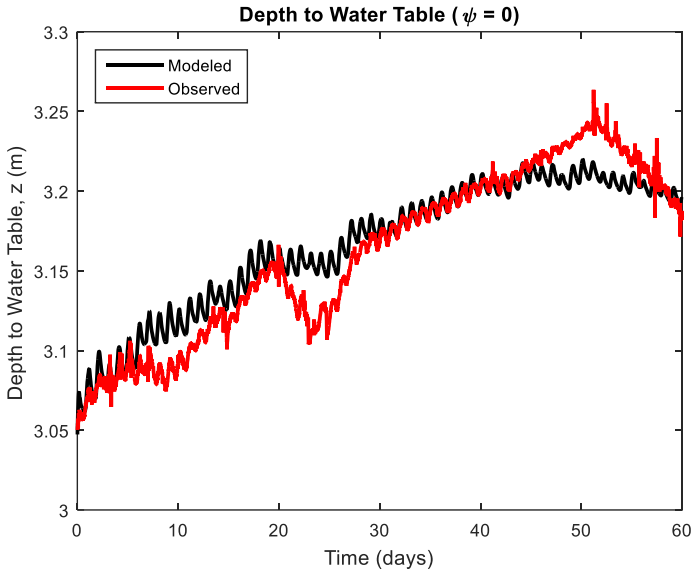

Figure 8. 6. Model run with $RW = 85\ m/m^3$(root density), $C_s = 920$, $C_r = 1.0 \times 10^5\ days/m$, $Zr_{max} =$ 3.29 m (the rooting depth, from the surface to a length of 3.29 meters).

The previous figures all display diurnal fluctuations in the water table, which is an indicator of the RET signal. By either changing the rooting depth or the root density there are significant changes in the water table variations produced by the model. If the rooting depth decreases the model shows a rise in ground water table and if the rooting density decreases (i.e. plant water uptake is reduced), then the diurnal signal is not as evident. Furthermore if the rooting density and rooting depth increase, the model responds with a much deeper and more prevalent signal as one would expect.

In the second version of the numerical model, the field estimated RET-values were uniformly distributed across a rooting depth of 3.3 meters as a sink term. Three different periods during the 2012 growing season were examined with the goal of modeling the soil moisture changes induced by the measured RET. A secondary goal was to compare the modeled total soil moisture change using the entire numerical model grid with that obtained using discrete sensor locations, to evaluate the limitations of the RET estimates

from the field. These periods were the same three periods that were shown in the previous chapter (refer to chapter VII). The distributed RET sink term was specified by constructing a diurnally varying function representing the average estimated RET for that specific period. The Q_{in} (when positive) or Q_{out} (when negative) term was precribed as a flux boundary condition at the bottom of the domain which is assumed as explained from the conceptual model. The following series of figures illustrates the results from the model and field observations. Figures 8.7 through 8.10 show the results and observations for period 1 (5/21-28/2012), figures 8.11 through 8.14 show the results and observations for period 2 (6/8-13/2012) and figures 8.15 through 8.18 show the results and observations for period 3 (7/18-27/2012). The red lines correspond to the RET estimates obtained by integrating the total soil moisture changes over the entire depth profile (RET_{model}) while the blue (RET_{full}) and green (RET_{top}) lines only use soil moisture values at a few discrete depths, which correspond to the depths of soil moisture sensors and the water table. The RET estimates obtained based on the soil moisture values at discrete depths followed the same procedure as the field data analysis:

1) A trapezoidal integration across 6 or 7 discrete soil moisture values was employed to estimate TSM_{top} or TSM_{full}.
2) The daily Q_{in} or Q_{out} values were estimated from the nighttime TSM slope, similar to the process followed in estimating Q_{in} or Q_{out} for the RET calculations from field measurements.

The estimated RET from the entire depth profile (RET_{model}) and using seven discrete points (RET_{full}) were very similar while the RET estimates obtained using only the six soil moisture sensors (RET_{top}) gave the lowest values (the six soil moisture sensors are

distributed across a depth of 1.6 m, which is less than half the depth of 3.3 m over which the RET sink term was uniformly distributed in this modeling exercise). Figures 8.7, 8.11 and 8.15 shown below compare the three different estimated RET results. During the first period RET_{model} estimated an average of 7.9 mm/day and 7.2 mm/day for RET_{full} and 4.1 mm/day for RET_{top}. The second period averaged 9.2, 7.8 and 4.7 mm/day respectively of RET. For the third period the estimated RET averaged 5.1 mm/day for RET_{model}, 4.2 mm/day for RET_{full} and 2.5 mm/day for RET_{top}.

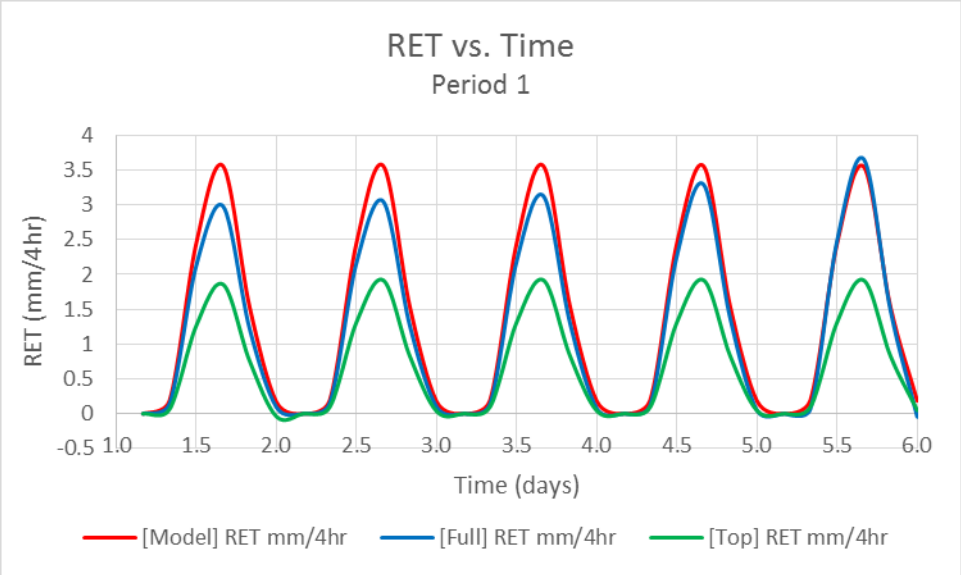

Figure 8. 7. Modeled RET by integrating the TSM across the entire depth(red line), RET estimated by using six discrete points and the water table location (blue line) and RET estimated by only using six discrete points for period 1.

Figures 8.8, 8.12 and 8.16 show the calculated Q_{in} or Q_{out} values obtained from the nighttime TSM slope. The Q values from the modeled TSM did not vary much through the five-day simulation run as did the Q values from the TSM_{top} and TSM_{full}. During the first period, Q values from the TSM model results remained around 4 mm/day while the values from the TSM_{full} varied from 1.3 to 3.8 mm/day and -0.9 to 0.1 mm/day from TSM_{top}. During

the second period, Q values from the modeled TSM stayed consistently around 5 mm/day and varied between 0.6 to 3.3 mm/day and -0.9-1.9 mm/day from the TSM_{full} and TSM_{top} nighttime slopes, respectively. Lastly during the third period Q values from the modeled TSM stayed around 3 mm/day and ranged from -0.5 to 1.1 mm/day from TSM_{full} and Q values from TSM_{top} remained negative throughout the five-day simulation and varied between -1.6 and -0.6 mm /day.

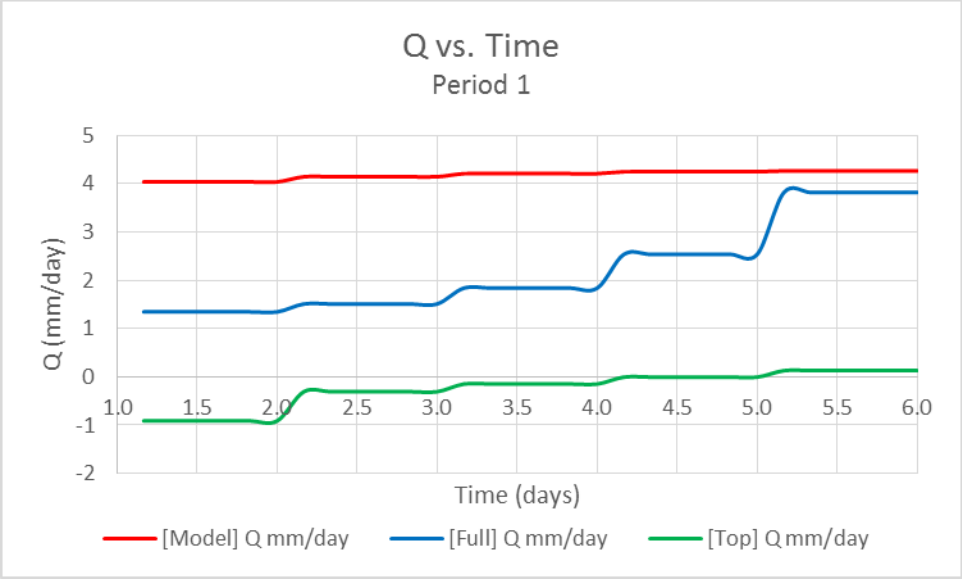

Figure 8. 8. Calculated daily Q_{in} or Q_{out} values that were determined from the nighttime TSM slope from the three different methods for period 1.

Figures 8.9, 8.13 and 8.17 show the change in soil moisture at six depth locations ($\Delta\theta_1$, $\Delta\theta_2$, $\Delta\theta_3$, $\Delta\theta_4$, $\Delta\theta_5$, and $\Delta\theta_6$). These locations correspond to the soil moisture sensor locations. Figures 8.9a, 8.13a and 8.17a show the modeled soil moisture changes and figures 8.9b, 8.13b, 8.17b show the observed soil moisture changes from the field. Even though the modeled and observed soil moisture changes do not match extactly, they do show some similarities. For example, during the first period as seen in figure 8.9 both the

modeled and observed $\Delta\theta_3$ (magenta colored line) shows some of the highest soil moisture changes. The magnitudes of changes in the water content are not too disparate.

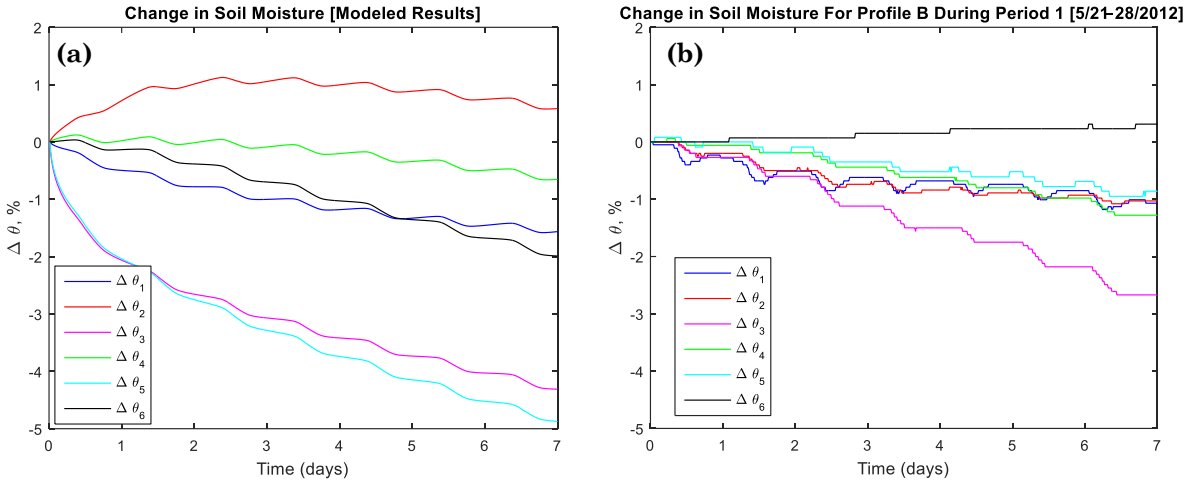

Figure 8. 9. Change in soil moisture at six depth locations for period 1 (5/21-28/2012); a) modeled results; b) field observations.

Figures 8.10, 8.14 and 8.18 shown below compare the total soil moisture changes using the three different methods previoulsy described (refer to chapter 5) - TSM changes based on the entire model grid (Model TSM), the TSM changes based on six sensor locations and the water table (TSM_{full}), and TSM changes only based on the six sensors (TSM_{top}). Both the modeled TSM and TSM_{full} show a recovery during the night time but TSM_{top} does not, rather it only seems to plateau during period 1. During period 2 as shown in figure 8.14 all three methods show a recovery during the night and during period 3. TSM_{top} has a small decline during the night or what is generally considered as the recovery (see figure 8.18).

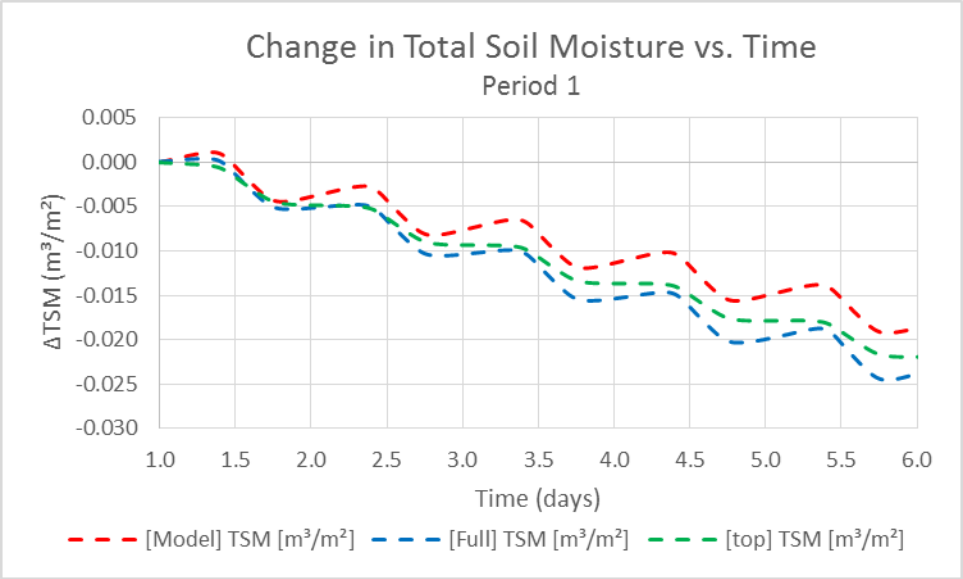

Figure 8. 10. Change in total soil moisture using three different approaches. Red dotted line uses the results from the entire profile, green dashed line uses values from six depths, and the blue dashed line also uses the same six depth location in addition to location of the water table.

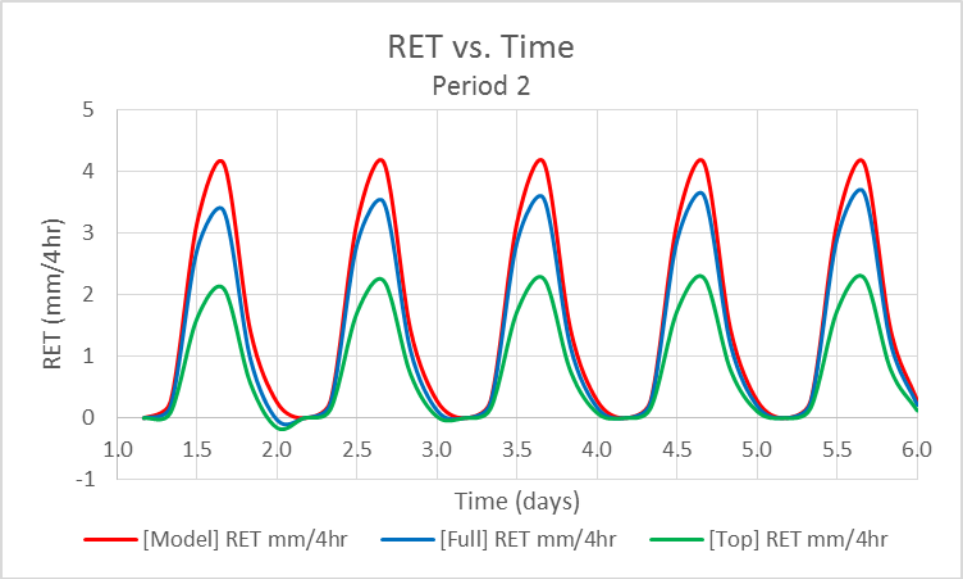

Figure 8. 11. Modeled RET by integrating the TSM across the entire depth(red line), RET estimated by using six discrete points and the water table location (blue line) and RET estimated by only using six discrete points for period 2.

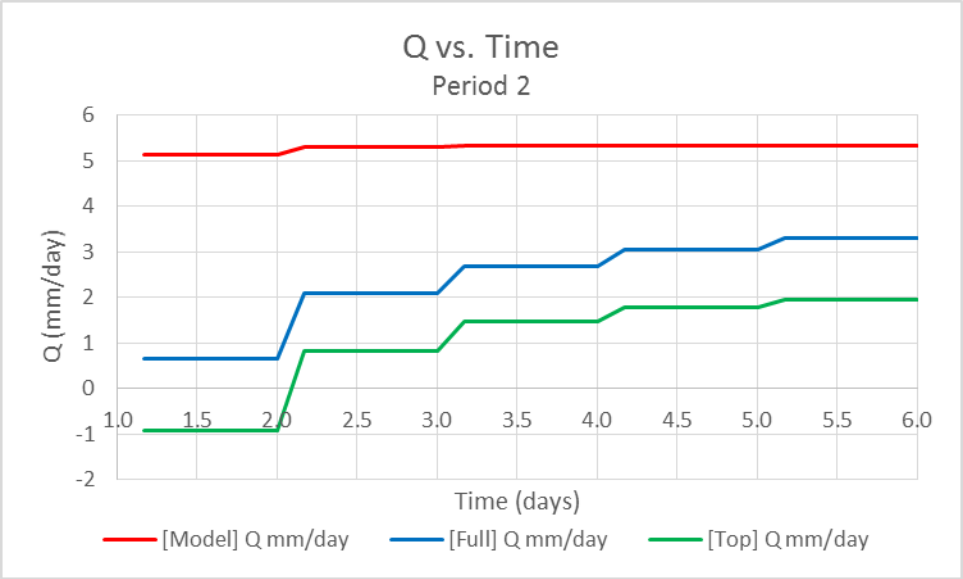

Figure 8. 12. Calculated daily Q_{in} or Q_{out} values that were determined from the nighttime TSM slope from the three different methods for period 2.

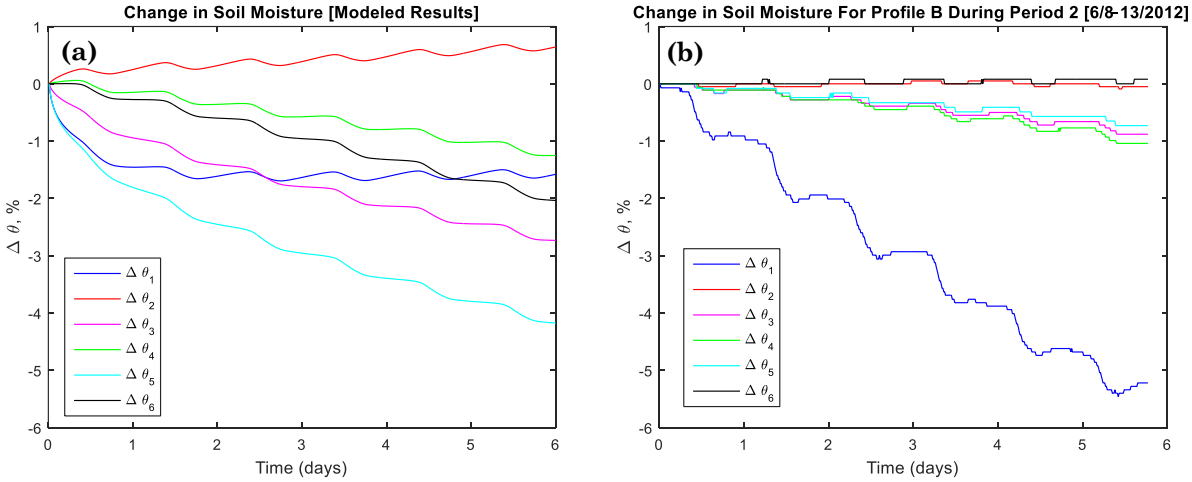

Figure 8. 13. Change in soil moisture at six sensor locations. (a) modeled results (b) field observations.

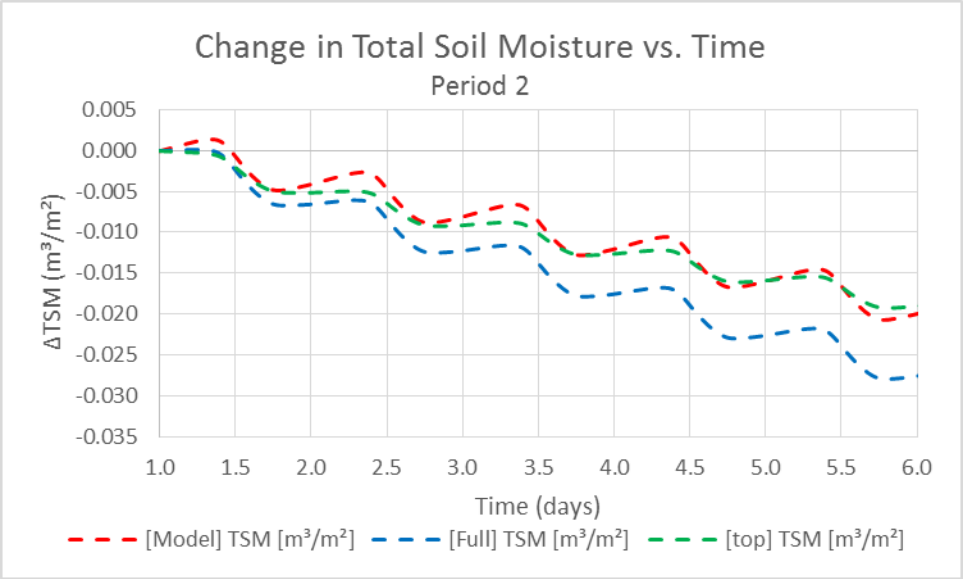

Figure 8. 14. Change in total soil moisture using three different approaches for period 2. Red dotted line uses the results from the entire profile, green dotted line uses values from six depths, and the blue dotted line also uses the same six depth location in addition to location of the water table.

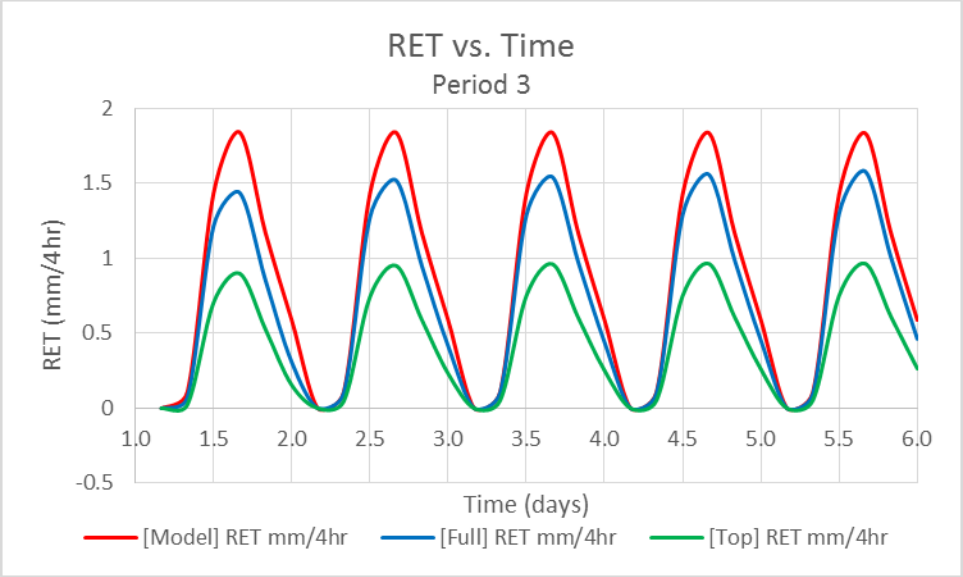

Figure 8. 15. Modeled RET by integrating the TSM across the entire depth(red line), RET estimated by using six discrete points and the water table location (blue line) and RET estimated by only using six discrete points for period 3.

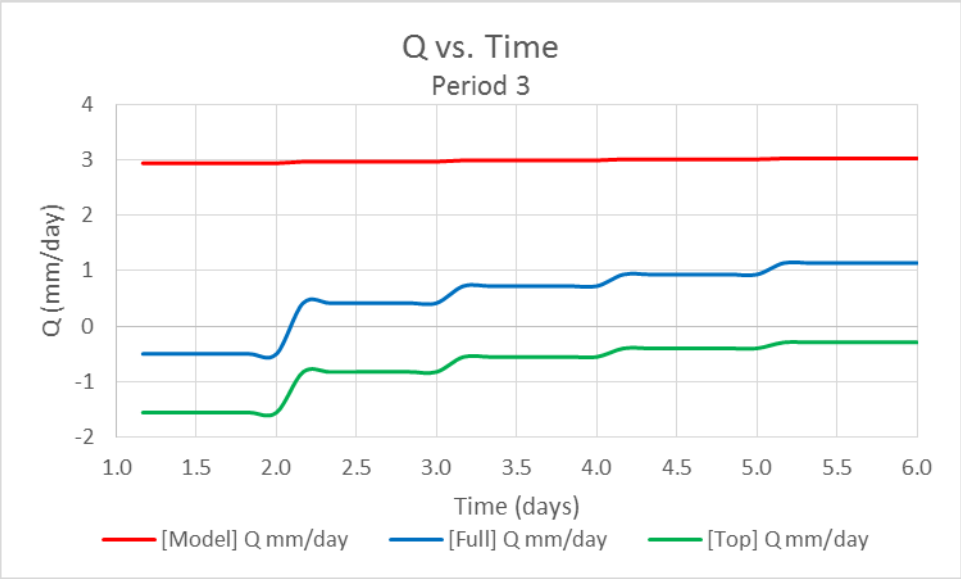

Figure 8. 16. Calculated daily Q_{in} or Q_{out} values that were determined from the nighttime TSM slope from the three different methods for period 3.

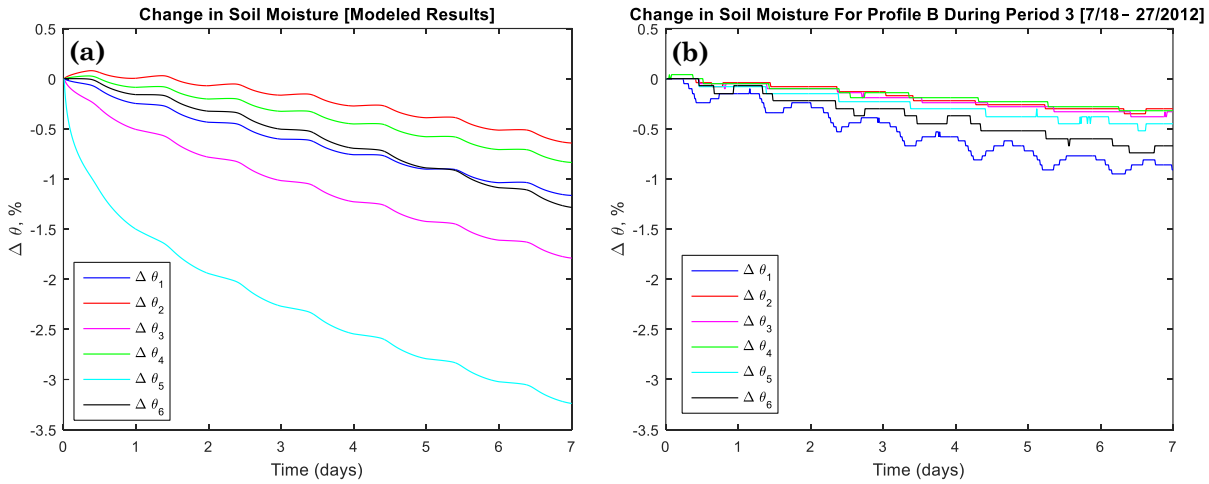

Figure 8. 17. Change in soil moisture at six sensor locations. (a) modeled results (b) field observations.

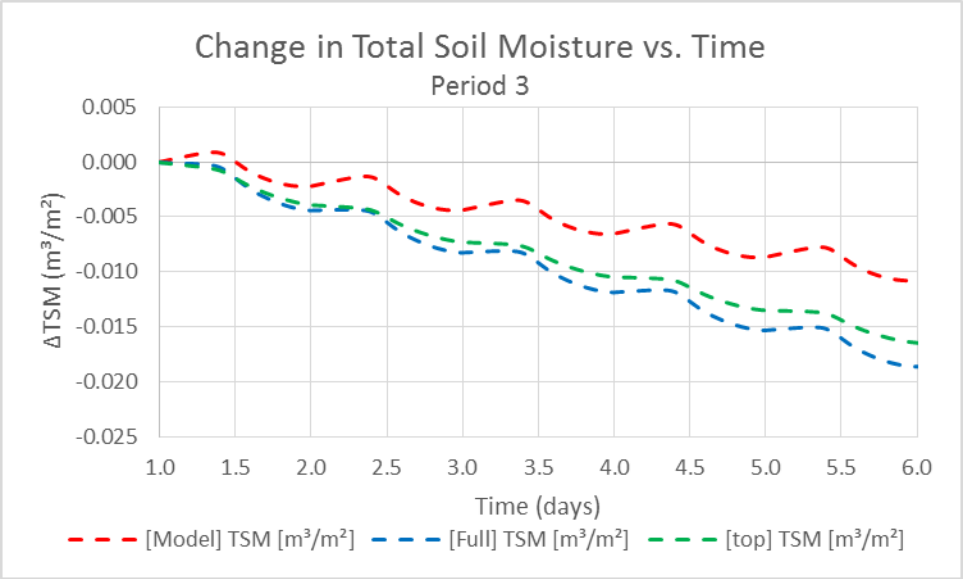

Figure 8. 18. Change in total soil moisture using three different approaches for period 3. Red dotted line uses the results from the entire profile, green dotted line uses values from six depths, and the blue dotted line also uses the same six depth location in addition to location of the water table.

These modeling exercises where helpful in understanding how much of a difference there is in the calculation of RET estimates using the different methods. What can be concluded is that even though it is understandable that by estimating the RET using discrete soil moisture measurements there will be some errors in the estimates, the errors seem to be minimal when using the TSM_{full} method when compared to modeled TSM where it uses the entire depth profile.

CHAPTER IX

SUMMARY AND CONCLUSIONS

This thesis focused on evaluating a subsurface water balance (SSWB) approach for estimating riparian evapotranspiration (RET) in a thick vadose zone (depth to water table ranged between 2 and 4 meters), where the soil moisture contribution to plant water uptake is significant, in contrast to many previous studies where the water balance could be accomplished based on groundwater table elevations. The study site was adjacent to Rock Creek in the Whitewater basin, south-central Kansas, on a 100 meter long reach, where the riparian zone width averages 45 m (Chapter II). The soils are comprised largely of silty loam and clay, with gravel fragments at greater depths (Chapter II). The deeper alluvial sediment in the riparian zone is primarily clay that acts as an aquitard overlying the bedrock and overlying this layer is more permeable alluvial sediment and soil. The SSWB approach was based on a monitoring network that included six soil moisture profilers (locations A-F) with capacitance sensors at 4-6 depths (during different periods of the study), 4 water table wells, a deep bedrock well, and a weather station (Chapter III). Due to technical challenges, cost, and limitations of readily available instrumentation, we could not install soil moisture sensors below a depth of about 1.8 m, which allows for the length of the access tube supplied with the capacitance sensors and a reasonable stick-up above the ground. Thus, the soil moisture sensors did not extend all the way down to the water table.

Preliminary observations indicated significant diurnal fluctuations in the total soil moisture (TSM) integrated over the depth range from the surface to the lowest sensor, and in shallow water table wells. These observations document the response of the subsurface

to the diurnal cycles in uptake of water by plants (primarily trees) and released as RET. A detailed examination of these observations led to the formulation of a conceptual model for the hydrogeology at the site (Chapter IV). The conceptual model developed in Chapter IV suggests that the stream is largely disconnected from the alluvium in the riparian zone, except during very high storm events that raise stream stage significantly, causing flow from the stream into a more permeable zone in the unconfined aquifer in the riparian alluvium. The unconfined aquifer in the alluvium is somewhat patchy, given the difficulties in measuring a water table at two of the shallow water table wells during relatively long durations. It is evident that RET is supplied by soil moisture and groundwater in the shallow alluvium (2.4-3 m deep). The water storage in the shallow alluvium is supplied directly by precipitation, and by rare high streamflow events that produce lateral flow from the stream. Although the deep bedrock well shows higher potentiometric head elevations than the shallow water-table wells, upward leakage from the confined aquifer below the deep alluvium is expected to be very small due to the low permeability and large thickness of the aquitard unit in-in the lower alluvium.

Based on the conceptual model developed in Chapter IV, a framework for water balance analysis was proposed and illustrated in Chapter V. The water balance analysis essentially employs a one-dimensional vertically integrated estimate of total soil moisture (TSM) that included the water-table data where available, but mostly involved the TSM between the ground surface and the lowest soil moisture sensor (TSM_{top}). Increase in TSM_{top} results from precipitation and exfiltration/capillary rise from the shallow water table. Decrease in TSM_{top} results from RET and downward infiltration (gravity drainage) at the depth of the lowest sensor. A key assumption in the SSWB approach is that the

upward or downward fluxes at the depth of the lowest sensor are slowly varying and may thus be estimated as constant values over 24-hour periods, based on the nighttime slope of TSM_{top} trends. Each profile location was analyzed independently and then combined to estimate transect-scale and reach-scale RET. The RET estimates also thus represent plant water uptake from the depth interval between the ground surface and the lowest soil moisture sensor.

The major findings of the study are contained in Chapters VI and VII, which report RET estimates at monthly time scales (Chapter VI) and during shorter periods within the growing season (Chapter VII). Chapter VII also reports a comparison of RET estimates obtained using the SSWB approach with LIDAR-based estimates. The study period extended from July 2010 to the end of 2013. There was significant variability in the precipitation between the three full years covered by the study - 2011, 2012 and 2013. While 2011 was a fairly wet year with storms in summer and late fall, 2012 was an extremely dry year. In 2013, relatively dry conditions during the first half of the year gave way to several high precipitation events in late July. In general TSM at all profile locations responded coherently to precipitation events. Yet, the actual TSM values differed significantly among the profile locations, as did the changes in TSM during periods of RET. There is a net loss in soil moisture storage in 2012 at all profile locations, whereas there is a general gain in soil moisture storage in the other years. In the annual cycle, TSM recovery tended to be highest during the spring, between around March and May on a consistent basis. In 2013, there was significant late summer increase in soil moisture due to higher than normal precipitation events in July and August. Continued precipitation events in the fall resulted in persistence of high soil moisture through the end of the year.

The RET estimates obtained from the different profile locations vary significantly, even though they typically exhibit coherent trends. In 2011, all locations exhibited the highest RET values in June (ranging from 2.21 to 5.55 mm/day). The RET is much lower from September through November. In 2012, the highest RET values were again observed in June (ranging from 3.47 to 7.44 mm/day, higher than in 2011; even though the American Society of Civil Engineers (ASCE) standardized reference evapotranspiration (ETsz) for June 2012 is slightly lower than in 2011). RET values in July 2012 were only slightly higher than in July 2011, and there was a steep drop in RET at all profile locations during the very dry period from August to November 2012. The duration from August 2012 to April 2013 shows the lowest TSM values over the entire study period, due to almost no precipitation. Between April and June 2013, RET values at all profiles continued to be extremely low. Following late summer precipitation events, TSM increased significantly and higher values of RET persisted through August and into October. This behavior was very much in contrast with 2011 and 2012 when the depletion of soil moisture during the summer resulted in very low RET values after August.

It is also useful to examine the net subsurface inflow/outflow, which was inferred from the nighttime slope of the TSM trends on a diurnal basis. During the summer growing season, profiles A, C, D and E tend to behave more like recharge zones (the G'-values are mostly negative), whereas profiles B and F (and to a small extent profile E) behave like discharge zones (positive G' values, suggesting exfiltration or capillary rise from groundwater). However the average values of G' for the entire study period (including periods outside the growing season) reveal that on average, all profile locations behave like

recharge zones, which is consistent with TSM_{top} not representing the full vertical thickness of the vadose zone down to the water table. Because TSM_{top} only reflects the upper 1.8 m of the vadose zone and the water table is typically at 3.5 m depth, it is expected that gravity drainage will dominate at the level of the lowest sensor through most of the year, except during periods in the growing season when capillary rise is driven by root water uptake. The G'-values exhibited the highest variability when compared to the other water balance variables. During the growing season G' ranged from minimum of -3 mm/day seen at profile A to a maximum of 2 mm/day seen at profile F.

In Chapter VII, soil moisture profiles and soil moisture variations at specific depths were described for three periods within the growing season - early, peak and late growing season. In 2011 and 2012, these periods correspond to replenished soil moisture (early), high RET rates driven by peak summer conditions (peak) and reduced RET due to depleted soil moisture (late). In 2013, the late period continued to show high RET rates because of late summer precipitation. The general behavior of the soil moisture profiles, TSM variations and soil moisture variations at individual sensor locations is consistent with the precipitation forcing and inferred behavior of RET and net subsurface inflow/outflow. Examination of individual soil moisture sensors provided additional insights on the depth interval from which moisture was being extracted by roots. For instance, during the extremely dry conditions of period 3 from 2012, the deeper sensors at all profile locations began to indicate significant depletion, suggesting that trees were attempting to extract water from greater depths due to the extremely dry surface conditions. At times when significant soil moisture was available across a range of depths, the shallowest depths typically showed the greatest soil moisture depletions at all profile locations early in the

growing season. During periods 2 (peak growing season), soil moisture depletion was distributed over a greater range of depths. In some periods and profile locations, moisture depletion was significant at isolated intermediate depths, behavior that cannot be explained based on hydrologic factors alone.

The behavior during three periods in 2011-2013 further accentuates understanding of the heterogeneity in soil moisture depletion and RET estimates across the six profile locations. The variability in RET is particularly surprising because with the exception of profile D (which was on the edge of the riparian zone), all other profile locations are well within the riparian zone. However, variations in local vegetation cover were clearly observable between the profile locations. Profile location F and B generally behaved like "discharge zones" during the growing season, suggesting that plant water uptake was driving capillary rise or exfiltration. Profile location D always behaves like a "recharge zone", which makes sense since it is the location furthest away from the stream. The remaining profiles behaved mostly as recharge zones. The RET estimates from within the same period varied by up to a factor of 3 between the profile locations A, B and F (Table 7.2). Across all periods and profiles, the ratio of RET to the ASCE standardized ETsz varied from 0.3 to 1.08 (exceedance of 1.0 likely reflects the difference in crop coefficient between a well-watered grass and riparian vegetation). It is also interesting to note that profile F showed the highest RET rates more or less consistently through the study period, except following the long dry spell in 2012. The RET in period 1 of 2013 at profile F is surprising low compared to the RET estimates from profile F at other times, suggesting impairment of vegetation health during the long dry spell in 2012-13. In the second two periods of 2013, the RET estimates at profile A were slightly higher than at profile F.

The comparison of SSWB based RET estimates with the LIDAR estimates was a very useful exercise. A detailed evaluation of the SSWB RET estimates during the days covered by the LIDAR campaign reveal daily RET variations of nearly a factor of 8 across the different profile locations (July 9, 2011). The RET estimated at profile F was significantly larger than at other profile locations. Fortuitously, the reach-scale RET estimated by trapezoidal integration of the RET estimates from individual profiles agreed reasonably well with the LIDAR estimated. Inclusion of profile F was critical to obtaining a good match between the LIDAR and SSWB RET estimates, which indicated the importance of areas of full canopy of trees within the riparian zone. The integrated RET estimate based only on the central transect (profiles A, B, C and D), which did not have a full canopy, did not match the LIDAR measurements very well.

In an overall assessment, we conclude that our field study was successful in obtaining reliable SSWB based estimates of RET from the depth range covered by the soil moisture sensor network (~1.8 m depth) at individual profile locations. However, based on the variability of the RET estimates across the different profile locations and the comparison with the LIDAR estimates, we conclude that a significantly larger number of sensors would be necessary to obtain reliable reach-scale RET estimates in riparian zones with thick vadose zones and spatial variability in vegetation type and density. Unlike in groundwater-dominated riparian zones where lateral groundwater flows readily occur in high permeability zones and can potentially play a role in smoothing out variations over small scales, in thick vadose zones with low-permeability sediments, a lack of horizontal correlation in the dynamics of vadose zone processes may be anticipated in response to

heterogeneous root water uptake. At the study site, the unconfined aquifer within the alluvium is also relatively patchy and root water uptake relies largely on soil moisture. For all these reasons, the significant spatial variability in one-dimensional vertical SSWB based estimates of RET within even the relatively short reach (100 m) is not surprising. The agreement between the LIDAR and reach-integrated SSWB RET estimates was rather fortuitous as noted earlier. Another reason to be cautious in inferring agreement between the LIDAR and SSWB based estimate is evident from chapter VIII - the numerical simulation results shown in chapter VIII suggest that RET estimates based on TSM_{top} can significantly underestimate the true RET if the rooting depth of vegetation extends over the entire thickness of the vadose zone and down below the water table. At the study site, the rooting depth is not well constrained and likely also varies across the profile locations. The SSWB based RET estimation approach is not very expensive compared to other approaches for estimating RET. Thus, it may be feasible to install a larger number of soil moisture profilers across a reach. It is also important to consider using multiple access tubes in sequence to install soil moisture sensors all the way down to the water table in future research. However, this may be challenging to accomplish when the vadose zone is very deep.

REFERENCES

Aber, J.S. (1991). Surficial Geology of Butler County, Kansas. *Kansas Geological Survey Open-file Report* 1991-48.

Allen, R. G., L. S. Pereira, D. Raes, and M. Smith., (1998). Crop evapotranspiration guidelines for computing crop water requirements. Rome: *Food and Agriculture Organization. FAO Irrigation and Drainage Paper No. 56.*

Allen, R. G., I. A. Walter, R. L. Elliott, T. A. Howell, D. Itenfisu, M. E. Jensen, and R. L. Snyder, (Eds.). (2005). The ASCE Standardized Reference Evapotranspiration Equation. *ASCE Publications*.

Alva, A. K. (2008). "Setpoints for Potato Irrigation in Sandy Soils Using Real-Time, Continuous Monitoring of Soil-Water Content in Soil Profile." *Journal of Crop Improvement*, 21(2), 117–137.

Akindunni, F. F. and R. W. Gillham. (1992), Unsaturated and Saturated Flow in Response to Pumping of an Unconfined Aquifer: Numerical Investigation of Delayed Drainage. *Ground Water*, 30: 873–884. doi: 10.1111/j.1745-6584.1992.tb01570.x

Bond BL, J. A. Jones, G. Moore, N. Phillips, D. Post, J.J. McDonnell. (2002). The zone of vegetation influence on baseflow revealed by diel patterns of streamflow and vegetation water use in a headwater basin. *Hydrological Processes* 16: 1671–1677.

Bren, L.J. (1997). Effects of slope vegetation removal on the diurnal variations of a smallmountain stream. *Water Resources Research*, Vol. 33, No. 2, p. 321–331, ISSN 0043-1397.

Busch, D. E., N. L. Ingraham, and S. D. Smith. (1992). Water uptake in woody riparian phreatophytes of the southwest- ern United States: A stable isotope study. *Ecological Applications* 2:450–459.

Butler, J. J., G. J. Kluitenberg, D. O. Whittemore, S. P. Loheide, W. Jin, M. A. Billinger, and X. Zhan, (2007). A field investigation of phreatophyte-induced fluctuations in the water table. *Water Resources Research*, 43(2), 1–12.

Celia, M.A., E. T. Bouloutas, and R. L. Zarba. (1990). A general mass-conservative numerical solution of the unsaturated flow equation. *Water Resources Research*, 26: 1483-1496.

Clement, T. P., W. R. Wise, and F. J. Molz. (1994). A physically based, two-dimensional, finite-difference algorithm for modeling variably saturated flow. *Journal of Hydrology*, *161*(1-4), 71-90. doi:10.1016/0022-1694(94)90121-X

Cooper, D. (2000). Spatial and Temporal Properties of Water Vapor and Latent Energy Flux over a Riparian Canopy. *Agricultural and Forest Meteorology* 105 (1-3): 161–83.

Cooper, D. I., W. E. Eichinger, J. Archuleta, L. Hipps, J. Kao, M. Y. Leclerc, C. M. Neale, and J. Prueger. (2003). Spatial Source-Area Analysis of Three-Dimensional Moisture Fields from Lidar, Eddy Covariance, and a Footprint Model. *Agricultural and Forest Meteorology* 114 (3-4): 213–34. doi:10.1016/S0168-1923(02)00175-2.

Eddy, T. A. (1995). Phreatophyte survey and water-use estimates for nine river systems in Kansas. In Proceedings of the Fourteenth North American Prairie Conference, edited by DC Hartnett (pp. 171-173).

Eichinger, W. (2000). Estimation of Spatially Distributed Latent Heat Flux over Complex Terrain from a Raman Lidar. *Agricultural and Forest Meteorology* 105 (1-3): 145–59. doi:10.1016/S0168-1923(00)00183-0.

Eichinger, W.E., D.I. Cooper, L.E. Hipps, W.P. Kustas, C.M.U. Neale, and J.H. Prueger. (2006). Spatial and Temporal Variation in Evapotranspiration Using Raman Lidar. *Advances in Water Resources* 29 (2): 369–81.

Eichinger, W., and D. I. Cooper. (2007). Using Lidar Remote Sensing for Spatially Resolved Measurements of Evaporation and Other Meteorological Parameters. *American Society of Agronomy Journal* 99(1): 255-271.

Gatewood, J. S., T. W. Robinson, B. R. Colby, J. D. Hem, and L. C. Halpenny (1950). Use of water by bottom-land vegetation in lower Safford Valley, Arizona. *U.S. Geol. Surv. Water Supply Pap.*, 1103.

Gribovszki, Z., P. Kalicz, J. Szilágyi, and M. Kucsara. (2008). Riparian zone evapotranspiration estimation from diurnal groundwater level fluctuations. *Journal of Hydrology*, 349(1), 6-17.

Grimm, N. B., A. Chacon, C. N. Dahm, S. W. Hostetler, O. W. Lind, P. L. Starkweather, and W. W. Wurtsbaugh. (1997). Sensitivity of aquatic ecosystems to climatic and anthropogenic changes: The basin and range, American Southwest and Mexico. *Hydrological Processes* 11:1023–1041.

Grossman, R. L., (1992) Convective boundary layer budgets of moisture and sensible heat over an unstressed prairie. *J. Geophys. Res.*, 97, 18 425–18 438.

Goodrich, D. C., R. Scott, J. Qi, B. Goff, C. L. Unkrich, M. S. Moran, D. Williams, S. Schaeffer, K. Snyder, R. MacNish, T. Maddock, D. Pool, A. Chehbouni, D. I. Cooper, W. E. Eichinger, W. J. Shuttleworth, Y. Kerr, R. Marsett, and W. Ni. (2000). Seasonal estimates of riparian evapotranspiration using remote and in situ measurements. *Agricultural and Forest*, 105(November), 281–309

Guswa, A. J., M. A. Celia, and I. Rodriguez-Iturbe. (2002). Models of soil moisture dynamics in ecohydrology: A comparative study. *Water Resources Research*, 38(9).

Guswa, A. J. (2005). Soil-moisture limits on plant uptake: An upscaled relationship for water-limited ecosystems. *Advances in Water Resources*, 28(6), 543–552.

Harvey, J.W., K.E. Bencala and G.W. Zellweger. (1991). Preliminary investigation of the effect of hillslope hydrology on the mechanics of solute exchange between streams and subsurface gravel zones. U.S.G.S. Toxic Substances Hydrology Program, Proceedings of the Technical Meeting, Monterey, California, *U.S. Geological Survey Water Resources Investigations Report* 91-4034, 413-418.

Hays, K. B. (2003). Water use by saltcedar (Tamarix sp.) and associated vegetation on the Canadian, Colorado and Pecos Rivers in Texas (Doctoral dissertation, Texas A&M University).

Hipps, L. E., D. I. Cooper, W. Eichinger, D. G. Williams, S. M. Schaeffer, K. A. Snyder, R. Scott, A. Chehbouni, C. Watts, O. Hartogensis, J. -P. Lhomme, B. Monteny, J. -P. Brunel, G. Boulet, J. Schieldge, H. A. R. DeBruin, W. J. Shuttle- worth, and Y. Kerr. (1998). A summary of processes which are connected to evaporation of riparian and heterogeneous upland vegetation in arid regions. Pages 43–48 in E. F. Wood, A. G. Chehbouni, D. C. Goodrich, D. J. Seo, J. R. Zimmerman (eds.). Proceedings from the Special Symposium on Hydrology American Meteorological Society, 11– 16 January 1998. Phoenix, Arizona.

Irmak, S., I. Kabenge, D. Rudnick, S. Knezevic, D. Woodward, and M. Moravek. (2013). Evapotranspiration Crop Coefficients for Mixed Riparian Plant Community and Transpiration Crop Coefficients for Common Reed, Cottonwood and Peach-Leaf Willow in the Platte River Basin, Nebraska-USA. *Journal of Hydrology* 481 (February): 177–90.

Jabro, J. D., B. G. Leib, and A. D. Jabro. (2005). Estimating soil water content using site-specific calibration of capacitance measurements from Sentek EnviroSCAN systems. *Applied Engineering in Agriculture*, 21(3), 393–400.

Lautz, L. K. (2008). Estimating groundwater evapotranspiration rates using diurnal water-table fluctuations in a semi-arid riparian zone. Hydrogeology Journal 16(3), 483-497.

Lee, Philip, C. Smyth, and S. Boutin. (2004). Quantitative Review of Riparian Buffer Width Guidelines from Canada and the United States. *Journal of Environmental Management* 70 (2): 165–80. doi:10.1016/j.jenvman.2003.11.009.

LeMone, M. A., R. L. Grossman, R. T. McMillen, K. Liou, S. C. Ou, S. McKeen, W. Angevine, K. Ikeda, and F. Chen. (2002). Cases-97: Late-Morning Warming And Moistening Of The Convective Boundary Layer Over The Walnut River Watershed. *Boundary-Layer Meteorology* 104 (1): 1–52. doi:10.1023/A:1015569104180.

Loheide, S. P., J. J. Butler Jr., and S. M. Gorelick (2005), Estimation of groundwater consumption by phreatophytes using diurnal water table fluctuations: A saturated-unsaturated flow assessment. *Water Resources Research*., 41, W07030, doi:10.1029/2005WR003942.

Lundquist J., and D. Cayan. (2002). Seasonal and spatial patterns in diurnal cycles in streamflow in the Western United States. *Journal of Hydrometeorology* 3: 591–603

Jobbágy, E. G., M. D. Nosetto, P. E. Villagra, and R. B. Jackson. (2011). Water subsidies from mountains to deserts: their role in sustaining groundwater-fed oases in a sandy landscape. *Ecological Applications*, 21(3), 678-694.

Machavaram, M. V., D.O. Whittemore, M.E. Conrad and N.L.Miller. (2006). Precipitation induced stream flow: An event based chemical and isotopic study of a small stream in the Great Plains region of the USA. *Journal of Hydrology*, 330, 470-480, 2006.

McMaster, G S, and W W Wilhelm. (1997). Growing Degree-Days: One Equation, Two Interpretations. *Agricultural and Forest Meteorology* 87: 291–300.

Mac Nish, R.D., C. L. Unkrich, E. Smythe, D. C. Goodrich, T. Maddock. (2000). Comparison of riparian evapotranspiration estimates based on a water balance approach and sap flow measurements. *Special SALSA Edition of Journal of Agricultural and Forest Meteorology*, 105, 271–279.

Miller, G. R., X. Chen, Y. Rubin, S. Ma,and D.D. Baldocchi. (2010). Groundwater uptake by woody vegetation in a semiarid oak savanna. *Water Resources Research*, 46(10).

Moncrieff, J., P. Jarvis, and R. Valentini. (2000). Canopy fluxes. In: Sala, O.E., Jackson, R.B., Mooney, H.A. (Eds.), *Methods in Ecosystem Science*. Springer, New York, pp. 161–180.

Mould, D. J., E. Frahm, T. Salzmann, K. Miegel, and M. C. Acreman. (2010). Evaluating the use of diurnal groundwater fluctuations for estimating evapotranspiration in wetland environments: case studies in southeast England and northeast Germany. *Ecohydrology*, 3(3), 294-305.

Mualem, Y. (1976). A new model for predicting the hydraulic conductivity of unsaturated porous media. *Water Resources Research*, American Geophysical Union, 12(3), 513–522.

Nagler, P.L., E. P. Glenn, and T.L. Thompson. (2003). Comparison of transpiration rates among saltcedar, cottonwood, and willow trees by sap flow and canopy temperature methods. *Agricultural and Forest Meteorology*. 116: 73-89.

National Research Council. (2002) Riparian Areas: Functions and Strategies for Management. Washington, DC: The National Academies Press. http://www.nap.edu/read/10327/chapter/3#33

Nachabe, M., N. Shah, M. Ross, and J. Vomacka. (2005). Evapotranspiration of two vegetation covers in a shallow water table environment. *Soil Science Society of America Journal*, 69(2), 492. Soil Science Society.

Newman, B. D., B. P. Wilcox, S. R. Archer, D. D. Breshears, C. N. Dahm, C. J. Duffy, N. G. McDowell, F. M. Phillips, B. R. Scanlon, and E. R. Vivoni. (2006). Ecohydrology of Water-Limited Environments: A Scientific Vision. *Water Resources Research* 42 (6): 1–15. doi:10.1029/2005WR004141.

Ojha, C. S., K. S. Prasad, V. Shankar, and C. A. Madramootoo, (2009). Evaluation of a Nonlinear Root-Water Uptake Model. *Journal of Irrigation and Drainage Engineering*, 135(3), 303.

Orellana, F., P. Verma, S. P. Loheide, and E. Daly. (2012). Monitoring and modeling water-vegetation interactions in groundwater-dependent ecosystems. *Reviews of Geophysics*, 50(3).

Paltineanu, I. C., and J. L. Starr. (1997). Real-time soil water dynamics using multisensor capacitance probes: Laboratory calibration. *Soil Science Society of America Journal*, 61(6), 1576–1585.

Paltineanu, I. C., and J. L. Starr. (2000). Real-time soil water dynamics. *Standard Handbook of Environmental Science, Health, and Technology*, J. H. Lehr and J. K. Lehr, eds., McGraw-Hill Standard Handbooks, 4.45–4.57.

Penner, H.L., S. C. Ekart, D. A. Ewing, G. Schmidt, and J. Smith. (1975). Soil survey of Butler County, Kansas: U.S. Department Agriculture, Soil Conservation Service.

Peters, A, and W. Durner, W. (2008). Simplified evaporation method for determining soil hydraulic properties. *Journal of Hydrology*, 356(1-2), 147–162.

Rahgozar, M., N. Shah, and M. Ross. (2012). Estimation of evapotranspiration and water budget components using concurrent soil moisture and water table monitoring. *ISRN Soil Science*, vol. 2012, Article ID 726806, 15 pages, doi:10.5402/2012/726806

Rosenberry, D. O., and T. C. Winter. (1997), Dynamics of water-table fluctuations in an upland between two prairie-pothole wetlands in North Dakota. *Journal of Hydrology*, Volume 191, Issues 1–4, 266-289.

Rowland, R., Y. A. Pachepsky, and A. K. Guber. (2011). "Sensitivity of a Capacitance Sensor to Artificial Macropores." *Soil Science*, 176(1), 9–14.

Schaeffer, S.M., D. G. Williams, and D.C. Goodrich. (2000). Transpiration of cottonwood forest estimated from sap flux. *Agricultural and Forest Meteorology*. 105: 257-270

Schilling, K. E. (2007). Water table fluctuations under three riparian land covers, Iowa (USA). *Hydrologic Processes* 21:2415–2424, DOI 10.1002/hyp.6393

Schilling, K. E., and P. Jacobson. (2009). Water uptake and nutrient concentrations under a floodplain oak savanna during a non-flood period, Lower Cedar River, Iowa. *Hydrologic Processes*, 23(21), 3006–3016.

Scott, R.L., W. J. Shuttleworth, D. C. Goodrich, and T. Maddock III. (2000). The water use of two dominant vegetation communities in a semiarid riparian ecosystem. *Agricultural and Forest Meteorology* 150, 241–256.

Scott, R. L., C. Watts, J. Garatuza, E. Edwards, D. C. Goodrich, and D. Williams. (2002). Measuring the distribution of surface energy and water fluxes in a riparian mesquite savannah-type ecosystem. *paper presented at 2nd Annual Meeting, Semi-Arid Hydrol. and Riparian Areas (SAHARA)*, Tucson, Ariz.

Scott, Russell L., C. Watts, J. G. Payan, E. Edwards, D. C. Goodrich, D. Williams, and W. J. Shuttleworth. (2003). The Understory and Overstory Partitioning of Energy and Water Fluxes in an Open Canopy, Semiarid Woodland. *Agricultural and Forest Meteorology* 114 (3-4): 127–319. doi:10.1016/S0168-1923(02)00197-1..

Scott, R.L., E. A. Edwards, W. J. Shuttleworth, T. E. Huxman, C. Watts, and D. C. Goodrich. (2004). Interannual and seasonal variation in fluxes of water and carbon dioxide from a riparian woodland ecosystem. *Agricultural and Forest Meteorology* 122, 65–84.

Scott, R. L.,W. L. Cable, T. E. Huxman, P. L. Nagler,M. Hernandez, and D. C. Goodrich (2008), Multiyear riparian evapotranspiration and groundwater use for a semiarid watershed. *Journal of Arid Environment*, 72(7), 1232–1246.

Sleezer, R.O., (1990). Drainage development and chert gravel deposits in Butler County, Kansas: Unpub. Master's thesis, Emporia State University, 37 p.

Smiley, P. C., K. W. King, and N. R. Fausey. (2011). Influence of Herbaceous Riparian Buffers on Physical Habitat, Water Chemistry, and Stream Communities within Channelized Agricultural Headwater Streams. *Ecological Engineering* 37 (9). Elsevier B.V.: 1314–23. doi:10.1016/j.ecoleng.2011.03.020.

Starr, J. L., and I. C. Paltineanu. (1998). Real-time soil water dynamics over large areas using multisensor capacitance probes and monitoring system. *Soil Science Society American Journal*, 47(1-2), 43–49.

Stromberg, J. C. (1993). Fremont cottonwood-Goodding willow riparian forests: A review of their ecology, threats, and recovery potential. *Journal of the Arizona-Nevada Academy of Science* 26(3):97–110.

Stull, R., (1988). An Introduction to Boundary Layer Meteorology. Kluwer Academic Publishers, Boston.

Troxell, H. C. (1936), The diurnal fluctuation in the ground-water and flow of the Santa Ana river and its meaning. *Eos, Transactions American Geophysical Union*, 17(4), 496– 504.

Unland, H.E., A.M. Arain, C. Harlow, P.R. Houser, J. Garatuza-Payan, P. Scott, O.L. Sen, and W.J. Shuttleworth.(1998) Evaporation from a Riparian System in a Semi-Arid Environment. *Hydrologic Processes*. 12: 527-542.

van Genuchten, M. T. (1980). A closed-form equation for predicting the hydraulic conductivity of unsaturated soils. *Soil Science Society of America Journal*, 8, 892–898.

Weeks, E. P., and M. L. Sorey (1973), Use of finite-difference arrays of observation wells to estimate evapotranspiration from ground water in the Arkansas River Valley, Colorado. *U.S. Geologic Survey Water Supply Pap*er. 2029-C, 27 pp.

Westenburg, C.L., D. P. Harper, and G. A. DeMeo. (2006). Evapotranspiration by phreatophytes along the lower Colorado River at Havasu National Wildlife Refuge, Arizona. *U.S. Geological Survey Scientific Investigations Report* 2006-5043, 44 p. Available at URL: <http://pubs.water.usgs.gov/sir20065043>.

White W., (1932), A method of estimating groundwater supplies based on discharge by plants and evaporation from soil. *U.S. Geologic Survey Water Supply Paper*, 659, 105pp.

Wicht, C. L. (1941). Diurnal fluctuation in Jonkershoek streams due to evaporation and transpiration. *Journal of the South African Forestry Association*, 7, 34-49

Williams, D., Scott, R. L. (2009). Vegetation-hydrology interactions: dynamics of riparian plant water use. *Ecology*, 37-56.

Zeller, D.E., (ed.), (1968). The stratigraphic succession in Kansas. *Kansas Geological Survey, Bulletin*, 189, 81 p.

APPENDIX A: Visual Soil Analysis

Table A 1. Visual inspection of soil core sample no. 4 (Well D, furthest from creek)

CORE SAMPLE NO. 4				
Soil Core	Depth penetrated (ft)	Depth recovered (ft)	Observational depths (ft)	Observational descriptions
4-1	0.00	0.00		
	5.00	3.64	3.64	Unconsolidated material has a dark brown color seems to have a lot of organic material (like compost)
4-2	5.00	0.00		
			1.67	Unconsolidated material has a dark brown color seems to have a lot of organic material (like compost)
			1.10	brown soil with more rock/shale broken particles unconsolidated
			0.28	darker brown material clayish more compacted or consolidated
	10.00	4.61	0.51	redish brown with more light tan mix, very loose has some broken shale
			0.50	redish brown with tan mix unconsolidated material
			0.55	redish brown color consolidated material
4-3	10.00	0.00		
	15.00	5.00	5.00	Full core, redish brown with streaks of light tan soil consolidated clay material at bottom still wet and very clayish the light color soil is more sticky than redish brown soil, the clear plastic has (core sieve) has white streaks as if had a hard time going into the soil.
4-4	15.00	0.00		
	17.50	4.88	4.74	Full core, redish brown with light tan color streaks mixture and consolidated
			0.14	Was in a plasitc Ziplock bag (is lables as the bottom of this core sample). Is very hard as it is dry.
4-5	17.50	0.00		
	18.50	2.83	2.83	Redish brown with light gray tan color, and seems more unconsolidated then other samples. At the bottom, the solis was broken like clay hard particles (crumbly).
4-6	18.50	0.00		
	19.50	2.94	2.44	Light brown soil with grey, looks unconsolidated as previous core sample
			0.50	bottom 6" looks more silty with more greyish brown color.
4-7	19.50	0.00		
	20.00	0.95	0.95	Light tan with grey consolidated all the way through at the top of the sample the it has some pieces that came apart and sounds very hard like dry clay
4-8	20.00	0.00		
	21.75	2.47	2.47	Light brown with tan mix at the top the soil is more crumbly and at the bottom looks very consolidated.

Table A 2. Visual inspection of soil core sample no. 5 (Well C, 2nd furthest from creek)

CORE SAMPLE NO. 5				
Soil Core	Depth penetrated (ft)	Depth recovered (ft)	Observational depths (ft)	Observational descriptions
5-1	0.00	0.00		
			2.00	First 2 feet is clay-silt material
	5.00	3.28	0.17	About 2 inches ther is a sand layer
			1.11	Rest is unconsolidated sand/clay-silt mix
5-2	5.00	0.00		
			1.67	at 1 foot 8 inches has unconsolidated sand/clay-silt mix this soil has a redish color
	10.00	3.80	0.29	at 3.5 inches unconsolidated silt-shale mix
			1.84	the rest is clay-sand mix
5-3	10.00	0.00		
	12.50	3.99	3.99	Clay-shale with some gravel mix reddish in color. Toward the bottom the material starts to turn to a lighter color (light grey)
5-4	12.50	0.00		
	15.00	4.33	4.33	Silt clay mix mor dense light brown with gray color
5-5	15.00	0.00		
			4.00	silt clay mix 4 feet light brown color
	17.50	5.00	1.00	Last 1 foot is reddish color and seems to be shale
5-6	17.50	0.00		
			0.33	4 inches of clay
	18.75	3.73	2.00	2 feet of silt shale mix (unconsolidated)
			1.40	The rest seems wetter and more consolidated
5-7	18.75	0.00		
	20.00	2.60	2.60	Last 6 to 9 inches it was very slow to penetrate. Gray clay at the bottom not wet, not very cohesive
5-8	20.00	0.00		
	20.40	0.40	0.40	It was difficult to tell exactly how much recovery there was especially since there was water in the tube. The water that seeped in from the previous night rain or it also could have seeped from the formation. The material consisted of the same material as the previous core. Gray clay shale (bed rock)

Table A 3. Visual inspection of soil core sample no. 6 (Well B, 2nd closest to creek)

CORE SAMPLE NO. 6				
Soil Core	Depth penetrated (ft)	Depth recovered (ft)	Observational depths (ft)	Observational descriptions
6-1	0.00	0.00		
	5.00	3.60	3.60	Silty unconsolidated
6-2	5.00	0.00		
			3.00	1 to 3 feet Reddish silt clay
	10.00	3.42	0.42	grayish shale
				rest is reddish silt clay again
6-3	10.00	0.00		
	12.50	3.94	3.94	Silty unconsolidated then coarser, very dense, (wet) last 1' or so
6-4	12.50	0.00		
			2.20	Uncosolidated reddish silt clay
			2.25	grayish shale
	15.00	5.00	0.45	light brown dense clay
6-5	15.00	0.00		
			3.44	brown clay (dense)
	16.50	4.02	0.88	reddish silt clay
6-6	16.50	0.00		
			2.23	reddish-grey mix of shale
	18.00	3.53	1.30	Uncosolidated reddish silt clay
6-7	18.00	0.00		
	20.00	3.41	3.41	Grayish clay (dense) the end turns to a light brown
6-8	20.00	0.00		
	20.80	0.95	0.95	Light brown clay and pulled up water as well.

Table A 4. Visual inspection of soil core sample no. 10 (Well A, closest to creek)

CORE SAMPLE NO. 10				
Soil Core	Depth penetrated (ft)	Depth recovered (ft)	Observational depths (ft)	Observational descriptions
10-1	0.00	0.00		
	5.00	3.51	3.51	Dark brown soil, almost black, looks very organic like compost, soil seems to be unconsolidated
10-2	5.00	0.00		
			1.00	At about 1 foot from top of the soil sample th soils is similar that of the previous sample
	7.50	2.43	1.09	From 1 foot to the bottom the soil starts to turn a lighter brown color
			0.33	The bottom 4 inches the soil tends to turn more to a redish brown color and looks more consolidated
10-3	7.50	0.00		
	10.00	3.86	3.86	Has a mixture of redish brown with some greyish tan brown. The lighter color looks like broken shale some parts of the sample tends to have some consolidated sections and some unconsolidated
10-4	10.00	0.00		
	12.00	5.00	5.00	Full core sample, soil tends to turn to more of a lighter greyish brown color from previous sample and tends to remain the same consistant color through out the sample execpt at the bottom it strats to turn a redish brown color and has some brokien shale peices and is semi consolidated.
10-5	12.00	0.00		
	13.50	3.13	3.13	The soil consits of redish and light greyish brown mixture. The soil seems unconsolidated which could have separated in the transportation process. Ther are some broken shale pieces
10-6	13.50	0.00		
			0.74	Soil seems to follow the same color and soil type as the bottom of the previous sample
	15.00	3.00	2.26	At about 8 7/8 inches the soil changes color from a light brownish color to a solid grey color that likes like wet cement and looks very consolidated
10-7	15.00	0.00		
	16.50	3.69	3.69	Soil continues with the same grey color and the top is darker then the bottom of the sample. The soil becomes lighter toward the bottom but is still grey. Soil is still bery moist and the bottom som water
10-8	16.50	0.00		
	18.00	2.29	2.29	Soil settled on one side, it looks very wet and consolidated clayish material. The top is grey and towards the bottom the color starts to turn more of a greyish tan color. Lighter color at the bottom.
10-9	18.00	0.00		
	20.00	2.14	2.14	Soil is still very saturated and see water at the top. The color of soil changes from a light greyish tan to more of a tan color towards the bottom.

APPENDIX B: Laboratory Soil Analysis

The following figures and tables show the percent finer vs. grain size relationship, mass of soil samples retained in each sieve, cumulative percent retained, and percent finer, and the obtained D_{60}, D_{30}, D_{10}, C_u, and C_c results. These samples were taken from profiles A, C, D, E, and F.

Profile A:

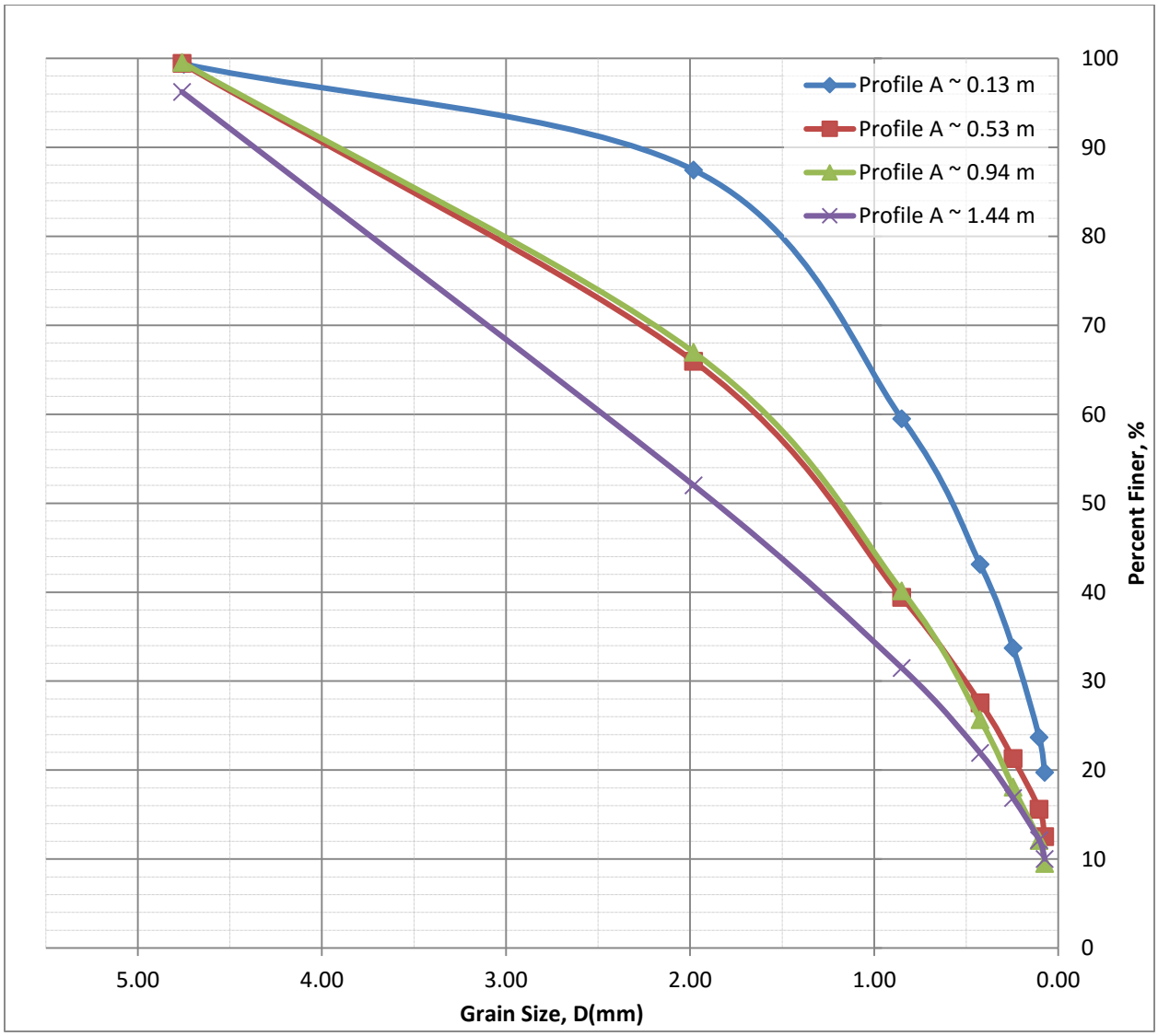

Figure B 1. Percent finer vs. Grain size relationship for soil located at Profile A at various depths from the surface.

Table B 1. Mass of soil samples retained in each sieve, cumulative percent retained, and percent finer for soil at Profile A at 0.13 m from the surface.

Sieve No.	Opening (mm)	Mass of Soil retrained on each sieve, W_s (g)	Percent of mass retained on each sieve, R_n (%)	Cumulative percent retained, $\sum R_n$ (%)	Percent finer, $100-\sum R_n$
4	4.750	0.60	0.66	0.66	99.34
10	1.981	10.90	11.90	12.55	87.45
20	0.833	25.60	27.95	40.50	59.50
40	0.419	15.00	16.38	56.88	43.12
60	0.246	8.60	9.39	66.27	33.73
140	0.104	9.20	10.04	76.31	23.69
200	0.074	3.60	3.93	80.24	19.76
Pan	0.000	18.10	19.76	100.00	0.00
Total		91.60			

Table B 2. Mass of soil samples retained in each sieve, cumulative percent retained, and percent finer for soil at Profile A at 0.53 m from the surface.

Sieve No.	Opening (mm)	Mass of Soil retrained on each sieve, W_s (g)	Percent of mass retained on each sieve, R_n (%)	Cumulative percent retained, $\sum R_n$ (%)	Percent finer, $100-\sum R_n$
4	4.750	0.50	0.57	0.57	99.43
10	1.981	29.40	33.49	34.05	65.95
20	0.833	23.30	26.54	60.59	39.41
40	0.419	10.40	11.85	72.44	27.56
60	0.246	5.50	6.26	78.70	21.30
140	0.104	5.00	5.69	84.40	15.60
200	0.074	2.70	3.08	87.47	12.53
Pan	0.000	11.00	12.53	100.00	0.00
Total		87.80			

Table B 3. Mass of soil samples retained in each sieve, cumulative percent retained, and percent finer for soil at Profile A at 0.84 m from the surface.

Sieve No.	Opening (mm)	Mass of Soil retrained on each sieve, W_s (g)	Percent of mass retained on each sieve, R_n (%)	Cumulative percent retained, $\sum R_n$ (%)	Percent finer, $100-\sum R_n$
4	4.750	0.40	0.45	0.45	99.55
10	1.981	28.80	32.58	33.03	66.97
20	0.833	23.70	26.81	59.84	40.16
40	0.419	12.80	14.48	74.32	25.68
60	0.246	6.70	7.58	81.90	18.10
140	0.104	5.30	6.00	87.90	12.10
200	0.074	2.30	2.60	90.50	9.50
Pan	0.000	8.40	9.50	100.00	0.00
Total		88.40			

Table B 4. Mass of soil samples retained in each sieve, cumulative percent retained, and percent finer for soil at Profile A at 1.44 m from the surface.

Sieve No.	Opening (mm)	Mass of Soil retrained on each sieve, W_s (g)	Percent of mass retained on each sieve, R_n (%)	Cumulative percent retained, $\sum R_n$ (%)	Percent finer, 100-$\sum R_n$
4	4.750	3.20	3.77	3.77	96.23
10	1.981	37.50	44.22	48.00	52.00
20	0.833	17.40	20.52	68.51	31.49
40	0.419	8.10	9.55	78.07	21.93
60	0.246	4.30	5.07	83.14	16.86
140	0.104	4.00	4.72	87.85	12.15
200	0.074	1.80	2.12	89.98	10.02
Pan	0.000	8.50	10.02	100.00	0.00
Total		84.80			

Table B 5. Values of D_{10}, D_{30}, and D_{60} along with the C_u and C_c from soil at Profile A at four distinct depths and their most probable classifications.

Sample Depth (meters)	Classification Variables					Most Probable Classification
	D_{60}	D_{30}	D_{10}	C_U	C_C	
0.13	0.85	0.19	0.03	28.33	1.42	SW,SM,SC
0.53	1.08	0.50	0.05	21.60	4.63	SW,SP,SM,SC
0.94	1.08	0.52	0.08	14.40	3.34	SW,SP,SM,SC
1.44	1.12	0.80	0.07	15.14	7.72	SW,SP,SM,SC

Profile C:

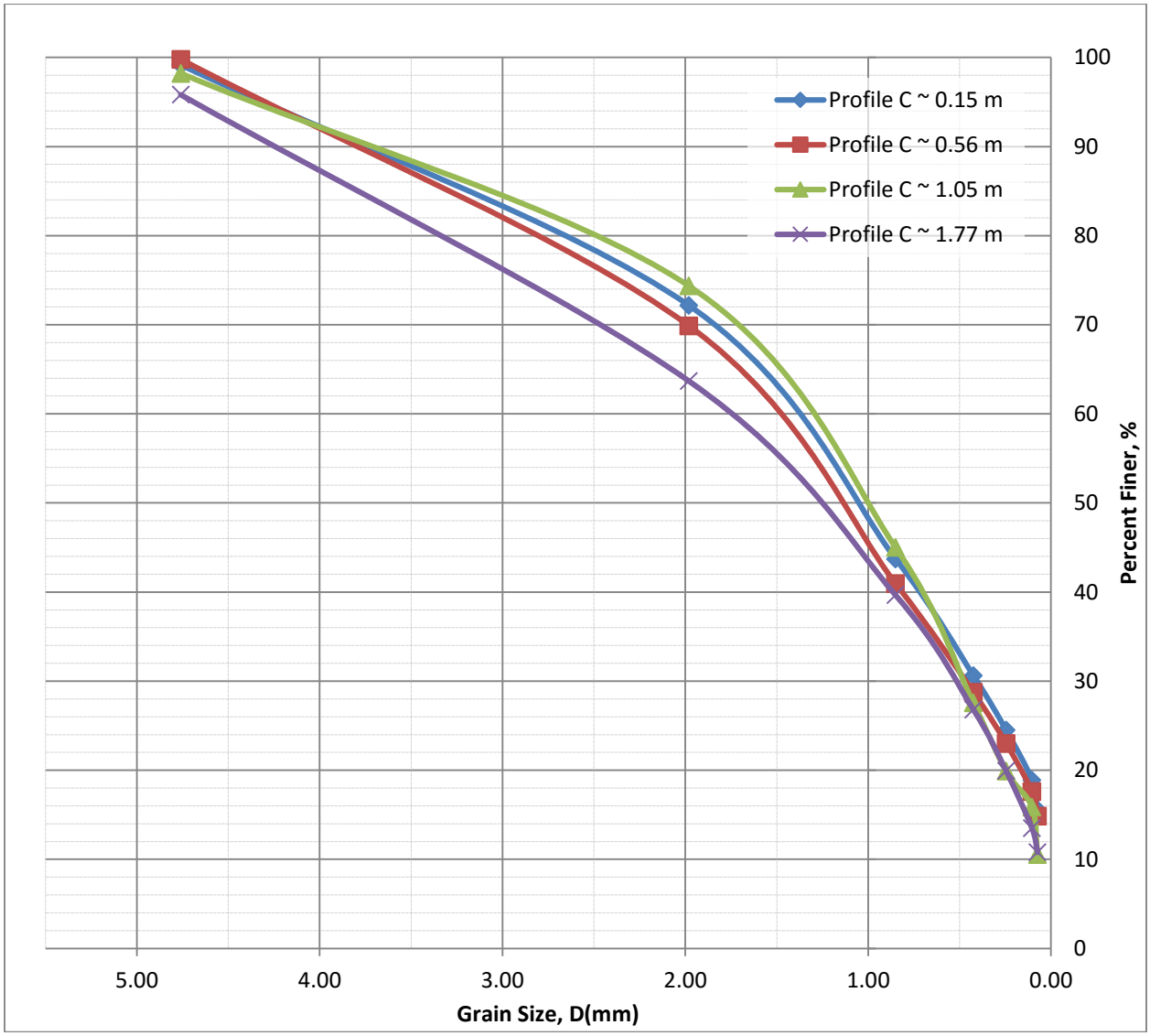

Figure B 2. Percent finer vs. Grain size relationship for soil located at Profile C at various depths from the surface.

Table B 6. Mass of soil samples retained in each sieve, cumulative percent retained, and percent finer for soil at Profile C at 0.15 m from the surface.

Sieve No.	Opening (mm)	Mass of Soil retrained on each sieve, W_s (g)	Percent of mass retained on each sieve, R_n (%)	Cumulative percent retained, $\sum R_n$ (%)	Percent finer, $100-\sum R_n$
4	4.760	0.8	0.8	0.8	99.2
10	1.981	26	27.0	27.8	72.2
20	0.850	27.4	28.5	56.3	43.7
40	0.425	12.6	13.1	69.4	30.6
60	0.246	5.9	6.1	75.5	24.5
140	0.104	5.4	5.6	81.1	18.9
200	0.074	3.2	3.3	84.4	15.6
Pan	0.000	15	15.6	100.0	0
Total		96.3			

Table B 7. Mass of soil samples retained in each sieve, cumulative percent retained, and percent finer for soil at Profile C at 0.56 m from the surface.

Sieve No.	Opening (mm)	Mass of Soil retrained on each sieve, W_s (g)	Percent of mass retained on each sieve, R_n (%)	Cumulative percent retained, $\sum R_n$ (%)	Percent finer, $100-\sum R_n$
4	4.760	0.2	0.2	0.2	99.8
10	1.981	28.2	29.9	30.1	69.9
20	0.850	27.3	29.0	59.1	40.9
40	0.425	11.5	12.2	71.3	28.7
60	0.246	5.4	5.7	77.0	23.0
140	0.104	5.1	5.4	82.4	17.6
200	0.074	2.6	2.8	85.2	14.8
Pan	0.000	14	14.8	100.0	0
Total		94.3			

Table B 8. Mass of soil samples retained in each sieve, cumulative percent retained, and percent finer for soil at Profile C at 1.05 m from the surface.

Sieve No.	Opening (mm)	Mass of Soil retrained on each sieve, W_s (g)	Percent of mass retained on each sieve, R_n (%)	Cumulative percent retained, $\sum R_n$ (%)	Percent finer, $100-\sum R_n$
4	4.760	2.3	1.8	1.8	98.2
10	1.981	30.8	23.9	25.6	74.4
20	0.850	37.9	29.4	55.0	45.0
40	0.425	22.5	17.4	72.4	27.6
60	0.246	9.9	7.7	80.1	19.9
140	0.104	5.2	4.0	84.1	15.9
200	0.074	6.9	5.3	89.5	10.5
Pan	0.000	13.6	10.5	100.0	0
Total		129.1			

Table B 9. Mass of soil samples retained in each sieve, cumulative percent retained, and percent finer for soil at Profile C at 1.77 m from the surface.

Sieve No.	Opening (mm)	Mass of Soil retrained on each sieve, W_s (g)	Percent of mass retained on each sieve, R_n (%)	Cumulative percent retained, $\sum R_n$ (%)	Percent finer, $100-\sum R_n$
4	4.760	5.1	4.2	4.2	95.8
10	1.981	39.3	32.1	36.3	63.7
20	0.850	29.4	24.0	60.3	39.7
40	0.425	15.7	12.8	73.2	26.8
60	0.246	8.4	6.9	80.0	20.0
140	0.104	7.9	6.5	86.5	13.5
200	0.074	3.3	2.7	89.2	10.8
Pan	0.000	13.2	10.8	100.0	0
Total		122.3			

Table B 10. Values of D_{10}, D_{30}, and D_{60} along with the C_u and C_c from soil at Profile C at four distinct depths and their most probable classifications.

Sample Depth (meters)	Classification Variables					Most Probable Classification
	D_{60}	D_{30}	D_{10}	C_U	C_C	
0.15	1.50	0.42	0.04	39.47	3.09	SW,SP,SM,SC
0.56	1.60	0.47	0.04	43.24	3.68	SW,SP,SM,SC
1.05	1.40	0.48	0.07	19.72	2.32	SW,SM,SC
1.77	1.75	0.53	0.07	25.74	2.39	SW,SM,SC

Profile D:

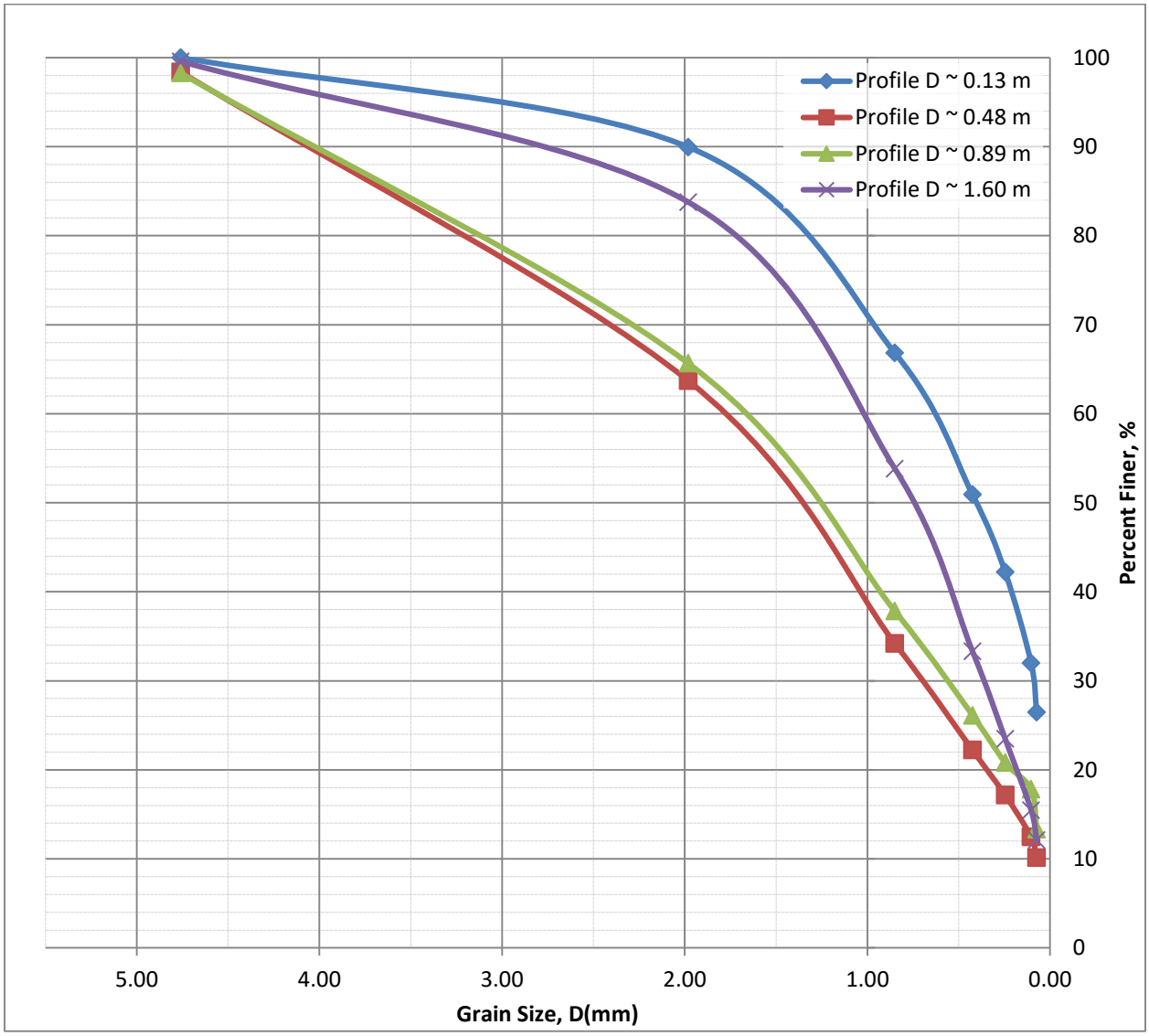

Figure B 3. Percent finer vs. Grain size relationship soil located at Profile D at various depths from the surface.

Table B 11. Mass of soil samples retained in each sieve, cumulative percent retained, and percent finer for soil at Profile D at 0.08 m from the surface.

Sieve No.	Opening (mm)	Mass of Soil retrained on each sieve, W_s (g)	Percent of mass retained on each sieve, R_n (%)	Cumulative percent retained, $\sum R_n$ (%)	Percent finer, $100-\sum R_n$
4	4.760	0	0.0	0.0	100.0
10	1.981	6	10.1	10.1	89.9
20	0.850	13.8	23.1	33.2	66.8
40	0.425	9.5	15.9	49.1	50.9
60	0.246	5.2	8.7	57.8	42.2
140	0.104	6.1	10.2	68.0	32.0
200	0.074	3.3	5.5	73.5	26.5
Pan	0.000	15.8	26.5	100.0	0
Total		59.7			

Table B 12. Mass of soil samples retained in each sieve, cumulative percent retained, and percent finer for soil at Profile D at 0.48 m from the surface.

Sieve No.	Opening (mm)	Mass of Soil retrained on each sieve, W_s (g)	Percent of mass retained on each sieve, R_n (%)	Cumulative percent retained, $\sum R_n$ (%)	Percent finer, $100-\sum R_n$
4	4.760	1.3	1.6	1.6	98.4
10	1.981	28.1	34.7	36.3	63.7
20	0.850	23.9	29.5	65.8	34.2
40	0.425	9.7	12.0	77.8	22.2
60	0.246	4.1	5.1	82.8	17.2
140	0.104	3.8	4.7	87.5	12.5
200	0.074	1.9	2.3	89.9	10.1
Pan	0.000	8.2	10.1	100.0	0
Total		81			

Table B 13. Mass of soil samples retained in each sieve, cumulative percent retained, and percent finer for soil at Profile D at 0.89 m from the surface.

Sieve No.	Opening (mm)	Mass of Soil retrained on each sieve, W_s (g)	Percent of mass retained on each sieve, R_n (%)	Cumulative percent retained, $\sum R_n$ (%)	Percent finer, $100-\sum R_n$
4	4.760	1.9	1.7	1.7	98.3
10	1.981	36.2	32.6	34.3	65.7
20	0.850	30.9	27.8	62.2	37.8
40	0.425	13	11.7	73.9	26.1
60	0.246	5.9	5.3	79.2	20.8
140	0.104	3.3	3.0	82.2	17.8
200	0.074	5	4.5	86.7	13.3
Pan	0.000	14.8	13.3	100.0	0
Total		111			

Table B 14. Mass of soil samples retained in each sieve, cumulative percent retained, and percent finer for soil at Profile D at 1.60 m from the surface.

Sieve No.	Opening (mm)	Mass of Soil retrained on each sieve, W_s (g)	Percent of mass retained on each sieve, R_n (%)	Cumulative percent retained, $\sum R_n$ (%)	Percent finer, $100-\sum R_n$
4	4.760	0.5	0.4	0.4	99.6
10	1.981	18.8	15.8	16.2	83.8
20	0.850	35.6	29.9	46.2	53.8
40	0.425	24.4	20.5	66.7	33.3
60	0.246	11.7	9.8	76.5	23.5
140	0.104	9.5	8.0	84.5	15.5
200	0.074	4	3.4	87.9	12.1
Pan	0.000	14.4	12.1	100.0	0
Total		118.9			

Table B 15. Values of D_{10}, D_{30}, and D_{60} along with the C_u and C_c from soil at Profile D at four distinct depths and their most probable classifications.

Sample Depth (meters)	Classification Variables					Most Probable Classification
	D_{60}	D_{30}	D_{10}	C_U	C_C	
0.08	0.63	0.09	0.03	24.23	0.49	SM,SC
0.48	1.85	0.73	0.07	25.34	3.89	SW,SP,SM,SC
0.89	1.75	0.57	0.06	29.17	3.06	SW,SP,SM,SC
1.60	1.00	0.38	0.06	17.54	2.47	SW,SM,SC

Profile E:

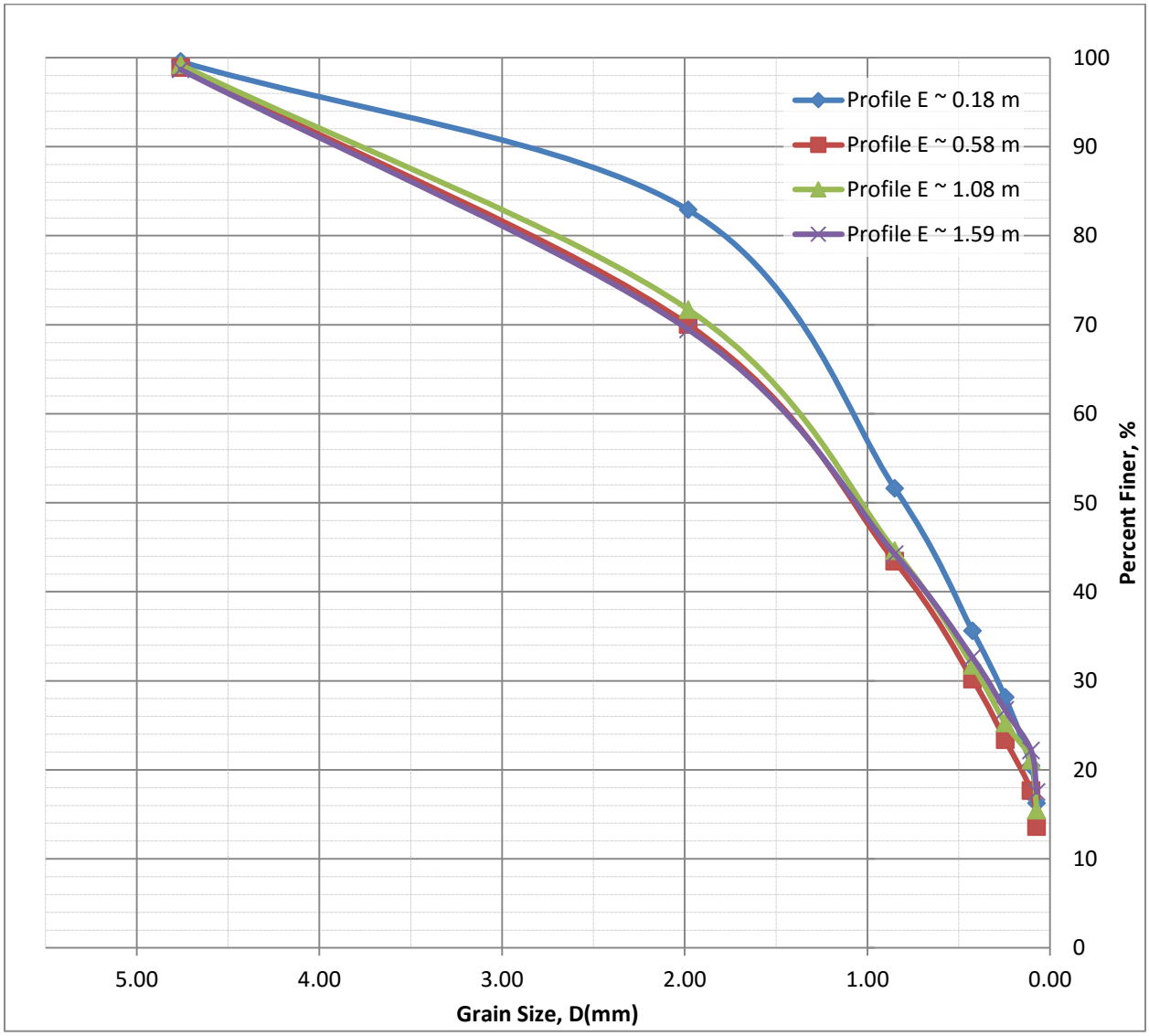

Figure B 4. Percent finer vs. Grain size relationship for soil located at Profile E at various depths from the surface.

Table B 16. Mass of soil samples retained in each sieve, cumulative percent retained, and percent finer for soil at Profile E at 0.18 m from the surface.

Sieve No.	Opening (mm)	Mass of Soil retrained on each sieve, W_s (g)	Percent of mass retained on each sieve, R_n (%)	Cumulative percent retained, $\sum R_n$ (%)	Percent finer, $100-\sum R_n$
4	4.760	0.4	0.4	0.4	99.6
10	1.981	15.4	16.7	17.1	82.9
20	0.850	28.9	31.3	48.4	51.6
40	0.425	14.8	16.0	64.4	35.6
60	0.246	6.9	7.5	71.9	28.1
140	0.104	7.1	7.7	79.5	20.5
200	0.074	3.9	4.2	83.8	16.2
Pan	0.000	15	16.2	100.0	0
Total		92.4			

Table B 17. Mass of soil samples retained in each sieve, cumulative percent retained, and percent finer for soil at Profile E at 0.58 m from the surface.

Sieve No.	Opening (mm)	Mass of Soil retrained on each sieve, W_s (g)	Percent of mass retained on each sieve, R_n (%)	Cumulative percent retained, $\sum R_n$ (%)	Percent finer, $100-\sum R_n$
4	4.760	1.2	1.1	1.1	98.9
10	1.981	31.4	28.9	30.0	70.0
20	0.850	28.9	26.6	56.6	43.4
40	0.425	14.4	13.2	69.8	30.2
60	0.246	7.4	6.8	76.6	23.4
140	0.104	6.2	5.7	82.3	17.7
200	0.074	4.4	4.0	86.4	13.6
Pan	0.000	14.8	13.6	100.0	0
Total		108.7			

Table B 18. Mass of soil samples retained in each sieve, cumulative percent retained, and percent finer for soil at Profile E at 1.08 m from the surface.

Sieve No.	Opening (mm)	Mass of Soil retrained on each sieve, W_s (g)	Percent of mass retained on each sieve, R_n (%)	Cumulative percent retained, $\sum R_n$ (%)	Percent finer, $100-\sum R_n$
4	4.760	1	0.8	0.8	99.2
10	1.981	34.3	27.5	28.3	71.7
20	0.850	33.8	27.1	55.4	44.6
40	0.425	16.1	12.9	68.3	31.7
60	0.246	8.1	6.5	74.8	25.2
140	0.104	5.2	4.2	78.9	21.1
200	0.074	7	5.6	84.5	15.5
Pan	0.000	19.3	15.5	100.0	0
Total		124.8			

Table B 19. Mass of soil samples retained in each sieve, cumulative percent retained, and percent finer for soil at Profile E at 1.59 m from the surface.

Sieve No.	Opening (mm)	Mass of Soil retrained on each sieve, W_s (g)	Percent of mass retained on each sieve, R_n (%)	Cumulative percent retained, $\sum R_n$ (%)	Percent finer, $100-\sum R_n$
4	4.760	1.6	1.3	1.3	98.7
10	1.981	35.2	29.2	30.5	69.5
20	0.850	30.4	25.2	55.8	44.2
40	0.425	14	11.6	67.4	32.6
60	0.246	7.1	5.9	73.3	26.7
140	0.104	5.5	4.6	77.8	22.2
200	0.074	5.6	4.6	82.5	17.5
Pan	0.000	21.1	17.5	100.0	0
Total		120.5			

Table B 20. Values of D_{10}, D_{30}, and D_{60} along with the C_u and C_c from soil at Profile E at four distinct depths and their most probable classifications.

Sample Depth (meters)	Classification Variables					Most Probable Classification
	D_{60}	D_{30}	D_{10}	C_U	C_C	
0.18	1.20	0.26	0.05	26.09	1.22	SW,SM,SC
0.58	1.60	0.43	0.06	29.09	2.13	SW,SM,SC
1.08	1.50	0.38	0.06	26.79	1.72	SW,SM,SC
1.59	1.60	0.35	0.04	37.21	1.78	SW,SM,SC

Profile F:

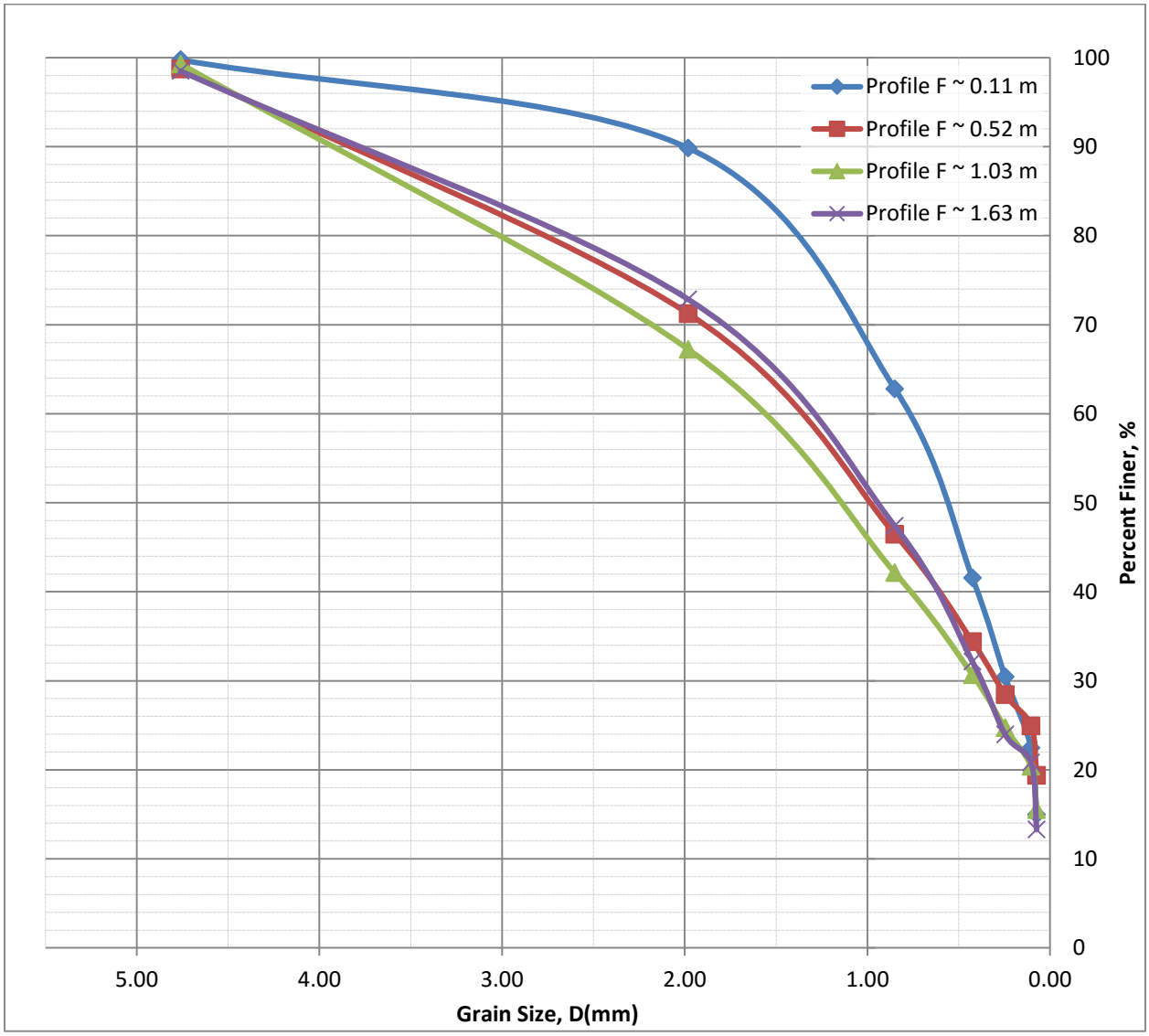

Figure B 5. Percent finer vs. Grain size relationship for soil located at Profile F at various depths from the surface.

Table B 21. Mass of soil samples retained in each sieve, cumulative percent retained, and percent finer for soil at Profile F at 0.11 m from the surface.

Sieve No.	Opening (mm)	Mass of Soil retrained on each sieve, W_s (g)	Percent of mass retained on each sieve, R_n (%)	Cumulative percent retained, $\sum R_n$ (%)	Percent finer, $100-\sum R_n$
4	4.760	0.1	0.2	0.2	99.8
10	1.981	4.1	9.9	10.1	89.9
20	0.850	11.2	27.1	37.2	62.8
40	0.425	8.8	21.3	58.5	41.5
60	0.246	4.6	11.1	69.6	30.4
140	0.104	3.3	8.0	77.5	22.5
200	0.074	3.1	7.5	85.0	15.0
Pan	0.000	6.2	15.0	100.0	0
Total		41.4			

Table B 22. Mass of soil samples retained in each sieve, cumulative percent retained, and percent finer for soil at Profile F at 0.52 m from the surface.

Sieve No.	Opening (mm)	Mass of Soil retrained on each sieve, W_s (g)	Percent of mass retained on each sieve, R_n (%)	Cumulative percent retained, $\sum R_n$ (%)	Percent finer, $100-\sum R_n$
4	4.760	1.6	1.3	1.3	98.7
10	1.981	34.6	27.5	28.8	71.2
20	0.850	31.2	24.8	53.5	46.5
40	0.425	15.2	12.1	65.6	34.4
60	0.246	7.5	6.0	71.6	28.4
140	0.104	4.4	3.5	75.1	24.9
200	0.074	7	5.6	80.6	19.4
Pan	0.000	24.4	19.4	100.0	0
Total		125.9			

Table B 23. Mass of soil samples retained in each sieve, cumulative percent retained, and percent finer for soil at Profile F at 1.03 m from the surface.

Sieve No.	Opening (mm)	Mass of Soil retrained on each sieve, W_s (g)	Percent of mass retained on each sieve, R_n (%)	Cumulative percent retained, $\sum R_n$ (%)	Percent finer, $100-\sum R_n$
4	4.760	0.8	0.7	0.7	99.3
10	1.981	35.5	32.0	32.8	67.2
20	0.850	27.8	25.1	57.9	42.1
40	0.425	12.7	11.5	69.3	30.7
60	0.246	6.6	6.0	75.3	24.7
140	0.104	4.8	4.3	79.6	20.4
200	0.074	5.4	4.9	84.5	15.5
Pan	0.000	17.2	15.5	100.0	0
Total		110.8			

Table B 24. Mass of soil samples retained in each sieve, cumulative percent retained, and percent finer for soil at Profile F at 1.63 m from the surface.

Sieve No.	Opening (mm)	Mass of Soil retrained on each sieve, W_s (g)	Percent of mass retained on each sieve, R_n (%)	Cumulative percent retained, $\sum R_n$ (%)	Percent finer, $100-\sum R_n$
4	4.760	1.6	1.5	1.5	98.5
10	1.981	27.6	25.7	27.1	72.9
20	0.850	27.4	25.5	52.6	47.4
40	0.425	16.4	15.2	67.8	32.2
60	0.246	8.8	8.2	76.0	24.0
140	0.104	3.4	3.2	79.2	20.8
200	0.074	8.1	7.5	86.7	13.3
Pan	0.000	14.3	13.3	100.0	0
Total		107.6			

Table B 25. Values of D_{10}, D_{30}, and D_{60} along with the C_u and C_c from soil at Profile F at four distinct depths and their most probable classifications.

Sample Depth (meters)	Classification Variables					Most Probable Classification
	D_{60}	D_{30}	D_{10}	C_U	C_C	
0.11	0.73	0.25	0.06	11.63	1.35	SW,SP,SM,SC
0.52	1.40	0.30	0.05	29.17	1.34	SW,SM,SC
1.03	1.70	0.40	0.06	29.82	1.65	SW,SM,SC
1.63	1.35	0.38	0.07	20.77	1.60	SW,SM,SC

Profile A Sample Calculations and Notes

A

5”

Variables	Values
D_{60}	0.85
D_{30}	0.19
D_{10}	0.03
C_U	28.3
C_C	1.42

Coarse-Grained
Sand
Well-Graded

Sand Fraction
79.6

Sieve	% Finer
10	87.4
40	43.1
200	19.8

Classification	Possible	Most Probable
A-1-b	SW,SP,SM	SW,SM,SC
A-2	SM,SC	

21”

Variables	Values
D_{60}	1.08
D_{30}	0.50
D_{10}	0.05
C_U	21.6
C_C	4.63

Coarse-Grained
Sand
Poorly Graded

Sand Fraction
86.9

Sieve	% Finer
10	65.9
40	27.6
200	12.5

Classification	Possible	Most Probable
A-1-b	SW,SP,SM	SW,SP,SM,SC
A-2	SM,SC	

37”

Variables	Values
D_{60}	1.08
D_{30}	0.52
D_{10}	0.08
C_U	14.4
C_C	3.34

Coarse-Grained
Sand
Poorly Graded

Sand Fraction
90.0

Sieve	% Finer
10	67.0
40	25.7
200	9.5

Classification	Possible	Most Probable
A-1-b	SW,SP,SM	SW,SP,SM,SC
A-2	SM,SC	

56.5”

Variables	Values
D_{60}	1.12
D_{30}	0.8
D_{10}	0.07
C_U	15.1
C_C	7.72

Coarse-Grained
Sand
Poorly Graded

Sand Fraction
86.2

Sieve	% Finer
10	52.0
40	21.9
200	10.0

Classification	Possible	Most Probable
A-1-a	SW,SP	SW,SP,SM,SC
A-2	SM,SC	

Profile C Sample Calculations and Notes

C

6"	Variables	Values	Coarse-Grained	Sieve	% Finer	Classification	Possible	Most Probable
			Sand	10	72.2	A-1-b	SW,SP,SM	SW,SP,SM,SC
	D_{60}	1.5	Poorly Graded	40	30.6	A-2	SM,SC	
	D_{30}	0.42		200	15.6			
	D_{10}	0.04	Sand Fraction					
	C_U	39.5	83.6					
	C_C	3.09						

22"	Variables	Values	Coarse-Grained	Sieve	% Finer	Classification	Possible	Most Probable
			Sand	10	69.9	A-1-b	SW,SP,SM	SW,SP,SM,SC
	D_{60}	1.6	Poorly Graded	40	28.7	A-2	SM,SC	
	D_{30}	0.47		200	14.8			
	D_{10}	0.04	Sand Fraction					
	C_U	43.2	84.9					
	C_C	3.68						

41.5"	Variables	Values	Coarse-Grained	Sieve	% Finer	Classification	Possible	Most Probable
			Sand	10	74.4	A-1-b	SW,SP,SM	SW,SM,SC
	D_{60}	1.4	Well-Graded	40	27.6	A-2	SM,SC	
	D_{30}	0.48		200	10.5			
	D_{10}	0.07	Sand Fraction					
	C_U	19.7	87.7					
	C_C	2.32						

69.5"	Variables	Values	Coarse-Grained	Sieve	% Finer	Classification	Possible	Most Probable
			Sand	10	63.7	A-1-b	SW,SP,SM	SW,SM,SC
	D_{60}	1.75	Well-Graded	40	26.8	A-2	SM,SC	
	D_{30}	0.53		200	10.8			
	D_{10}	0.07	Sand Fraction					
	C_U	25.7	85.0					
	C_C	2.39						

Profile D Sample Calculations and Notes

D

3"	Variables	Values	Coarse-Grained	Sieve	% Finer	Classification	Possible	Most Probable
			Sand	10	89.9	A-2	SM,SC	SM,SC
	D_{60}	0.63	Poorly Graded	40	50.9			
	D_{30}	0.09		200	26.5			
	D_{10}	0.026	Sand Fraction					
	C_U	24.2	73.5					
	C_C	0.49						

19"	Variables	Values	Coarse-Grained	Sieve	% Finer	Classification	Possible	Most Probable
			Sand	10	63.7	A-1-a	SW,SP	SW,SP,SM,SC
	D_{60}	1.85	Poorly Graded	40	22.2	A-2	SM,SC	
	D_{30}	0.725		200	10.1			
	D_{10}	0.73	Sand Fraction					
	C_U	2.53	88.3					
	C_C	0.39						

35"	Variables	Values	Coarse-Grained	Sieve	% Finer	Classification	Possible	Most Probable
			Sand	10	65.7	A-1-a	SW,SP	SW,SP,SM,SC
	D_{60}	1.75	Poorly Graded	40	26.1	A-2	SM,SC	
	D_{30}	0.567		200	13.3			
	D_{10}	0.06	Sand Fraction					
	C_U	29.2	85.0					
	C_C	3.06						

63"	Variables	Values	Coarse-Grained	Sieve	% Finer	Classification	Possible	Most Probable
			Sand	10	83.8	A-1-a	SW,SP	SW,SM,SC
	D_{60}	1	Well-Graded	40	33.3	A-2	SM,SC	
	D_{30}	0.375		200	12.1			
	D_{10}	0.057	Sand Fraction					
	C_U	17.5	87.5					
	C_C	2.47						

Profile E Sample Calculations and Notes

E

7"

Variables	Values
D_{60}	1.2
D_{30}	0.26
D_{10}	0.05
C_U	26.1
C_C	1.22

Coarse-Grained
Sand
Well-Graded

Sand Fraction
83.3

Sieve	% Finer
10	82.9
40	35.6
200	16.2

Classification	Possible	Most Probable
A-1-b	SW,SP,SM	SW,SM,SC
A-2	SM,SC	

23"

Variables	Values
D_{60}	1.6
D_{30}	0.43
D_{10}	0.06
C_U	29.1
C_C	2.13

Coarse-Grained
Sand
Well-Graded

Sand Fraction
85.3

Sieve	% Finer
10	70.0
40	30.2
200	13.6

Classification	Possible	Most Probable
A-1-b	SW,SP,SM	SW,SM,SC
A-2	SM,SC	

42.5"

Variables	Values
D_{60}	1.5
D_{30}	0.38
D_{10}	0.06
C_U	26.8
C_C	1.72

Coarse-Grained
Sand
Well-Graded

Sand Fraction
83.7

Sieve	% Finer
10	71.7
40	31.7
200	15.5

Classification	Possible	Most Probable
A-1-b	SW,SP,SM	SW,SM,SC
A-2	SM,SC	

62.5"

Variables	Values
D_{60}	1.6
D_{30}	0.35
D_{10}	0.04
C_U	37.2
C_C	1.78

Coarse-Grained
Sand
Well-Graded

Sand Fraction
81.2

Sieve	% Finer
10	69.5
40	32.6
200	17.5

Classification	Possible	Most Probable
A-1-b	SW,SP,SM	SW,SM,SC
A-2	SM,SC	

Profile F Sample Calculations and Notes

F

4.5″	Variables	Values	Coarse-Grained	Sieve	% Finer	Classification	Possible	Most Probable
			Sand	10	89.9	A-1-b	SW,SP,SM	SW,SP,SM,SC
	D_{60}	0.73	Poorly Graded	40	41.5	A-2	SM,SC	
	D_{30}	0.25		200	15.0			
	D_{10}	0.06	Sand Fraction					
	C_U	11.6	84.8					
	C_C	1.35						

20.5″	Variables	Values	Coarse-Grained	Sieve	% Finer	Classification	Possible	Most Probable
			Sand	10	71.2	A-1-b	SW,SP,SM	SW,SM,SC
	D_{60}	1.40	Well-Graded	40	34.4	A-2	SM,SC	
	D_{30}	0.30		200	19.4			
	D_{10}	0.05	Sand Fraction					
	C_U	29.2	79.3					
	C_C	1.34						

40.5″	Variables	Values	Coarse-Grained	Sieve	% Finer	Classification	Possible	Most Probable
			Sand	10	67.2	A-1-b	SW,SP,SM	SW,SM,SC
	D_{60}	1.70	Well-Graded	40	30.7	A-2	SM,SC	
	D_{30}	0.40		200	15.5			
	D_{10}	0.06	Sand Fraction					
	C_U	29.8	83.8					
	C_C	1.65						

64″	Variables	Values	Coarse-Grained	Sieve	% Finer	Classification	Possible	Most Probable
			Sand	10	72.9	A-1-b	SW,SP,SM	SW,SM,SC
	D_{60}	1.35	Well-Graded	40	32.2	A-2	SM,SC	
	D_{30}	0.38		200	13.3			
	D_{10}	0.07	Sand Fraction					
	C_U	20.8	85.2					
	C_C	1.60						

Standard Practice for Classification of Soils for Engineering Purposes (Unified Soil Classification System)

TABLE 1 Soil Classification Chart

Criteria for Assigning Group Symbols and Group Names Using Laboratory Tests[A]				Soil Classification	
				Group Symbol	Group Name[B]
COARSE-GRAINED SOILS	Gravels	Clean Gravels	Cu ≥ 4 and 1 ≤ Cc ≤ 3[C]	GW	Well-graded gravel[D]
More than 50 % retained on No. 200 sieve	More than 50 % of coarse fraction retained on No. 4 sieve	Less than 5 % fines[E]	Cu < 4 and/or 1 > Cc > 3[C]	GP	Poorly graded gravel[D]
		Gravels with Fines	Fines classify as ML or MH	GM	Silty gravel[D,F,G]

TABLE 1 *Continued*

Criteria for Assigning Group Symbols and Group Names Using Laboratory Tests[A]				Soil Classification	
				Group Symbol	Group Name[B]
		More than 12 % fines[E]	Fines classify as CL or CH	,urule;1>GC	Clayey gravel[D,F,G]
	Sands	Clean Sands	Cu ≥ 6 and 1 ≤ Cc ≤ 3[C]	SW	Well-graded sand[H]
	50 % or more of coarse	Less than 5 % fines[I]	Cu < 6 and/or 1 > Cc > 3[C]	SP	Poorly graded sand[H]
	fraction passes No. 4 sieve	Sands with Fines	Fines classify as ML or MH	SM	Silty sand[F,G,H]
		More than 12 % fines[I]	Fines classify as CL or CH	SC	Clayey sand[F,G,H]
FINE-GRAINED SOILS	Silts and Clays	inorganic	PI > 7 and plots on or above "A" line[J]	CL	Lean clay[K,L,M]
50 % or more passes the No.	Liquid limit less than 50		PI < 4 or plots below "A" line[J]	ML	Silt[K,L,M]
200 seive		organic	Liquid limit – oven dried> < 0.75	OL	Organic clay[K,L,M,N]
			Liquid limit – not dried	OL	Organic silt[K,L,M,O]
	Silts and Clays	inorganic	PI plots on or above "A" line	CH	Fat clay[K,L,M]
	Liquid limit 50 or more		PI plots below "A" line	MH	Elastic silt[K,L,M]
		organic	Liquid limit – oven dried < 0.75	OH	Organic clay[K,L,M,P]
			Liquid limit – not dried		Organic silt[K,L,M,Q]
HIGHLY ORGANIC SOILS	Primarily organic matter, dark in color, and organic odor			PT	Peat

[A] Based on the material passing the 3-in. (75-mm) sieve.
[B] If field sample contained cobbles or boulders, or both, add "with cobbles or boulders, or both" to group name.
[C] $Cu = D_{60}/D_{10}$ $Cc = (D_{30})^2 / D_{10} \times D_{60}$
[D] If soil contains ≥15 % sand, add "with sand" to group name.
[E] Gravels with 5 to 12 % fines require dual symbols:
GW-GM well-graded gravel with silt
GW-GC well-graded gravel with clay
GP-GM poorly graded gravel with silt
GP-GC poorly graded gravel with clay
[F] If fines classify as CL-ML, use dual symbol GC-GM, or SC-SM.
[G] If fines are organic, add "with organic fines" to group name.
[H] If soil contains ≥15 % gravel, add "with gravel" to group name.
[I] Sands with 5 to 12 % fines require dual symbols:
SW-SM well-graded sand with silt
SW-SC well-graded sand with clay
SP-SM poorly graded sand with silt
SP-SC poorly graded sand with clay
[J] If Atterberg limits plot in hatched area, soil is a CL-ML, silty clay.
[K] If soil contains 15 to 29 % plus No. 200, add "with sand" or "with gravel," whichever is predominant.
[L] If soil contains ≥30 % plus No. 200, predominantly sand, add "sand " to group name.
[M] If soil contains ≥30 % plus No. 200, predominantly gravel, add "gravelly" to group name.
[N] PI ≥ 4 and plots on or above "A" line.
[O] PI < 4 or plots below" A" line.
[P] PI plots on or above "A" line.
[Q] PI plots below "A" line.

Citation (ASTM D2487-11, Standard Practice for Classification of Soils for Engineering Purposes (Unified Soil Classification System), ASTM International, West Conshohocken, PA, 2011, www.astm.org)

APPENDIX C: Normalized Total Soil Moisture Time Series

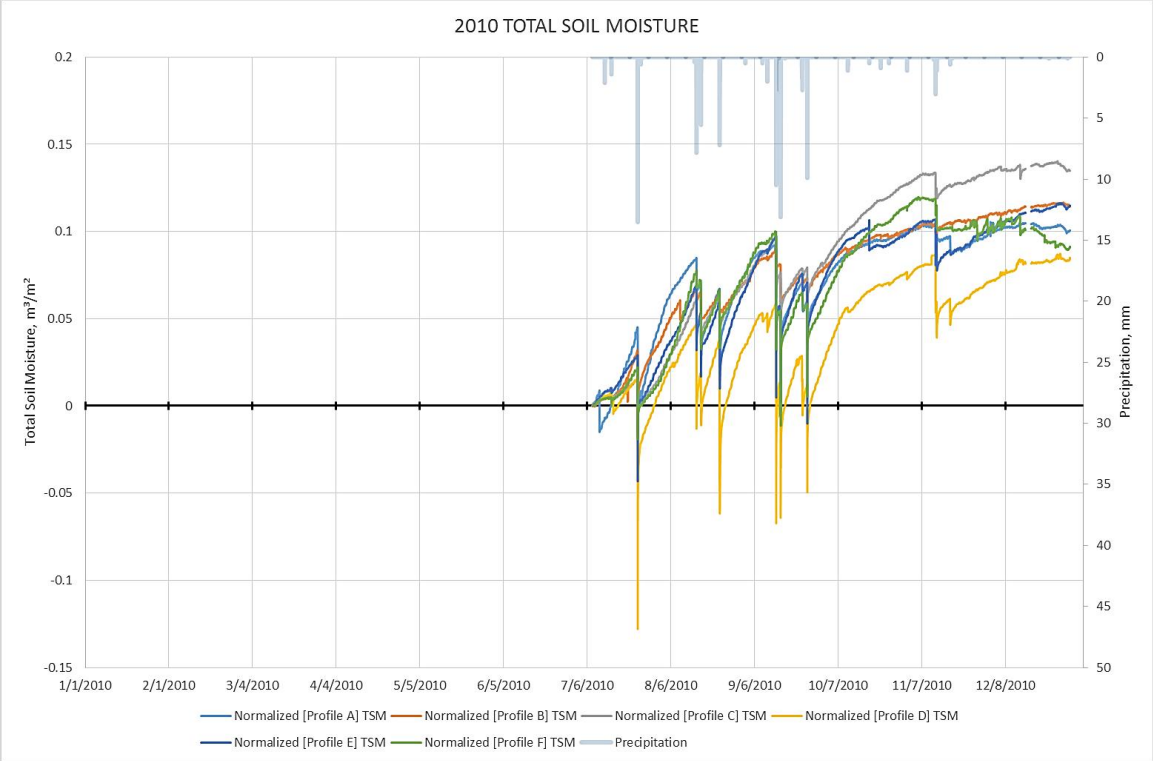

Figure C 1. Normalized total soil moisture for all profiles in 2010.

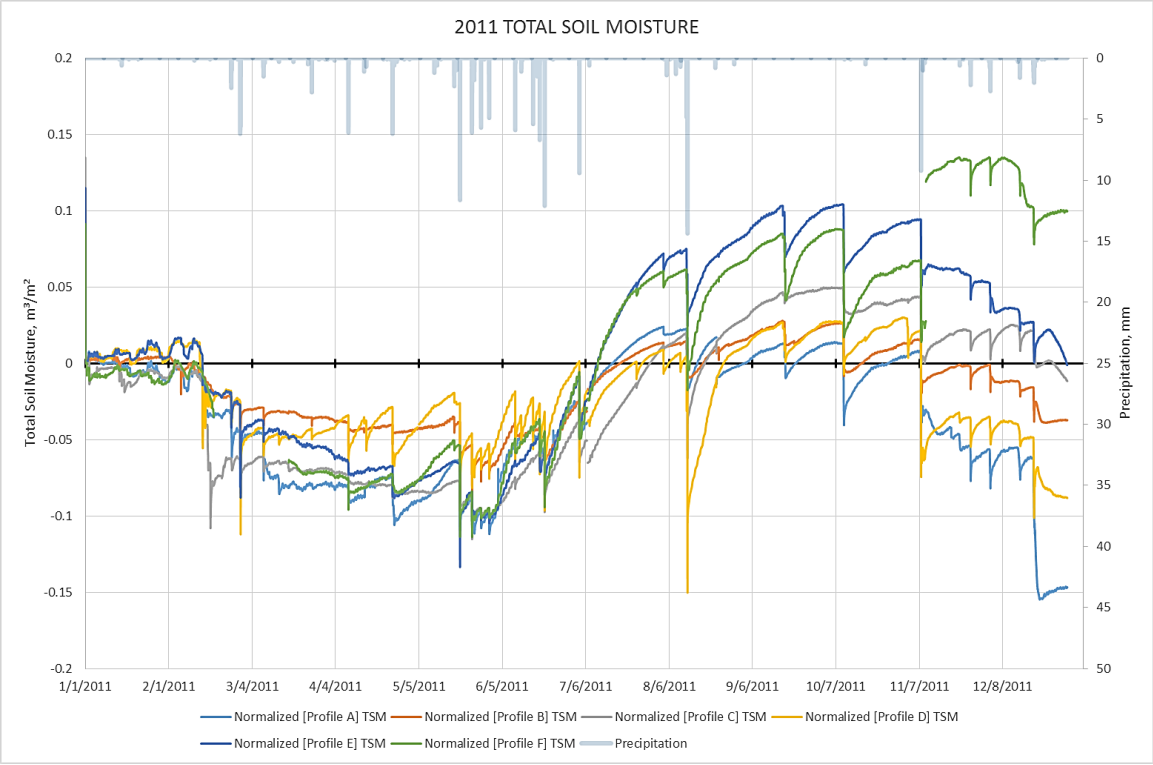

Figure C 2. Normalized total soil moisture for all profiles in 2011.

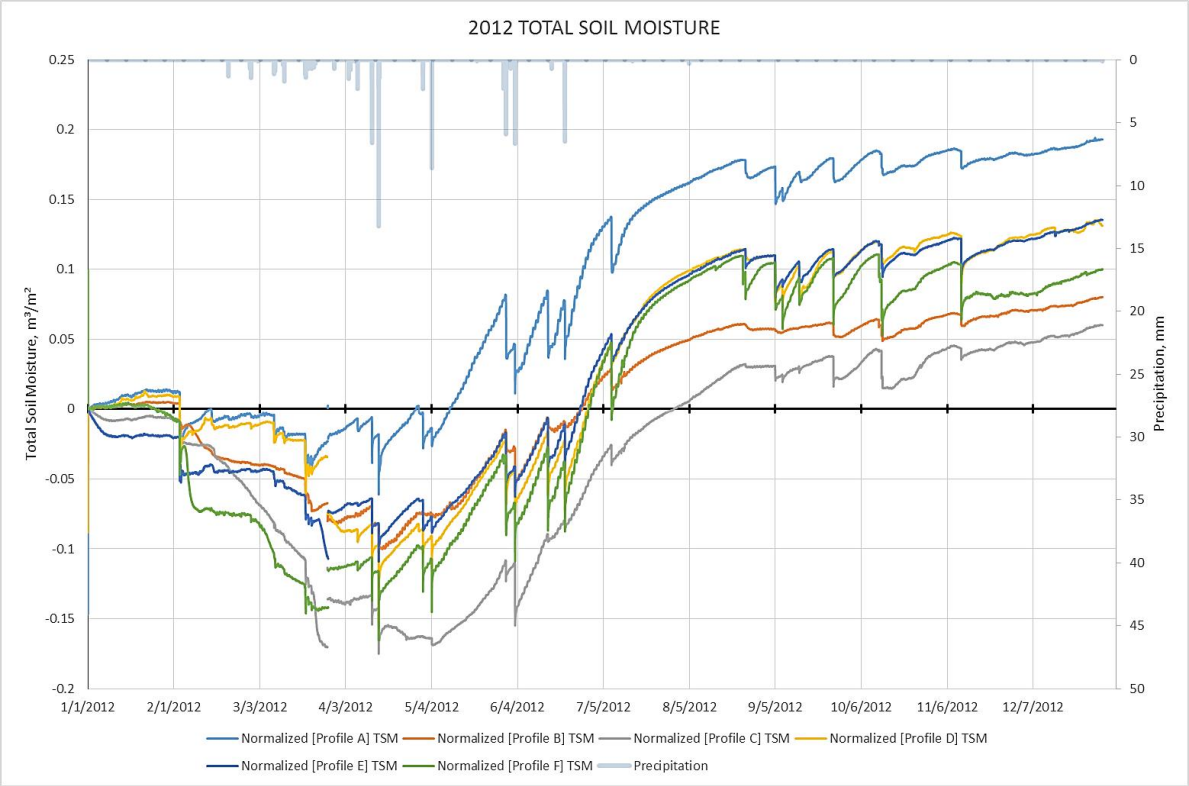

Figure C 3. Normalized total soil moisture for all profiles in 2012.

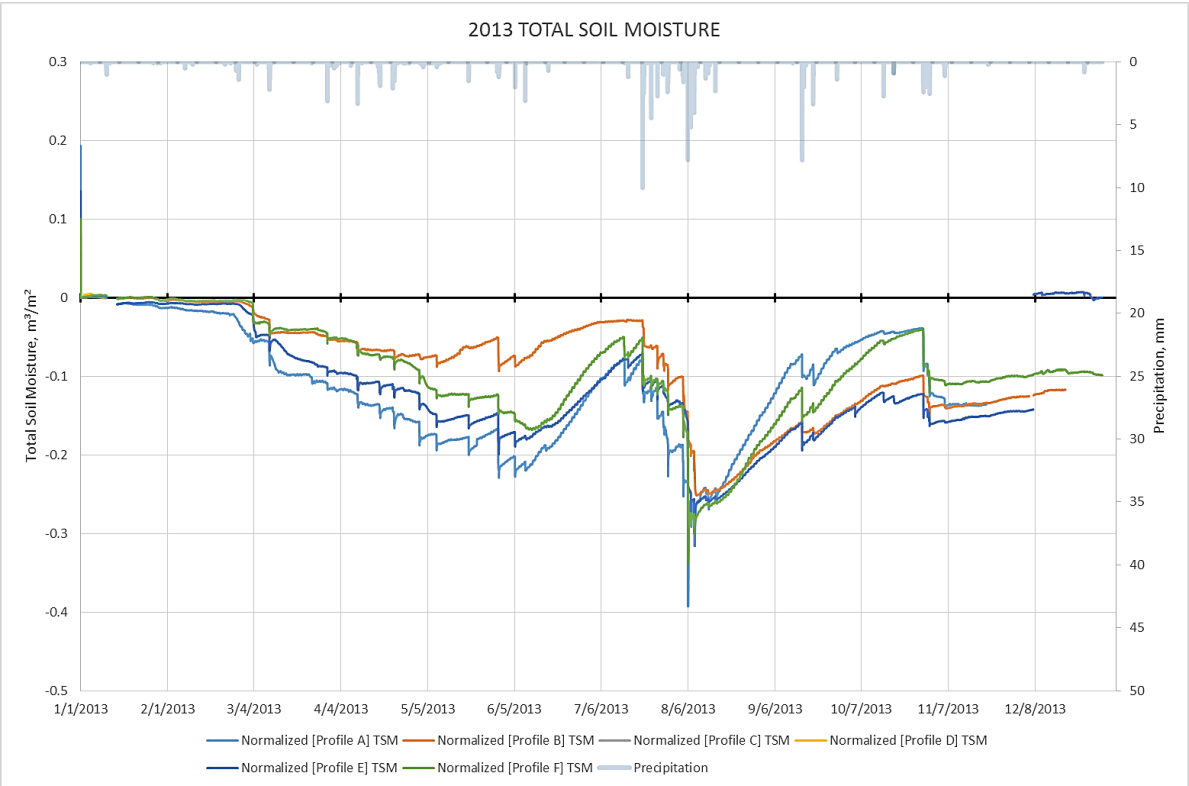

Figure C 4. Normalized total soil moisture for all profiles in 2013.

APPENDIX D: Annual Soil Moisture Time Series Plots

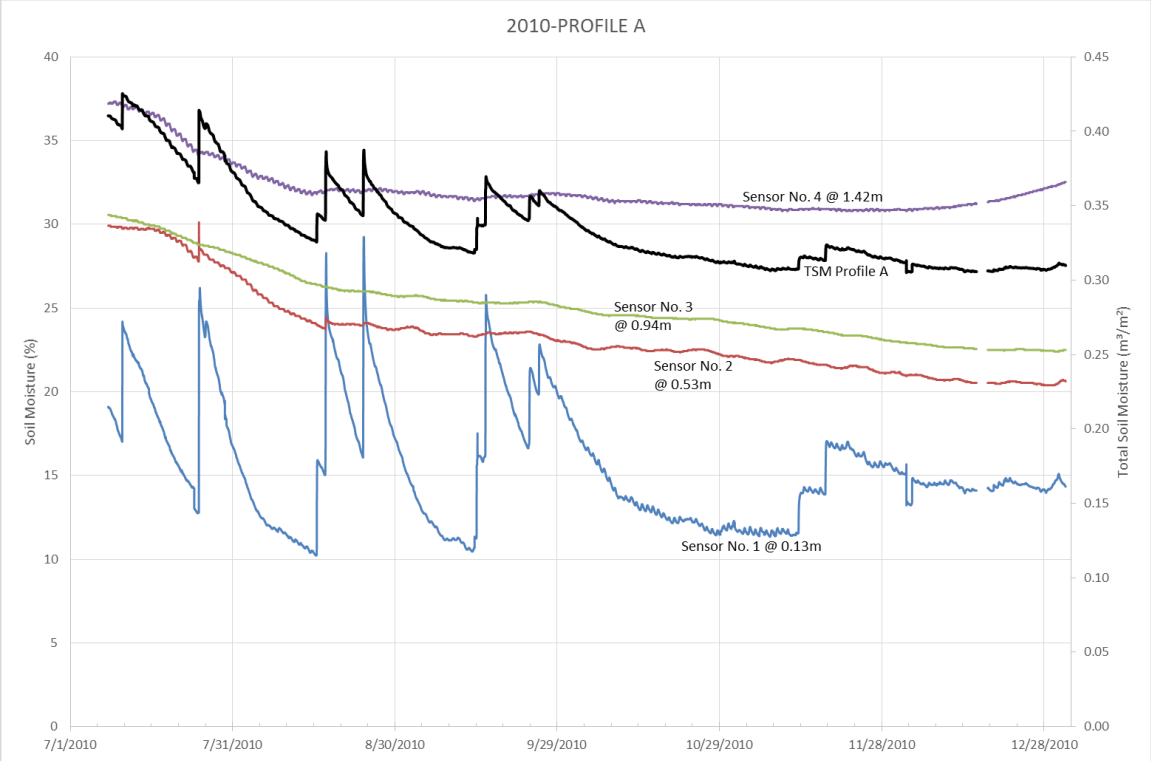

Figure D 1. Soil moisture and total soil moisture for profile A in 2010.

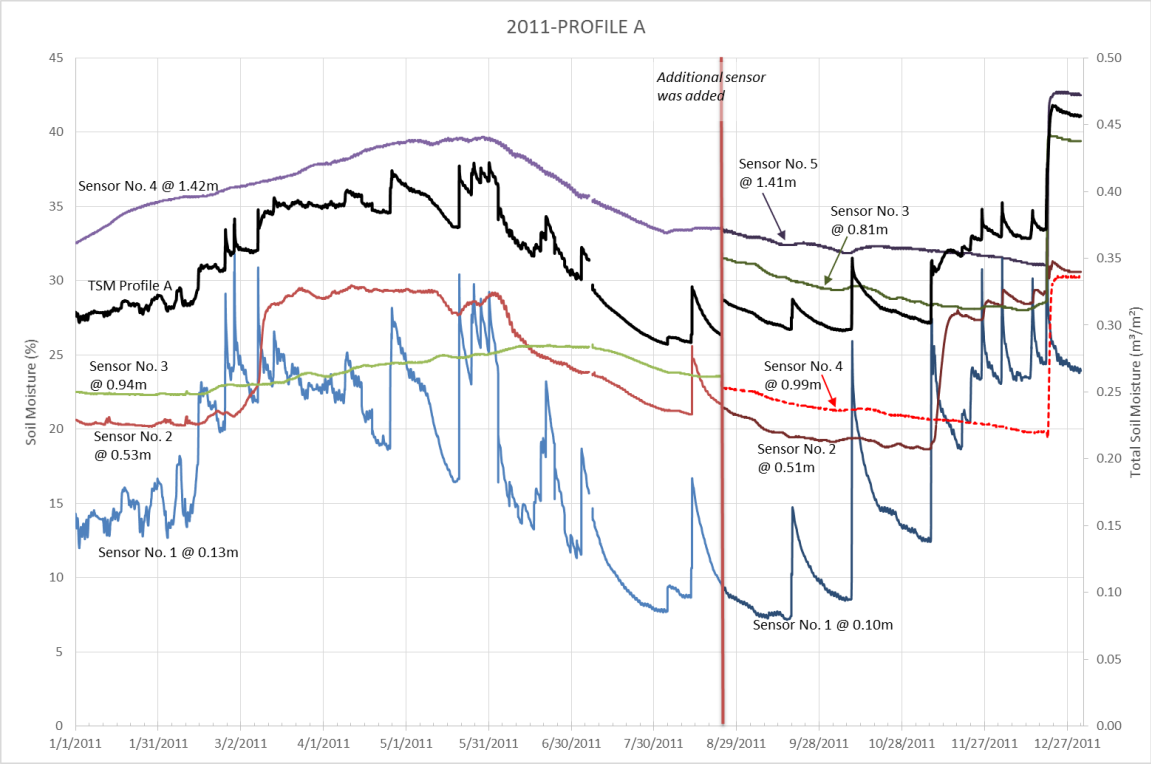

Figure D 2. Soil moisture and total soil moisture for profile A in 2011.

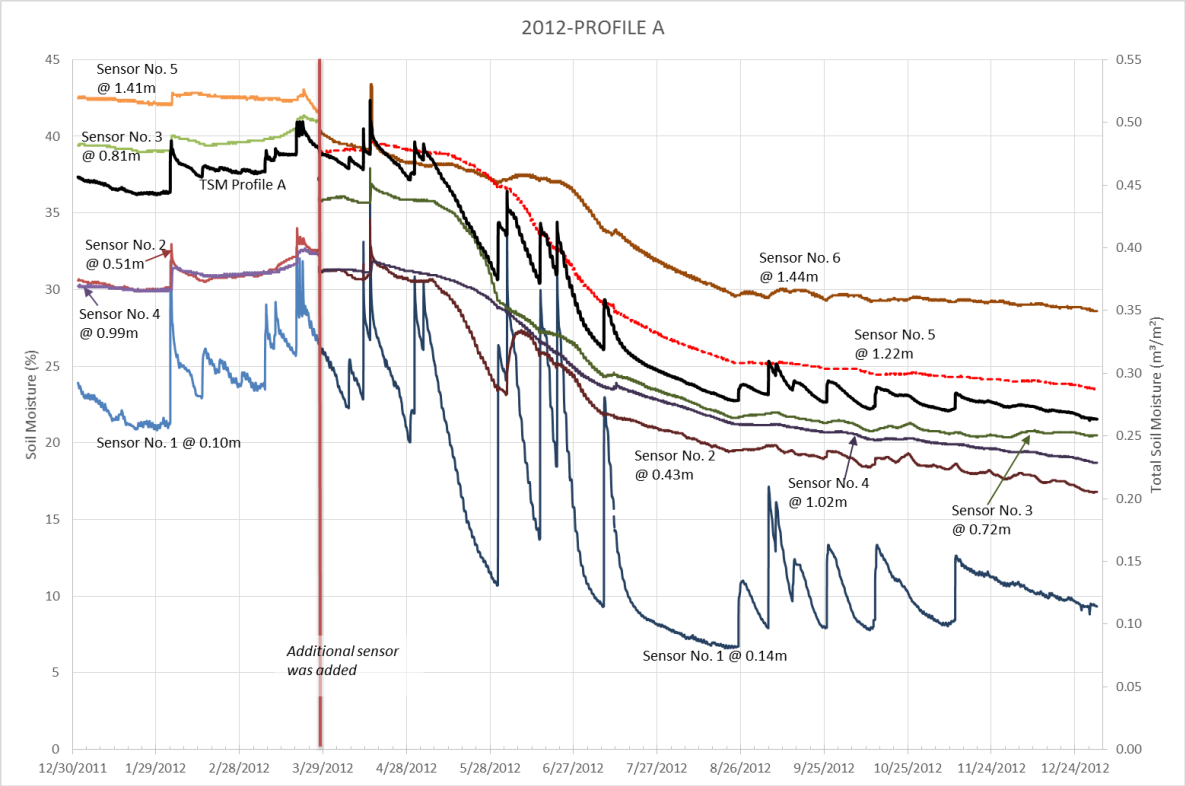

Figure D 3. Soil moisture and total soil moisture for profile A in 2012.

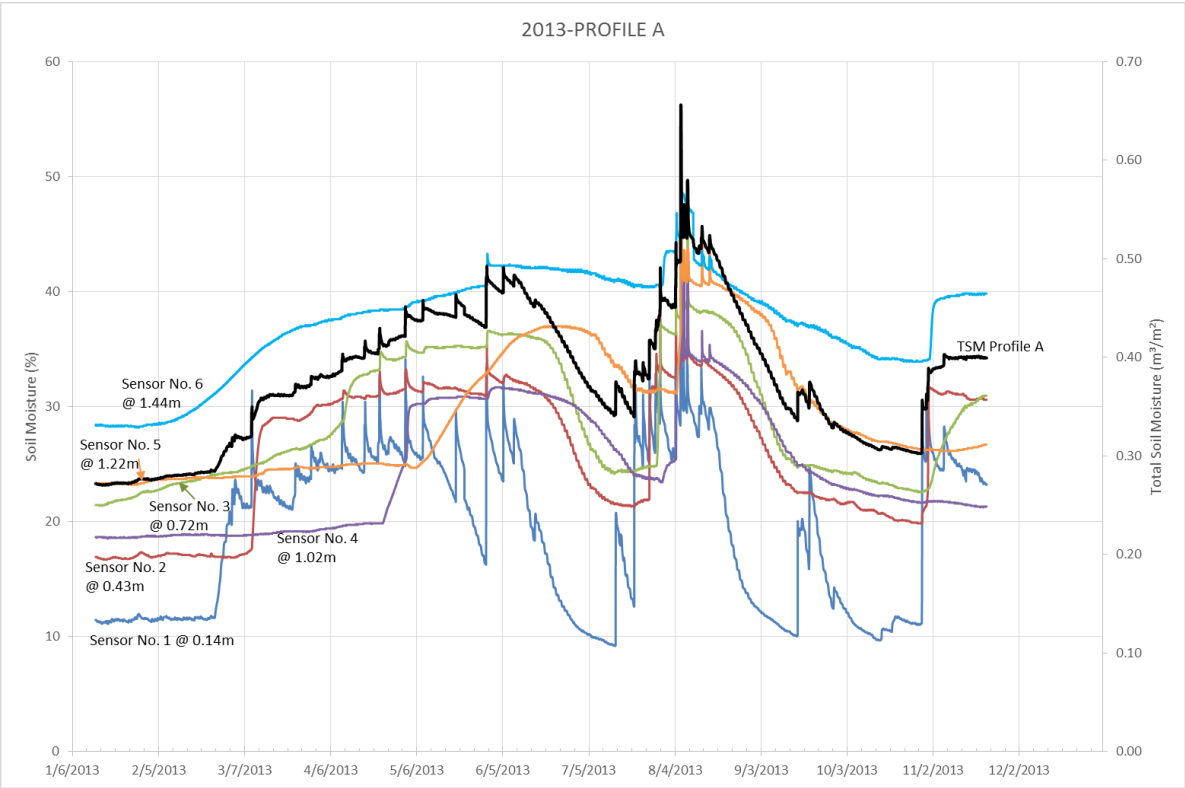

Figure D 4. Soil moisture and total soil moisture for profile A in 2013.

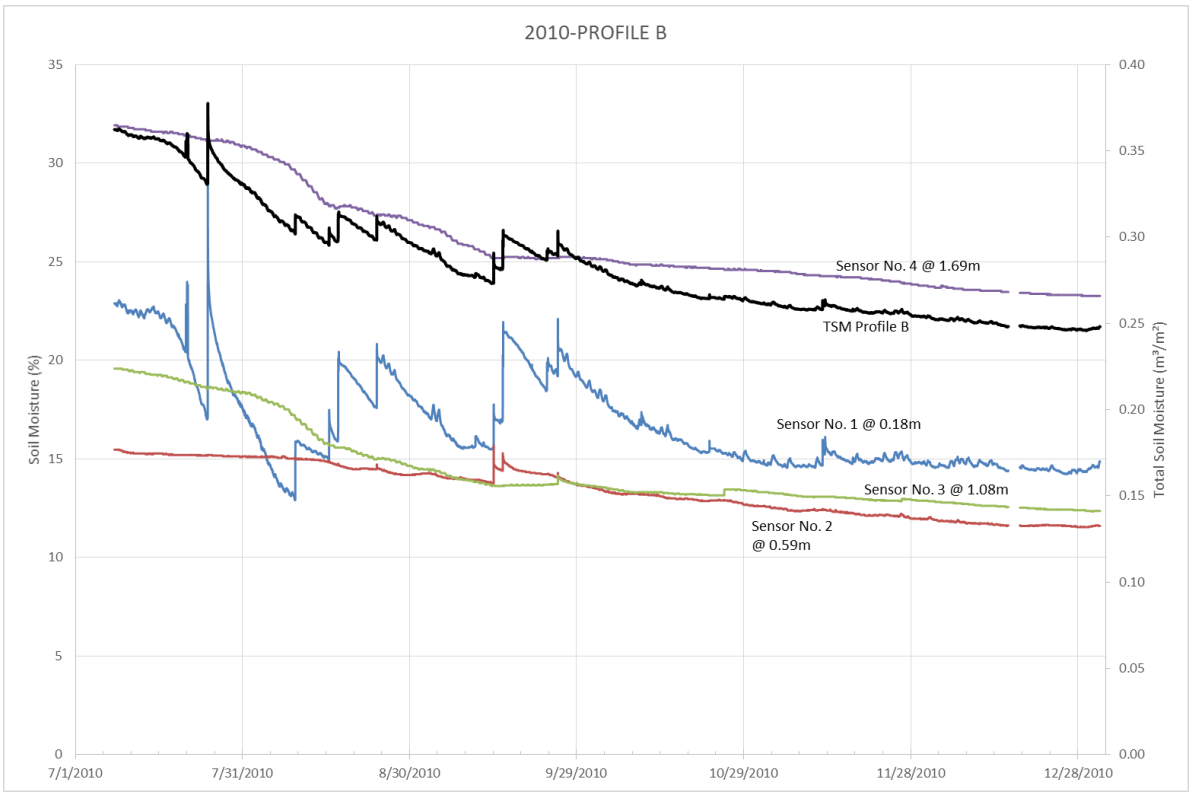

Figure D 5. Soil moisture and total soil moisture for profile B in 2010.

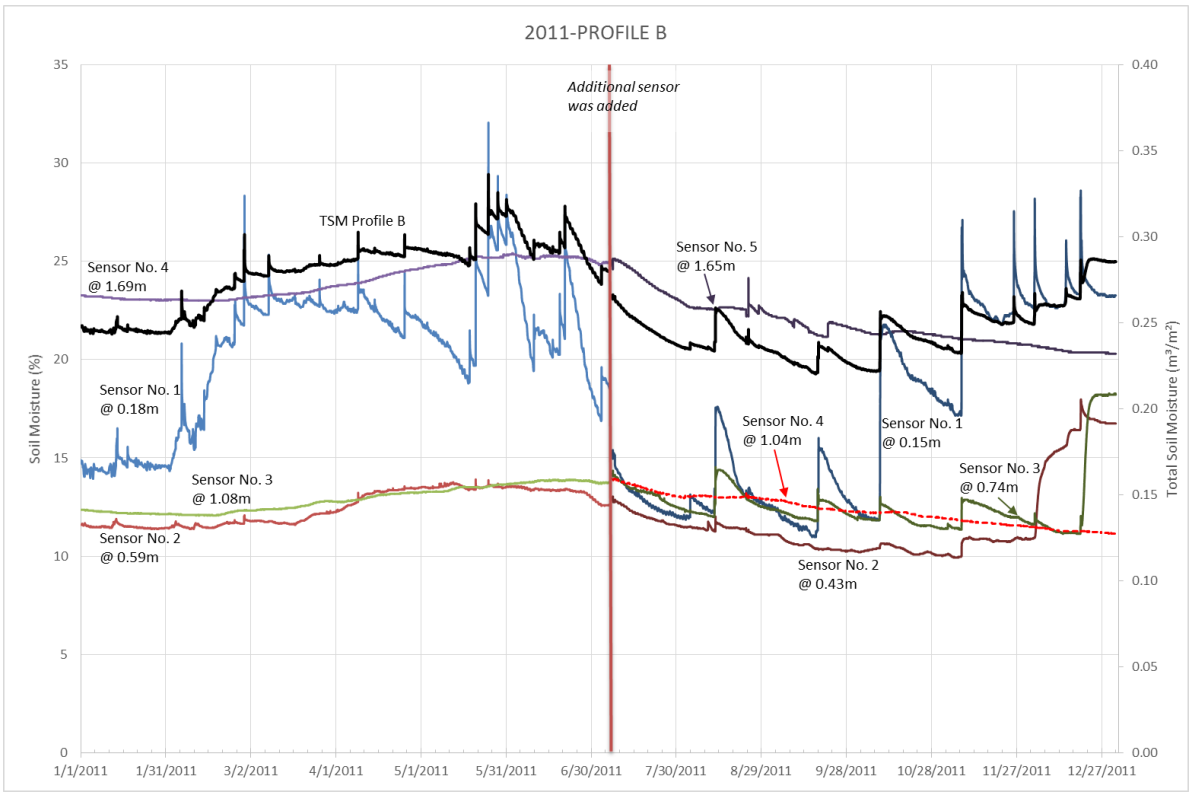

Figure D 6. Soil moisture and total soil moisture for profile B in 2011.

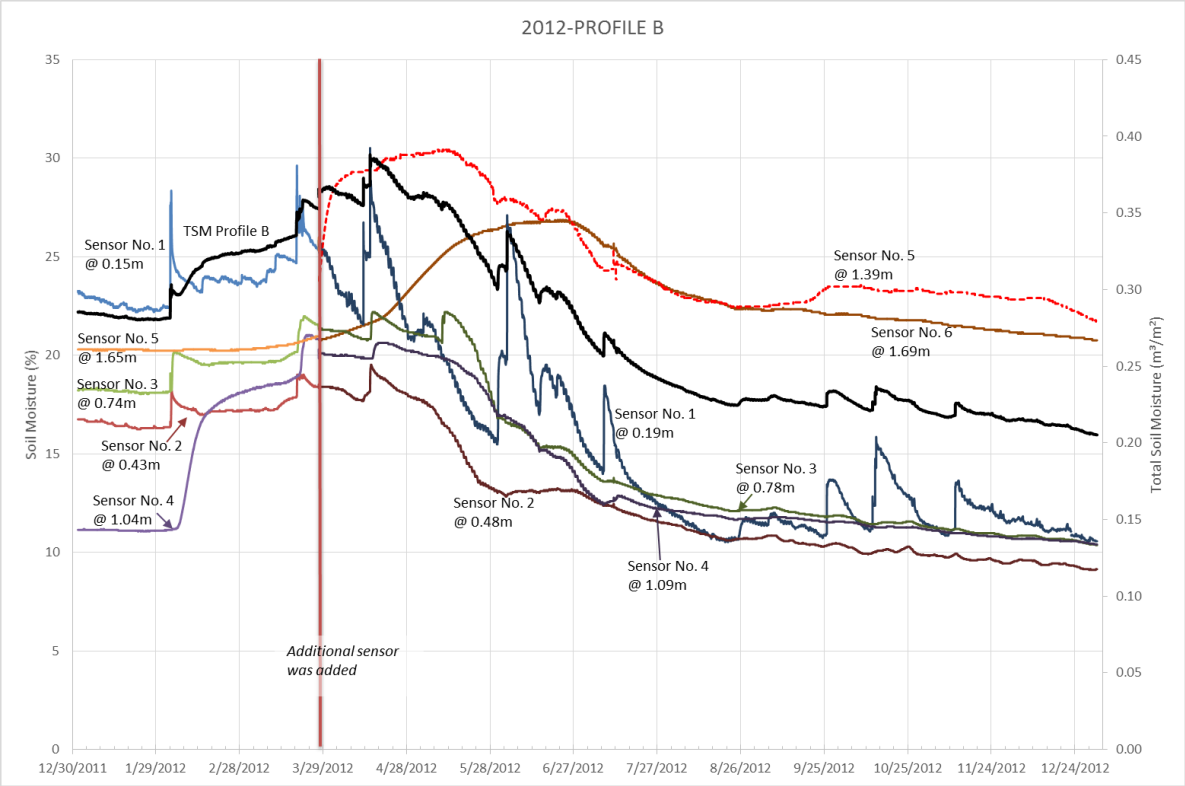

Figure D 7. Soil moisture and total soil moisture for profile B in 2012.

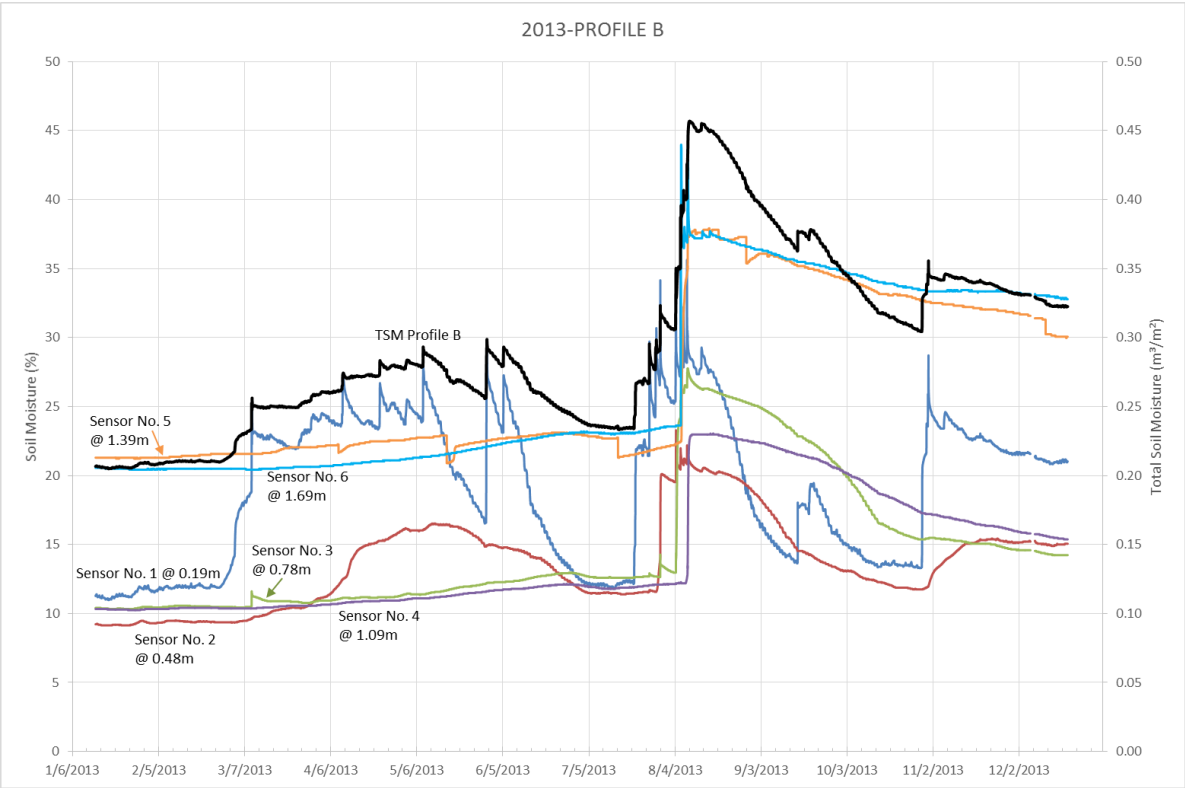

Figure D 8. Soil moisture and total soil moisture for profile B in 2013.

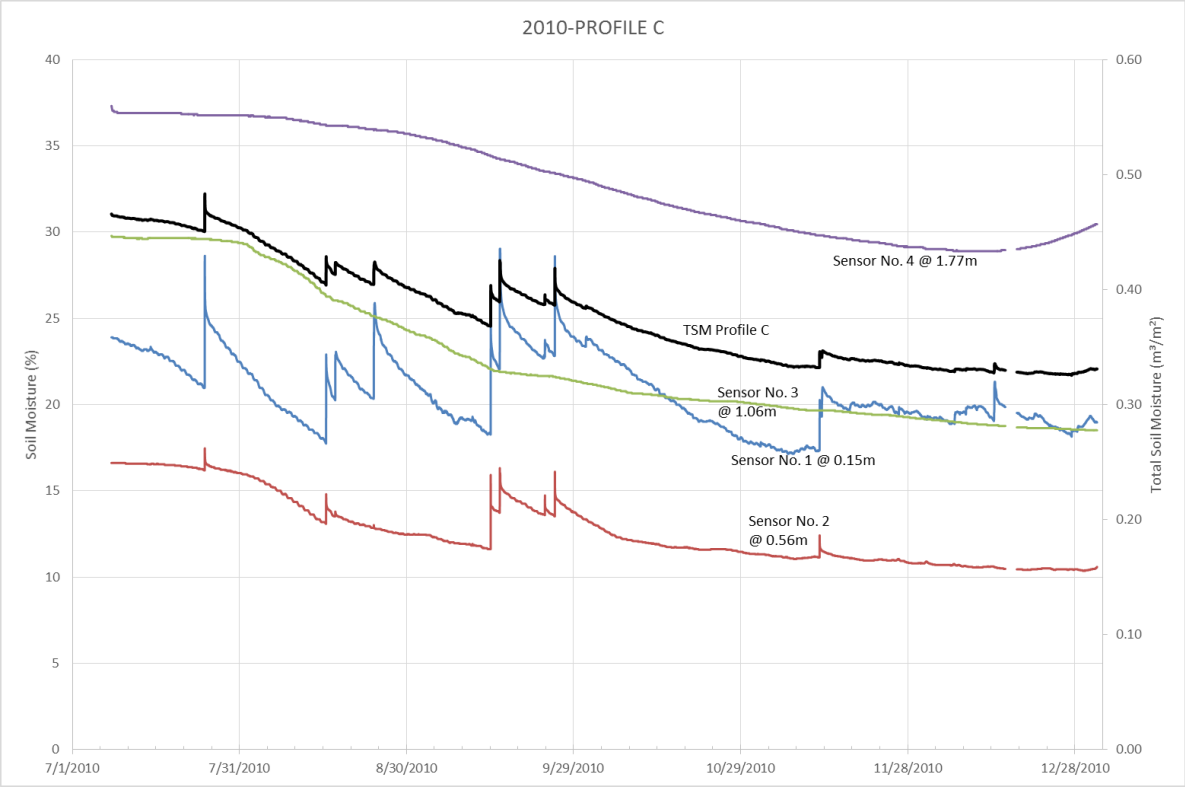

Figure D 9. Soil moisture and total soil moisture for profile C in 2010.

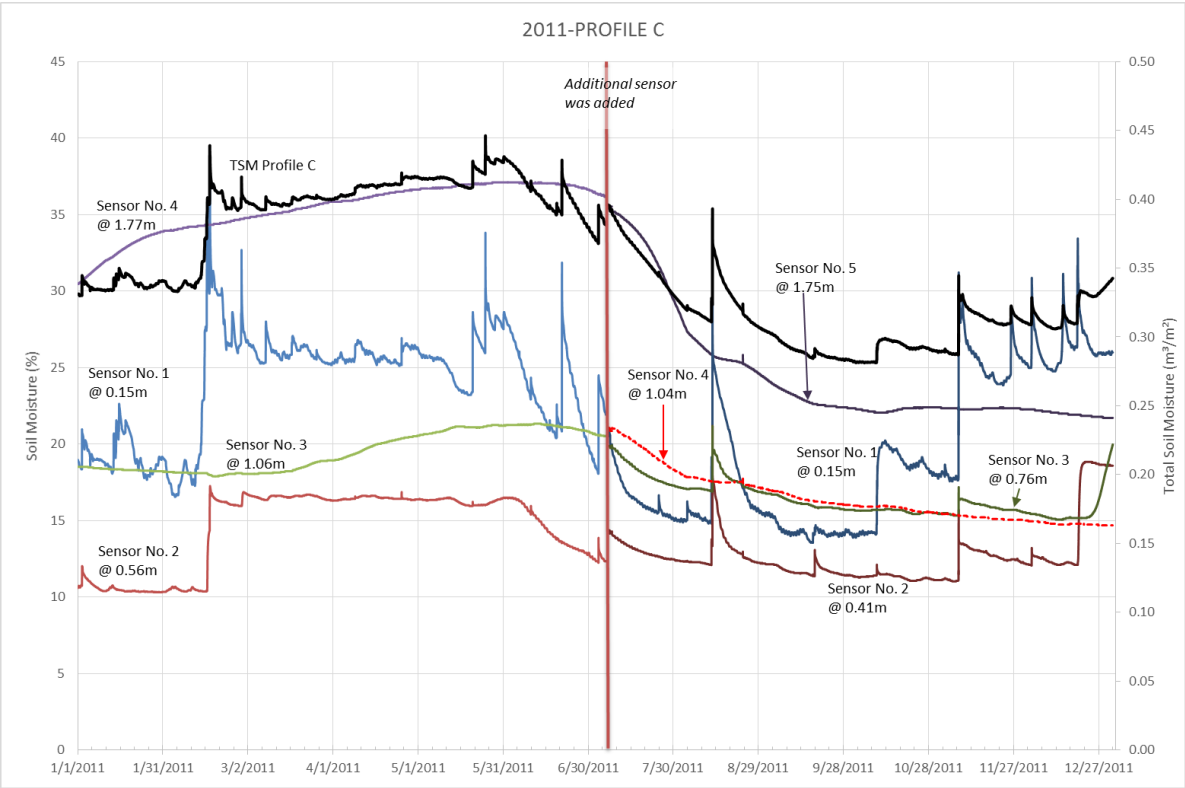

Figure D 10. Soil moisture and total soil moisture for profile C in 2011.

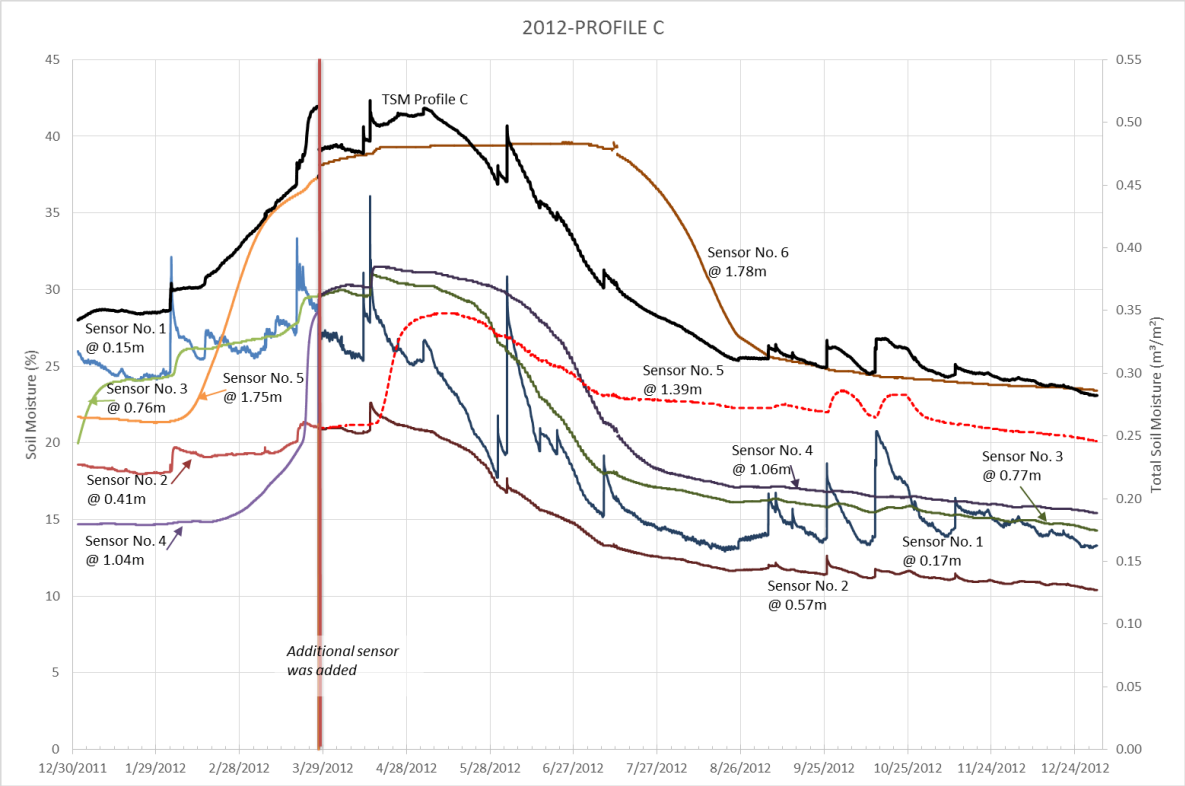

Figure D 11. Soil moisture and total soil moisture for profile C in 2012.

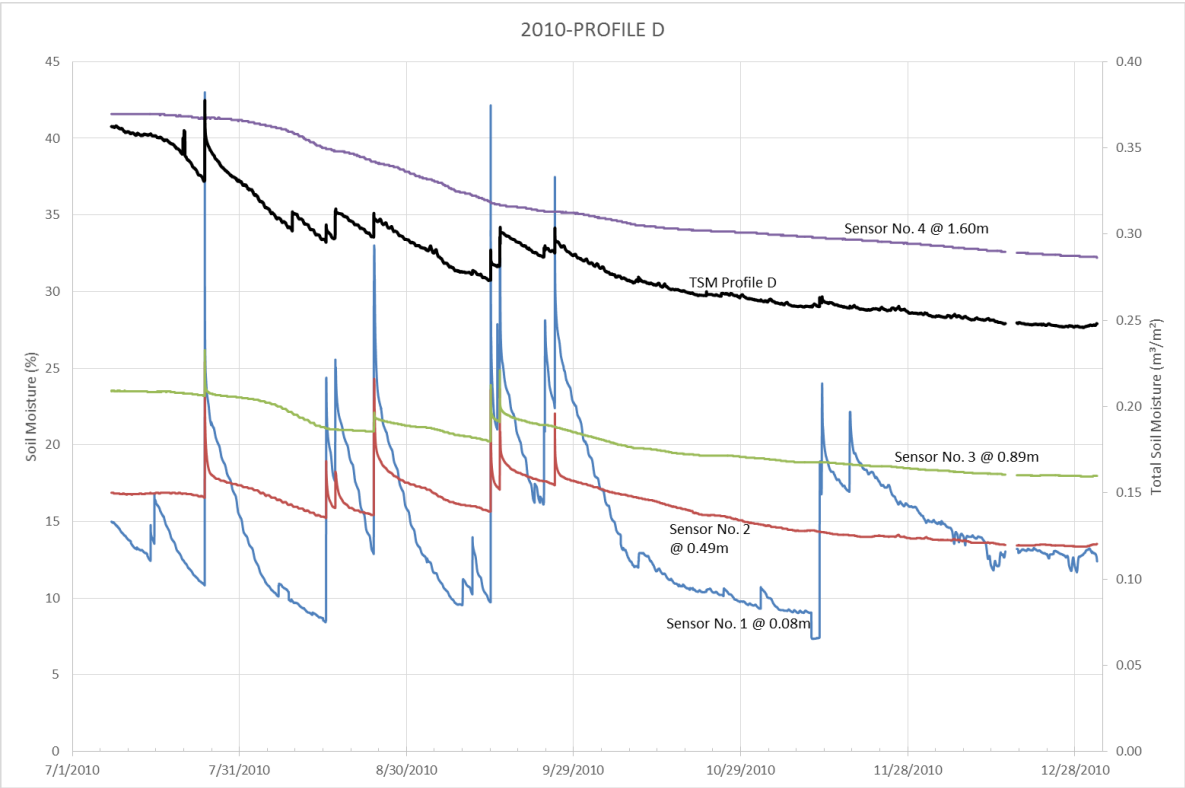

Figure D 12. Soil moisture and total soil moisture for profile D in 2010.

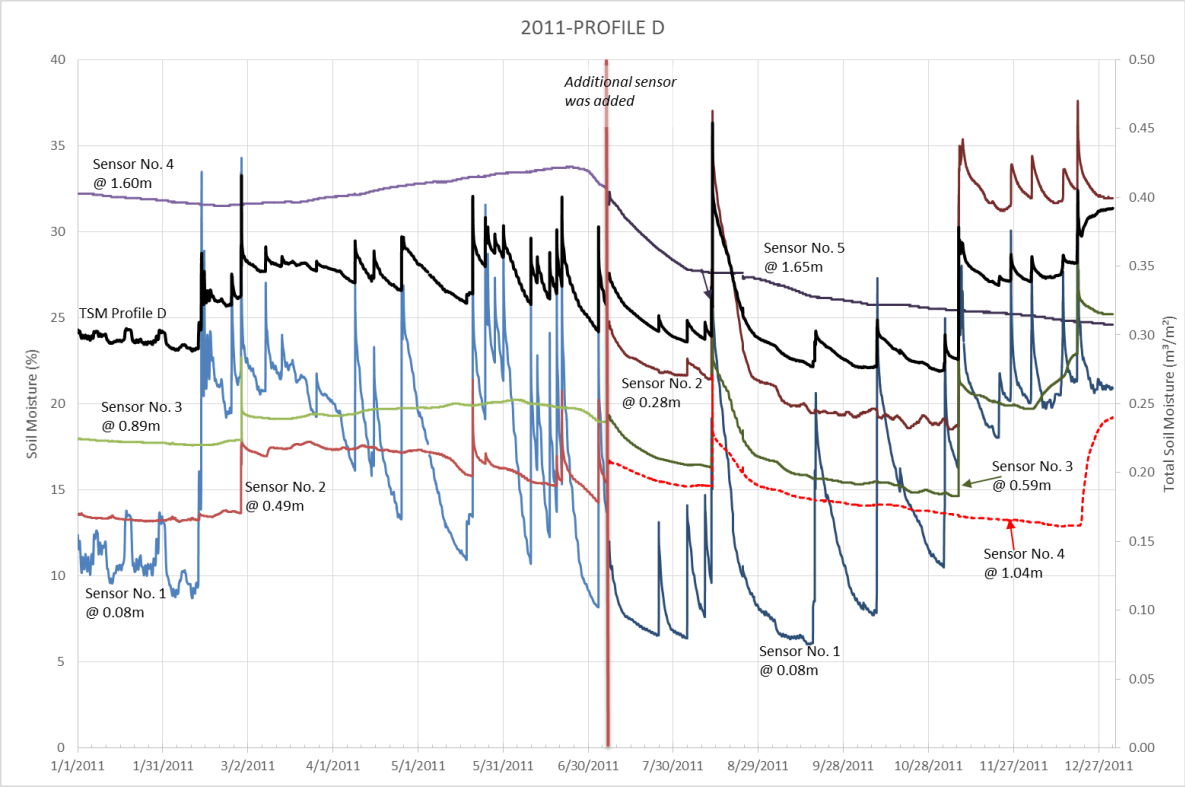

Figure D 13. Soil moisture and total soil moisture for profile D in 2011.

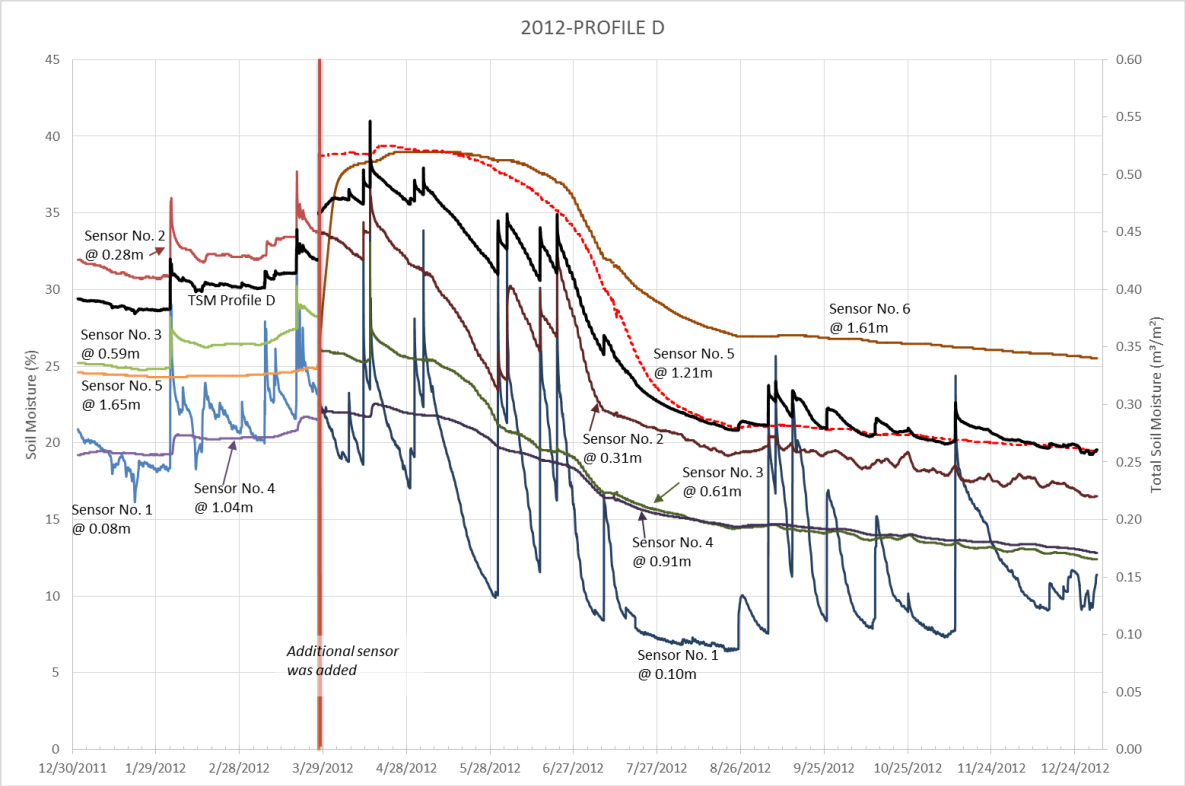

Figure D 14. Soil moisture and total soil moisture for profile D in 2012.

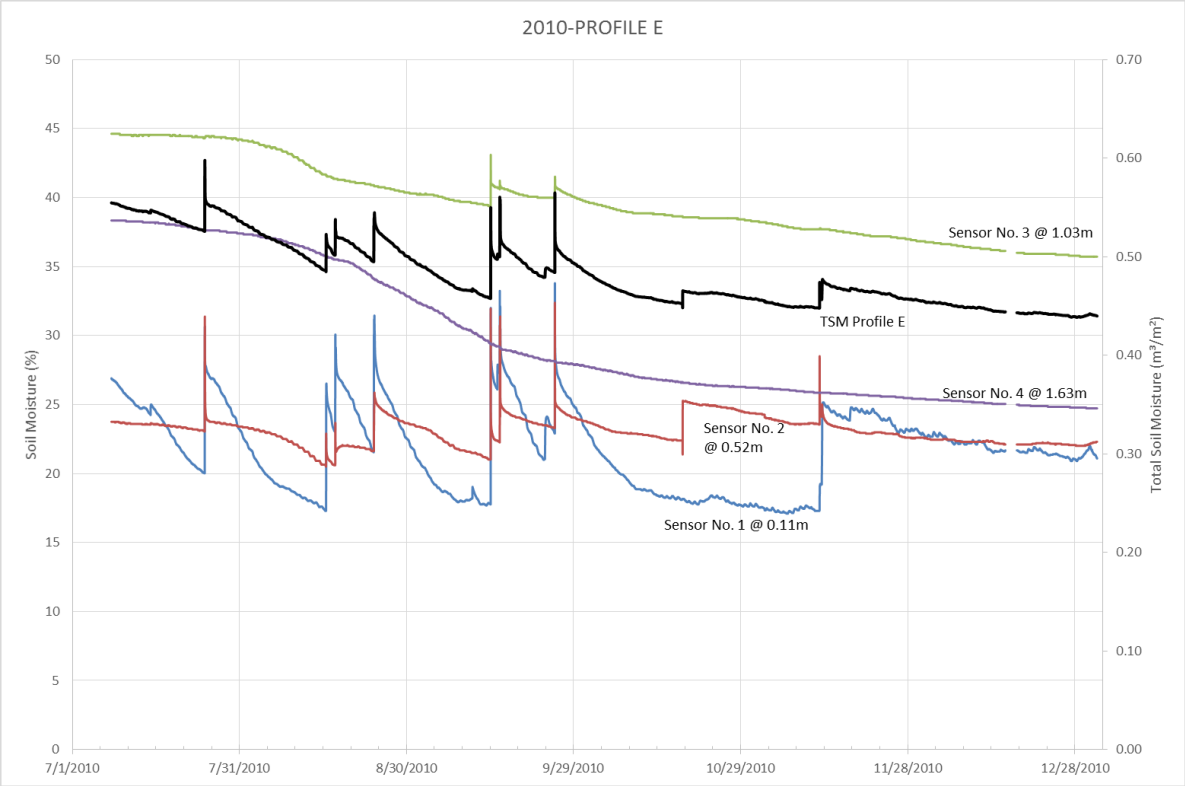

Figure D 15. Soil moisture and total soil moisture for profile E in 2010.

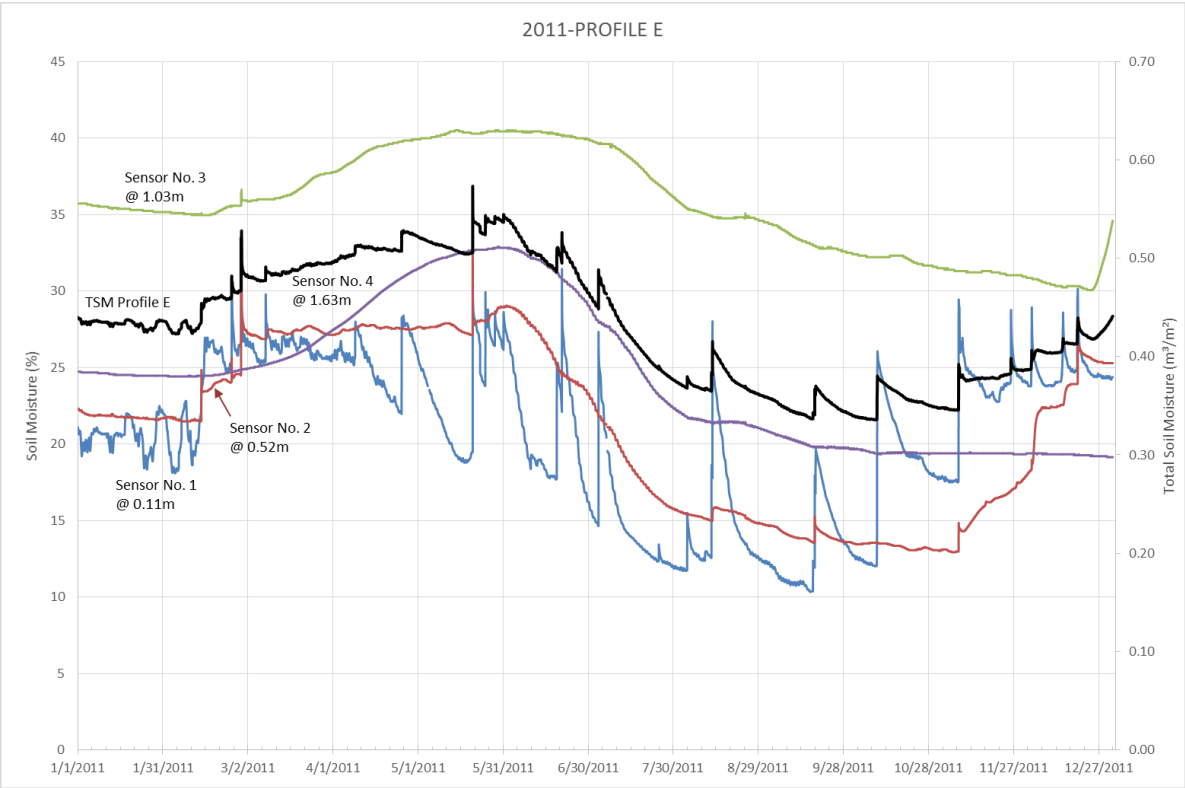

Figure D 16. Soil moisture and total soil moisture for profile E in 2011.

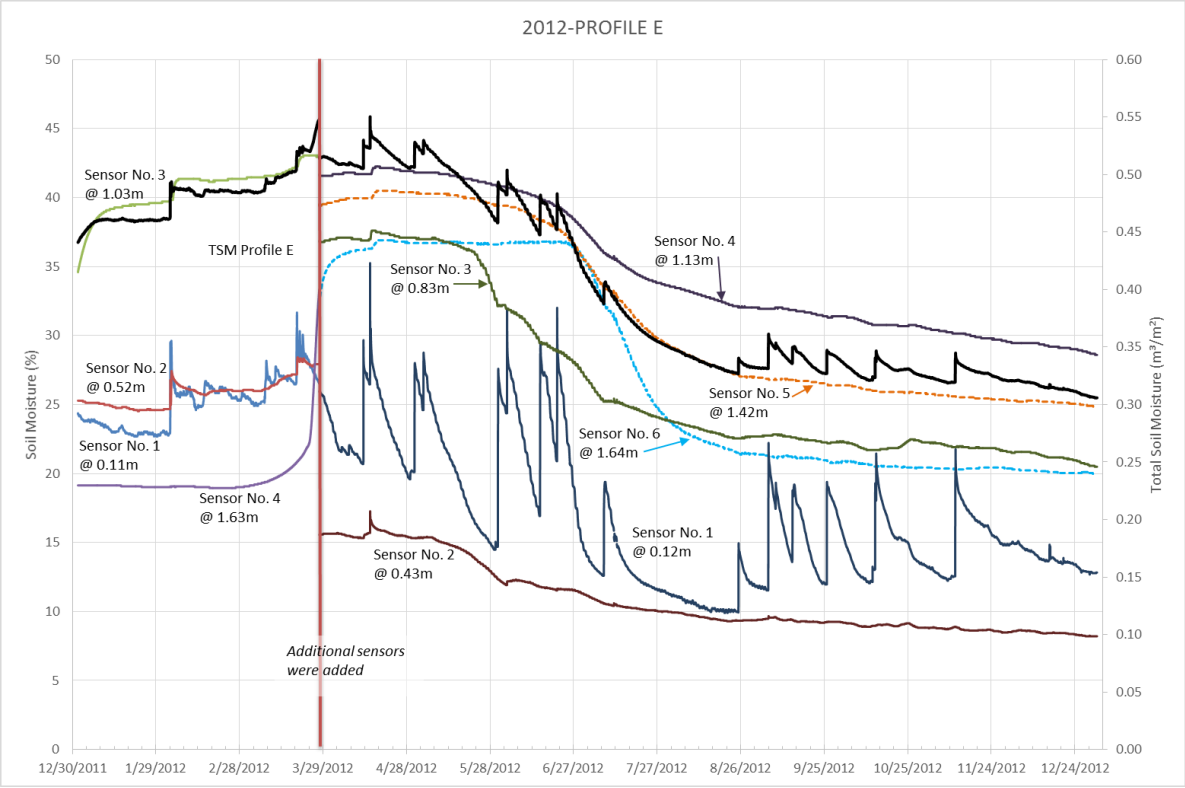

Figure D 17. Soil moisture and total soil moisture for profile E in 2012.

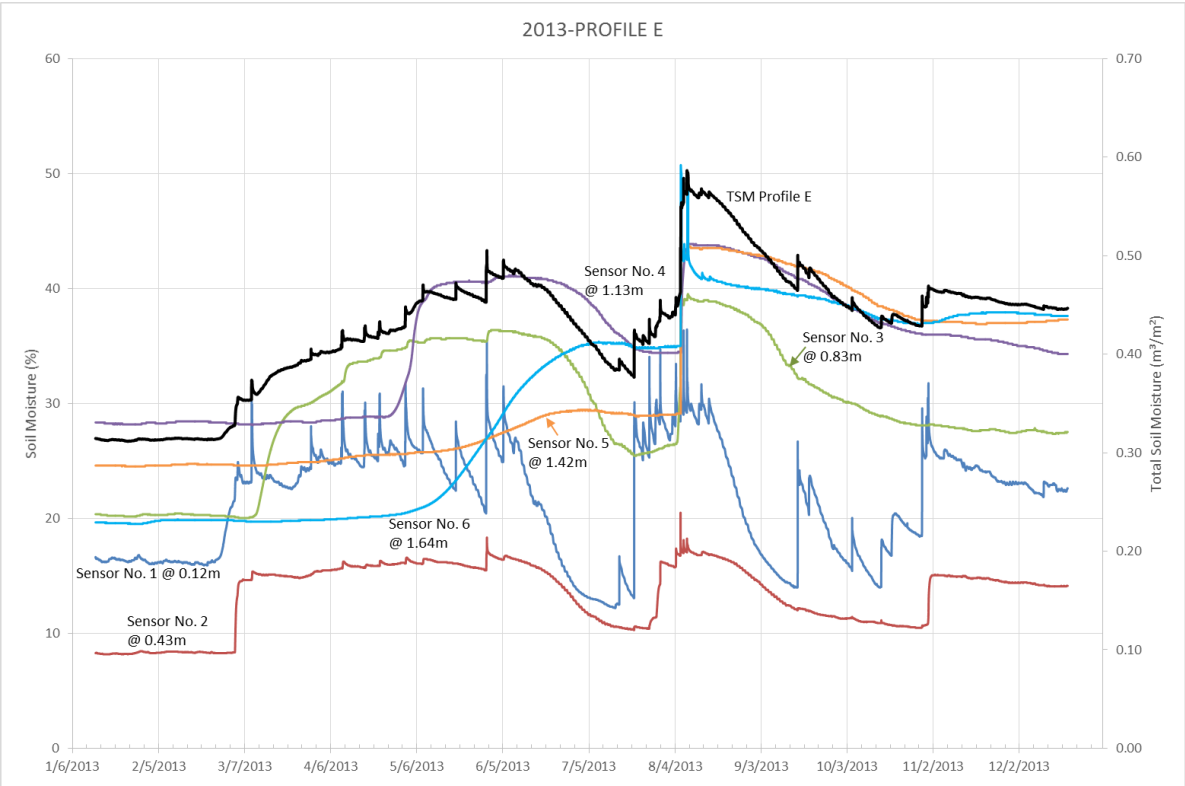

Figure D 18. Soil moisture and total soil moisture for profile E in 2013.

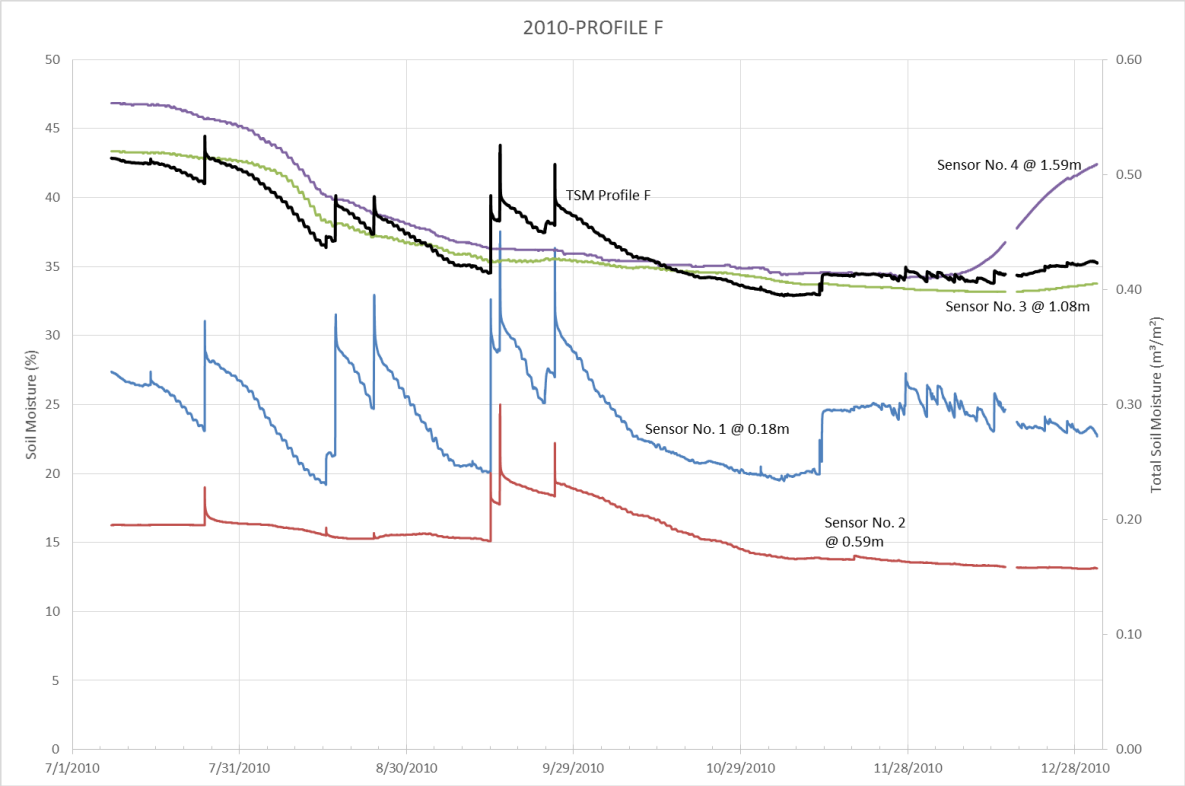

Figure D 19. Soil moisture and total soil moisture for profile F in 2010.

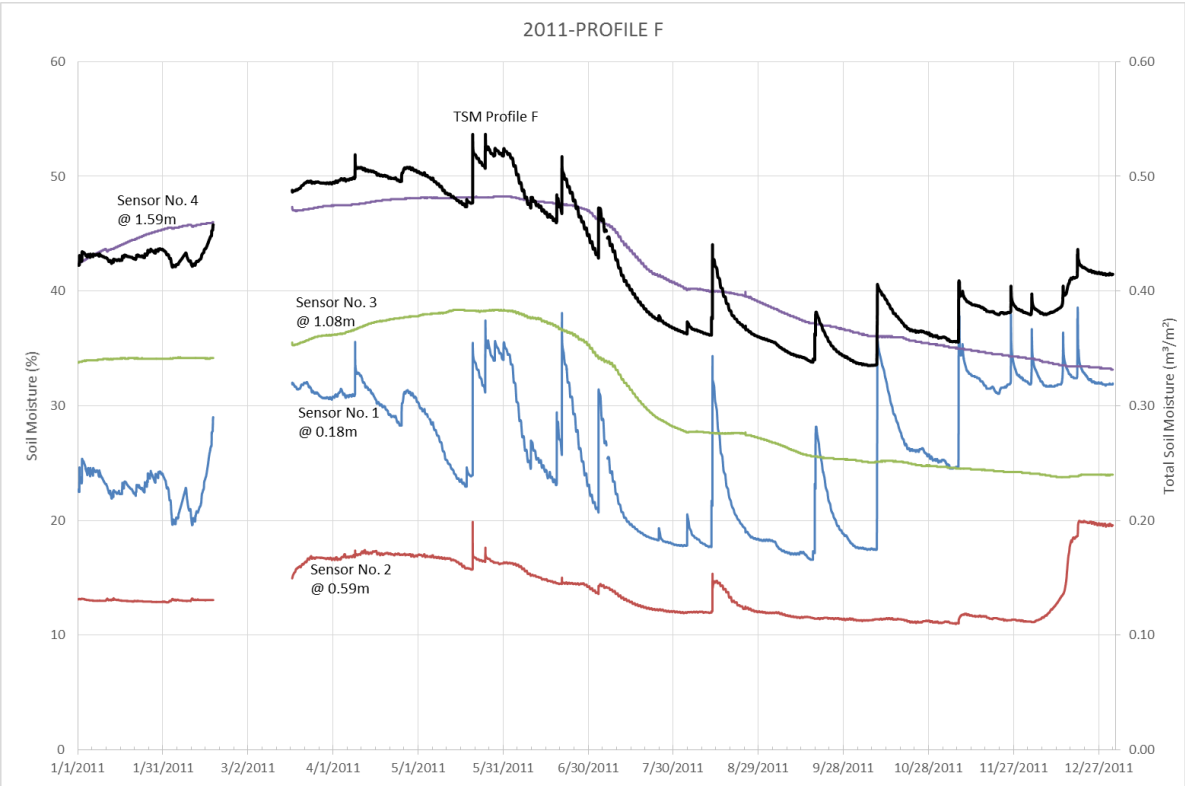

Figure D 20. Soil moisture and total soil moisture for profile F in 2011.

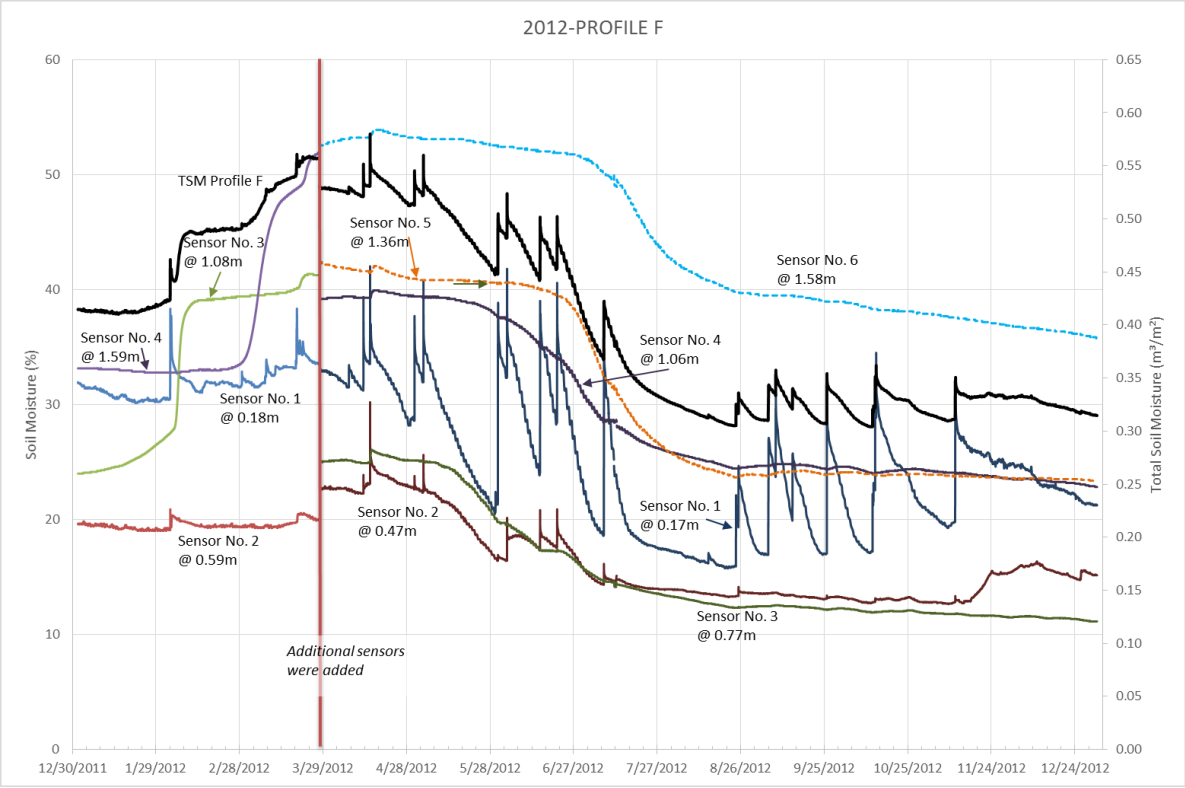

Figure D 21. Soil moisture and total soil moisture for profile F in 2012.

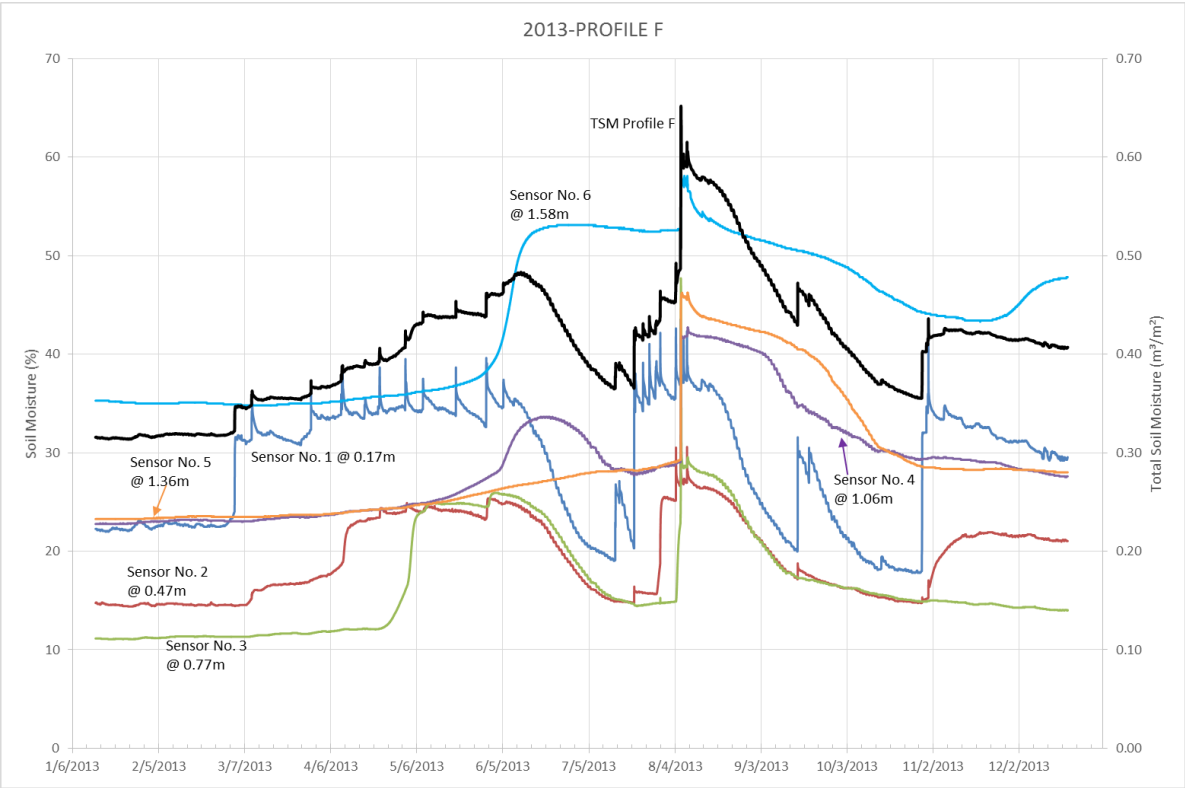

Figure D 22. Soil moisture and total soil moisture for profile F in 2013.

APPENDIX E: Annual Reference Evapotranspiration on a monthly time scale.

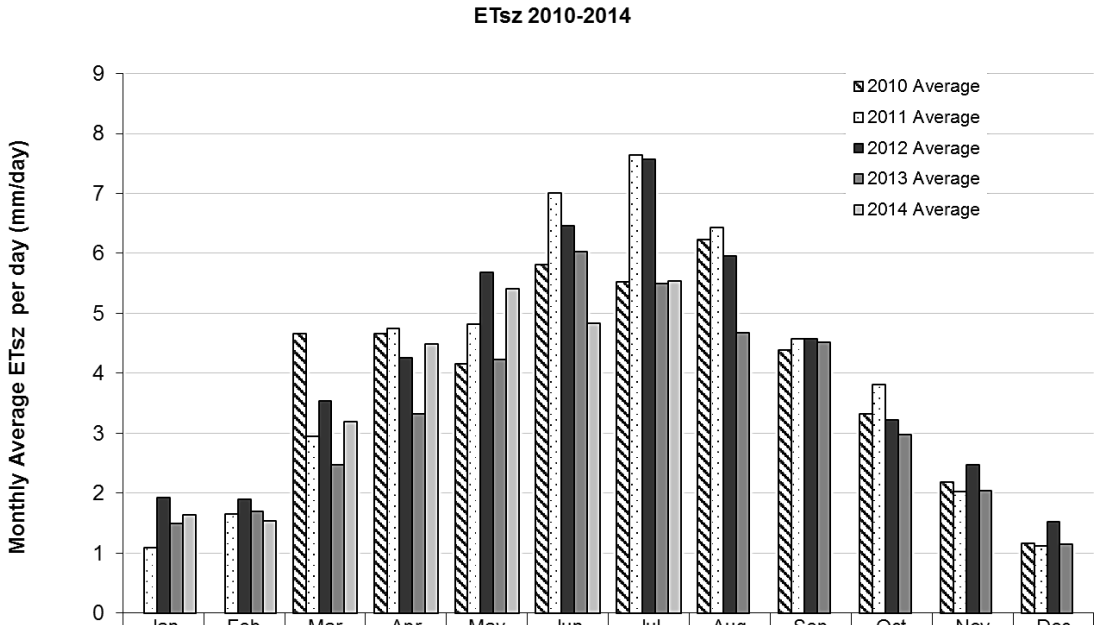

	Jan	Feb	Mar	Apr	May	Jun	Jul	Aug	Sep	Oct	Nov	Dec
2010 Average			4.66	4.66	4.16	5.82	5.52	6.22	4.38	3.32	2.18	1.16
2011 Average	1.09	1.65	2.95	4.75	4.82	7.01	7.64	6.44	4.57	3.81	2.02	1.12
2012 Average	1.92	1.90	3.53	4.26	5.68	6.46	7.57	5.96	4.57	3.22	2.47	1.53
2013 Average	1.49	1.69	2.48	3.33	4.24	6.03	5.50	4.67	4.52	2.98	2.03	1.15
2014 Average	1.63	1.54	3.19	4.49	5.41	4.83	5.54					

Figure E 1. ASCE standardized evapotranspiration, ETsz on monthly average extending from March 2010 to July 2014.

APPENDIX F: Annual water table hydrograph measurements for shallow wells

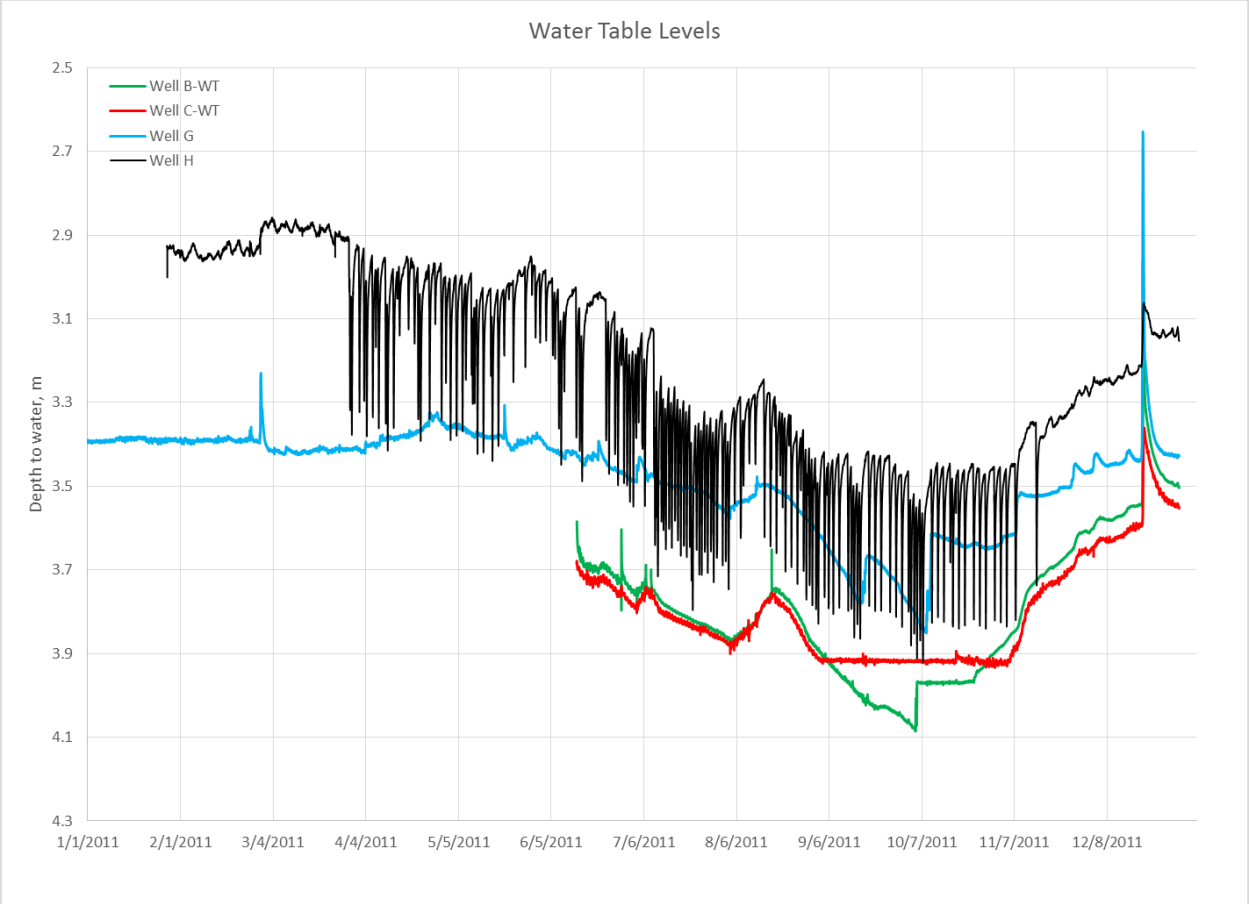

Figure F 1. 2011 Annual water table hydrograph measurements for shallow wells B (green line) and C (red line), and deep bedrock well (well H, black line) and for the well located in the stream (well G, light blue line).

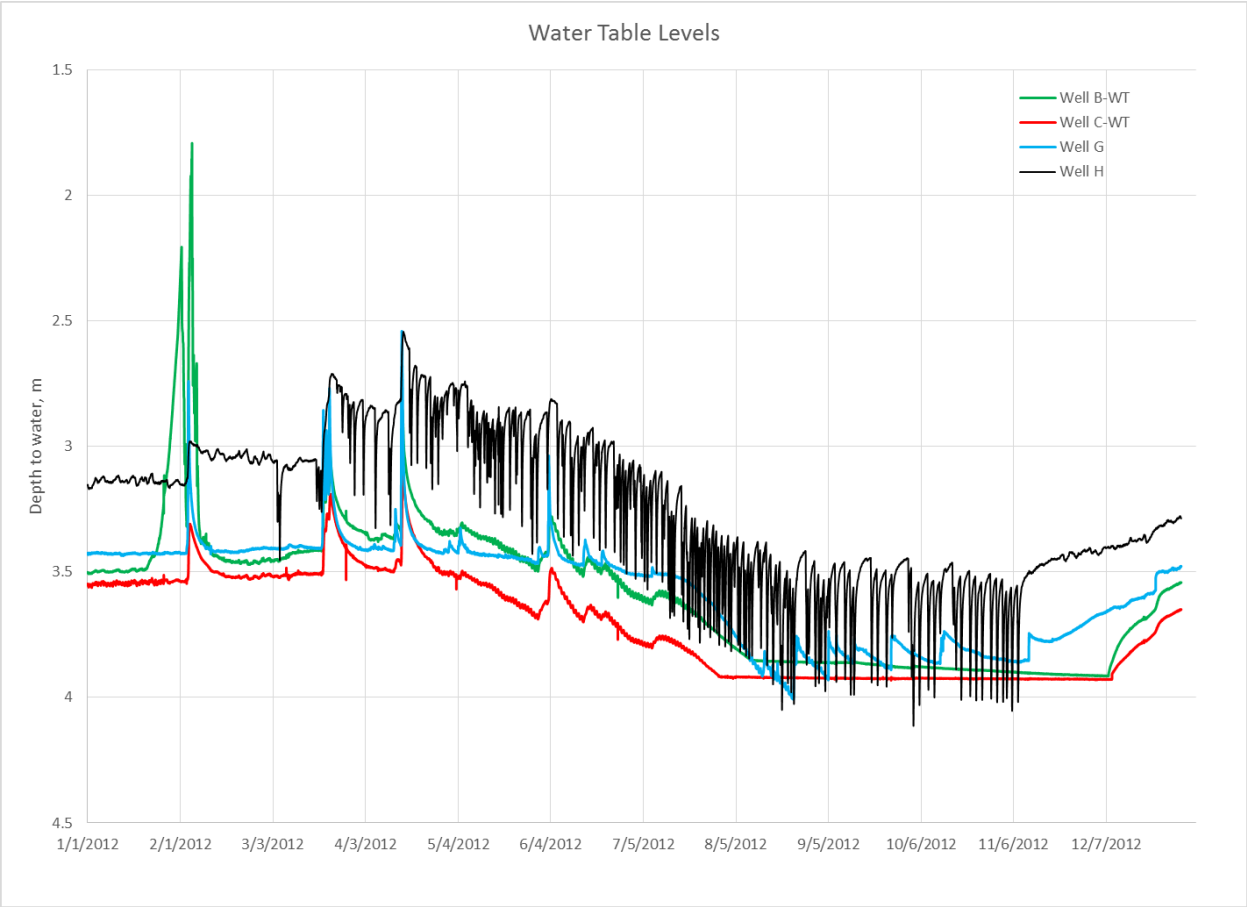

Figure F 2. 2012 Annual water table hydrograph measurements for shallow wells B (green line) and C (red line), and deep bedrock well (well H, black line) and for the well located in the stream (well G, light blue line).

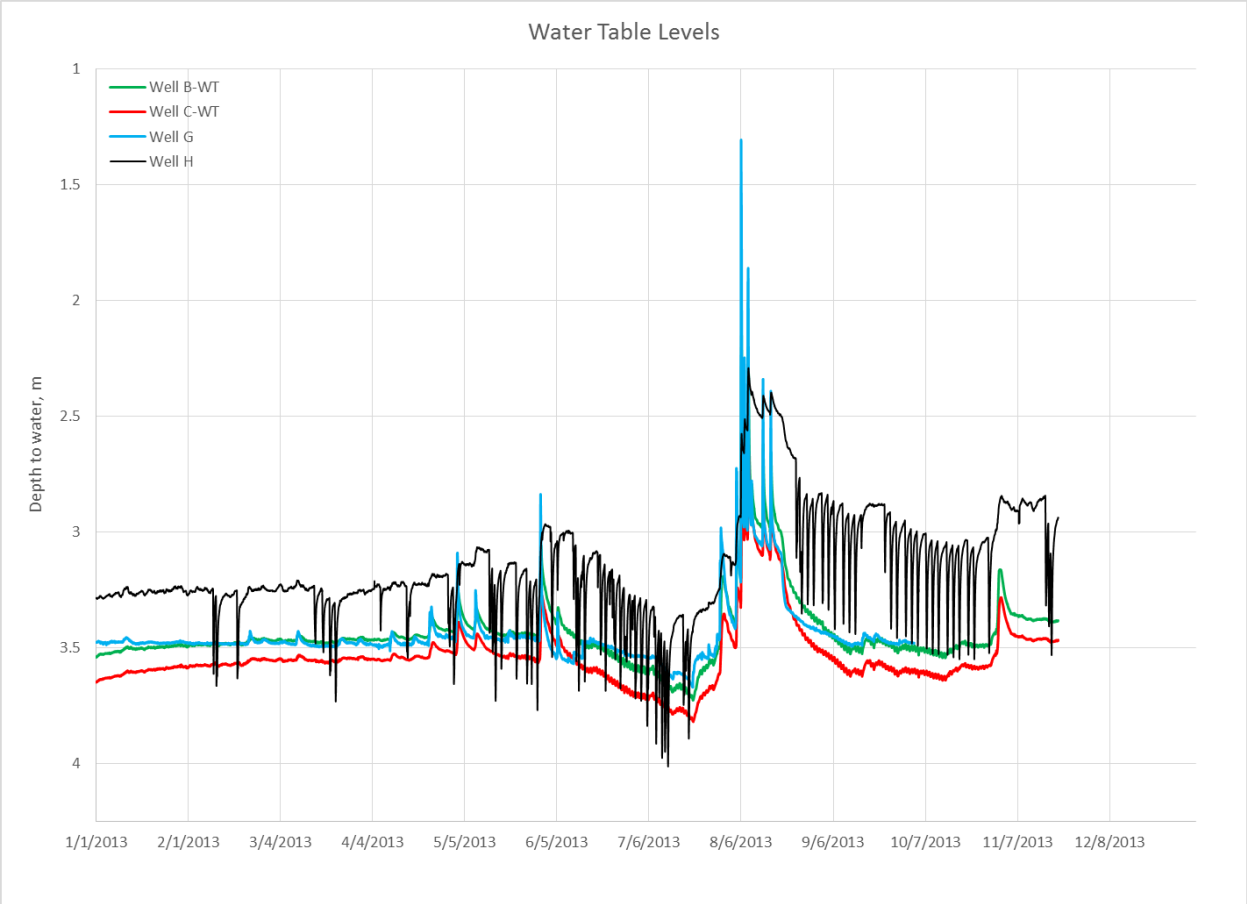

Figure F 3. 2013 Annual water table hydrograph measurements for shallow wells B (green line) and C (red line), and deep bedrock well (well H, black line) and for the well located in the stream (well G, light blue line).

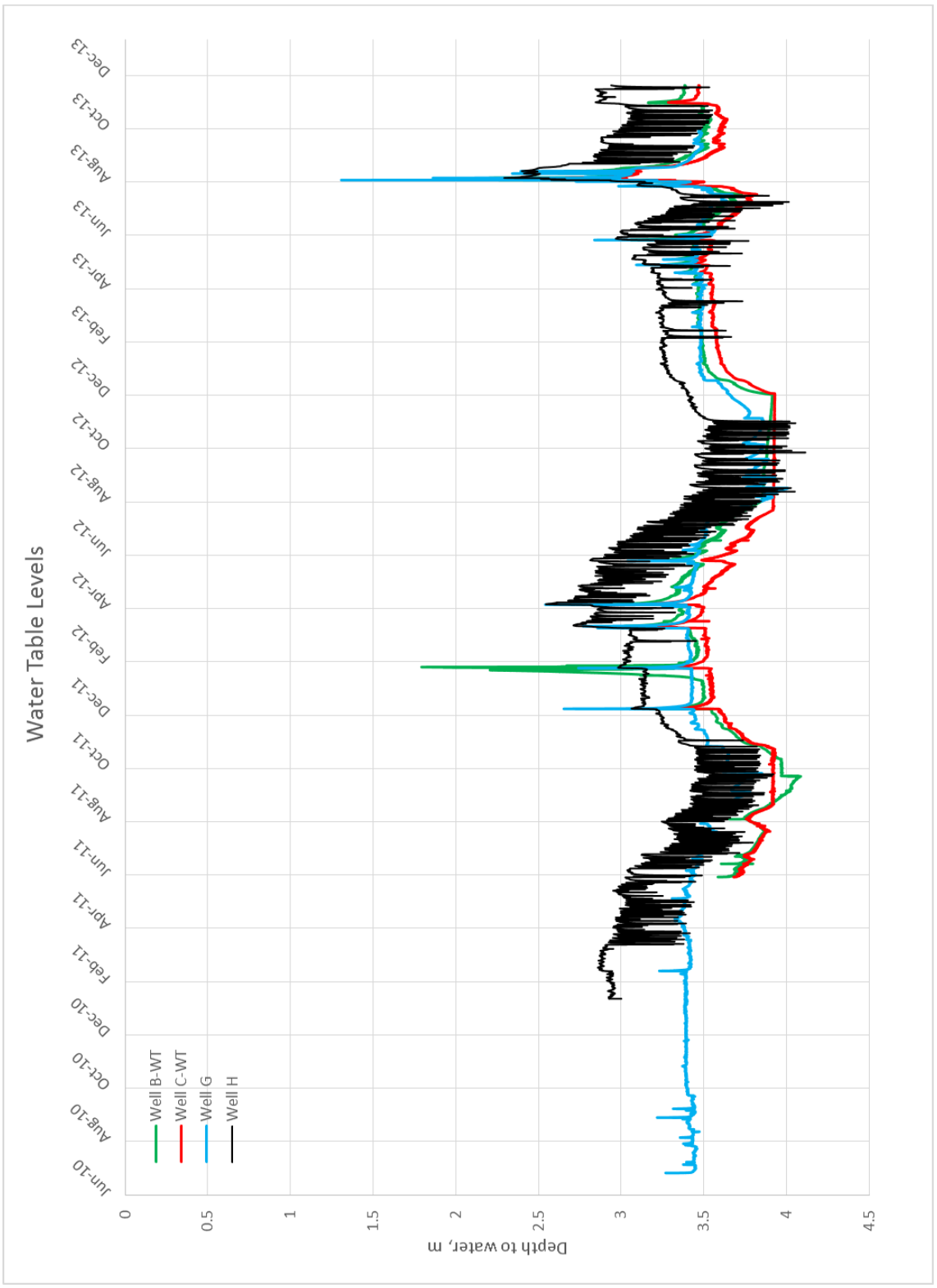

Figure F 4. 2013 Annual water table hydrograph measurements for shallow wells B (green line) and C (red line), and deep bedrock well (well H, black line) and for the well located in the stream (well G, light blue line).